THE RELATIONSHIP BETWEEN TDAG51 AND GDF10 IN THE CONTEXT OF MEDIAL VASCULAR CALCIFICATION AND FATTY LIVER

THE RELATIONSHIP BETWEEN TDAG51 AND GDF10 IN THE CONTEXT OF MEDIAL VASCULAR CALCIFICATION AND FATTY LIVER

By
Khrystyna Platko, B.Sc., M.Sc.

A Thesis Submitted to the School of Graduate Studies in Partial Fulfillment of the Requirements for the Degree Doctor of Philosophy

McMaster University
© Copyright by Khrystyna Platko, 2020

McMaster University DOCTOD OF PHILOSOPHY (2020) Hamilton, Ontario (Medical Sciences, Blood and Vasculature)

TITLE: The relationship between TDAG51 and GDF10 in the context of medial vascular calcification and liver injury

AUTHOR: Khrystyna Platko, B.Sc., M.Sc. (McMaster University)

SUPERVISOR: Richard C. Austin, PhD.

NUMBER OF PAGES: xiv, 198

ABSTRACT

Background: Disturbances in metabolic homeostasis, resulting in cardiovascular disease, are the major cause of morbidity and mortality in patients with chronic kidney disease (CKD). Mineral deposition in the vascular smooth muscle cell (VSMC)-rich medial layer of the vessel wall is a prominent driver of mortality in these patients. Vascular calcification (VC) is now recognized as an important predictor and independent risk factor for all-cause and cardiovascular mortality in patients with advanced CKD. Prolonged impairment in kidney functions, characteristic of chronic CKD, results in marked changes in blood biochemistry, namely elevated circulating levels of inorganic phosphate (P_i) and calcium. These changes in circulating mineral content trigger osteogenic transdifferentiation and apoptosis of the VSMCs, subsequently leading to VC. In addition to kidney-related metabolic changes, chronic inflammation and liver disease are also associated with increased VC. T-cell death-associated gene 51 (TDAG51) and growth differentiation factor 10 (GDF10) have been previously reported to contribute to metabolic regulation in conditions of atherogenic VC, osteogenesis, and adipogenesis. However their role in medial VC and associated morbidities remains unknown. **Methods and Results:** Using a combination of *in vitro*, *ex vivo* and *in vivo* models findings presented in this thesis demonstrate that TDAG51 is an important modulator of VC, and as such is upregulated by conditions of hyperphosphatemia. I show that VSMCs from *TDAG51*$^{-/-}$ mice exhibit reduced expression and activity of key driver of osteogenic transdifferentiation, Runt-related transcription factor 2 (Runx2). To explain these observations, I demonstrate reduced expression of type III sodium-dependent P_i transporter, Pit-1, as well as intracellular P_i in

these cells. Additionally, GDF10, an established inhibitor of osteogenesis, was identified to be significantly upregulated in *TDAG51*$^{-/-}$ VSMCs and mice. In line with these observations, knockdown of human homologue of TDAG51, pleckstrin homology-like domain, family A, member 1, resulted in increased expression of *GDF10*. Consistent with the anti-osteogenic role of GDF10, treatment with recombinant human GDF10 reduced P_i-mediated hydroxyapatite deposition, Runx2 expression and activity in primary mouse VSMCs. Interestingly, *GDF10*$^{-/-}$ mice develop severe adiposity, hepatic lipid accumulation, injury and inflammation. To explain this phenotype, a marked increase in the expression and activity of established driver of adipogenesis, peroxisome-proliferator-activated receptor γ (PPAR γ) in the livers of *GDF10*$^{-/-}$ mice was demonstrated. Complementary experiments in cultured hepatocytes demonstrate that treatment with recombinant human GDF10 attenuates nuclear PPAR γ expression and subsequent lipid accumulation, inflammation and fibrosis in these cells. **Conclusion:** This work highlights TDAG51 as an important regulator of P_i-mediated VC through downregulation of Pit-1, Runx2, and GDF10. Additionally, GDF10 has been described as a novel systemic inhibitor and a potential diagnostic marker for VC. Lastly, this work further characterizes GDF10 as an adipokine important in the regulation of hepatic lipid levels, which can indirectly affect vascular health.

ACKNOWLEDGEMENTS

I would like to express my deepest gratitude to my supervisor, Dr. Richard Austin. Thank you for providing me with an opportunity to grow as an individual and a scientist. Above all, thank you for your unwavering guidance, support and optimism.

Thank you Dr. Joan Krepinsky for your mentorship and encouragement during my PhD studies. It was a privilege to have you on my supervisory committee and I will continue to look up to you in many ways.

Thank you to Dr. Suleiman Igdoura for your support and insight into my projects.

Thank you to the Austin lab members both present and past for their continuous help and support throughout this journey. Your friendship, encouragement and advice have made the lab days as enjoyable as they were. Special thanks to Melissa, for providing a tremendous amount of help with countless animal experiments. Jae, thank you for your help with many of the projects that we have worked on together. Finally, Paul, thank you for your support and patience. Although frustrating at times, your constant state of calmness is what kept me grounded and focused on what matters.

Last but not least, I wish to express my deepest gratitude to my mother, who has unconditionally supported and encouraged me throughout my life. I would not be where I am today without the sacrifices that you've made. For that I am eternally grateful.

TABLE OF CONTENTS

ABSTRACT iii

ACKNOWLEDGEMENTS v

TABLE OF CONTENTS vi

LIST OF FIGURES viii

LIST OF TABLES ix

LIST OF ABBREVIATIONS x

DECLARATION OF ACADEMIC ACHIEVEMENT xii

CHAPTER 1: INTRODUCTION *1*

1.1 NATURAL HISTORY OF ARTERIAL STIFFNESS DUE TO CALCIFICATION ... 2

1.1.0 Intimal vs. medial vascular calcification 3

1.1.1 The link between impaired renal function and cardiovascular death 7

1.1.1 The role of phosphate in the development of vascular calcification 10

1.2 MOLECULAR MECHANISMS DRIVING MEDIAL VASCULAR CALCIFICATION 14

1.2.1 Genetic determinants of vascular calcification 17

1.2.2 Osteogenic transdifferentiation of the VSMCs 20

1.2.3 Apoptotic cell death as a driver of VC 23

1.3 T-CELL DEATH-ASSOCIATED GENE 51 (TDAG51) AND ITS HUMAN HOMOLOGUE PLECKSTRIN HOMOLOGY-LIKE DOMAIN FAMILY A, MEMBER 1 (PHLDA1) 25

1.3.1 Protein structure and homology 25

1.3.2 The role of TDAG51/PHLDA1 in health and disease 28

1.4 THE FUNCTION OF TGF-β SUPERFAMILY IN HEALTH AND DISEASE 30

1.4.1 TGF-β superfamily overview 30

1.4.2 The role of TGF-β superfamily in vascular function 32

1.4.3 The role of TGF-β superfamily in fibrosis and tissue repair 34

1.4.4 GDF10 is a divergent member of the TGF-β superfamily similar to BMP3 36

1.5 THE FUNCTION OF PPARs IN HEALTH AND DISEASE 40

1.5.1 PPAR superfamily overview 40

1.5.2 The biological function of PPARγ 41

1.6 PROJECT RATIONALE, HYPOTHESIS, OBJECTIVES, AND THESIS OUTLINE 43

1.6.1 Project rationale and hypothesis 43

1.6.2 Objectives and experimental approach 45

1.6.3 Thesis outline 46

CHAPTER 2: MANUSCRIPT 1 ..... *49*

TDAG51 (T-cell death-associated gene 51) is a key modulator of vascular calcification and osteogenic transdifferentiation of arterial smooth muscle cells. 49
Chapter link 50
Author's contribution 50

CHAPTER 3: MANUSCRIPT 2 83

GDF10 is a negative regulator of vascular calcification of vascular smooth muscle cells . 83
Chapter link 84
Author's contribution 84

CHAPTER 4: MANUSCRIPT 3 123

GDF10 blocks hepatic PPARγ activation to protect against diet-induced liver injury ... 123
Chapter link 124
Author's contribution 124

CHAPTER 5: GENERAL DISCUSSION 148

5.1 The pathogenesis of VC 148
5.1.1 TDAG51 is a key modulator of vascular calcification and osteogenic transdifferentiation of arterial smooth muscle cells 151
5.1.2 GDF10 is a negative regulator of vascular calcification of vascular smooth muscle cells 154

5.2 The relationship between CKD and NAFLD 158
5.2.1 GDF10 blocks hepatic PPARγ activation to protect against diet-induced liver injury 159

5.3 Conclusion and future directions 161

CHAPTER 6: REFERENCES 164

APPENDICES 185

APPENDIX 1-ER stress in response to vitamin D3 186

APPENDIX 2-Adenine model of VC pilot 187

APPENDIX 3-Structural similarity between mouse TGF-β and GDF10 active ligands . 196

APPENDIX 4-HDAC3 expression in VSMCs from *TDAG51*$^{+/+}$ and *TDAG51*$^{-/-}$ mice 198

APPENDIX REFERENCES 199

LIST OF FIGURES

Chapter 1: Introduction	Page number
Figure 1 Intimal vs. Medial VC	6
Figure 2 P_i homeostasis	13
Figure 3 Cellular and systemic drivers of VC	16
Figure 4 PHLDA1 structure and function	27
Figure 5 GDF10 structure and function	39

Appendices	
Supplemental Figure S1 Aortas from *TDAG51*$^{-/-}$ mice exhibit an attenuation of ER stress in response to vitamin D3 treatment	182
Supplemental Figure S2 A schematic representation of adenine-mediated CKD models	186
Supplemental Figure S3 Assessment of adenine-mediated model of renal damage and VC	187-189
Supplemental Figure S4: Assessment of adapted adenine model of renal damage and VC	192
Supplemental Figure S5 Comparison of GDF10 and TGF-β protein sequences	193
Supplemental Figure S6 *TDAG51*$^{-/-}$ VSMCs exhibit increase expression of HDAC3	194

LIST OF TABLES

Appendices	Page number
Supplemental Table 1 Diet compositions	191
Supplemental Table 2 NCBI protein blast input summary	192

LIST OF ABBREVIATIONS

aa-amino acid
ABCC6- ATP binding cassette subfamily C, member 6
AKT-protein kinase B
ALK-activin receptor-like kinase
AMP-adenosine monophosphate
ATP-adenosine triphosphate
ALP-alkaline phosphatase
BMP-bone morphogenic protein
CAC-coronary artery calcification
CA2-carbonicanhydrase-2
CD73-cluster of differentiation 73
CHOP- C/EBP homologous protein
CKD-chronic kidney disease
Col I- type I collagen
CV-cardiovascular
CVD-cardiovascular disease
DBD-DNA-binding domain
ECM-extracellular matrix
ENPP1- ectonucleotide pyrophosphatase/phosphodiesterase 1
EMT-epithelial to mesenchymal transition
ER-endoplasmic reticulum
ESRD-end-stage renal disease
eGFR-estimated glomerular filtration rate
DM-diabetes mellitus
FGF23-fibroblast growth factor 23
GDF-growth differentiation factor
HA-hydroxyapatite
HFD-high fat diet
KL-klotho
KO-knock out
LBD-ligand-binding domain
MAPK-mitogen-activated protein kinase
MGP-Matrix-gla protein
Msx2-Msh homeobox2
NAFLD-non-alcoholic fatty liver disease
OPN-osteopontin
Osx-osterix
OCN-osteocalcin
PARP- poly [ADP-ribose] polymerase
PCSK9-proprotein convertase subtilisin/kexin type 9
PH-proline-histidine
PHLD-pleckstrin homology-like domain

PHLDA1-pleckstrin homology-like domain family A, member 1
P-phosphate (organic)
P_i-inorganic phosphate
PP_i-pyrophosphate
PPARγ- peroxisome proliferator-activated receptor γ
PPARE- peroxisome proliferator response elements
Pit-1-type III sodium-dependent phosphate transporter 1
PTH-parathyroid hormone
PQ-proline-glutamine
R-receptor
RXR-retinoid X receptor
Runx2-runt-related transcription factor 2
QQ-polyglutamate
SNPs-single-nucleotide polymorphisms
SMAD- SMA-related and MAD-related protein
α-SMA- α-smooth muscle actin
Tdag51-T-cell death-associated gene 51
TGF-β-transforming growth factor- β
VC-vascular calcification
VSMC-vascular smooth muscle cell

DECLARATION OF ACADEMIC ACHIEVEMENT

This PhD thesis is presented in a sandwich thesis format and is comprised of 6 chapters. *Chapter 1*, general introduction, provides background information relevant to findings presented in subsequent chapters. *Chapters 2-4* are journal articles that outline the overall basis of the thesis. *Chapters 2* and *4*, have been published at the time of the thesis preparation, while *Chapter 3* was being prepared for submission at the *Journal of Biological Chemistry*. I am the primary author of *Chapters 2* and *3*, and a co-author of *Chapter 4*. The *author's contribution* section and *chapter link* section preceding each chapter describes the contributions of all authors of a given manuscript, as well as the rationale for the studies. *Chapter 5*, highlights the implications of the work described in *Chapters 2-4*, as well as limitations and future directions of this research. References cited in *Chapters 1* and *5* are found in *Chapter 6*, a reference chapter, while references cited within each manuscript are independent.

In addition to work used to produce this thesis, I also contributed to the following manuscripts that have been published or are under review, and are not directly relevant to this thesis.

Studies not directly related to the Ph.D. thesis topic	Contribution	Status
The hypocholesterolemic PCSK9 Q152H variant protects against liver injury by enhancing ER chaperone stability. Lebeau PF*, Wassef H*, Byun JH, **Platko K**, Ménard J, Ason B, Jackson S, Dobroff J, Shetterly S, Richards WG, Al-hashimi AA, Won KD, Mbikay M, Prat A, Tang A, Paré G, Pasqualini R, Arap W, Seidah NG, Chrétien M, Austin RC. *, Both authors contributed equally to this work	Assisted with tissue processing, histological and immunohistochemical analysis. Assisted with experiments for journal article revisions.	In-press *JCI* 2020.
Interstitial Cell Promotes Aberrant Adipogenesis in Dystrophic Muscles. Camps J*, Breuls N*, Sifrim A, Giarratana N, Corvelyn M, Danti L, Grosemans H, Vanuytven S, Thiry I, Belicchi M, Meregalli M, **Platko K**, Macdonald ME, Austin RC, Gijsbers R, Cossu G, Torrente Y, Voet T, Sampaolesi M. *, Both authors contributed equally to this work	Assisted with *in vivo* experiments for journal article revisions.	*Cell Rep. 2020*
Pcsk9 knockout exacerbates diet-induced non-alcoholic steatohepatitis, fibrosis and liver injury in mice. Lebeau PF*, Byun JH*, **Platko K***, Al-Hashimi AA, Lhoták Š, MacDonald ME, Mejia-Benitez A, Prat A, Igdoura SA, Trigatti B, Maclean KN, Seidah NG, Austin RC. *, All authors contributed equally to this work	Performed the majority of *in vivo* experiments, tissue processing and histological analysis, as well as some immunohistochemical staining.	*JHEP Rep. 2019*
The trypan blue cellular debris assay: a novel low-cost method for he rapid quantification of cell death. Lebeau PF*, Chen J*, Byun JH, **Platko K**, Austin RC. *, Both authors contributed equally to this work	Assisted with manuscript editing.	*MethodsX. 2019*

Diet-induced hepatic steatosis abrogates cell-surface LDLR by inducing de novo PCSK9 expression in mice. Lebeau PF*, Byun JH*, **Platko K**, MacDonald ME, Poon SV, Faiyaz M, Seidah NG, Austin RC. *, Both authors contributed equally to this work	Performed *in vivo* experiments, tissue processing and histological analysis, as well as some immunohistochemical staining.	*J. Biol Chem. 2019*
4-Phenylbutyrate protects against atherosclerotic lesion growth by increasing the expression of HSP25 in macrophages and in circulation in Apoe-/- mice. Lynn EG, Lhoták Š, Lebeau P, Byun JH, Chen J, **Platko K**, Shi C, O'Brien ER, Austin RC.	Assisted with *in vitro* experiments for journal article revisions.	*FASEB J. 2019*
Anti-GRP78 autoantibodies induce endothelial cell activation and accelerate the development of atherosclerotic lesions. Crane ED, Al-Hashimi AA, Chen J, Lynn EG, Won KD, Lhoták Š, Naeim M, **Platko K**, Lebeau P, Byun JH, Shayegan B, Krepinsky JC, Rayner KJ, Marchiò S, Pasqualini R, Arap W, Austin RC.	Assisted with *in vivo* experiments for journal article revisions.	*JCI Insight. 2018*
Loss-of-function PCSK9 mutants evade the unfolded protein response sensor GRP78 and fail to induce endoplasmic reticulum stress when retained. Lebeau P, **Platko K**, Al-Hashimi AA, Byun JH, Lhoták Š, Holzapfel N, Gyulay G, Igdoura SA, Cool DR, Trigatti B, Seidah NG, Austin RC	Assisted with tissue processing and immunohistochemical analysis.	*J. Biol Chem. 2018*
Mapping the kinase landscape of macrophage activation. **Platko K**, Lebeau P, Austin RC. *, Both authors contributed equally to this work	Completed a portion of the literature research and writing.	*J. Biol Chem. 2018*
Caffeine *blocks SREBP2-induced hepatic PCSK9 expression to enhance LDLR-mediated cholesterol clearance.* Lebeau PF, Byun JH, **Platko K**, Saliba P, Pare G, Steinberg GR, Janssen LJ, Wayne Chen SR, Seidah NG, Magolan J, Austin RC.	Performed *in vivo* caffeine experiments, tissue processing and histological analysis of harvested tissues.	The manuscript is under revisions at *Nat. Commun*

CHAPTER 1: INTRODUCTION

1.1 NATURAL HISTORY OF ARTERIAL STIFFNESS DUE TO CALCIFICATION

The large elastic arteries play an important role in buffering the cyclical cardiac flow. In a healthy individual, the vasculature maintains low systolic blood pressure by expanding to accommodate the stroke volume during systole and subsequently recoiling in order to preserve adequate blood pressure to allow for sufficient cardiac perfusion during diastole[1,2]. As stiffening of the vasculature progressively increases with age, it accelerates the development of cardiovascular (CV) disease (CVD) and deterioration of major organs[3]. An increase in the arterial stiffening is recognized as an independent predictor of myocardial infarction, hypertension, stroke, left ventricular hypertrophy and atherosclerosis as well as CV complications in patients with diabetes mellitus (DM) and chronic kidney disease (CKD)[4-6]. Vascular stiffening is further exacerbated by CVD, metabolic syndrome, DM, and CKD[3]. Additionally, the aortic pulse wave velocity – the indicator arterial stiffness – is also an important predictor of CV risk in the healthy general population[7].

Extensive pathophysiological studies have elucidated numerous mechanisms contributing to the progressive increase in arterial stiffness. Structural and functional changes that occur in the vasculature as a result of aging, CVD, and metabolic syndrome are thought to drive this process[2]. In patients with essential hypertension, arterial stiffness is elevated in response to persistent arterial pulsatile stress due to the elevated blood pressure, which occurs as a result of vascular remodeling[8]. Studies also demonstrate that chronic hyperglycemia, observed in patients with DM, results in persisting activation of the renin-angiotensin system leading to vascular smooth muscle cell (VSMC) proliferation,

inflammation, advanced glycation end products formation, and collagen crosslinking, subsequently leading to structural alterations of the arterial wall and increased vascular stiffness[6]. Activation of the renin-angiotensin system also occurs independent of hyperglycemia in patients with CKD[9]. Emerging evidence demonstrates a link between arterial mineral deposition, commonly referred to as vascular calcification (VC), and arterial stiffness which accelerates the development of CVD[2,10,11].

A variety of arterial wall cell types contribute to arterial stiffening, including endothelial cells, fibroblasts, inflammatory cells, and VSMCs[2,3]. Among these, VSMCs are essential for maintaining vascular elasticity and compliance[2,3]. Under normal heathy condition, VSMCs regulate vascular tone by producing crucial extracellular matrix (ECM) components, such as collagens and elastin. The bi-directional cross-talk between the VSMCs and the ECM also helps maintain vascular homeostasis[2]. However, in conditions of vascular stress, due to toxicity or elevated blood pressure, ECM remodeling promotes arterial stiffness in-part due to VC and overproduction of ECM components. Conversely, mineral deposition in the VSMCs drives ECM remodeling further exacerbating this unique pathophysiological adaptations that lead to an increase in arterial stiffness and subsequent increase in CV risk[2,10,12].

1.1.0 Intimal vs. medial vascular calcification

VC of the large arteries is a phenomenon dating as far back as >2,000 years. Computed tomography scans of mummies from the Egyptian empire show presence of mineral deposits in various vessels, including aorta, coronary, carotid, iliac, and femoral arteries[13].

Abundant evidence now demonstrates that VC is a pathophysiologic condition prevalent in aging, DM, dyslipidemia, CKD, and some genetic conditions[2,10,14]. In a meta-analysis, Wang *et al.*[15] conclude that 53-68 % of patients with CKD have coronary artery calcification. There are two major types of VC: intimal calcification and medial calcification[16]. As the name suggests, intimal calcification is present within the tunica intima, and is associated with hyperlipidemia, macrophage infiltration, and vascular inflammation[16]. Medial VC, also known as Mönckeberg sclerosis, is found within the VSMC-rich tunica media, and occurs independent of atherosclerosis (Figure 1)[10]. Numerous epidemiological studies have linked the prevalence and the extent of VC with increased risk of all-cause and CV mortality both in heathy and diseased populations[17-19].

Calcification of the intimal layer of the vessel wall is defined by lipid deposits in a form of fatty streaks spanning the large elastic arteries and is prevalent in progressive atherosclerotic lesions[16]. On the other hand, medial VC, which presents as sheet-like mineral deposits within the medial layer of the vessel wall, occurs independent of intimal calcification[10]. Medial VC is a unique and prominent type of vascular mineral deposition that is almost exclusively associated with mineral metabolism dysregulation observed in patients with advanced CKD[17,20,21]. Significant medial VC of coronary arteries is present in the absence of intimal mineral deposition and is associated with an increase in serum creatinine – indicative of reduced renal function[22]. Similarly, Moe *et al.*[23] show an increase in medial VC of the epigastric artery in the absence of classical atherosclerosis in patient with CKD. Additionally, medial VC is present in vessels of both the central and the peripheral circulatory system in patients with CKD[24]. Autopsy studies reveal an

increased hydroxyapatite (HA) mineral deposition within vasculature in patients with CKD[25,26]. In line with these studies, the frequency of calcific atherosclerotic plaque formation is increased in patients with CKD compared to age-matched subjects with normal renal function[26,27]. Furthermore, the presence of medial VC is a strong predictor of CV and all-cause mortality in patients with CKD[17].

Although morphologically distinct, clinical and pathophysiological studies demonstrate that there are many similarities between the pathogenesis of intimal and medial VC[20]. In particular, increased oxidative stress- and hyperglycemia-mediated systemic and local inflammation are associated with both intimal and medial VC in patients with CKD as well as those presenting with classical atherosclerosis[20]. The state of chronic inflammation is also associated with increased CV mortality, a condition that is further exacerbated in patients with CKD[28]. In line with these findings, there exists a positive correlation between systemic inflammation and presence of both intimal and medial calcification in hemodialysis patients[29,30]. Additionally, expression of markers of inflammation in calcified arteries from patients with CKD differs from that of non-uremic controls[31]. However, even though patients with CKD frequently present with both types of VC, medial VC is more prevalent due to kidney-induced changes in blood biochemistry. For this reason, patients with advanced CKD exhibit an additive CVD-associated risk due to the presence of both types of VC.

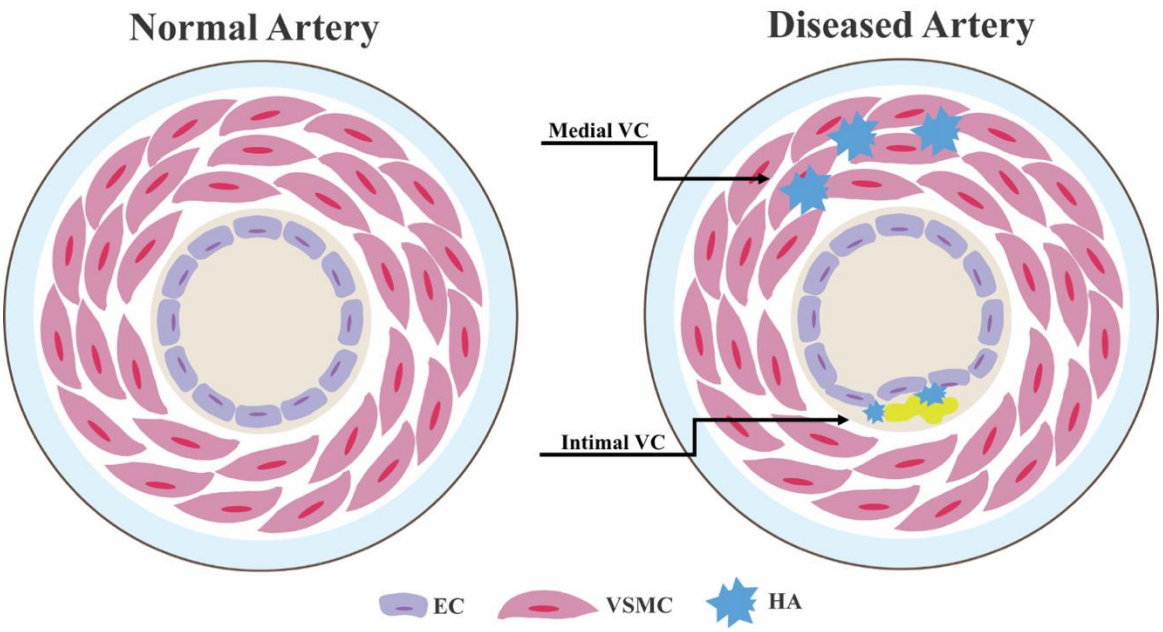

Figure 1. Intimal vs. medial VC. Healthy large elastic arteries are broadly divided into tunica intima, composed of endothelial cells (EC), and tunica media that is rich in vascular smooth muscle cell (VSMC). Pathological deposition of hydroxyapatite (HA) mineral crystals can occur within both layers of the vessel wall. HA mineral deposition in the intimal layer of the vessel wall is associated with atherosclerotic plaques, whereas mineral deposition in the medial layer of the vessel wall almost exclusively occurs in patients with chronic kidney disease. Figure adapted from Kakani *et al*[21].

1.1.1 The link between impaired renal function and cardiovascular death

CKD is a major cause of morbidity and mortality both nationally and internationally[15]. The prevalence of CKD is 13% worldwide, while approximately 15% of individuals suffer from this disease in Canada and USA[32]. A numbers which are likely to increase with increase in aging population. CKD is characterized by the presence of kidney damage or decline of kidney function lasting longer than 3 months, and is classified by a degree of renal impairment, measured by the estimated glomerular filtration rate (eGFR), urinary albumin-to-creatinine ratio and presence or absence of kidney damage[33]. Currently CKD is defined by eGFR of less than 60 mL/min per 1.73 m^2 or urinary albumin-to-creatinine ration of greater than 30 mg/g. CKD can be further classified into 5 stages based on eGFR, as well as recently modified 3 stage classification of albuminuria. The newly adopted classification system emphasizes the prognostic value of these key drivers of CKD[33]. The progressive decline in renal function results in end-stage renal disease (ESRD) which requires renal replacement therapy delivered either in the form of dialysis or renal transplantation[34]. Chronic renal insufficiency is associated with increased risk of all-cause and CVD-associated mortality[35-38].

Patients with CKD present with a multitude of CVD outcomes, including ischemic heart disease, heart failure, arrythmias, and peripheral vascular disease[11]. The evidence from several epidemiological studies conducted in the general population as well as various clinical populations demonstrates a strong relationship between renal insufficiency and the CVD[35-37,39]. The Framingham Heart Study assessed the effect of reduced renal function on CV death in general population. Over a 15 year follow-up period, the study showed that

impaired renal function correlates with an increase in CV events and all-cause mortality in men, while no significant association was observed in women[39]. In a cohort of 1,120,295 adults, Go *et al.*[35] defined an independent inverse association between renal function – assessed by eGFR – and the rate of CV event, death, and hospitalization. Similarly, a meta-analysis including 266,975 patients showed a correlation between renal disfunction, measured by eGFR and albuminuria, and CV mortality[36]. Consistent with these findings, Manjunath *et al.*[37] reported a 5% increase in risk of CV mortality with every 10 mL/min per 1.73m^2 reduction in eGFR. CVD in turn can exacerbate the progression on CKD, as shown by a 29% higher risk of decline in renal function in patients with heart failure[40].

CV mortality is about 15 to 30 times higher in patients with advanced CKD compared to age-adjusted rate of CVD-associated mortality in the general population[41]. Despite the presence of traditional CVD risk factors in patients with CKD, they can only partially explain the strikingly high prevalence of CVD mortality in this patient population. Thus many studies have now delineated the relationship between non-traditional risk factors that are almost exclusively unique to patients with CKD and CV risk. These include, but are not limited to, albuminuria, hyperparathyroidism, as well as mineral and bone disorders[11]. Importantly, both traditional and non-traditional risk factors have an additive effect in patients with CKD, expediating CVD progression.

In addition to low eGFR, renal disease is also defined by the presence of excess albumin in the urine, which is now regarded as an independent marker of CV risk[42]. Microalbuminuria, defined as urinary albumin excretion rate of 30 to 300 mg per 24 hours, is recognized as a predictor of CV mortality in the general population and patients with

DM[41]. In a cohort of 40,548 adults between ages 28 and 75, the Prevention of Renal and Vascular End Stage Disease Study group demonstrated a positive dose-response relationship between urinary albumin concentration and all-cause mortality, as well as CV mortality[43]. In a similar manner, the Heart Outcomes Prevention and Evaluation study reported that microalbuminuria increased the adjusted relative risk of CV events, congestive heart failure, and all-cause mortality in those with and without DM[38]. In a similar population, Zeeuw *et al.*[44] showed that albuminuria was a strong independent predictor of CV risk in patients with diabetic nephropathy. Importantly, recent studies have established that any degree of rise of albuminuria, even within currently defined normal range (< 30 mg per 24 hours), leads to an increase in CV risk[41].

Similar to albuminuria, hyperthyroidism develops in the early stages of renal insufficiency as an adaptive mechanism to maintain calcium homeostasis[11]. Under normal healthy conditions, the parathyroid hormone (PTH) maintains a narrow range of blood calcium by regulating calcium resorption in the cortical bone, its absorption in the intestine, and excretion by the kidney[45]. However, disturbances in calcium and vitamin D metabolism that occur as a result of CKD lead to secondary hyperthyroidism defined by an increase in PTH secretion, synthesis, and parathyroid gland hyperplasia[45]. It is also important to note that abnormalities in phosphate (P) metabolism, observed in patients with progressive CKD, can contribute parathyroid gland dysfunction, while PTH abnormalities also exacerbate hyperphosphatemia[46]. Aberrant PTH regulation is related to atherosclerosis, endothelial dysfunction, inflammation, elevated blood pressure, VC, and increased risk of CV events; conditions that are further heightened in patients with CKD[47].

Mineral and bone disorders are also prevalent in patients with CKD, and occur as a result of persistent mineral and hormonal imbalances described above[48]. Patients with CKD exhibit higher risk of fractures compared to age-adjusted general population[49]. There also exists an inverse relationship between bone mineral density and VC, suggesting that these two processes occur in parallel[50,51]. Pathomorphological studies show presence of structures resembling bone, cartilage, and bone marrow elements in calcified vasculature[23,24,52]. Thus, a combination of pre-existing traditional CV risk factors and non-traditional pathologies that occur as a result of impaired kidney function, lead to increased risk of CV mortality in patients with advanced CKD.

1.1.1 The role of phosphate in the development of vascular calcification

The majority of P in the body is found in the form of organic P, which is essential for cellular structure and function, energy production, glucose synthesis, as well as cellular signaling[53]. In humans, 85% of P is found in bone, 14% is in the intracellular space and 1% is found in the extracellular fluid[54]. The free P found in the extracellular space, mainly in the form of inorganic P (P_i), functions as a buffering system[55]. Similar to extracellular calcium, maintenance of normal serum P_i depends on absorption in the gut, reabsorption and excretion in the kidney, and the flux between blood content and skeletal system[53]. Under healthy conditions, the narrow normal range of extracellular P_i concentration is regulated by complex crosstalk between the bone, intestine, kidney, and parathyroid gland. At the cellular level, PTH, calcitriol and fibroblast growth factor 23 (FGF23) are the main regulators of extracellular P_i content[53]. Dysregulation of this homeostasis has serious health

consequences. Studies show that even a small increase in serum P_i, within or outside of the normal range, correlate with increased CV mortality in patients with CKD and those with normal renal function[56-58].

In humans, an increase in serum P_i triggers a subsequent increase in the secretion of PTH and FGF23 from the parathyroid glad and bone cells respectively[53]. Both PTH and FGF23 inhibit P_i reabsorption in the kidney by decreasing the expression of sodium-dependent phosphate transporters, NaPi-2a and NaPi-2c. Additionally, FGF23 also decreases P_i absorption in the intestine by reducing the expression of NaPi-2b in the gut and suppressing circulating calcitriol levels[53]. There also exists a reciprocal regulatory cascade between FGF23 and PTH, where PTH increases FGF23 expression directly and indirectly via calcitriol, and FGF23 inhibits PTH expression[53]. Thus, an increase in renal P_i excretion and a decrease of intestinal P_i absorption lower the concentration of free P_i in the circulation (Figure 2).

Chronic renal insufficiency combined with abnormalities in bone-mineral turnover and hormonal imbalance lead to a persistent state of hyperphosphatemia and eventually P_i toxicity in patients with CKD[59]. Therefore, hyperphosphatemia is a complication of late stage CKD, and as such is an important predictor of CV mortality in these patients[56]. An increase in serum P_i concentrations, even within normal range, can increase both valvular and vascular calcification in patients with both normal and impaired renal function[58,59]. Consistently, elevated calcium x P_i product is associated with increased medial VC in dialysis patients[56]. Additionally, high P_i *ex vivo* culture of arterial rings from patients with CKD promotes mineral deposition within the arterial tissue[60]. Consistent with these

findings, El-Abbadi *et al.*[61] reported that high P_i loading is significantly associated with VC in uremic mice. Likewise, high P_i levels in VSMC culture leads to an induction of pro-osteogenic phenotype and mineral deposition in these cells[62]. Conversely, lowering serum P_i slows the progression of VC in patients with ESRD[63,64]. Collectively, current knowledge leads to the conclusion that P_i is a clinically important modulator of vascular function and CVD in the general population and patients with renal insufficiency.

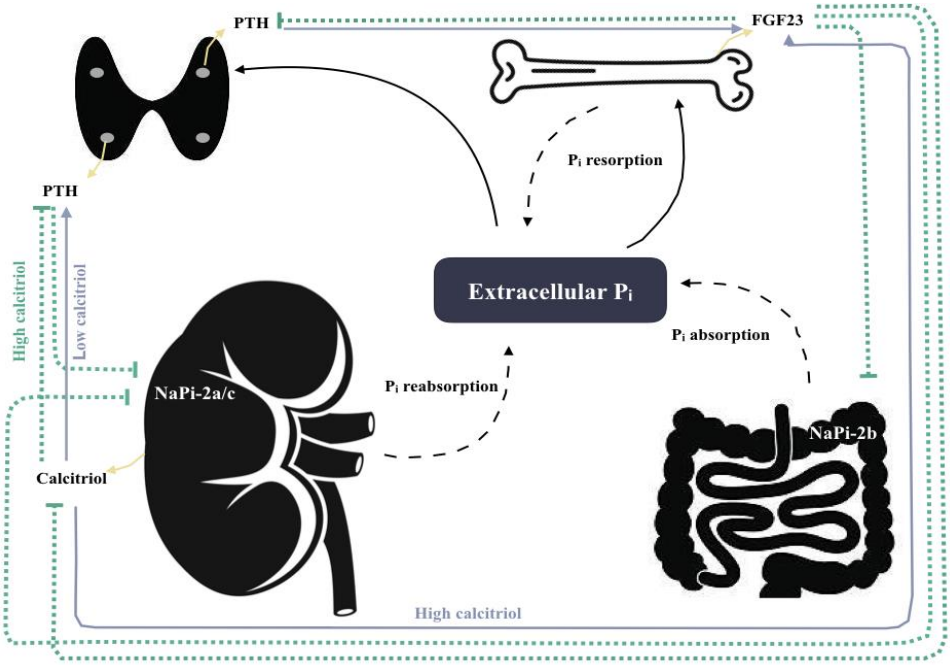

Figure 2. P_i homeostasis. In a healthy individual P_i homeostasis is maintained by the complex crosstalk between the parathyroid gland, bone, intestine, and kidney. An increase in serum P_i occurs as a result of (i) P_i reabsorption in the kidney via NaPi-2a/b cotransporters, (ii) P_i absorption in the intestine via NaPi-2b cotransporter, and (iii) P_i resorption from the bone. An increase in extracellular P_i then triggers secretion of PTH and FGF23 from the parathyroid gland and bone, respectively. PTH and FGF23 both inhibit P_i reabsorption in the kidney by decreasing the expression of NaPi-2a/c P_i cotransporters. Additionally, FGF23 reduces P_i absorption in the gut by decreasing the expression of NaPi-2b P_i cotransporters, as well as suppressing circulating calcitriol. High circulating levels of calcitriol inhibit PTH and stimulate FGF23 secretion, whereas low calcitriol levels stimulate PTH secretion. There also exits a reciprocal relationship between FGF23 and PTH, whereby PTH increases FGF23, and FGF23 inhibits PTH. Figure adapted from Ritter and Slatopolsky[53]

1.2 MOLECULAR MECHANISMS DRIVING MEDIAL VASCULAR CALCIFICATION

Although previously thought of as a passive phenomenon, VC is now recognized as a highly regulated process that shares many similarities with bone formation, and is defined by osteogenic transdifferentiation, matrix maturation, and mineralization stages[12,16]. This multifaceted process is regulated by a number of intra- and extra-cellular stimuli as well as environmental factors[16]. Osteogenic transdifferentiation of vascular cells, mainly VSMCs, is a common feature present in both intimal and medial VC[16]. The plasticity of VSMCs is critical for the phenotypic transition that occurs during osteogenic transdifferentiation, as well as transdifferentiation into other cell types of mesenchymal lineages, such as chondrocytes and adipocytes[65-67]. Osteogenic transdifferentiation of VSMCs is characterized by the loss of contractile phenotype followed by the transition to osteoblast-like phenotype; the process which features an increase in bone markers accompanied by a concurrent decrease in smooth muscle markers[23,24,65]. Similar to osteoblast differentiation of bone cells, increased expression of alkaline phosphatase (ALP) and type I collagen (Col I) is also observed in the VSMCs undergoing the osteogenic switch[23]. There are a number of intra- and extra-cellular regulators of VC, including elevation of oxidative stress, hyperglycemia, dysregulation of mineral metabolism, and initiation of pro-osteogenic program in the VSMC[20]. Additionally, multiple genetic regulator of VC have also been identified[68]. However, broadly speaking, apart from the genetic pre-dispositions, external stimuli affect the two main pathophysiological processes that facilitate the development of VC, namely pro-

osteogenic phenotype transition and apoptosis of the VSMCs (Figure 3)[2,10,12].

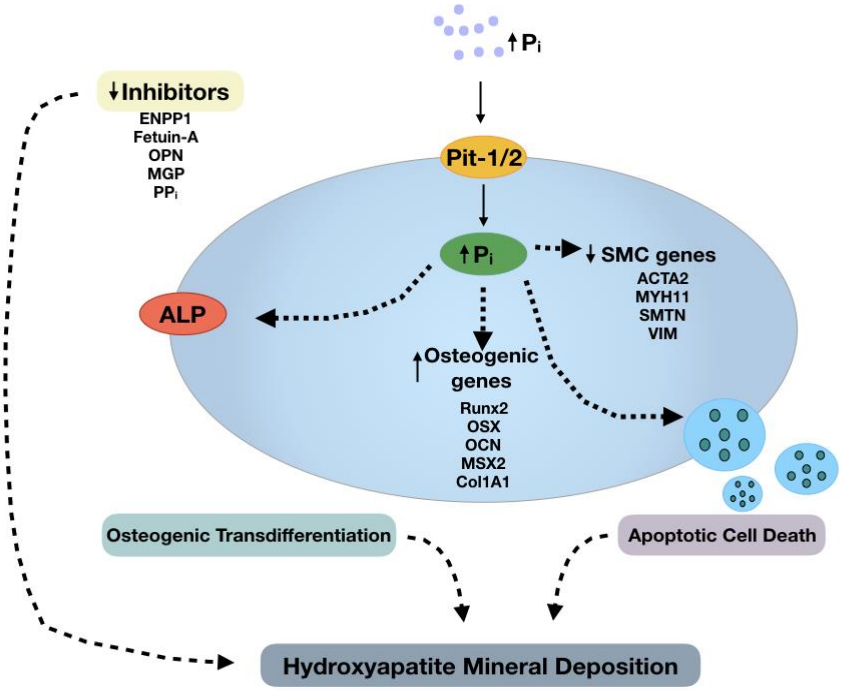

Figure 3. Cellular and systemic drivers of VC. The two major pathophysiological mechanisms that contribute to VC are apoptotic cell death and osteogenic transdifferentiation of VSMCs. Additionally, downregulation of inhibitors of VC, including ENPP1, Fetuin-A, OPN, MGP, PP_i, exacerbates this process. In a setting of CKD, elevated extracellular P_i is one of the major drivers of VC. In VSMCs, P_i transporter is regulated by sodium-dependent Pi transporters, Pit-1 and Pit-2. Elevated intracellular P_i promotes pro-osteogenic phenotype, characterized by decrease in smooth muscle cell-specific genes, including ACTA2, MYH11, SMTN, VIM, and a concurrent increase in pro-osteogenic genes, including Runx2, OSX, OCN, MSX2, Col A1. Additionally, P_i toxicity promotes apoptosis of VSMCs, which further contributes to vascular mineralization. Figure adapted from Li *et al.* and Shanahan *et al*[10,69].

1.2.1 Genetic determinants of vascular calcification

Genetic studies have established that VC of the large contractile arteries is heavily influenced by heritability[70,71]. The Framingham Heart Study concluded that 49% of variability in the abdominal artery calcification can be attributed to genetic variations[70]. In a different study, Peyser *et al.*[71] examined coronary artery calcification (CAC) in 698 adults and also concluded that 41.8% of variation in CAC is attributable to genetic factors. Although arterial calcification of the aorta, coronary, carotid, and peripheral arteries increases with age, DM, CKD, as well as other metabolic disorders, genetic factors play a key role in modulating VC[14,20]. To date many key regulators of VC have been identified through genetic studies in human as well as animal models. These include matrix proteins, circulating calcium-binding proteins, regulators of P_i and pyrophosphate (PP_i) metabolism and many others[68].

Matrix-Gla protein (MGP) is a vitamin K-dependent protein secreted predominantly by chondrocytes and VSMCs[20,68]. MGP acts as a powerful endogenous inhibitor of VC by binding to calcium in order to prevent the accumulation of mineral deposits[68]. In clinical studies, single-nucleotide polymorphisms (SNPs) in the *MGP* gene have been linked to Keutel syndrome and severe arterial calcification[72,73]. In line with these studies, *MGP*$^{-/-}$ mice develop severe ectopic mineral deposition in soft tissues, such as arteries and cartilage[74]. MGP deficient *ApoE*$^{-/-}$ mice develop extensive medial VC when compared to *ApoE*$^{-/-}$[75]. Consistently, inhibition of vitamin K metabolism leads to the production of functionally-deficient MGP and subsequent VC[76]. Likewise, SNPs in the vitamin K epoxide reductase, a protein essential for vitamin K function, are also associated

with aortic calcification[77]. Osteopontin (OPN) is another matrix protein that acts as an inhibitor of VC through adhesion to apatite crystals[68]. OPN level is associated with CAC presence and severity in dialysis patients[78]. Furthermore, exogenous addition of OPN prevents mineral deposition and promotes regression of ectopic calcification[79].

Fetuin-A is a systemic calcification inhibitor, that in a manner similar to MGP and OPN, prevents VC by directly interacting with the mineral particles to prevent HA crystal precipitation[68,80]. Variations in *fetuin-A* allele are associated with reduction in circulating fetuin-A and an increase in circulating P_i in healthy individuals[81]. A decrease in circulating fetuin-A levels is also associated with increased VC in patients with atherosclerosis, DM, and CKD[82-84]. In their study, Lehtinen *et al.*[85] identified four different SNPs in fetuin-A gene that are associated with the extent of CAC in patients with DM. In line with these findings, Fetuin-A knock out (KO) mice develop severe calcification of soft tissues, supporting its key role of powerful circulating inhibitor of VC[86].

The homeostasis between P_i and PP_i is critical for the maintenance of vascular health[12,68]. Genetic and pathophysiological studies identified three key proteins that work in concert to suppress spontaneous arterial calcification by modulating P_i and PP_i homeostasis[68]. Ectonucleotide pyrophosphatase/phosphodiesterase 1 (ENPP1) is an enzyme that hydrolyzes adenosine triphosphate (ATP) into adenosine monophosphate (AMP) and PP_i at the cell membrane, where it is thought to be subsequently transported to the extracellular matrix via the ANK transporter[68,87]. PP_i is a well-known inhibitor of HA formation, and ENPP1 deficiency in humans is associated with severe arterial calcification of infancy, characterized by extensive mineral deposition in the soft tissues[87]. Additionally,

polymorphisms in the ENPP1 gene are associated with significantly higher CAC in patients with ESRD[88]. In support of these findings, the *ENPP1*$^{-/-}$ mice also develop increased arterial mineral deposition[89]. Similarly, mice with mutations in the *ANK* gene exhibit defects in PP_i metabolism and as a result increased VC[90]. The cluster of differentiation 73 (CD73) is also a cell surface enzyme that hydrolyzes the AMP produced by ENPP1 to generate adenosine, which in turn suppresses tissue nonspecific ALP expression, vascular inflammation, and P_i production[68]. In humans, deficiencies in CD73 lead to calcification of joints and arteries[91]. On the other hand the ATP binding cassette subfamily C, member 6 (ABCC6) is a transmembrane ATP and adenosine transporter though to aid in the maintenance of extracellular PP_i/P_i homeostasis[68]. Similar to phenotype observed in ENPP1 and CD73 deficient mice and humans, ABCC6 deficiencies lead to calcification of the soft tissues, such as skin, retina, aorta, and vena-cava[92]. Thus, monogenic mutations in ENPP1, CD73, and ABCC6 are established drivers of molecular changes that subsequently lead to prominent arterial calcification.

Recent association analyses have identified additional diverse mediators of VC in human and mouse studies, including adiponectin, klotho (KL), and carbonicanhydrase-2 (CA2)[93-95]. Adiponectin is a systemic an anti-inflammatory hormone produced by adipocytes. SNPs in the adiponectin gene are associated with increased prevalence of CAC in African American population[93]. In support of these findings, adiponectin-deficient mice develop age-onset aortic calcification[96]. Similar to adiponectin, KL is a circulating protein known to regulate oxidative stress and insulin sensitivity[94]. Although there currently there exists no associations between mutations in the human KL gene and VC, *KL*-deficient mice

develop arterial stiffening, osteoporosis, and ectopic calcification[68,94]. Consistently, KL abundance declines with renal insufficiency[94]. CA2 is an ion transporter crucial for normal bone turnover[68]. In humans, loss of CA2 function leads to cerebral calcificatio[97]. Likewise, mice deficient in *Ca2* develop extensive age-onset medial VC[98].

Additionally, the transforming growth factor-β (TGF-β) superfamily signaling has fundamental roles in embryonic skeletal development and postnatal bone homeostasis, as well as regulation of soft-tissue calcification[99]. SMA-related and MAD-related protein (SMAD) 6 is a negative regulator of the TGF-β signaling and a known inhibitor of VC[100]. Mice deficient in *SMAD6* develop arterial calcification[100]. On the other hand, bone morphogenic protein (BMP) 7 protects against VC and promotes a VSMC-specific phenotype by upregulating the expression of α-smooth muscle actin (α-SMA)[101]. Furthermore, SNPs in BMP7 gene are associated with arterial calcification in patients with DM[102].

1.2.2 Osteogenic transdifferentiation of the VSMCs

Chronic renal insufficiency promotes changes in both systemic and local stimuli that drive the development of VC[14,20,23,28]. Osteogenic transdifferentiation of VSMCs is a highly regulated pathophysiological process that shares many common features with differentiation of bone cells[10,16,20]. In VSMCs, this process is characterized by increased expression of bone-specific markers and concurrent decrease in the expression of VSMC-specific markers[24,65]. Bone-related transcription factors, including Runt-related transcription factor 2 (Runx2), Msh homeobox 2 (MSX2) and osterix (OSX) have been

detected in calcified vessels[60,103,104]. These transcription factors are well-established regulators of osteoblast and chondrocyte differentiation, and are now also recognized as crucial mediators of VC. Among them, Runx2 is regarded as a specific and indispensable regulator of osteogenic differentiation of the VSMCs[12,20].

Various experimental approaches have determined the essential role of Runx2 in the development of VC. Clinical studies and animal models highlight an increase in the expression of Runx2 and its downstream targets osteocalcin (OCN), ALP, and Col I in calcified vessels[23,60,105]. Overexpression of Runx2 in the VSMCs and adipose-derived stem cells is sufficient to induce osteogenic transdifferentiation of these cells[106,107]. In support of these findings, Runx2 expression is necessary for hyperphosphatemia-induced VC in mice[108]. Conversely, VSMC-specific ablation or downregulation of Runx2 expression attenuates VC[109,110]. In addition to its role as a regulator of osteogenic transdifferentiation of the VSMCs, Runx2 expression is also associated with calcification of other vascular cells, including endothelial cells and vascular progenitor cells[20].

A diverse abundance of extracellular stimuli are known to regulate the expression and transcriptional activation of Runx2 leading to subsequent osteogenic transdifferentiation of the VSMCs. In their study, Byon *et al.*[106] show that reactive oxygen species induce osteogenic transdifferentiation of the VSMCs by increasing the expression of Runx2 and its downstream targets ALP, OCN, and Col I. Similarly, hyperglycemia and glucose metabolites increased Runx2 expression and transcriptional activity in vascular cells[111]. Serum from uremic patients with CKD increased Runx2 expression, while simultaneously decreasing the expression of α-SMA in human VSMCs[112]. However, in the

context of advanced CKD, high P_i plays a key role in the pro-osteogenic transdifferentiation of VSMCs[113]. An increase in P_i concentration can also induce Runx2 expression and transcriptional activity, leading to mineralization of the VSMCs as well as *ex vivo* aortic ring cultures[60,65,114].

In VSMCs, P_i transport is mediated by the type III sodium-dependent P_i cotransporters Pit-1 and Pit-2[62]. Pit-1 is the predominant P_i cotransporter found in human VSMCs, and as such is necessary for P_i-mediated mineralization[69]. Pit-1 knock-down inhibits P_i uptake and HA deposition, while Pit-1 overexpression leads to increased P_i-mediated calcification[69]. In their study, Koleganova *et al.*[115] reported that together with other well-established drivers of VC, including Runx2, MSX2 and OCN, Pit-1 expression was also increased in calcified arteries from patient with CKD. Similar to the master-regulator of osteogenic transdifferentiation of the VSMCs, Runx2, Pit-1 expression is also induced by P_i, calcium, and BMP2[114,116,117].

Extensive research has identified multiple cellular signaling pathways that regulate Runx2-mediated osteogenic transdifferentiation of the VSMCs. Activation of the protein kinase B (AKT) signaling pathway by oxidative stress leads to upregulation of Runx2 expression and transcriptional activity, resulting in osteogenic transdifferentiation of the VSMCs[106]. Additionally, activation of the mitogen-activate- protein kinase (MAPK) pathway increases Runx2 phosphorylation resulting in enhanced mineral deposition *in vitro* and *in vivo*[118]. Conversely, downregulation of the p38 MAPK expression in the VSMCs attenuates Runx2 transcriptional activity and osteogenic transdifrentiation[118]. In their study, Fujuta *et al.*[119] show that intracellular P_i content regulates nuclear shuttling of Runx2 in

osteoblast cells. Collectively, the intra- and extra-cellular stimuli that lead to enhanced Runx2 expression via the activation of various cellular pathways are exacerbated in conditions of oxidative stress, hyperglycemia, and dysregulation of mineral metabolism.

Additionally, recent evidence highlights the importance of a reciprocal relationship between peroxisome proliferator-activated receptor γ (PPARγ) and osteogenic pathways[120-122]. PPARγ-deficient mesenchymal stem cells differentiate into osteoblast-like cells, while PPARγ-deficient mice exhibit an increase in bone mass[123,124]. In mesenchymal bone marrow cells, conditions that lead to osteoblast differentiation inhibit adipogenesis, while those promoting adipocyte formation supress osteoblast differentiation[125]. Consistent with these observations, MAPK-mediated phosphorylation of Runx2 and PPARγ is necessary for osteoblast differentiation[120]. VSMC-specific deletion of PPARγ accelerates VC in low density lipoprotein receptor deficient mice[126]. Similarly, P_i-mediated inhibition of PPARγ expression exacerbated CKD-associated VC[127]. Together these findings suggest that a fine balance between, PPARγ and Runx2 is necessary for the maintenance of vascular phenotype.

1.2.3 Apoptotic cell death as a driver of VC

Accumulating evidence suggests that apoptosis of the VSMCs is another key cellular process that mediates VC[10,12]. In their study, Proudfoot *et al.*[128] report that apoptosis precedes mineral deposition *in vivo*. Additionally, apoptotic bodies released by damaged VSMCs are known to contain high mineral content and act as nucleating agents further driving VC[12]. Consistently, increased apoptosis and matrix vesicle release was also

observed in calcifying human VSMCs[129]. Similarly, treatment of *ex vivo* cultured aortic rings from patients with CKD in high P_i-containing calcifying medium lead to an increase apoptotic cell death and subsequent calcification of these vessels[60]. Calcified vessels from pediatric patients undergoing dialysis treatment also exhibit severe apoptosis[130]. Conversely, inhibition of apoptotic cell death attenuates the secretion of mineral-rich matrix vesicles as well as VC[60,128].

Experimental studies in a variety of disease models have identified key modulators of cell death and VC. Endoplasmic reticulum (ER) stress has long been recognized as a critical regulator of vascular health in the context of atherosclerosis[131]. However, emerging evidence has also defined the role of ER stress in the development of VC[132]. Tumor necrosis factor α-mediated activation of C/EBP homologous protein (CHOP) – a known regulator of apoptotic cell death – lead to increased VC in a CKD-dependent model of VC[133]. Consistent with these findings, CHOP deficiency attenuated CKD-dependent apoptotic cell death and VC[134]. Studies also demonstrate an increase in the expression of know modulator of DNA damage response machinery and markers of apoptosis, poly [ADP-ribose] polymerase (PARP) 1 and 2, at the site of VC in human and animal vessels, as well as calcified VSMCs[135,136]. These enzymes are activated in response to calcifying medium, and their inhibition can attenuate mineral deposition in VSMCs[135].

Although under normal healthy conditions, apoptotic cell death and osteogenic differentiation are two distinct physiological processes, in the state of chronic renal insufficiency, changes in systemic stimuli lead to these two processes being tightly intertwined. Activation of ER stress-mediated cell death also results in an increase in ALP

activity, which is a well-established indicator of increased Runx2 activation[133,134]. Similarly, PARP signaling regulates Runx2 protein levels and osteogenic transdifferentiation of the VSMCs[137]. It has also been previously suggested that osteogenic transdifferentiation and apoptosis are both adaptive processes that occur in response to elevated extracellular mineral content. In their study, Shroff *et al.*[130] suggest that VSMC undergo phenotypic switch in order to avoid mineral overload, where those cells that fail to transdifferentiate undergo apoptotic cell death and thus contribute to HA deposition in that manner.

1.3 T-CELL DEATH-ASSOCIATED GENE 51 (TDAG51) AND ITS HUMAN HOMOLOGUE PLECKSTRIN HOMOLOGY-LIKE DOMAIN FAMILY A, MEMBER 1 (PHLDA1)

1.3.1 Protein structure and homology

The pleckstrin homology-like domain (PHLD) class of proteins is composed of two separate families of multifunctional proteins, including PHLDA and PHLDB[138]. Both PHLDA and PHLDB families are highly evolutionary conserved and consists of three structurally-similar proteins, including PHLDA1, PHLDA2, PHLDA3, PHLDB1, PHLDB2 and PHLDB3[138,139]. As their name suggests, all PHLD proteins contain a PHL domain that is 100-120 amino acids (aa) in length and has been demonstrated to bind to phosphatidylinositol lipids[139]. Proteins containing the PHL domain have been found to participate in cellular signaling, vesicular trafficking, and maintenance of cytoskeletal integrity[139,140]. However, to date majority of the studies have focused on the role of

PHLDA, more specifically PHLDA1, in health and disease.

PHLDA1 and its mouse homologue TDAG51 were first identified as a transcription factor necessary for Fas-mediated apoptosis[141,142]. TDAG51 and PHLDA1 share 89% sequence homology, with most variability observed in the N-terminal domain. PHLDA1 gene is located on chromosome 12q21.2 and encodes a protein that is 401 aa in length containing regions rich in polyglutamine (QQ), proline-glutamine (PQ) and proline-histidine (PH) in addition to the PHL domain[138,143]. Full length TDAG51 and PHLDA1 both contain PH and PQ repeats, also known as the *death domain*, which are located in the C-terminus of the protein and are responsible for pro-apoptotic properties of PHLDA1[144]. Similar to the PHL and the PQ domains, the QQ domain is also well-conserved in a variety of eukaryotic cells and is predominantly found in proteins known to regulate transcriptional activation[143]. The evolutionary conserved PHL domain is located in the N-terminal domain of PHLDA1 (Figure 4A)[138,143].

A

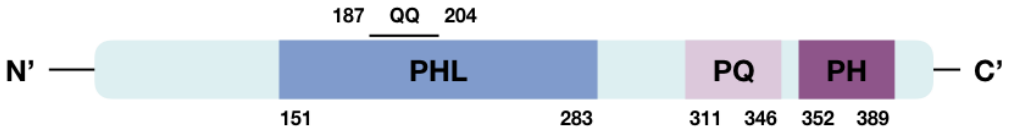

B

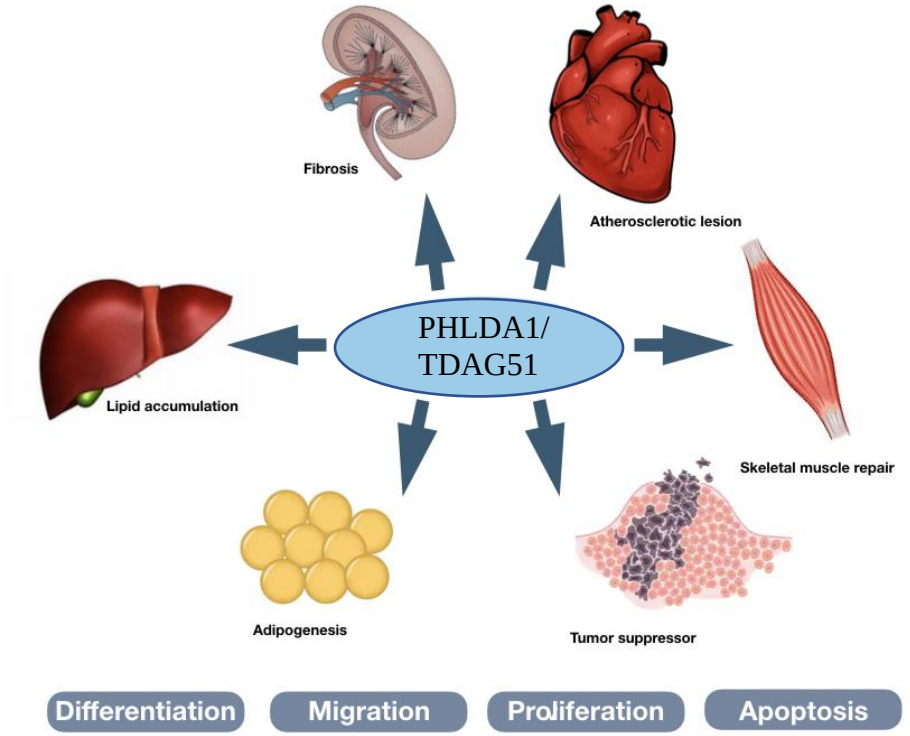

Figure 4. PHLDA1 structure and function . (A) Schematic representation of PHLDA1 protein structure. PHL, plecktrin homology-like domain; PQ, proline-glutamine-rich region; PH, proline-histidine-rich region; QQ, polyglutamine-rich region. (B) The expression of PHLDA1 and its mouse homologue TDAG51 is associated with atherosclerotic plaque formation, skeletal muscle repair, tumorigenesis, adipogenesis, hepatic lipid accumulation, and renal fibrosis. Figure adapted from Nagai *et. al* and Fuselier *et. al*[138,143].

1.3.2 The role of TDAG51/PHLDA1 in health and disease

TDAG51 was first identified as a transcription factor necessary for T-cell receptor-induced Fas-mediated apoptosis[141]. Since then, the expression of TDAG51 and PHLDA1 was found in a variety of tissues, including lung, thymus, liver, VSMCs, and white adipose tissue[114,143,145]. TDAG51 is predominantly found in the cytoplasm, however, it is also present in the perinuclear and nuclear cellular compartments[114,142,143]. Although the exact molecular and biological function of TDAG51 remains to be elucidated, diverse extracellular stimuli induce TDAG51 expression in a variety of cell types. In their study, Kastrati *et al.*[146] demonstrate that PHLDA1 expression is modulated by crosstalk between estrogen receptor and the inflammatory nuclear factor *k*B in breast cancer cells. Similarly, insulin-like growth factor 1 upregulates TDAG51 expression in fibroblast cells[147]. ER stress-inducing agents, such as tunicamycin, thapsigargin, cyclosporin A, homocysteine, peroxinitrate, and farnesol can also induce TDAG51 expression in a variety of cell types[143]. Additionally, elevated P_i content, common in the state of hyperphosphatemia observed in patient with CKD, increases TDAG51 expression[114].

Downregulation PHLDA1 expression is found in a variety of tumors, suggesting that it predominantly functions as a tumor suppressor (Figure 4B)[143]. In melanoma, downregulation of PHLDA1 expression is present in metastatic lesions and its expression is associated with cell growth and apoptosis[142]. Similarly, reduced PHLDA1 expression is also observed in patients with oral carcinoma[148]. In lung and breast carcinomas, PHLDA1 overexpression inhibits cell proliferation, colony formation, and cell migration[149]. Patients with increased PHLDA1 expression in estrogen receptor-negative tumors have a more

favorable outcome, whereas, high PHLDA1 expression is associated with metastatic state in estrogen receptor positive tumors[146,150]. An increase in PHLDA1 expression is also present in osteosarcoma and colorectal carcinoma[150]. Thus, suggesting that PHLDA1 may have a different function depending on cells type and state.

In addition to its tumor suppressor role, PHLDA1 is also important in the regulation of apoptotic cell death[143]. In agreement with its proapoptotic role, antibody-mediated neutralization of PHLDA1 increases while its overexpression decreases cell survival[151]. Hossain *et al.*[152] reported a significant increase in TDAG51 expression in atherosclerotic lesions form *ApoE*$^{-/-}$ mice, which also correlated with apoptotic cells death. Transient overexpression of PHLDA1 results in substantial changes in cellular morphology and adhesion, which promotes detachment-mediate cell death of endothelial cells[152]. Similarly, PHLDA1 overexpression attenuates cell growth, and colony formation while increasing apoptotic cell death in a variety of melanoma cell lines[149]. Furthermore, stress-induced heat-shock proteins inhibit its pro-apoptotic function by direct binding to the PHL domain of PHLDA1 in mouse embryonic fibroblasts[144]. These findings further supporting its role as a robust modulator of apoptosis (Figure 4B).

Although the initial studies have focused on the role of PHLDA1 and TDAG51 as mediators of apoptosis and tumorigenesis, our understanding of TDAG51/PHLDA1-mediated cellular processes have evolved. Findings from our laboratory demonstrate that TDAG51 is an important modulator of adipogenesis and as such, its expression is inversely correlated with mature-onset obesity, hepatic steatosis and insulin resistance[145]. More specifically, TDAG51 expression is downregulated during adipogenesis, while loss of

TDAG51 leads to enhanced lipid accumulation in *TDAG51*$^{-/-}$ primary preadipocytes. In line with these findings, *TDAG51*$^{-/-}$ mice develop increased adiposity, hepatic steatosis, and insulin resistance (Figure 4B). To explain these observations, enhanced expression of key drivers of adipogenesis, PPARy and CCAAT/enhancer binding protein α, was observed[145].

Additionally, TDAG51 mediates epithelial to mesenchymal transition (EMT) in human proximal epithelial cells (Figure 4B). Carlisle *et al.*[153] found that similar to changes observed in endothelial cells, transient TDAG51 overexpression results in changes in cell shape and morphology that exacerbate TGF-β mediated EMT. Consistent with these observations, *TDAG51*$^{-/-}$ mice are resistant to TGF-β induced EMT and peritoneal fibrosis[153]. Findings from our laboratory also identify TDAG51 as a key modulator of P_i-induced VC[114]. Given that TGF-β superfamily is composed of many well-established mediators cellular signaling, tissue fibrosis, VC, and tumorigenesis, processes that are all affected by changes in TDAG51 expression, additional studies are necessary to delineate the potential crosstalk between TDAG51 and the TGF-β superfamily and their role in disease state.

1.4 THE FUNCTION OF TGF-β SUPERFAMILY IN HEALTH AND DISEASE

1.4.1 TGF-β superfamily overview

The TGF-β superfamily is comprised of thirty three multifunctional proteins, including three TGF-β isoforms, activins, inhibins, nodals, anti-mullerian hormone, BMPs, and growth differentiation factors (GDFs)[154]. Although structurally similar, these ligands elicit different responses based on their tissue/cell-specific expression, and unique molecular

interactions with a variety of inhibitory molecules and receptor complexes[154,155]. They all elicit their signaling effect via the serine/threonine transmembrane receptors and SMAD transcription factors[156]. The TGF-β superfamily signaling has fundamental roles in embryonic development, adult tissue homeostasis, and in pathogenesis of variety of diseases, including cancer, fibrosis, and CVD. The TGF-β signaling exerts its control by regulating a multitude of cellular processes, such as cell growth, differentiation, migration, apoptosis, and ECM production[154].

All TGF-β superfamily members are encoded as a large precursor polypeptides comprised of the amino-terminal signal peptide, pro-segment, and carboxy-terminal active polypeptide[154]. The amino-terminal signal peptide is removed during the translocation of the peptide into the lumen of the rough ER[154]. The inactive precursor protein is then cleaved by the furin protein convertase to generate a mature ligand. Although, the majority of the studies delineating the activation mechanism have focused on TGF-β1, all TGF-β superfamily members contain a pro-segment with putative furin cleavage sites (RXXR, RXK, RR)[157]. The mature protein contains seven to nine cysteine residues that modulate inter- and intra-molecular interaction and are conserved in most TGF-β superfamily members[154].

Despite the large number of TGF-β ligands, only a few receptors mediate the transduction of intracellular signaling cascades. The ligands that belong to the TGF-β superfamily elicit their response via the type I and type II serine/threonine kinase transmembrane receptors[154,155]. To date, seven type I receptors have been identified, known as activin receptor-like kinases (ALKs), ALKs1-7. Additionally, five type II receptors have

been identified, including activin receptor type IIA and B, BMP type II receptor, TGF-β type II receptor, and anti-mullerian hormone type II receptor[154]. Different ligands can bind to different combinations of type I and type II receptors, resulting in different responses. Importantly, the abundance of each receptor type varies between tissues, which can explain a multitude of signaling responses mediated by TGF-β superfamily[155,156].

TGF-β and TGF-β-like ligands bind to the constitutively active type II receptor, leading to phosphorylation and activation of type I receptor[154-156]. Upon activation, the type I receptor undergoes a conformational change that allows direct binding and phosphorylation of the appropriate receptor (R-) SMAD[156]. SMADs are the canonical signaling proteins responsible for eliciting the TGF-β response. TGF-β and activins predominantly induce phosphorylation of SMAD2 and SMAD3, whereas BMPs induce phosphorylation of SMAD1, SMAD5, and SMAD8[154,156,158]. Phosphorylation of R-SMADs leads to its subsequent association with common partner SMAD4 and nuclear translocation of the complex, where it can regulate the expression of TGF-β target genes[156]. Additionally, the TGF-β superfamily of proteins are known to elicit their response via several non-SMAD signaling pathways[155].

1.4.2 The role of TGF-β superfamily in vascular function

Genetic analyses in mice and humans have identified TGF-β signaling to be essential for vascular development and homeostasis[159]. Using a variety of knockout models, studies report that inactivation of various components of TGF-β signaling results in either embryonic lethality due to vascular defects or severe abnormalities in the vessel structure

and function[100,160,161]. In humans, dysregulation of TGF-β signaling can lead to a myriad of vascular pathologies, such as arteriovenous malformations, aneurysms, hypertension, atherosclerosis and CVD[159]. In endothelial cells, TGF-β signaling regulates proliferation, migration and vascular permeability. Additionally, TGF-β signaling plays an important role in the regulation of VSMC differentiation and function. The interaction between the endothelial cells and VSMCs maintains healthy vessel tone and function[154]. Consistent with this notion, perturbations in the TGF-β signaling cascade result in impaired blood flow due to hypertension[162]. Similarly, loss of BMP receptor II in endothelial cells and VSMCs leads to dysregulation in pulmonary arterial hypertension in humans and mice[163]. Furthermore, expression of various TGF-β superfamily members is found in advanced atherosclerotic plaques[164,165].

Arterial calcification is regarded as a hallmark of advanced vascular disease[166]. Several studies provide evidence that TGF-β signaling contributes to mineral deposition in both intimal and medial layers of the vessel wall. In particular, BMPs play an important role in osteogenic transdifferentiation of vascular cells which leads to VC[159]. Consistent with these findings, exogenous BMP2 treatment leads to VC in the aortas of high fat diet-fed *LRLR*$^{-/-}$ mice[167]. Furthermore, treatment of VSMCs with BMP2 enhances osteogenic transdifferentiation and VC by increasing P_i uptake and Runx2 expression[117,168,169]. Activation of the BMP2 and BMP4 signaling promotes osteoblast-like phenotypic switch and increases the expression of osteoblast-specific genes, such as ALP, OCN, OSX and MSX2[117,168-171]. In line with these observations, inhibition of BMP2 signaling in *ApoE*$^{-/-}$ mice attenuates arterial calcification[75].

Studies also show that in addition to pro-osteogenic BMPs discussed above, there also exist BMPs that oppose this process. BMP7 promotes a VSMC-specific phenotype by upregulating the expression of α-SMA[101]. Additionally, BMP3 is another negative regulator of osteogenesis, a process similar to VC[16,172]. Mice lacking the *BMP3* gene display increased bone mass, whereas transgenic mice overexpressing *BMP3* develop spontaneous rib fractures due to altered endochondral bone formatio[172,173]. BMP-3b, also known as GDF10, is a divergent member of the TGF-β superfamily that is closely related to BMP3 and signals through TGF-β receptors[174,175]. GDF10 expression correlates with osteoblast differentiation and in a manner similar to BMP3, is able to inhibit this process[176,177]. Furthermore, GDF10 acts as an inhibitor of ALP activity and mineralization in pre-osteoblast cells[178]. Given that VC is a highly regulated process that draws many similarities with osteoblast differentiation, GDF10 may also play a role in maintaining vascular function by regulating osteogenic transdifferentiation of the VSMCs.

1.4.3 The role of TGF-β superfamily in fibrosis and tissue repair

Under normal healthy conditions, TGF-β signaling regulates wound healing by modulating cell proliferation, migration, ECM production, and tissue remodeling. However, chronic tissue injury leads to persistent need for healing, thus resulting in excessive scarring or fibrogenesis, the process in which TGF-β signaling plays a critical role[179]. The balance between activation of TGF-β and BMP pathways through both canonical and non-canonical signaling modulates the fibrotic response in various organ tissues[180]. In their seminal discovery, Roberts *et al.*[181] reported that a subcutaneous injection of TGF-β1 can induce

fibrotic lesion formation at the site of the injection. Consistently, administration of TGF-β adenoviral vector results in fibrotic response in lung and peritoneum[153,182]. In hepatocytes, activation of TGF-β signaling contributes to hepatocyte cell death and lipid accumulation, leading to increased hepatic fibrosis[183]. Activation of the TGF-β signaling cascade in the liver leads to production of Col I, fibronectin as well as other ECM components, subsequently resulting in hepatic fibrosis[180]. In contrast, inhibition of TGF-β signaling attenuates liver fibrosis in mice[184]. Consistent with the crucial role of TGF-β-SMAD pathway in fibrogenesis, *SMAD3* knockout mice are resistant to bleomycin-induced lung fibrosis, and unilateral ureteral obstruction-induced renal fibrosis[185,186].

Several studies demonstrate that other components of the TGF-β signaling cascade are also important in mitigating the fibrotic response. Increase in circulating BMP9 levels are observed in patients with liver fibrosis, while *BMP9* knockout mice develop an increase in perivascular hepatic fibrosis[187,188]. In line with these findings, treatment of primary liver sinusoidal endothelial cells with exogenous BMP9 attenuates the fibrotic response[188]. Similarly, BMP7 treatment inhibits tubulointerstitial fibrosis in a rodent model of renal injury[189]. Consistent with these findings, exogenous BMP7 also ameliorates the expression of profibrotic genes in the aortas of uremic rats[190]. *GDF15* expression is dramatically increased following liver injury, while its overexpression can reduce ischemia reperfusion injury in the heart and improve functional recovery following a traumatic spinal cord injury[191-193]. Additionally, treatment with exogenous GDF10 promotes axonal sprouting and functional recovery after stroke in rodents[194]. In line with its potential role as a modulator of tissue repair, *GDF10*$^{-/-}$ mice develop severe hepatic fibrosis and lipid

accumulation, whereas mice overexpressing GDF10 are protected against diet-induced obesity[195,196]. Additionally, almost a 12-fold decrease in *GDF10* was observed in a model of wound healing[197].

The pro-fibrotic activity of TGF-β is also mediated by several members of the nuclear receptor superfamily, such as vitamin D receptor and PPAR-γ[154]. Vitamin D treatment attenuates TGF-β-induced EMT in a model of subepithelial fibrosis[198]. Additionally, activation of the vitamin D3 receptor by its ligands inhibits TGF-β-mediated hepatic stellate cell activation and fibrosis, while vitamin D receptor knockout mice develop severe hepatic fibrosis[199]. Similarly, PPAR-γ inhibits TGF-β-mediated pro-fibrotic response in hepatic stellate cells[200]. Studies also show that activation of PPAR-γ inhibits TGF-β signal transduction and fibrosis in liver, lung, kidney, and heart[200-203].

1.4.4 GDF10 is a divergent member of the TGF-β superfamily similar to BMP3

GDF10, also known as BMP-3b, is a member of the TGF-β superfamily of growth and differentiation factors, and is closely related to BMP3 in sequence homology[204]. BMP3 and GDF10 share 82% homology in the mature region, while homology in the pro-region is only 37%. The *GDF10* gene encodes a protein of 476 aa with a predicted molecular mass of approximately 52 kDa[174,204]. Similar to other TGF-β family members, GDF10 is synthesized as a large precursor protein containing a hydrophobic signal sequence, carboxyl-terminal domain, and amino-terminal pro-domain[174,178]. The active/secreted form of GDF10 is generated by proteolytic cleavage of the precursor protein at the putative RXXR site. Like BMP3, GDF10 also has two potential cleavage sites, which give rise to

two different sizes of mature protein (Figure 5A)[178,205]. Several studies have characterized the expression of GDF10 in a variety of rodent and human tissues, such as adipose, brain, spleen, uterus and bone[174,176,178,204]. Our group has also characterized murine *GDF10* mRNA expression using *in situ* hybridization analysis. Similar to other reports, we observe *GDF10* mRNA expression in the brain, bone, uterus, aorta as well as lung Additionally, *GDF10* expression was also detected in spleen, parathyroid, and adrenal glands (Chapter 2; Fig. 1B &C, Fig. S2).

Similar to BMP3, GDF10 was originally discovered in bone and thus though to have osteogenic activity[174,204]. *GDF10* expression increases upon BMP2-induced differentiation of rat calvarial osteoblasts. In contrast, TGF-β1 inhibits osteoblast differentiation and *GDF10* expression[176]. Similarly, primate studies show an increase in *GDF10* expression in a model of ectopic bone formation induced by TGF-β2[206]. Although the expression of GDF10 in the bone is relatively high, treatment with recombinant-purified GDF10 does not induce ectopic mineral deposition[174]. Similar to BMP3, GDF10 is a negative regulator of osteogenesis, and as such GDF10 inhibits ALP activity and osteoblast differentiation[172,178]. Additionally, GDF10 is necessary for head formation and acts as an antagonist of BMP2 during embryogenesis[178,205]. Mechanistically GDF10 inhibits osteoblast differentiation by inhibiting BMP-2, -5, -6, and -7-induced expression of Runx2 and OCN via the SMAD 2/3 pathway[177].

Although initial studies have focused on the role of GDF10 in osteogenesis and embryogenesis, our understanding of its function has expanded beyond these roles. Recent studies highlight that GDF10 plays an important role in metabolic regulation. GDF10 is

highly expressed in adipose tissue and its expression is induced by high fat diet (HFD)[207]. Furthermore,GDF10 is secreted from adipocytes and that its expression is higher in preadipocytes than mature adipocytes, suggesting that GDF10 is a regulator of adipogenesis[207]. In support of its role as a regulator of adipogenesis, overexpression of GDF10 inhibits adipocyte differentiation, while its inhibition enhances adipogenesis in 3T3-L1 pre-adipocytes[207]. Consistent with these findings, adipose-specific overexpression of GDF10 in mice reduced adiposity and improved insulin sensitivity in HFD-fed mice through downregulation of PPARγ and its target genes[196]. Likewise, GDF10 knockout mice develop severe HFD-induced obesity and hepatic steatosis that occurs as a result of increased PPARγ expression and activity[195]. Taken together these findings suggest that there exists a fine balance between GDF10 and PPARγ signaling (Figure 5B).

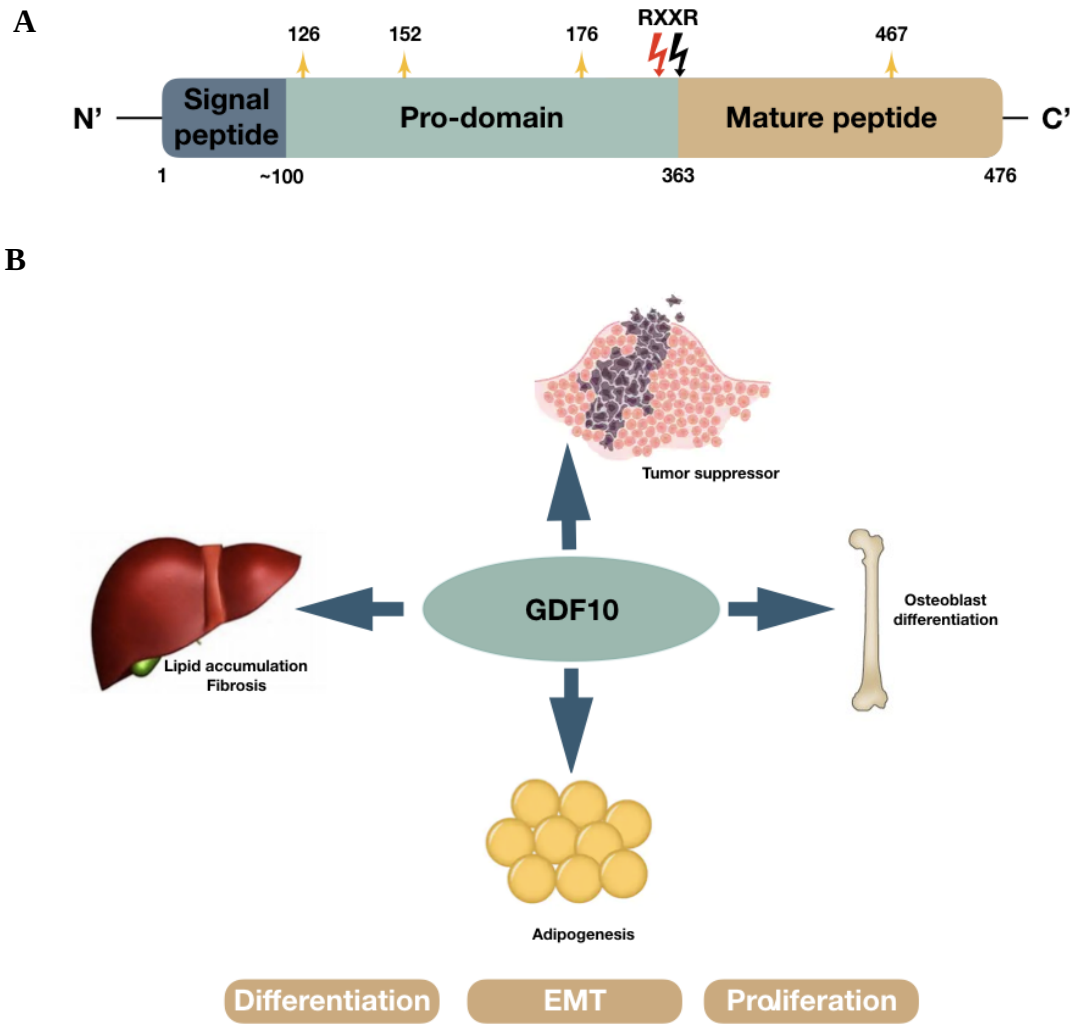

Figure 5. GDF10 structure and function. (A) Schematic representation of GDF10 protein structure. Yellow arrows represent glycosylation sites. Black and red arrow represents an established and a potential alternative cleavage sites, respectively. (B) The expression of GDF10 is associated with tumorigenesis, osteoblast differentiation, hepatic lipid accumulation and fibrosis. Structure of GDF10 protein is based on Hino *et al.* and Takao *et al*[174,178].

1.5 THE FUNCTION OF PPARs IN HEALTH AND DISEASE

1.5.1 PPAR superfamily overview

The PPAR nuclear receptor superfamily is composed of three isoforms, PPARγ, PPARα, and PPARδ, which are all encoded by their respective genes[208]. All PPARs contain the N-terminal transactivating domain, central DNA-binding domain (DBD), and C-terminal ligand-binding domain (LBD)[208]. The DBD is composed of two zinc-finger domains that uniquely bind the PPREs. Additionally, the C-terminal LBD of PPARs is composed of 13 α-helices and 4 β-sheets, which is known to create a large ligand binding pocket. The large ligand binding pocket of PPARs is thought to facilitate the ability of these transcription factors to be activated by a large variety of ligands[208,209]. The DBD and LBD are most conserved between the three receptors[208,209]. Additionally, PPARs also possess two activations domains, AF-1 and AF-2, which are responsible for ligand-independent and -dependent recruitment of coregulatory proteins, respectively[208,210].

Upon ligand-mediated activation, each of the PPAR nuclear receptors binds to its respective peroxisome proliferator response elements (PPARE) as a heterodimer with retinoid X receptor (RXR), which is then followed by coactivator recruitment[211]. Additionally, phosphorylation of PPARs is critical for their function[212]. A large variety of naturally occurring free fatty acids and synthetic compounds serve as ligands, and PPARs possess varying degree of responsiveness dependent on the ligand[213]. Studies have also shown that PPARs are found in a variety of tissues, including adipose, liver, cardiovascular system, immune system, and nervous system, where they have distinct function based on ligand binding[213,214]. The PPARs play a crucial role in cell differentiation, development,

and metabolism. PPARα function has been predominantly characterized in the liver, where it modulates lipid homeostasis by regulating fatty acid transports, β-oxidation, and ketogenesis. In contrast, PPARδ is highly expressed in the muscle where regulates fatty acid metabolism. Additionally, PPARγ is crucial for adipose differentiation. Various studies also highlight the role of PPARs in the regulation of atherosclerotic plaque formation, vascular tone, angiogenesis, and variety of cancers[208,213,214].

1.5.2 The biological function of PPARγ

PPARγ expression is crucial for adipocyte differentiation and healthy function[215]. PPARγ expression is highest in adipose tissues, where it mainly regulates the expression of genes involved in lipid homeostasis, including aP2, PEPCK, acyl-CoA synthase, FATP-1 and CD36[215,216]. Aberrant PPARγ expression is associated with obesity, insulin resistance, and fibrosis[208,216]. Conversely, PPARγ-deficient mice develop reduced adipose tissue stores[217]. Interestingly, PPARγ activation exerts differential effect based on adipose depot. In white adipose tissue, PPARγ is essential for insulin sensitivity, lipogenesis, and adipocyte function. On the other hand, PPARγ activation in brown adipose tissue regulates thermogenesis and mitochondrial biogenesis[218]. Overexpression of PPARγ in fibroblast cells leads to a pro-adipogenic program in these cells[218]. Thus, PPARγ is both necessary and sufficient to induce adipogenesis.

Although under normal healthy conditions PPARγ is most abundantly expressed in adipose tissue, its hepatic expression is robustly induced in conditions of hepatic lipid accumulation[218,219]. In the liver, pro-steatotic effect of PPARγ is due to upregulation of

genes involved in lipogenesis, triglyceride synthesis, and lipid droplet formation. In conditions of metabolic stress, elevated dietary free fatty acids modulate PPARγ activity[216,218]. Conversely, hepatocytes and mice that do not express PPARγ in the liver are resistant to HFD-induced hepatic lipid accumulation, but this exacerbates insulin resistance[220]. Similarly, inhibition of PPARγ or RXR using pharmacological agents also ameliorates hepatic steatosis[221]. Taken together, these studies demonstrate that PPARγ plays an important role in regulating hepatic lipid metabolism in conditions of metabolic stress.

Our understanding of PPARγ function has now extended beyond its role in lipid metabolism. PPARγ activation in endothelial cells inhibits inflammation and the expression cellular adhesion molecules[214]. Endothelial cell migration and apoptosis are also regulated in PPARγ-dependent manner. In VSMCs PPARγ expression is upregulated in hypertensive conditions and upon injury. Similar to its role in endothelial cells, PPARγ also regulates VSMCs migration, proliferation and apoptosis[214]. Furthermore, recent studies have demonstrated that activation of PPARγ inhibited VC by inhibiting Wnt5a signaling in VSMCs[126]. PPARγ-mediated upregulation of Klotho also inhibited VC[222]. In their study, Liu *et al.*[127] reported that high P_i conditions, downregulated PPARγ expression which contributed to increased CKD-associated VC. In line with these findings, PPARγ inhibits pro-osteoblastic phenotype by directly biding to Runx2 and preventing its association with the osteoblast-specific element-2 promoter[223]. Similarly, overexpression of PPARγ co-factor, peroxisome proliferator-activated receptor-γ coactivator-1α, attenuates mineral deposition in adenine-induced model of VC[224]. Thus in addition to its established role in

adipogenesis and tissue fibrogenesis, PPARγ is also a modulator of vascular health.

1.6 PROJECT RATIONALE, HYPOTHESIS, OBJECTIVES, AND THESIS OUTLINE

1.6.1 Project rationale and hypothesis

The overall objective of this thesis is to (i) determine the role of TDAG51 and GDF10 in VC, and (ii) identify the mechanism(s) by which these proteins regulate mineral deposition in the VSMCs. Additionally, observations during these studies brough to light the importance of GDF10 as a regulator of metabolic homeostasis. Thus the focus of the final chapter of this thesis is on the mechanism by which GDF10 regulates hepatic lipid metabolism.

Medial VC is the predominant pathophysiological mechanism contributing to vascular dysfunction and poor prognosis in patients with CKD[17,21,52]. In support of these findings, VC in patients with CKD has been linked to disturbances in P_i homeostasis, and is now recognized as the major risk factor for CVD in these patients[35]. TDAG51 is most frequently characterized as a pro-apoptotic gene involved in both intrinsic and extrinsic mechanisms of apoptosis; however, this relationship is variable across different tissues and species[143]. We and others have reported that TDAG51 contributes to vascular disease in the setting of atherosclerosis, and is induced by a variety of stimuli. In addition to a reduction in atherogenesis, however, a significant reduction in intimal calcification within advanced atherosclerotic lesions in mice with global deletion of TDAG51 was also observed[152]. Given that in clinical studies medial and intimal calcification are frequently present at the

same time, I hypothesize that TDAG51 also acts as a modulator of CKD-associated medial VC.

A micro-array analysis identified GDF10 to be significantly upregulated in *TDAG51*$^{-/-}$ VSMCs. Although it's role in VC is unknown, a recent study has demonstrated that GDF10 inhibits osteoblast differentiation, a process that draws many parallels with VC[176,177]. In support of these findings, GDF10 overexpression inhibits ALP activity in mouse calvarial pre-osteoblast cells[178]. Additionally, GDF10 acts as a antagonist of BMP2, a well-established driver of osteogenesis, during embryogenesis[205]. Given these data, I hypothesize that GDF10 is a novel systemic inhibitor of VC.

During my studies I also observed that *GDF10*$^{-/-}$ mice develop increased body weight, adiposity, and hepatic lipid accumulation when fed normal control diet. Consistent with these findings, mice overexpressing GDF10 are protected against HFD-induced obesity[196]. In their studies, Hino *et al.*[196] reported that GDF10 regulates adipogenesis and free fatty acid β-oxidation in adipose tissue. Despite the established role of the adipose-secreted adipokine GDF10 in modulating adipogenesis, its role in hepatic steatosis remains to be explored. Given that the preliminary findings showed increased adiposity and severe hepatic lipid accumulation in *GDF10*$^{-/-}$ mice, I hypothesize that GDF10 plays a pivotal role in the regulation of hepatic lipid metabolism.

In summary, the hypothesis of this PhD thesis consists of several parts: medial VC is mediated by (i) TDAG51 and (ii) systemic adipokine GDF10. (iii) GDF10 also acts as an inhibitor of non-alcoholic fatty liver disease (NAFLD) progression. Given that in clinical

studies there exists a correlation between NAFLD and VC, GDF10 may also regulate VC indirectly by modulating other metabolic parameters.

1.6.2 Objectives and experimental approach

To assess my hypothesis, studies focused on examining the following objectives.

1. Examine the mechanism(s) by which TDAG51 regulates hyperphosphatemia-associated VC.
2. Determine whether GDF10 acts as an inhibitor of VC and the mechanism(s) involved in its regulatory action.
3. Define mechanism(s) by which GDF10 regulates hepatic lipid metabolism.

In order to examine the objectives of this thesis, *in vitro*, *in vivo*, and *ex vivo* approaches were used.

For experiments examining VC, primary mouse and human VSMCs were used. Primary mouse VSMCs were derived using the explant method, while human VSMCs were purchased from a commercially available source[225]. Although biologically relevant, these cells have a finite lifespan, and thus were only used up to passage 8. When appropriate and permitting, the results were also corroborated in mouse *ex vivo* aortic rings and *in vivo* models of VC. Additionally, experiments examining the mechanisms by which GDF10 regulates hepatic lipid homeostasis utilized Huh7 and HepG2 immortalized human hepatocyte cell lines, as well as primary human hepatocytes that were acquired from commercial source. The results of *in vitro* studies were also confirmed using *in vivo* models

of HFD-induced hepatic lipid accumulation.

Male *TDAG51*$^{-/-}$ and *TDAG51*$^{+/+}$ littermate control mice were used to examine VC in a model of hyperphosphatemia-associated vitamin D3-induced model of VC. Similarly, *in vivo* studies examining the role of GDF10 in VC utilized male *GDF10*$^{-/-}$ and *GDF10*$^{+/+}$ littermate control mice in a similar setting. For studies examining the role of GDF10 in hepatic lipid accumulation, male *GDF10* knockout (KO) and wild-type (C67Bl/6J) mice were used. Widely-used HFD model of hepatic lipid accumulation was utilized for these experiments. All animals were bred in-house or purchased from Jackson Laboratories. Experimental procedures were performed with accordance to McMaster University Animal Research Ethics Board guidelines.

Tissue samples collected from the experiments described above were analyzed using a combination of laboratory techniques, including but not limited to, quantitative real-time polymerase chain reaction, western blotting, immunohistochemistry, immunofluorescent staining, morphological staining (H&E, Masson's Trichrome), mineral staining (Von Kossa, Alizarin Red), ELISAs, as well as variety of functional assays.

1.6.3 Thesis outline

The thesis objectives and experimental results are summarized in three manuscripts (*Chapter 2-4*) that are presented as follows:

Chapter 2: TDAG51 (T-cell death-associated gene 51) is a key modulator of vascular calcification and osteogenic transdifferentiation of arterial smooth muscle cells.

This journal article, published in *Atherosclerosis, Thrombosis, and Vascular Biology* (2020), was accepted for publication on May 4, 2020. According to the AHA/ASA journal policies, the authors retain the right to include full journal article for print thesis at this time and electronic thesis 12 months after the article publication, provided that the journal is cited as the original source. Therefore the published article and relevant supplemental materials are included as *Chapter 2*.This journal article demonstrated that TDAG51 mediates VC by regulating RUNX2 transcriptional activity and Pit-1 expression. To this end, *TDAG51*$^{-/-}$ mice were protected from hyperphosphatemia-associated VC.

Chapter 3: GDF10 is a negative regulator of vascular calcification of vascular smooth muscle cells.

This journal article currently being prepared for submission to *Journal of Biological Chemistry*. Findings outlined in the manuscript identified GDF10 as a novel mediator of mineral deposition in the VSMCs, and as such a potential novel therapeutic avenue for diagnosis and management of this disease.

Chapter 4:GDF10 blocks hepatic PPARγ activity to protect against diet-induced liver injury.

This journal article, published in *Molecular Metabolism* (2019), was accepted for publication on June 24, 2019. According to the Elsevier publishing group guidelines, the authors retain the right to include full journal article as a part of thesis dissertation, provided that (i) it is not published commercially, and (ii) the journal is sited as the original source.

Therefore the published article and relevant supplemental materials are included as *chapter 4*. This journal article demonstrated that GDF10 knock out mice develop severe diet-induced obesity, hepatic steatosis, and hepatic fibrosis. To explain these observations, heightened PPARγ expression and activity was observed in these mice. Additionally, GDF10 attenuated lipid accumulation and PPARγ activity in cultured hepatocytes.

CHAPTER 2: MANUSCRIPT 1

TDAG51 (T-cell death-associated gene 51) is a key modulator of vascular calcification and osteogenic transdifferentiation of arterial smooth muscle cells.

Khrystyna Platko, Paul F. Lebeau, Gabriel Gyulay, Šárka Lhoták, Melissa E. MacDonald, Giusepina Pacher, Jae Hyun Byun, Felix J. Boivin, Suleiman A. Igdoura, Jean-Claude Cutz, Joan C. Krepinsky, Richard C. Austin

Atherosclerosis, Thrombosis, and Vascular Biology (2020). 40(7):1664-1679. doi: 10.1161/ATVBAHA.119.313779.

© *Copyright by American Heart Association*

Chapter link: *TDAG51 regulates osteogenic transdifferentiation and subsequent VC of the VSMCs*. Previous studies demonstrate that TDAG51contributes to vascular disease in the setting of atherosclerosis[226]. In addition to reduction in atherogenesis, a significant reduction in intimal calcification was observed in the *TDAG51*$^{-/-}$ mice[152]. Although morphologically distinct, there are many similarities between the pathogenesis of intimal and medial VC, and both are frequently present in patients with advanced CKD[20]. However, medial VC, which mainly occurs as a result of changes in blood biochemistry, almost exclusively a feature of CKD-associated vascular impairment[58]. This journal article demonstrated that TDAG51 modulates osteogenic transdifferentiation and subsequent VC by regulating (i) transcriptional activity of master-regulator of pro-osteogenic switch in VSMCs, Runx2, and (ii) cellular P_i homeostasis via the regulation the expression of sodium-dependent phosphate transporter, Pit-1.

Author's contribution: K. Platko, R. C. Austin, and J.C. Krepinsky designed the study. K. Platko performed cell culture experiments, western blotting, immunofluorescence staining and related analysis with help of P.F. Lebeau, G. Gyulay, G. Pacher and J. Hyun Byun. F. J. Boivin performed PHLDA1 *in situ* hybridazation analysis. Human temporal arteries were provided by JC. Cutz. Animal experiments were conducted by K. Platko with help of M. E. MacDonald. K. Platko curated the data and wrote the manuscript. P. F. Lebeau helped revise the manuscript. K. Platko, R.C. Austin, J.C. Krepinsky, S.A. Igdoura, A.J. Ingram and D. Bridgewater reviewed and edited the manuscript. All authors approved the final submission.

Arteriosclerosis, Thrombosis, and Vascular Biology

BASIC SCIENCES

TDAG51 (T-Cell Death-Associated Gene 51) Is a Key Modulator of Vascular Calcification and Osteogenic Transdifferentiation of Arterial Smooth Muscle Cells

Khrystyna Platko, Paul F. Lebeau, Gabriel Gyulay, Šárka Lhoták, Melissa E. MacDonald, Giusepina Pacher, Jae Hyun Byun, Felix J. Boivin, Suleiman A. Igdoura, Jean-Claude Cutz, Darren Bridgewater, Alistair J. Ingram, Joan C. Krepinsky,* Richard C. Austin*

OBJECTIVE: Cardiovascular disease is the primary cause of mortality in patients with chronic kidney disease. Vascular calcification (VC) in the medial layer of the vessel wall is a unique and prominent feature in patients with advanced chronic kidney disease and is now recognized as an important predictor and independent risk factor for cardiovascular and all-cause mortality in these patients. VC in chronic kidney disease is triggered by the transformation of vascular smooth muscle cells (VSMCs) into osteoblasts as a consequence of elevated circulating inorganic phosphate (P_i) levels, due to poor kidney function. The objective of our study was to investigate the role of TDAG51 (T-cell death-associated gene 51) in the development of medial VC.

METHODS AND RESULTS: Using primary mouse and human VSMCs, we found that TDAG51 is induced in VSMCs by P_i and is expressed in the medial layer of calcified human vessels. Furthermore, the transcriptional activity of RUNX2 (Runt-related transcription factor 2), a well-established driver of P_i-mediated VC, is reduced in TDAG51$^{-/-}$ VSMCs. To explain these observations, we identified that TDAG51$^{-/-}$ VSMCs express reduced levels of the type III sodium-dependent P_i transporter, Pit-1, a solute transporter, a solute transporter, a solute transporter responsible for cellular P_i uptake. Significantly, in response to hyperphosphatemia induced by vitamin D_3, medial VC was attenuated in TDAG51$^{-/-}$ mice.

CONCLUSIONS: Our studies highlight TDAG51 as an important mediator of P_i-induced VC in VSMCs through the downregulation of Pit-1. As such, TDAG51 may represent a therapeutic target for the prevention of VC and cardiovascular disease in patients with chronic kidney disease.

VISUAL OVERVIEW: An online visual overview is available for this article.

Key Words: hyperphosphatemia ■ inorganic phosphate transporter ■ osteoblasts ■ risk factor ■ vascular calcification ■ vascular smooth muscle cells

Downloaded from http://ahajournals.org by on July 22, 2020

Cardiovascular disease (CVD) is the primary cause of mortality in patients with chronic kidney disease (CKD) as a result of vascular calcification (VC), a process known to reduce vascular compliance resulting in chronically elevated blood pressure.[1,2] Although VC of the intimal layer of the vessel wall is a common feature of atherosclerotic CVD, kidney-induced changes in blood biochemistry drive calcification of the vascular smooth muscle cell (VSMC)-enriched medial layer of the vessel wall. For this reason, patients with end-stage renal disease (ESRD) commonly exhibit an additive risk of CVD due to the presence of both forms of VC. Furthermore, calcification of the medial layer of the vessel wall is regarded as an established risk factor for sudden cardiac death in patients with CKD[3–5] and contributes to myocardial infarction, aortic valve stenosis, and limb

Correspondence to: Richard C. Austin, 50 Charlton Ave E, Room T-3313, Hamilton, Ontario, L8N 4A6, Canada. Email austinr@taari.ca
*These authors contributed equally to this article.
The Data Supplement is available with this article at https://www.ahajournals.org/doi/suppl/10.1161/ATVBAHA.119.313779.
For Sources of Funding and Disclosures, see page 1677.
© 2020 American Heart Association, Inc.
Arterioscler Thromb Vasc Biol is available at www.ahajournals.org/journal/atvb

Nonstandard Abbreviations and Acronyms

α-SMA	alpha smooth muscle actin
ALP	alkaline phosphatase
CKD	chronic kidney disease
CVD	cardiovascular disease
ESRD	end-stage renal disease
EV	empty vector
MSX2	Msh homeobox 2
OCN	osteocalcin
OPG	osteoprotegerin
OPN	osteopontin
OSE2	osteoblast-specific cis-acting element 2
OSX	osterix
PHLDA1	pleckstrin homology-like domain, family A, member 1
Pi	inorganic phosphate
Pit-1/2	type III sodium-dependent Pi transporter
PPARγ	peroxisome proliferator-activated receptor;
RUNX2	Runt-related transcription factor 2
TDAG51	T-cell death-associated gene 51
VC	vascular calcification
VD3	vitamin D3
VSMC	vascular smooth muscle cell
WTCCC	Welcome Trust Case Control Consortium

Highlights

- Vascular calcification resulting from elevated serum P_i content is an important predictor of cardiovascular mortality in patients with chronic kidney disease.
- Osteogenic transdifferentiation and apoptotic cell death are thought to be major contributors to mineral deposition within vessel wall.
- In this study, we identify TDAG51 (T-cell death-associated gene 51) as an important mediator of vascular calcification.
- We demonstrate TDAG51$^{-/-}$ vascular smooth muscle cells exhibit reduced RUNX2 (Runt-related transcription factor 2) transcriptional activity and Pit-1 expression.
- TDAG51$^{-/-}$ mice are protected from vitamin D3-mediated vascular calcification.

amputation in these patients.[6,7] Despite its clinical importance, understanding the cellular factors and molecular mechanisms modulating VC and the effective targeting of this process is a major unmet clinical need, since no reliable therapies currently exist.[8]

Although several pathophysiological processes are thought to contribute to the development of medial VC, inorganic phosphate (P_i)–mediated apoptotic cell death and the transdifferentiation of VSMCs into osteoblast-like cells are established causative factors.[9] Hydroxyapatite (HA) is the most abundant mineral within calcified regions of the artery, and its deposition has been shown to be essential for the osteogenic transdifferentiation of VSMC.[10] Currently, the osteogenic transdifferentiation process is incompletely understood. What is known, however, is that mineral abnormalities such as hyperphosphatemia play a key role by inducing the expression of procalcific bone matrix proteins in VSMCs as well as causing apoptotic cell death of VSMCs.[3,11] Elevated levels of P_i in the serum, due to a lack of excretion in patients with CKD, initiates this osteogenic switch. The state of hyperphosphatemia also increases intracellular P_i levels via active transport through type III sodium-dependent P_i transporters, Pit-1 and Pit-2, at the cell surface.[12,13] Pit-1, in particular, plays a major role in VC, with its downregulation preventing and overexpression promoting the pro-osteogenic phenotype.[12] Furthermore, higher expression of Pit-1 is observed in the calcified aortas of patients with CKD.[14]

RUNX2 (Runt-related transcription factor 2) is a key transcription factor necessary for osteoblast transdifferentiation and is involved in the transcriptional regulation of several genes, including bone matrix proteins like osteocalcin (OCN) and collagen I.[15] In both clinical studies and animal models, elevated RUNX2 expression is observed in calcified aortas.[14] Elevated intracellular P_i increases the expression of RUNX2 and its downstream target, OCN, in human aortic VSMCs.[16,17] Overexpression of RUNX2 in VSMCs and adipose-derived stem cells is sufficient to induce the expression of pro-osteogenic genes and leads to a phenotypic switch.[18–20] Although global RUNX2 knockout mice die shortly after birth, due to a complete absence of bone development as a result of impaired osteoblast maturation,[21] VSMC-specific deletion of RUNX2 protects against high-fat diet-induced VC.[22] Furthermore, RUNX2 expression in the VSMCs is required for vitamin D_3 (VD_3)-mediated VC, which is also driven largely by hyperphosphatemia.[23] Beyond the strong influence of RUNX2, functional disturbances in, or attenuation of, endogenous calcification inhibitors such as pyrophosphate, fetuin-A, maGLAP (matrix Gla protein), OPN (osteopontin), and OPG (osteoprotegerin) also represent an established avenue leading to VC in the setting of ESRD.[11] Overall, the plasticity of VSMCs is a critical characteristic for the phenotypic switch during the pathogenesis of VC.

TDAG51 (T-cell death-associated gene 51) and its human homologue PHLDA1 (pleckstrin homology-like domain, family A, member 1) are members of the pleckstrin homology-related domain gene family that have been traditionally regarded as tumor suppressor genes with the ability to cause apoptotic cell death in a variety

Downloaded from http://ahajournals.org by on July 22, 2020

of mammalian cells.[24–27] We[28–31] as well as others[32] have reported that TDAG51 contributes to vascular disease in the setting of atherosclerosis and that TDAG51 expression is induced by endoplasmic reticulum stress. The WTCCC (Welcome Trust Case Control Consortium) study showed that 5 single-nucleotide polymorphisms in the region that include the PHLDA1 gene are associated with CVD, while our findings highlight an association between 2 single-nucleotide polymorphisms and CVD using combined analysis of results from the WTCCC and the University of California, San Francisco case-control study.[31,33,34] In addition to a reduction in atherogenesis, a marked attenuation of intimal calcification within advanced atherosclerotic lesions was also observed in TDAG51$^{-/-}$ mice.[31] However, a specific role for TDAG51 in medial VC was not investigated.

Here, we report that TDAG51 is induced in VSMCs by P_i and is expressed in the medial layer of calcified human vessels. Although no direct interaction between TDAG51 and RUNX2 was detected, the transcriptional activity of RUNX2 was reduced in TDAG51$^{-/-}$ VSMCs and this was associated with reduced HA crystal formation. Furthermore, we identified that TDAG51$^{-/-}$ VSMCs express reduced levels of Pit-1. In contrast, overexpression of Pit-1 restored P_i uptake, RUNX2 activation and mineral deposition in the TDAG51$^{-/-}$ VSMCs. Our findings also show that siRNA-mediated RUNX2 knockdown reduced Pit-1 expression. In support of these in vitro findings, TDAG51 deletion protected against rapid mineral deposition induced by VD_3 administration in a mouse model of hyperphosphatemic medial VC. Collectively, these findings suggest that TDAG51 represents a novel driver of medial VC in the context of mineral imbalance—a condition commonly observed in patients with CKD.

METHODS

The authors declare that all supporting data are available within the article and in the Data Supplement.

Animal Handling and Procedures

TDAG51$^{-/-}$ mice were generated previously[35] and backcrossed onto a C57BL/6J (TDAG51$^{+/+}$) background for at least 9 generations (Tables I and II in the Data Supplement) as characterized by our group.[31,36] Mice were housed in a 12-hour light-dark cycle with access to a standard laboratory diet (2918, Envigo) and water ad libitum. At 6 to 10 weeks of age, male TDAG51$^{-/-}$ mice and age-matched TDAG51$^{+/+}$ littermate controls were euthanized under anesthesia and perfused with PBS, after which the thoracic and abdominal aortas were excised for experimentation. For studies examining VC, 8-week-old male TDAG51$^{+/+}$ and TDAG51$^{-/-}$ mice were randomly allocated into groups treated with VD_3 or a vehicle control (n=9–13 per group). Male mice were used in our study because estrogen has been demonstrated to affect mineral absorption via the PTH-VD_3 axis.[37] Mice were subcutaneously injected with 5.55×10^5 IU/kg per day of active VD_3 (Sigma-Aldrich) for 3 consecutive days[38,39] and were euthanized 7 days post-treatment. All animal procedures were approved by the McMaster University Animal Research Ethics Board.

VSMC and Aortic Ring Isolation and Treatment

TDAG51$^{+/+}$ and TDAG51$^{-/-}$ VSMCs were isolated from the aortas of 6- to 10-week-old male mice by the explant method[40] and cultured in DMEM (Gibco) supplemented with 10% v/v fetal bovine serum (Sigma-Aldrich), 100 IU/mL penicillin and 100 µg/mL streptomycin (Gibco). Human aortic VSMCs were purchased from Lonza (CC-2571, isolated from an 18-year-old healthy male donor) and cultured in SmGM-2 BulletKit medium (Lonza). All VSMCs were maintained in 5% CO_2 at 37°C. Cells were plated at a confluence of 50% to 70% and used at passage 4 to 6. Similarly, aortic rings were isolated for ex vivo studies. Briefly, thoracic aortas were removed, washed in PBS-anti/anti solution (Gibco) 6× while the adventitia and adipose layers were removed. Clean aortas were cut into 5 to 10 mm segments and cultured in suspension. To induce osteogenic differentiation of the VSMCs and ex vivo aortic rings, medium was supplemented with additional P_i to achieve a concentration of 2.6 mmol/L[41]; a clinically relevant concentration commonly observed in the plasma of patients with ESRD.[42]

Quantification of Ca^{2+} and P_i Content

After decalcification of cells or tissue with 0.6 N HCl for 48 to 72 hours, Ca^{2+}deposition in arteries or VSMCs was quantified using a colorimetric calcium kit via the o-cresolphthalein method (Sigma-Aldrich).[43] Data were normalized to cellular protein content or the dry weight of aortic tissue. For experiments examining intracellular P_i content, cells were lysed using the freeze-thaw method followed by scraping of the cells and sonication of the cell lysate suspension. P_i content in the suspension was quantified using a colorimetric phosphate kit (Sigma-Aldrich) according to the manufacturer's instructions and normalized to protein content.

OsteoImage HA Crystal Quantification Assay

HA levels were quantified using the OsteoImage fluorescent assay kit (Lonza) according to the manufacturer's instructions. Briefly, cells were plated in a black clear-bottom 96-well plate and cultured in calcification-inducing medium for 5 to 6 days. Cells were subsequently washed, fixed with 4% w/v paraformaldehyde, and stained with the fluorescent reagent for 30 minutes. HA levels were quantitatively assessed using a fluorescent microplate reader (Molecular Devices) at 492/520 nm wavelengths. Mineral deposition was normalized to either total cell number or protein content. Cells were also visualized using a fluorescent microscope (EVOS-FL, ThermoFisher Scientific).

Von Kossa and Alizarin Red S Calcium Staining

Von Kossa staining was performed on sections that were adjacent to the sections used for human temporal artery fluorescent in situ hybridization analysis. Staining was performed by the St. Joseph's Healthcare Pathology department using bone sections as positive controls. Briefly, 5 µm sections

Downloaded from http://ahajournals.org by on July 22, 2020

were deparaffinized, rinsed in distilled water, and incubated in a 1% w/v silver nitrate (Sigma-Aldrich) solution under UV light. Slides were then incubated in 5% w/v sodium thiosulfate (Sigma-Aldrich) solution for 5 minutes. Slides were subsequently counterstained with Nuclear Fast Red (Sigma-Aldrich), followed by dehydration and mounting. Calcium deposition was visualized by black and brown staining.[44] Alizarin Red S was used to visualize calcium deposition in mouse tissue sections. Following deparaffinization, sections were stained with 2% w/v Alizarin Red (Sigma-Aldrich) solution at a pH of 4.2 for 2 minutes, dehydrated, and mounted in synthetic mounting medium. Calcium deposition was visualized via orange-red staining.[45] All staining was imaged using a Nikon Eclipse Ci (DS-Ri2) light microscope.

Small Interfering RNA Transfection

To block PHLDA1 expression, targeting siRNA was purchased from Dharmacon (M-012389-01-0005); nontargeting siRNA (D-001210-01-05) was used as a control. Similarly, siRNA targeted against RUNX2 was purchased from ThermoFisher Scientific (MSS202674). Dharmafect 1 (GE Dharmacon) and Lipofectamine RNAiMAX (ThermoFisher Scientific) transfection reagents were used for siRNA transfections according to the manufacturer's instructions.

Transient Transfection and Luciferase Reporter Assay

TDAG51$^{+/+}$ and TDAG51$^{-/-}$ mouse VSMCs were seeded overnight before cotransfection with a RUNX2 luciferase reporter plasmid[46] and a β-galactosidase plasmid (631719, Takara Bio) using Lipofectamine 2000 (ThermoFisher Scientific) according to the manufacturer's instructions. At 24-hour post-transfection, cells were treated with either 2.6 mmol/L P_i or a vehicle control then harvested for a luciferase promoter assay (Promega) 48 hours following the treatments. The β-galactosidase enzyme assay (Promega) was used as a transfection control. In experiments designed to examine the role of Pit-1 in mineral metabolism and VC, mouse VSMCs were transfected with either the Pit-1 expression plasmid (MR209998, OriGene Technologie) or an empty vector (EV) control using Lipofectamine 2000. The cells were harvested for analysis at 48-hour post-transfection.

Cell Fractionation, RUNX2 Response Element Immunoprecipitation Assay and Immunoprecipitation Analysis

Nuclear extracts from TDAG51$^{+/+}$ and TDAG51$^{-/-}$ VSMCs were isolated using a Nuclear Extraction Kit (Abcam) according to the manufacturer's instruction. For studies examining RUNX2 binding to the OSE2 (osteoblast-specific cis-acting element 2), 500 µg of protein from nuclear extracts was incubated overnight on an orbital shaker at 4°C with an oligonucleotide (1 µg) consisting of 6× repeats of the OSE2 promoter (ACCACA), as well as RUNX2 or IgG control antibody. The samples were then incubated with protein G magnetic beads (Bio-Rad). For the OSE2-containing oligonucleotide was isolated by incubating samples at high heat (95°C for 5 minutes) and amplified via polymerase chain reaction using Platinum Taq DNA Polymerase High Fidelity (ThermoFisher Scientific). The amplified DNA product was electrophoretically resolved on agarose gels and visualized using Safe-Red (Applied Biosystems). For complete oligonucleotide sequences, please refer to Materials in the Data Supplement and Table V in the Data Supplement. For studies examining RUNX2 phosphorylation status and TDAG51-RUNX2 protein interaction, 500 µg of protein was incubated overnight on an orbital shaker at 4°C with RUNX2 or TDAG51 antibody (1 µg) respectively, using IgG (Invitrogen) as a control. The samples were then incubated with protein G magnetic beads (Bio-Rad). Immunoprecipitation samples were subsequently eluted in SDS-containing lysis buffer at high heat (100°C for 5 minutes) and resolved on an SDS-PAGE gel for analysis.

Patient Samples/Temporal Aortas

Biopsies were obtained from male and female patients between 67 and 73 years of age, who were previously diagnosed with diabetes mellitus or chronic obstructive pulmonary disease and suspected of exhibiting medial VC and temporal arteritis. All procedures were approved by the McMaster University Research Ethics Board.

Statistical Analysis

Data were analyzed using the unpaired Student *t* test or 1-way ANOVA with Tukey multiple comparison testing using Prism 6 (GraphPad). Data were not analyzed for normality and equal variance. Data are presented as the mean±SD, with $P<0.05$ considered significant between groups. All experiments were repeated at least 3×. Details of the biological replicates are listed in figure legends.

RESULTS

TDAG51 Is a Regulator of P_i-Induced VC in Primary Mouse and Human VSMCs

Intimal and medial arterial mineral deposition is prevalent in patients with CKD and is regarded as an important predictor of cardiovascular mortality.[4,10] Given our previous findings, in which intimal calcification was reduced in atherosclerotic lesions from TDAG51$^{-/-}$/ApoE$^{-/-}$ mice,[31] in situ hybridization was used to assess the expression of PHLDA1 (human homologue of TDAG51) in the medial layer of calcified human temporal arteries. An increase in PHLDA1 mRNA was observed within smooth muscle cells adjacent to the mineral deposits devoid of live cells (Figure 1A and Figure IA in the Data Supplement). To provide further insight into the location of healthy VSMCs, α-SMA (α smooth muscle actin) was also examined in adjacent sections using in situ hybridization (Figure 1A). Co-staining of PHLDA1 and α-SMA using fluorescent in situ hybridization revealed that PHLDA1 is found in healthy VSMCs, whereas regions where α-SMA expression is low, an occurrence which has previously been associated with mineral deposition in the arterial wall,[47] undetectable PHLDA1 expression (Figure 1B). PHLDA1 and α-SMA hybridization

Downloaded from http://ahajournals.org by on July 22, 2020

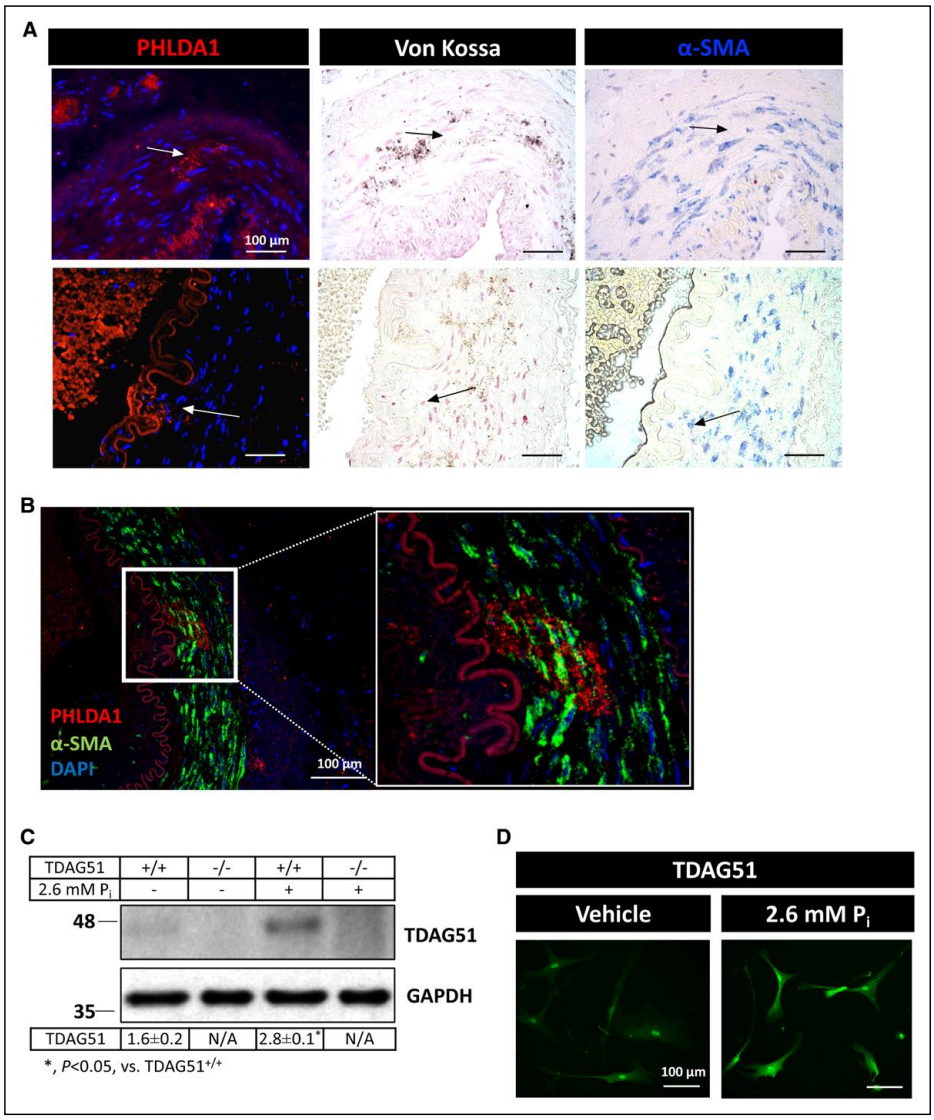

Figure 1. TDAG51 (T-cell death-associated gene 51) is expressed in human temporal arteries and induced in Pi-treated vascular smooth muscle cells (VSMCs).
A, Representative micrographs of PHLDA1 (pleckstrin homology-like domain, family A, member 1; human homologue) fluorescent in situ hybridization and von Kossa staining in serial sections of human temporal arteries. The arrow points to the area of TDAG51 upregulation. **B**, Immunofluorescence co-staining of PHLDA1 (red) and α-SMA (α-smooth muscle actin; green) in human temporal arteries. **C**, Immunoblot and densitometry analysis of TDAG51 protein following 4 days of inorganic phosphate (P_i) treatment in cultured mouse TDAG51$^{+/+}$ and TDAG51$^{-/-}$ VSMCs (n=5). **D**, Immunofluorescent staining of TDAG51 in mouse VSMCs. All data are shown as mean and error bars as SD. *P<0.05 by 2-tailed unpaired Student t test. Genotype is indicated as $^{+/+}$ and $^{-/-}$ for TDAG51$^{+/+}$ and TDAG51$^{-/-}$, respectively.

probes were validated via the staining of human hair follicles (Figure IB and IC in the Data Supplement).[48] Immunoblot and immunofluorescence staining revealed an increase in TDAG51 protein expression in primary mouse VSMCs treated with a pathophysiological dose of P_i (2.6 mmol/L) for 4 days[41,42] (Figure 1C and 1D). Overall, these early observations demonstrate that (1) in human temporal arteries, PHLDA1 expression is high in

Downloaded from http://ahajournals.org by on July 22, 2020

areas adjacent to HA deposits and (2) TDAG51 expression increases upon treatment with P_i in primary mouse VSMCs. We, therefore, hypothesized that TDAG51 may play an important role in the process of VC in conditions of hyperphosphatemia.

To further test this hypothesis, we next assessed the role of TDAG51 in the process of VC using a variety of knockdown and knockout VSMC models. Supporting its putative role in VC, reduced mineral deposition was observed in human VSMCs following PHLDA1 siRNA-mediated knockdown (Figure 2A, 2B, and 2C) and in TDAG51$^{-/-}$ VSMCs (Figure 2D), as well as in TDAG51$^{-/-}$ aortic ring cultures exposed to high P_i medium (Figure 2E). Because the pathogenesis of medial VC is predominantly associated with extracellular crystallization of HA in the medial layer of the arterial wall,[49,50] we first confirmed that P_i-mediated mineral deposition occurs in the extracellular matrix. Quantification of Ca^{2+} and HA formation assays both demonstrate an increase in mineral deposition in purified extracellular matrices (Figure IIA and IIB in the Data Supplement).[51] The quality of matrix preparations was verified by nuclear staining using DAPI (Figure IIC in the Data Supplement). Collectively, these data demonstrate that TDAG51 expression strongly correlates with regions adjacent to the calcified areas in the medial layer of the vessel wall and also suggest that TDAG51 may contribute to the process of P_i-mediated VC.

TDAG51$^{-/-}$ VSMCs Exhibit Reduced Basal P_i-Mediated RUNX2 Transcriptional Activity

Similar to bone formation, osteogenic transdifferentiation of VSMCs is a highly regulated process.[17] Given that RUNX2 activation is both necessary and sufficient for the development of VC,[18,19,22,23] our next aim was to assess RUNX2 expression in TDAG51$^{-/-}$ VSMCs. Interestingly, an increase in total cellular abundance of RUNX2 was observed in TDAG51$^{-/-}$ VSMCs cultured in regular medium, as well as in cells treated with P_i, although basal mRNA levels were lower in these cells (Figure 3A and 3B). Similarly, immunoblot analysis of subcellular fractions as well as immunofluorescence staining revealed increased nuclear abundance of RUNX2 in TDAG51$^{-/-}$ VSMCs following 24 hours of P_i treatment (Figure 3C and 3D). Concurrently, P_i treatment also increased the nuclear abundance of TDAG51 in the TDAG51$^{+/+}$ VSMCs (Figure 3C).

Given that RUNX2 expression was increased, we next examined RUNX2 transcriptional activity using a luciferase reporter assay with 6XOSE2-Luc, a RUNX2 target gene promoter that is widely used to study osteoblast development.[46] Despite the elevated abundance of RUNX2 observed in TDAG51$^{-/-}$ VSMCs, RUNX2-dependent activation of the OSE2 promoter was diminished in the TDAG51$^{-/-}$ VSMCs (Figure 4A). RUNX2 binding to the OSE2 promoter region was also examined in nuclear extracts from these cells. Consistent with reduced RUNX2 transcriptional activity, RUNX2 binding to the OSE2 promoter region was significantly diminished in the TDAG51$^{-/-}$ VSMCs (Figure 4B). Because RUNX2 phosphorylation sites associated with osteogenic transdifferentiation and mineral deposition predominantly occur on serine residues,[52] total serine phosphorylation of RUNX2 immunoprecipitated from TDAG51$^{+/+}$ and TDAG51$^{-/-}$ VSMCs was also examined via immunoblots. These studies demonstrated an increase in global RUNX2 serine phosphorylation in TDAG51$^{-/-}$ VSMCs (Figure 4C). In line with these findings, the mRNA expression of the RUNX2-regulated osteogenic marker, OCN, was also reduced (Figure 4D). Furthermore, we observed an increase in the expression of calcification inhibitors, including OPN, OPG, and maGLAP[11] in TDAG51$^{-/-}$ VSMCs (Figure III in the Data Supplement). To gain further insight in the mechanism by which TDAG51 modulates RUNX2 activity, studies examining the ability of TDAG51 to bind to either the OSE2 promoter region or act as a RUNX2 binding partner were performed. Co-immunoprecipitation studies demonstrate no direct interaction between RUNX2 and TDAG51 (Figure 4E). In a similar manner, TDAG51 does not bind to the OSE2 promoter region as illustrated by a promoter binding assay, using RUNX2 as a positive control (Figure 4F). Taken together, our results indicate that TDAG51 does not act as a promoter of P_i-induced RUNX2-mediated osteogenic differentiation in VSMCs by directly regulating RUNX2 function.

Apoptotic cell death is another major contributor to the development of VC and that TDAG51 has been previously shown to affect this process,[9] apoptotic cell death, and cell viability were also examined using the TUNEL (terminal deoxynucleotidyl transferase dUTP nick-end labeling) stain assay and a lactate dehydrogenase release assay. Our observations recapitulate previous findings where TDAG51$^{-/-}$ VSMCs were protected from apoptotic cell death and exhibit improved cell viability, suggesting that reduced cell death may be contributing to the observed phenotype (Figure IVA and IVB in the Data Supplement).

Pit-1 Inhibition in TDAG51$^{-/-}$ VSMCs Leads to a Reduction in Intracellular P_i Content

Pit-1 is the predominant P_i solute transporter and an established modulator of mineral deposition in VSMCs.[11,12,53] Given the established link between intracellular P_i content and RUNX2 activation,[16,17] we next examined Pit-1 expression. A reduction in Pit-1 mRNA transcript and protein expression was observed in TDAG51$^{-/-}$ VSMCs, while Pit-2 expression was unchanged (Figure 5A and 5B). Consistent with immunoblotting, immunofluorescence staining demonstrated

Downloaded from http://ahajournals.org by on July 22, 2020

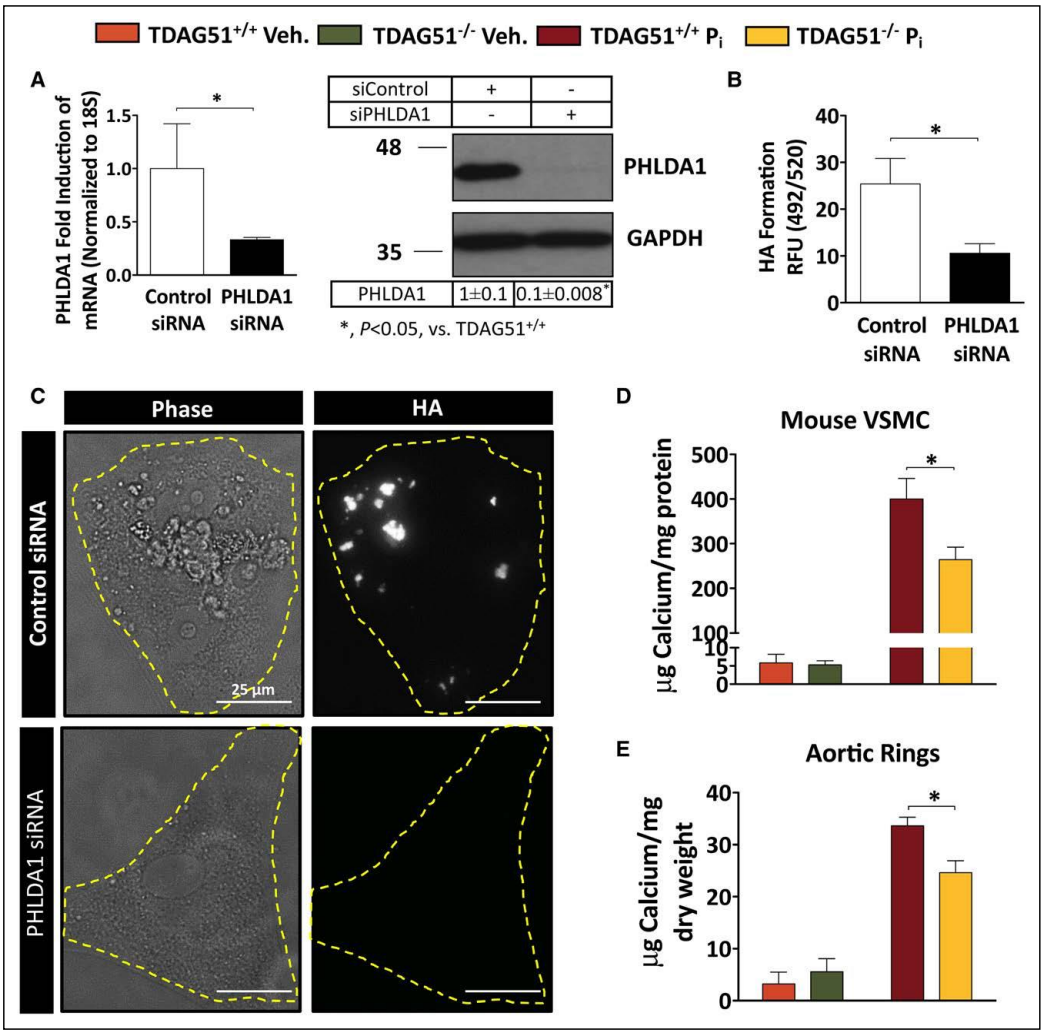

Figure 2. TDAG51 (T-cell death-associated gene 51) deficiency inhibits inorganic phosphate (P_i)-induced VC in vascular smooth muscle cells (VSMCs) and ex vivo aortic ring cultures.

A, Quantitative real-time polymerase chain reaction and immunoblot analysis of PHLDA1 (pleckstrin homology-like domain family A member 1) expression in human VSMCs transfected with either control siRNA or siRNA targeted against PHLDA1(n=3). **B**, Quantification of P_i-induced hydroxyapatite (HA) crystal formation in control or PHLDA1 siRNA-transfected human VSMCs (n=12). **C**, Brightfield microscopy depicting HA crystal formation after 5 days of 2.6 mmol/L P_i treatment in human VSMCs transfected with control or PHLDA1 siRNA. The outline of the representative cell is depicted as a dotted yellow line. **D** and **E**, Quantification of calcium deposition in TDAG51$^{+/+}$ and TDAG51$^{-/-}$ mouse VSMCs and ex vivo aortic ring cultures following 5 and 7 days of 2.6 mmol/L P_i treatment, respectively (n=5 and n=4). All data are shown as mean and error bars as SD. *P<0.05 by 2-tailed unpaired Student t test or 1-way ANOVA with Tukey multiple comparison testing using Prism 6 (GraphPad). Genotype is indicated as $^{+/+}$ and $^{-/-}$ for TDAG51$^{+/+}$ and TDAG51$^{-/-}$, respectively.

a reduction in cell-surface expression of Pit-1 both in the absence and in the presence of high P_i treatment in TDAG51$^{-/-}$ VSMCs (Figure 5C). Furthermore, immunoblotting and immunohistochemistry staining of thoracic aortas also revealed a decrease in Pit-1 abundance in TDAG51$^{-/-}$ compared with TDAG51$^{+/+}$ mice (Figure 5D through 5F). Immunofluorescence co-staining of Pit-1 and CD31 (endothelial cell marker) as well as Pit-1 and α-SMA (smooth muscle cell marker) confirmed that Pit-1 staining occurs within the smooth muscle cell layer of the vessel (Figure VA and VB in the Data Supplement). Next, we examined whether decrease in the expression

Downloaded from http://ahajournals.org by on July 22, 2020

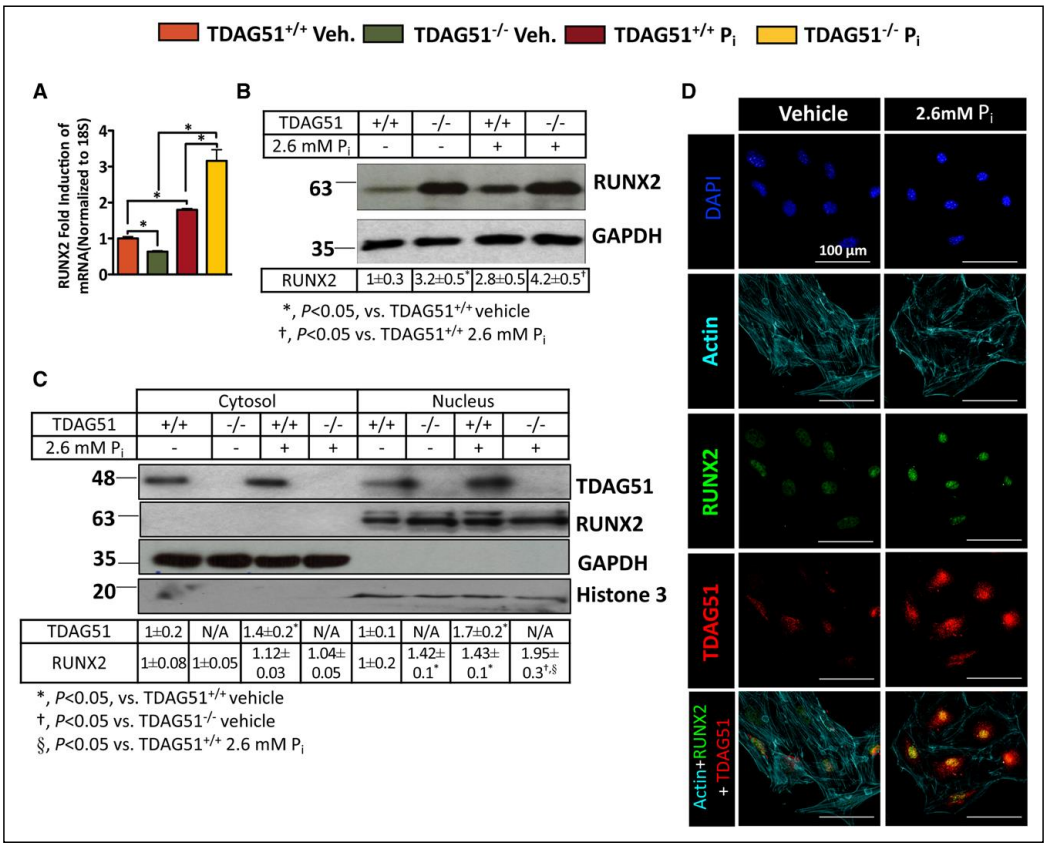

Figure 3. TDAG51$^{-/-}$ (T-cell death-associated gene 51) vascular smooth muscle cells (VSMCs) exhibit reduced expression of RUNX2 (Runt-related transcription factor 2).

A and **B**, Quantitative real-time polymerase chain reaction and immunoblot analysis of RUNX2 expression in mouse VSMCs after 4 days of inorganic phosphate (P_i) treatment (n=5). **C**, Immunoblot analysis of TDAG51 and RUNX2 in cytosolic and nuclear subcellular fractions from mouse VSMCs treated with 2.6 mmol/L P_i for 5 days (n=4). **D**, Representative micrograph of immunofluorescence staining in TDAG51$^{+/+}$ VSMCs with anti-TDAG51 antibody (red), anti-RUNX2 antibody (green), phalloidin (teal), and DAPI (blue) following 5 days of 2.6 mmol/L P_i treatment. All data are shown as mean and error bars as SD. * P<0.05 by 1-way ANOVA with Tukey multiple comparison testing using Prism 6 (GraphPad). Genotype is indicated as $^{+/+}$ and $^{-/-}$ for TDAG51$^{+/+}$ and TDAG51$^{-/-}$, respectively.

of cell-surface Pit-1 leads to a reduction in intracellular P_i content in TDAG51$^{-/-}$ VSMCs. Consistent with other observations, our data reveal that TDAG51$^{-/-}$ VSMCs exhibit lower levels of intracellular P_i content following 1, 2, and 3 day P_i treatment (Figure 5G).

Previous studies also report that Pit-1 expression is increased within calcified regions of the artery and has been shown to be modulated by well-established drivers of VC.[54,55] Furthermore, Pit-1 knockdown blocks P_i-induced mineralization of VSMCs.[12,13] Thus, to interrogate the role of Pit-1 in the context TDAG51 deficiency in vitro, and to determine whether Pit-1 overexpression can restore VC in response to P_i, we used a FLAG-tagged Pit-1 expression vector. Transfection efficiency was evaluated by immunoblotting of whole cell lysates and immunofluorescence staining in TDAG51$^{-/-}$ VSMCs (Figure 6A and 6B). Interestingly, we observed that overexpression of Pit-1 markedly increased RUNX2 expression (Figure 6A). In support of previous studies demonstrating a transient decrease in intracellular P_i uptake following Pit-1 knockdown, Pit-1 overexpression yielded increased intracellular P_i content following 48 hours of P_i treatment (Figure 6C).[12] In addition, the increased intracellular P_i content was accompanied by increased VC (Figure 6D). A promoter binding assay was also employed to confirm that Pit-1 overexpression restored the binding of RUNX2 to the OSE2 promoter region in TDAG51$^{-/-}$ VSMCs (Figure 6E).

Our observations as well as those of others,[12–14] strongly suggest that Pit-1 is a modulator of RUNX2 expression and activity. In human VSMCs, RUNX2

Downloaded from http://ahajournals.org by on July 22, 2020

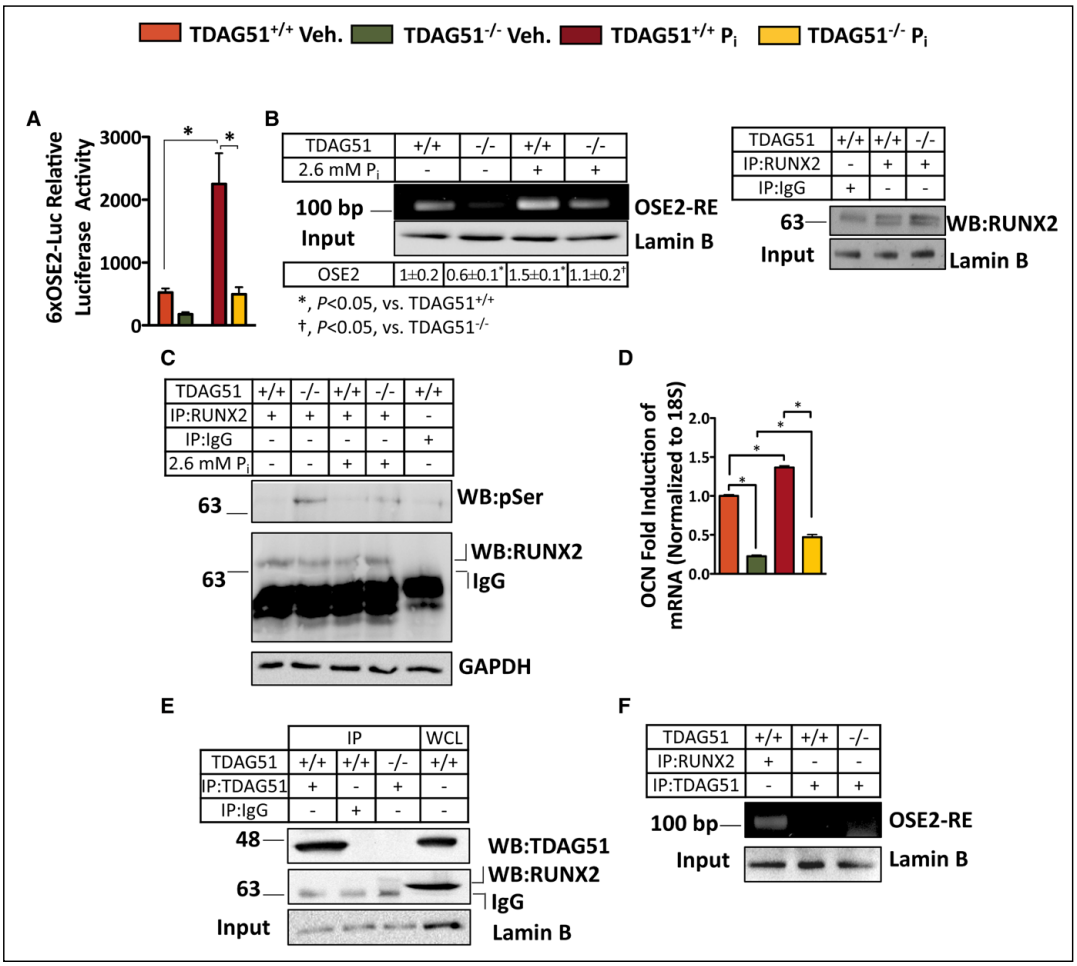

Figure 4. Inorganic phosphate (P_i) fails to induce RUNX2 (Runt-related transcription factor 2) transcriptional activity in TDAG51$^{-/-}$ (T-cell death-associated gene 51) vascular smooth muscle cells (VSMCs).
A, RUNX2 luciferase reporter assay following 2 days of P_i treatment (n=5). **B**, RUNX2-OSE2 (osteoblast-specific cis-acting element 2) binding assay and RUNX2 immunoprecipitation control in TDAG51$^{+/+}$ and TDAG51$^{-/-}$ VSMCs (n=3). **C**, Immunoblot of RUNX2 immunoprecipitation and global RUNX2 serine phosphorylation. **D**, Quantitative real-time polymerase chain reaction of OCN (osteocalcin) expression (n=5). **E**, Co-immunoprecipitation of TDAG51 and RUNX2 in TDAG51$^{+/+}$ VSMCs using TDAG51$^{-/-}$ VSMCs and whole cell lysate (WCL) as negative and positive controls. **F**, TDAG51-OSE2 binding assay. All data are shown as mean and error bars as SD. * P<0.05 by 1-way ANOVA with Tukey multiple comparison testing using Prism 6 (GraphPad). Genotype is indicated as $^{+/+}$ and $^{-/-}$ for TDAG51$^{+/+}$ and TDAG51$^{-/-}$, respectively.

Downloaded from http://ahajournals.org by on July 22, 2020

activity is dependent upon Pit-1 expression, and lack thereof prevents osteogenic transdifferentiation of these cells in a high P_i environment.[12] To our knowledge, however, the capacity of RUNX2 to regulate Pit-1 expression has never been reported. To determine whether the reduced RUNX2 activity in TDAG51$^{-/-}$ VSMCs contributes to decreased Pit-1 expression, we downregulated RUNX2 using siRNA. RUNX2 knockdown reduced Pit-1 protein and mRNA abundance (Figure 6F; Figure VI in the Data Supplement), suggesting that Pit-1 is a Runx2 responsive gene. Given that Pit-1 is known to impact the activity of Runx2, and that our studies show that Runx2 affects Pit-1 expression, our data suggest that TDAG51 enhances RUNX2 activity in a Pit-1-dependent manner.

TDAG51$^{-/-}$ Mice Are Protected Against VD_3-Induced Medial VC

To substantiate our findings on the role of TDAG51 in VC, a VD_3 overload mouse model of rapid VC was employed.[38,39]

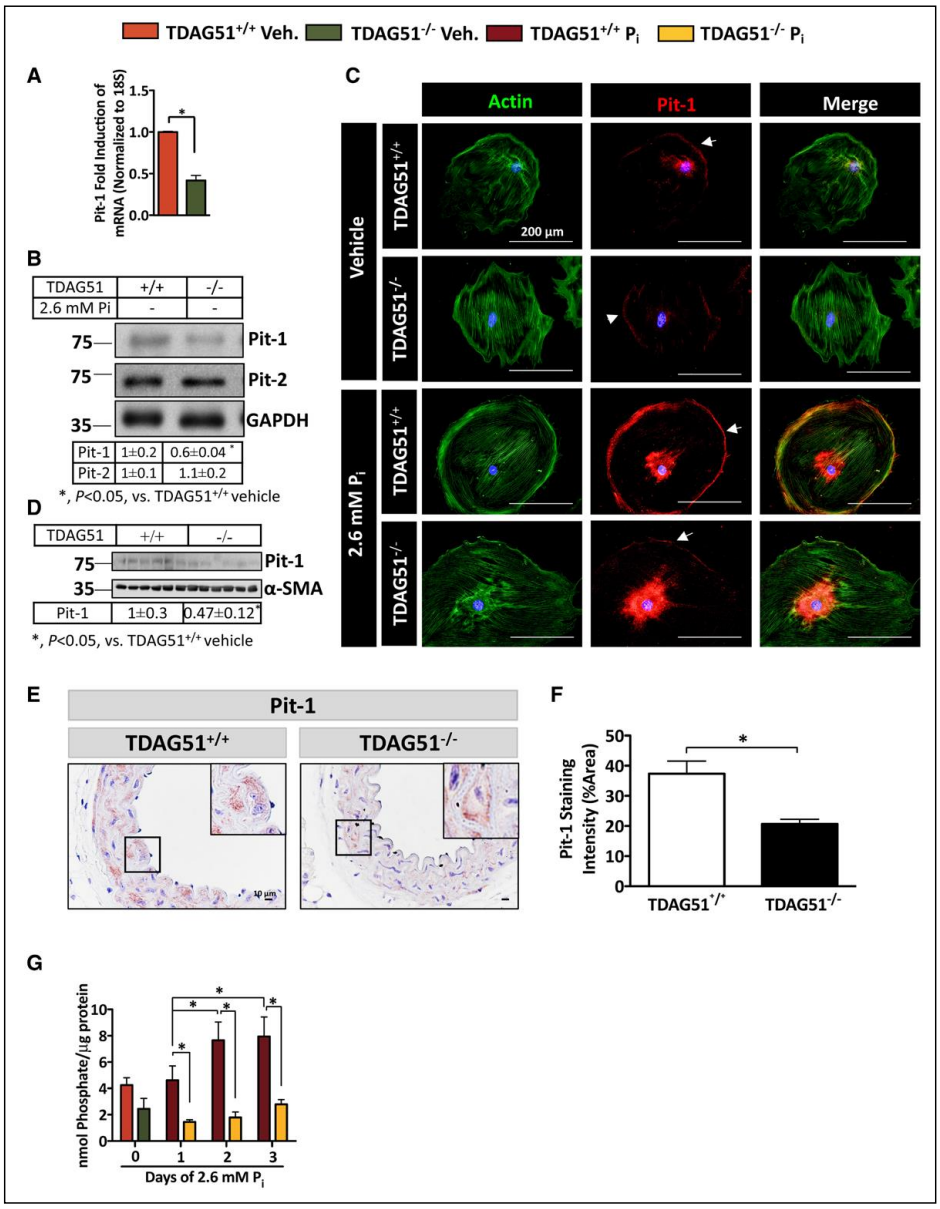

Figure 5. TDAG51 (T-cell death-associated gene 51) modulates intracellular inorganic phosphate (P_i) levels via Pit-1. **A** and **B**, Quantitative real-time polymerase chain reaction and immunoblot analysis of type III sodium-dependent P_i transporters (Pit-1/2) expression in TDAG51$^{+/+}$ and TDAG51$^{-/-}$ VSMCs (vascular smooth muscle cells; n=5). **C**, Immunofluorescence staining of Pit-1 (red), phalloidin (green), and DAPI (blue) in TDAG51$^{+/+}$ and TDAG51$^{-/-}$ VSMCs following 3 days of 2.6 mmol/L P_i treatment. **D**, Immunoblot analysis of Pit-1 expression in thoracic aortas from TDAG51$^{+/+}$ and TDAG51$^{-/-}$ mice (n=3). **E** and **F**, Immunohistochemistry staining and quantification of Pit-1 in TDAG51$^{+/+}$ and TDAG51$^{-/-}$ mouse aortas (n=5). **G**, Quantification of intracellular P_i content in TDAG51$^{+/+}$ and TDAG51$^{-/-}$ VSMCs following treatment with 2.6 mmol/L P_i for 0, 1, 2, and 3 days (n=3). All data are shown as mean and error bars as SD. *P<0.05 by unpaired 2-tailed Student t test or 1-way ANOVA with Tukey multiple comparison testing using Prism 6 (GraphPad). Genotype is indicated as $^{+/+}$ and $^{-/-}$ for TDAG51$^{+/+}$ and TDAG51$^{-/-}$, respectively.

Downloaded from http://ahajournals.org by on July 22, 2020

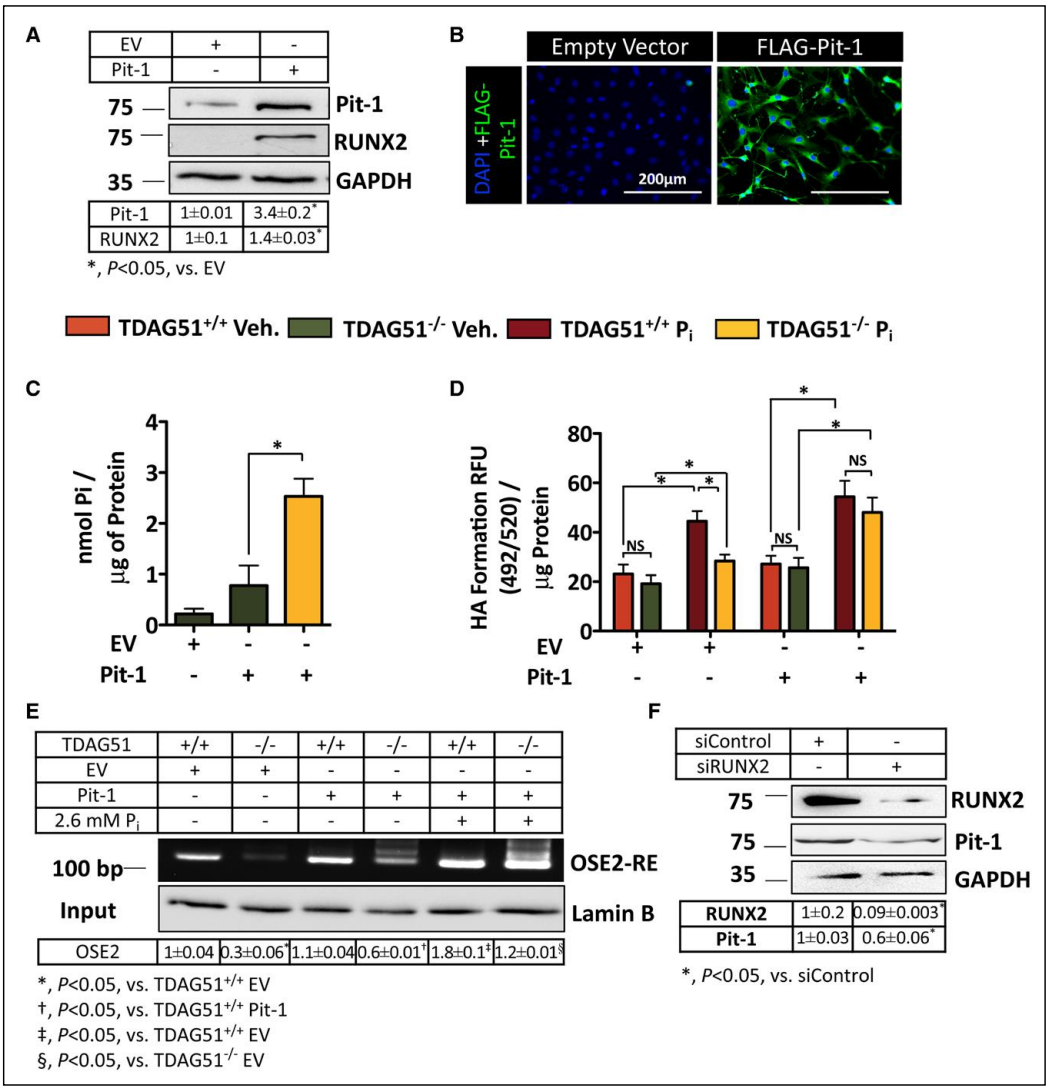

Figure 6. Pit-1 (type III sodium-dependent Pi transporter) overexpression restores inorganic phosphate (P_i) uptake and induces mineral deposition in TDAG51$^{-/-}$ (T-cell death-associated gene 51) vascular smooth muscle cells (VSMCs).
A and **B**, Immunoblot analysis and immunofluorescence staining of Pit-1 in TDAG51$^{-/-}$ VSMCs. **C**, Quantification of the intracellular P_i content in TDAG51$^{+/+}$ and TDAG51$^{-/-}$ VSMCs transfected with either Pit-1 or empty vector (EV) following 48 h of 2.6 mmol/L P_i (n=3). **D**, HA quantification in TDAG51$^{+/+}$ and TDAG51$^{-/-}$ VSMCs transfected with either Pit-1 or EV following 5 days of 2.6 mmol/L P_i (n=6). **E**, RUNX2 (Runt-related transcription factor 2)-OSE2 (osteoblast-specific cis-acting element 2) binding assay in TDAG51$^{+/+}$ and TDAG51$^{-/-}$ VSMCs transfected with either Pit-1 or EV following 48 h of 2.6 mmol/L P_i (n=3). **F**, Immunoblot analysis of RUNX2 and Pit-1 expression in TDAG51$^{+/+}$ VSMCs transfected with either control siRNA or siRNA targeted against RUNX2. All data are shown as mean and error bars as SD. *P<0.05 by unpaired 2-tailed Student *t* test or 1-way ANOVA with Tukey multiple comparison testing using Prism 6 (GraphPad). Genotype is indicated as $^{+/+}$ and $^{-/-}$ for TDAG51$^{+/+}$ and TDAG51$^{-/-}$, respectively.

Functionality of the model was first examined. Consistent with previous studies,[39] a significant increase in serum Ca^{2+} and P_i levels was observed in VD_3-treated mice and this was unaffected by the absence of TDAG51 (Table 1). Despite this expected finding, quantification of mineral deposition (Figure 7A) and Alizarin Red calcium stain (Figure 7E)

Downloaded from http://ahajournals.org by on July 22, 2020

Table. Serum Biochemistry

	Vehicle		Vitamin D_3	
	TDAG51$^{+/+}$	TDAG51$^{-/-}$	TDAG51$^{+/+}$	TDAG51$^{-/-}$
Serum calcium, mmol/L	2.6±0.21	2.37±0.11	3.70±0.47†	4.03±0.36*
Serum phosphate, mmol/L	1.83±0.14	1.93±0.25	2.88±0.45†	2.42±0.25*

Serum calcium and phosphate content in mice treated with vehicle control or VD3 for 7 days. TDAG51 indicates T-cell death-associated gene 51. All data are shown as mean±SD. *$P<0.05$ vs TDAG51$^{+/+}$; VD_3 †$P<0.05$ vs TDAG51$^{+/+}$ vehicle by 1-way ANOVA with Tukey multiple comparison testing using Prism 6 (GraphPad). Genotype is indicated as $^{+/+}$ and $^{-/-}$ for TDAG51$^{+/+}$ and TDAG51$^{-/-}$, respectively.

both revealed a reduction in deposition in TDAG51$^{-/-}$ aortas compared with controls. The increase in systolic blood pressure mediated by the calcified vessels, as seen in TDAG51$^{+/+}$ mice, was also abrogated in TDAG51$^{-/-}$ mice (Figure 7B). In line with our in vitro studies, immunoblot, quantitative real time polymerase chain reaction, and immunohistochemistry analysis also revealed a decrease in the expression of established drivers of osteogenic transdifferentiation of VSMCs, including MSX2 (Msh homeobox 2), ALP (alkaline phosphatase), and OSX (osterix), in the aortas of VD_3-treated TDAG51$^{-/-}$ mice (Figure 7C through 7E). Additionally, immunofluorescence co-staining of Runx2/MSX2/OCN and CD31 as well as Runx2/MSX2/OCN and α-SMA confirmed that these markers were predominantly expressed within the medial layer of the vessel wall (Figure VIIA and VIIB in the Data Supplement). Overall, these data demonstrate that TDAG51 plays a critical role as a regulator of VC.

DISCUSSION

VC in the medial layer of the vessel wall is a predictor of cardiovascular morbidity and mortality in patients with CKD.[1,2] However, its development is not completely understood.[1,3,9] High circulating P_i levels are considered to be a major driver in the development of arterial VSMC calcification in humans, as well as in in vivo and in vitro models.[4–6,10] In this study, we have identified TDAG51 as a regulator of osteogenic transdifferentiation and calcification of VSMCs in response to high P_i. We demonstrate an induction of TDAG51 expression in VSMCs treated with a pathophysiological dose of P_i, as well as within calcified regions of human temporal arteries. As bone formation and VC share a common pathway,[7–9] we examined the expression and transcriptional activity of the osteogenic transcription factor, RUNX2. Our findings show differential RUNX2 serine phosphorylation, diminished basal and P_i-mediated Runx2 activation, as well as decreased RUNX2 binding to the OSE2 promoter region in TDAG51$^{-/-}$ VSMCs. To explain these observations, we examined the expression of the predominant P_i transporter in VSMCs, Pit-1. In our studies, we observed a reduction in Pit-1 expression and intracellular P_i content in TDAG51$^{-/-}$ VSMCs compared with controls. In line with these findings, Pit-1 overexpression restored intracellular P_i content, HA crystal formation and the ability of RUNX2 to bind to the OSE2 promoter region in the presence of P_i. Furthermore, we demonstrated that siRNA-mediated knockdown of RUNX2 reduced Pit-1 abundance, suggesting that there exists a reciprocal relationship between Pit-1 and RUNX2. Collectively, these data support the concept that TDAG51 modulates P_i-induced RUNX2-mediated osteogenic transdifferentiation of VSMCs in a Pit-1-dependent manner by regulating RUNX2 activity.

The potential mechanisms underlying P_i-induced VC include osteogenic transdifferentiation of VSMCs, loss of calcification inhibitors, induction of procalcific genes, and apoptotic cell death.[6,9] Although conventionally described as a tumor suppressor,[24] we as well as others have reported that TDAG51 attenuates apoptosis,[28] endoplasmic reticulum stress[29,30] and oxidative stress,[31] all of which are well-established mediators of osteogenic transdifferentiation in VSMCs. It is, therefore, possible that TDAG51 may regulate VC via alternative cellular processes. In support of this notion, endoplasmic reticulum and oxidative stress-inducing agents, such as homocysteine,[28] tunicamycin,[56] and farnesol[57] have all been reported to induce TDAG51 expression in various cell types. Transient overexpression of TDAG51 has been shown to decrease cell adhesion and cause detachment-mediated programmed cell death in cultured human vascular endothelial cells[28] and cardiac muscle cells.[58] Furthermore, TDAG51-deficient ApoE$^{-/-}$ mice exhibit reduced apoptosis and mineral deposition in atherosclerotic lesions.[31] Consistent with these findings, we observed reduced apoptotic cell death and increased cell viability following P_i treatment in the TDAG51$^{-/-}$ VSMCs. Prior studies also illustrate an inverse relationship between TDAG51 and a well-established inhibitor of osteogenic transdifferentiation in VSMCs, PPARγ (peroxisome proliferator-activated receptor γ).[31,36] Specifically, TDAG51 was shown to negatively regulate the expression of PPARγ and its downstream targets, whereas TDAG51 deficiency enhanced PPARγ activity. Studies in 3T3-L1 preadipocytes and mouse embryonic fibroblasts also show that decreased TDAG51 expression inversely correlates with the induction of PPARγ expression,[36] suggesting that TDAG51 may act as a modulator of cellular differentiation. Therefore, even though these studies focus on Pit-1-RUNX2–mediated mechanism of VC, TDAG51$^{-/-}$ models may in

Downloaded from http://ahajournals.org by on July 22, 2020

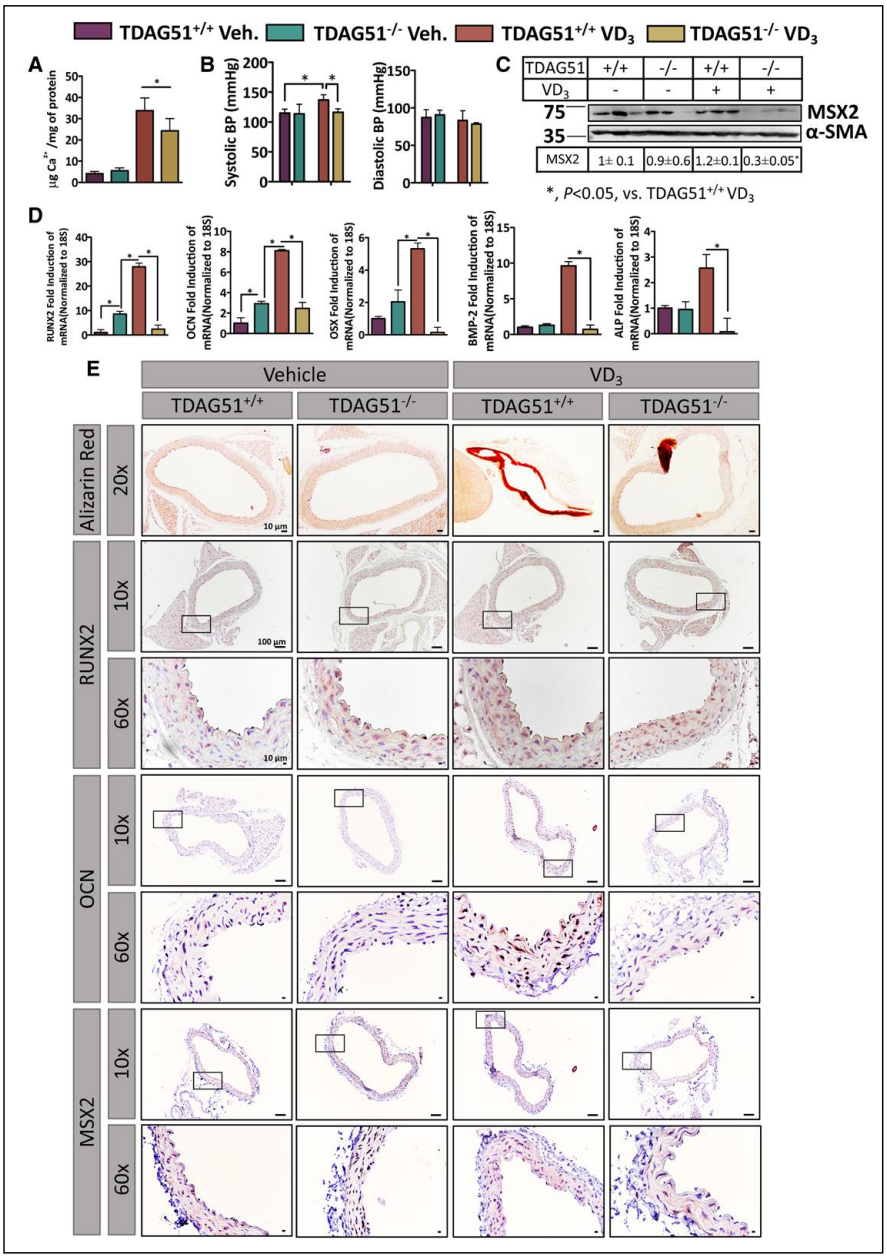

Figure 7. TDAG51$^{-/-}$ (T-cell death-associated gene 51) mice are protected against vitamin D3 (VD_3)-induced vascular calcification (VC).

A, Calcium quantification in the abdominal aortas (n=9–13 per group), as well as (**B**) systolic and diastolic blood pressure (BP) in TDAG51$^{+/+}$ and TDAG51$^{-/-}$ mice treated with VD_3 and vehicle-treated controls (n=5 per group). **C**, Immunoblot analysis of MSX2 (msh homeobox 2) expression in TDAG51$^{+/+}$ and TDAG51$^{-/-}$ mice treated with VD_3 and vehicle-treated controls (n=3 per group). **D**, Quantitative real-time polymerase chain reaction analysis of mRNA expression of RUNX2, OCN (osteocalcin), OSX (osterix), BMP-2 (bone morphogenic protein 2) and ALP (alkaline phosphatase). **E**, Alizarin Red staining and immunohistochemistry staining of RUNX2 (Runt-related transcription factor 2), OCN, and MSX2 in abdominal aortas. All data are shown as mean and error bars as SD. *$P<0.05$ by 1-way ANOVA with Tukey multiple comparison testing using Prism 6 (GraphPad). Genotype is indicated as $^{+/+}$ and $^{-/-}$ for TDAG51$^{+/+}$ and TDAG51$^{-/-}$, respectively.

Downloaded from http://ahajournals.org by on July 22, 2020

part exhibit additional cytoprotection through other cellular mechanisms, including increased PPARγ activity and attenuated apoptotic signaling.

The transdifferentiation of VSMCs is a highly regulated process that draws many parallels with bone formation. It is well-established that RUNX2 transcriptional activity is necessary for osteoblast differentiation, matrix production, and mineralization during bone development[59] as well as VC.[21–23] Recent studies demonstrate that P_i also plays a critical role in RUNX2-mediated skeletal development. Acute P_i restriction decreased the expression of RUNX2 downstream targets and markers of osteogenic lineage, including OSX and OCN.[60] Similarly, studies have also shown that RUNX2 activation is essential for P_i-mediated osteogenic differentiation of VSMCs.[23,24] Furthermore, overexpression of RUNX2 in adipose tissue-derived mesenchymal stem cells led to the development of an osteoblast-like phenotype and mineral deposition in these cells.[18] Although global knockout of RUNX2 is embryonically lethal due to skeletal malformations,[21] VSMC-specific deletion of RUNX2 protects against vascular mineral deposition.[22,23] Interestingly, while protected from VC, TDAG51$^{-/-}$ VSMCs exhibited an increase in RUNX2 expression accompanied by impaired RUNX2 transcriptional activity and VC. These findings suggest that increased RUNX2 expression occurs as a compensatory mechanism in response to impaired transcriptional activation. Similar to our findings in TDAG51$^{-/-}$ VSMCs, Liu et al[61] observed that ablation of MED23 in osteoblasts increased RUNX2 expression while reducing OSE2-Luc activity and attenuating osteoblast differentiation. We also demonstrate a decrease in the expression of key modulators of RUNX2 expression and transcriptional activity MSX2[15,62] as well as its downstream targets OCN and OSX[15,60] in VD_3-treated TDAG51$^{-/-}$ mice. The diminished mineral accumulation and osteogenic differentiation observed in TDAG51$^{-/-}$ VSMCs, despite increased RUNX2 expression, could potentially occur as a result of altered function of RUNX2. Additional studies are currently underway to investigate how TDAG51 regulates RUNX2 transcriptional activity.

Preclinical and clinical studies demonstrate that persistent hyperphosphatemia is associated with increased prevalence of VC and cardiovascular mortality in patients with ESRD.[3,6,11] Importantly, lowering serum P_i slows the progression of VC in patients with ESRD.[63,64] Consistent with these findings, exposure to pathophysiological levels of P_i leads to mineral deposition in vitro.[20] Active P_i transport into rat and human VSMCs is mediated by the type III sodium-dependent cotransporters, Pit-1 and Pit-2.[11] In VSMCs, Pit-1 is more abundant than Pit-2 and is critical for P_i-mediated VC. Similar to the knockdown of RUNX2, Pit-1 knockdown impaired mineralization and blocked the expression of osteogenic transdifferentiation markers, RUNX2 and OPN. Conversely, Pit-1 overexpression rescued P_i-induced mineralization of VSMCs.[12] Furthermore, Pit-1 and RUNX2 expression were found to be increased in calcified aortas of uremic rats.[20,55] Studies also show that during osteoblast differentiation, Pit-1 expression levels increase concomitantly with OCN, an established target of RUNX2 activation, while low basal Pit-2 expression remains unchanged.[63] Similarly, in our studies, a reduction in the expression of Pit-1 was observed in the absence of changes in Pit-2 expression in TDAG51$^{-/-}$ cells and aortas. Consistent with previous studies,[12] we also show impaired P_i-induced RUNX2-mediated osteogenic transdifferentiation in Pit-1 deficient TDAG51$^{-/-}$ VSMCs. Our studies also indicate that RUNX2 and Pit-1 mutually induce their expression to promote osteogenic differentiation. However, given the apparent cross-talk that occurs between RUNX2 and Pit-1, it is unclear whether TDAG51 regulates VC through (1) regulation of Pit-1 expression, (2) modulating RUNX2 transcriptional activity, or (3) whether both are affected by TDAG51. Therefore, further studies are necessary to elucidate the mechanism by which TDAG51 regulates these key drivers of VC.

In summary, we demonstrate that TDAG51 plays a central role in P_i-mediated calcification of the VSMCs. TDAG51 is induced in conditions of P_i-mediated osteogenic transdifferentiation, while loss of TDAG51 expression leads to a protective phenotype in both in vitro and in vivo models. Given the emerging role of TDAG51 in a variety of metabolic diseases known to contribute to VC,[28–32] additional tissue-specific knockout studies are required to further elucidate the mechanism by which the loss of TDAG51 protects against VC. Future studies examining the role of TDAG51 in CKD-mediated VC and in combination with high P_i feeding are also of interest.

ARTICLE INFORMATION

Received December 2, 2019; accepted May 4, 2020.

Affiliations

From the Division of Nephrology, Department of Medicine (K.P., P.F.L., G.G., Š.L., M.E.M., G.P., J.H.B., A.J.I., J.C.K., R.C.A.) and Department of Pathology and Molecular Medicine (J.-C.C.), McMaster University, and The Research Institute of St. Joseph's Hamilton, ON, Canada; and Department of Pathology and Molecular Medicine (F.J.B., S.A.I., D.B.) and Department of Biology (S.A.I.), McMaster University Medical Centre, Hamilton, ON, Canada.

Sources of Funding

This work was supported in part by research grants to R.C. Austin from the Heart and Stroke Foundation of Canada (G-13-0003064 and G-15-0009389) and the Canadian Institutes of Health Research (148539, 111239, and 126083) to R.C. Austin and J.C. Krepinsky from the CIHR (148539). Financial support from the Research Institute of St. Joseph's Healthcare Hamilton is acknowledged. R.C. Austin is a Career Investigator of the Heart and Stroke Foundation of Ontario and holds the Amgen Canada Research Chair in the Division of Nephrology at St. Joseph's Healthcare and McMaster University.

Disclosures

None.

REFERENCES

1. Sarnak MJ, Levey AS, Schoolwerth AC, Coresh J, Culleton B, Hamm LL, McCullough PA, Kasiske BL, Kelepouris E, Klag MJ, et al.; American Heart Association Councils on Kidney in Cardiovascular Disease, High Blood

Downloaded from http://ahajournals.org by on July 22, 2020

Pressure Research, Clinical Cardiology, and Epidemiology and Prevention. Kidney disease as a risk factor for development of cardiovascular disease: a statement from the American Heart Association Councils on Kidney in Cardiovascular Disease, High Blood Pressure Research, Clinical Cardiology, and Epidemiology and Prevention. *Circulation*. 2003;108:2154–2169. doi: 10.1161/01.CIR.0000095676.90936.80
2. Schiffrin EL, Lipman ML, Mann JF. Chronic kidney disease: effects on the cardiovascular system. *Circulation*. 2007;116:85–97. doi: 10.1161/CIRCULATIONAHA.106.678342
3. Block GA, Hulbert-Shearon TE, Levin NW, Port FK. Association of serum phosphorus and calcium x phosphate product with mortality risk in chronic hemodialysis patients: a national study. *Am J Kidney Dis*. 1998;31:607–617. doi: 10.1053/ajkd.1998.v31.pm9531176
4. Sigrist MK, Taal MW, Bungay P, McIntyre CW. Progressive vascular calcification over 2 years is associated with arterial stiffening and increased mortality in patients with stages 4 and 5 chronic kidney disease. *Clin J Am Soc Nephrol*. 2007;2:1241–1248. doi: 10.2215/CJN.02190507
5. McCullough PA, Agrawal V, Danielewicz E, Abela GS. Accelerated atherosclerotic calcification and Monckeberg's sclerosis: a continuum of advanced vascular pathology in chronic kidney disease. *Clin J Am Soc Nephrol*. 2008;3:1585–1598. doi: 10.2215/CJN.01930408
6. Abedin M, Tintut Y, Demer LL. Vascular calcification: mechanisms and clinical ramifications. *Arterioscler Thromb Vasc Biol*. 2004;24:1161–1170. doi: 10.1161/01.ATV.0000133194.94939.42
7. Jono S, Shioi A, Ikari Y, Nishizawa Y. Vascular calcification in chronic kidney disease. *J Bone Miner Metab*. 2006;24:176–181. doi: 10.1007/s00774-005-0668-6
8. Tölle M, Reshetnik A, Schuchardt M, Höhne M, van der Giet M. Arteriosclerosis and vascular calcification: causes, clinical assessment and therapy. *Eur J Clin Invest*. 2015;45:976–985. doi: 10.1111/eci.12493
9. Leopold JA. Vascular calcification: Mechanisms of vascular smooth muscle cell calcification. *Trends Cardiovasc Med*. 2015;25:267–274. doi: 10.1016/j.tcm.2014.10.021
10. Schlieper G, Aretz A, Verberckmoes SC, Krüger T, Behets GJ, Ghadimi R, Weirich TE, Rohrmann D, Langer S, Tordoir JH, et al. Ultrastructural analysis of vascular calcifications in uremia. *J Am Soc Nephrol*. 2010;21:689–696. doi: 10.1681/ASN.2009080829
11. Giachelli CM. The emerging role of phosphate in vascular calcification. *Kidney Int*. 2009;75:890–897. doi: 10.1038/ki.2008.644
12. Li X, Yang HY, Giachelli CM. Role of the sodium-dependent phosphate cotransporter, Pit-1, in vascular smooth muscle cell calcification. *Circ Res*. 2006;98:905–912. doi: 10.1161/01.RES.0000216409.20863.e7
13. Crouthamel MH, Lau WL, Leaf EM, Chavkin NW, Wallingford MC, Peterson DF, Li X, Liu Y, Chin MT, Levi M, et al. Sodium-dependent phosphate cotransporters and phosphate-induced calcification of vascular smooth muscle cells: redundant roles for PiT-1 and PiT-2. *Arterioscler Thromb Vasc Biol*. 2013;33:2625–2632. doi: 10.1161/ATVBAHA.113.302249
14. Koleganova N, Piecha G, Ritz E, Schirmacher P, Müller A, Meyer HP, Gross ML. Arterial calcification in patients with chronic kidney disease. *Nephrol Dial Transplant*. 2009;24:2488–2496. doi: 10.1093/ndt/gfp137
15. Liu TM, Lee EH. Transcriptional regulatory cascades in Runx2-dependent bone development. *Tissue Eng Part B Rev*. 2013;19:254–263. doi: 10.1089/ten.TEB.2012.0527
16. Jono S, McKee MD, Murry CE, Shioi A, Nishizawa Y, Mori K, Morii H, Giachelli CM. Phosphate regulation of vascular smooth muscle cell calcification. *Circ Res*. 2000;87:E10–E17. doi: 10.1161/01.res.87.7.e10
17. Graciolli FG, Neves KR, dos Reis LM, Graciolli RG, Noronha IL, Moysés RM, Jorgetti V. Phosphorus overload and PTH induce aortic expression of Runx2 in experimental uraemia. *Nephrol Dial Transplant*. 2009;24:1416–1421. doi: 10.1093/ndt/gfn686
18. Zhang X, Yang M, Lin L, Chen P, Ma KT, Zhou CY, Ao YF. Runx2 overexpression enhances osteoblastic differentiation and mineralization in adipose–derived stem cells *in vitro* and in vivo. *Calcif Tissue Int*. 2006;79:169–178. doi: 10.1007/s00223-006-0083-6
19. Byon CH, Javed A, Dai Q, Kappes JC, Clemens TL, Darley-Usmar VM, McDonald JM, Chen Y. Oxidative stress induces vascular calcification through modulation of the osteogenic transcription factor Runx2 by AKT signaling. *J Biol Chem*. 2008;283:15319–15327. doi: 10.1074/jbc.M800021200
20. Steitz SA, Speer MY, Curinga G, Yang HY, Haynes P, Aebersold R, Schinke T, Karsenty G, Giachelli CM. Smooth muscle cell phenotypic transition associated with calcification: upregulation of Cbfa1 and downregulation of smooth muscle lineage markers. *Circ Res*. 2001;89:1147–1154. doi: 10.1161/hh2401.101070
21. Komori T, Yagi H, Nomura S, Yamaguchi A, Sasaki K, Deguchi K, Shimizu Y, Bronson RT, Gao YH, Inada M, et al. Targeted disruption of Cbfa1 results in a complete lack of bone formation owing to maturational arrest of osteoblasts. *Cell*. 1997;89:755–764. doi: 10.1016/s0092-8674(00)80258-5
22. Sun Y, Byon CH, Yuan K, Chen J, Mao X, Heath JM, Javed A, Zhang K, Anderson PG, Chen Y. Smooth muscle cell-specific runx2 deficiency inhibits vascular calcification. *Circ Res*. 2012;111:543–552. doi: 10.1161/CIRCRESAHA.112.267237
23. Lin ME, Chen T, Leaf EM, Speer MY, Giachelli CM. Runx2 Expression in Smooth Muscle Cells Is Required for Arterial Medial Calcification in Mice. *Am J Pathol*. 2015;185:1958–1969. doi: 10.1016/j.ajpath.2015.03.020
24. Nagai MA. Pleckstrin homology-like domain, family A, member 1 (PHLDA1) and cancer. *Biomed Rep*. 2016;4:275–281. doi: 10.3892/br.2016.580
25. Park CG, Lee SY, Kandala G, Lee SY, Choi Y. A novel gene product that couples TCR signaling to Fas(CD95) expression in activation-induced cell death. *Immunity*. 1996;4:583–591. doi: 10.1016/s1074-7613(00)80484-7
26. Frank D, Mendelsohn CL, Ciccone E, Svensson K, Ohlsson R, Tycko B. A novel pleckstrin homology-related gene family defined by Ipl/Tssc3, TDAG51, and Tih1: tissue-specific expression, chromosomal location, and parental imprinting. *Mamm Genome*. 1999;10:1150–1159. doi: 10.1007/s003359901182
27. Gomes I, Xiong W, Miki T, Rosner MR. A proline- and glutamine-rich protein promotes apoptosis in neuronal cells. *J Neurochem*. 1999;73:612–622. doi: 10.1046/j.1471-4159.1999.0730612.x
28. Hossain GS, van Thienen JV, Werstuck GH, Zhou J, Sood SK, Dickhout JG, de Koning AB, Tang D, Wu D, Falk E, et al. TDAG51 is induced by homocysteine, promotes detachment-mediated programmed cell death, and contributes to the cevelopment of atherosclerosis in hyperhomocysteinemia. *J Biol Chem*. 2003;278:30317–30327. doi: 10.1074/jbc.M212897200
29. Dickhout JG, Hossain GS, Pozza LM, Zhou J, Lhoták S, Austin RC. Peroxynitrite causes endoplasmic reticulum stress and apoptosis in human vascular endothelium: implications in atherogenesis. *Arterioscler Thromb Vasc Biol*. 2005;25:2623–2629. doi: 10.1161/01.ATV.0000189159.96900.d9
30. Zhou J, Lhoták S, Hilditch BA, Austin RC. Activation of the unfolded protein response occurs at all stages of atherosclerotic lesion development in apolipoprotein E-deficient mice. *Circulation*. 2005;111:1814–1821. doi: 10.1161/01.CIR.0000160864.31351.C1
31. Hossain GS, Lynn EG, Maclean KN, Zhou J, Dickhout JG, Lhoták S, Trigatti B, Capone J, Rho J, Tang D, et al. Deficiency of TDAG51 protects against atherosclerosis by modulating apoptosis, cholesterol efflux, and peroxiredoxin-1 expression. *J Am Heart Assoc*. 2013;2:e000134. doi: 10.1161/JAHA.113.000134
32. Dai G, Kaazempur-Mofrad MR, Natarajan S, Zhang Y, Vaughn S, Blackman BR, Kamm RD, García-Cardeña G, Gimbrone MA Jr. Distinct endothelial phenotypes evoked by arterial waveforms derived from atherosclerosis-susceptible and -resistant regions of human vasculature. *Proc Natl Acad Sci U S A*. 2004;101:14871–14876. doi: 10.1073/pnas.0406073101
33. Wellcome Trust Case Control Consortium. Genome-wide association study of 14,000 cases of seven common diseases and 3,000 shared controls. *Nature*. 2007;447:661–678
34. Shiffman D, Kane JP, Louie JZ, Arellano AR, Ross DA, Catanese JJ, Malloy MJ, Ellis SG, Devlin JJ. Analysis of 17,576 potentially functional SNPs in three case-control studies of myocardial infarction. *PLoS One*. 2008;3:e2895. doi: 10.1371/journal.pone.0002895
35. Rho J, Gong S, Kim N, Choi Y. TDAG51 is not essential for Fas/CD95 regulation and apoptosis in vivo. *Mol Cell Biol*. 2001;21:8365–8370. doi: 10.1128/MCB.21.24.8365-8370.2001
36. Basseri S, Lhoták S, Fullerton MD, Palanivel R, Jiang H, Lynn EG, Ford RJ, Maclean KN, Steinberg GR, Austin RC. Loss of TDAG51 results in mature-onset obesity, hepatic steatosis, and insulin resistance by regulating lipogenesis. *Diabetes*. 2013;62:158–169. doi: 10.2337/db12-0256
37. Gallagher JC, Riggs BL, DeLuca HF. Effect of estrogen on calcium absorption and serum vitamin D metabolites in postmenopausal osteoporosis. *J Clin Endocrinol Metab*. 1980;51:1359–1364. doi: 10.1210/jcem-51-6-1359
38. Kang YH, Jin JS, Yi DW, Son SM. Bone morphogenetic protein-7 inhibits vascular calcification induced by high vitamin D in mice. *Tohoku J Exp Med*. 2010;221:299–307. doi: 10.1620/tjem.221.299
39. Price PA, June HH, Buckley JR, Williamson MK. Osteoprotegerin inhibits artery calcification induced by warfarin and by vitamin D. *Arterioscler Thromb Vasc Biol*. 2001;21:1610–1616. doi: 10.1161/hq1001.097102
40. Metz RP, Patterson JL, Wilson E. Vascular smooth muscle cells: isolation, culture, and characterization. *Methods Mol Biol*. 2012;843:169–176. doi: 10.1007/978-1-61779-523-7_16

Downloaded from http://ahajournals.org by on July 22, 2020

41. Akiyoshi T, Ota H, Iijima K, Son BK, Kahyo T, Setou M, Ogawa S, Ouchi Y, Akishita M. A novel organ culture model of aorta for vascular calcification. *Atherosclerosis*. 2016;244:51–58. doi: 10.1016/j.atherosclerosis.2015.11.005
42. Reynolds JL, Joannides AJ, Skepper JN, McNair R, Schurgers LJ, Proudfoot D, Jahnen-Dechent W, Weissberg PL, Shanahan CM. Human vascular smooth muscle cells undergo vesicle-mediated calcification in response to changes in extracellular calcium and phosphate concentrations: a potential mechanism for accelerated vascular calcification in ESRD. *J Am Soc Nephrol*. 2004;15:2857–2867. doi: 10.1097/01.ASN.0000141960.01035.28
43. El-Abbadi MM, Pai AS, Leaf EM, Yang HY, Bartley BA, Quan KK, Ingalls CM, Liao HW, Giachelli CM. Phosphate feeding induces arterial medial calcification in uremic mice: role of serum phosphorus, fibroblast growth factor-23, and osteopontin. *Kidney Int*. 2009;75:1297–1307. doi: 10.1038/ki.2009.83
44. Lomashvili K, Garg P, O'Neill WC. Chemical and hormonal determinants of vascular calcification *in vitro*. *Kidney Int*. 2006;69:1464–1470. doi: 10.1038/sj.ki.5000297
45. Puchtler H, Meloan SN, Terry MS. On the history and mechanism of alizarin and alizarin red S stains for calcium. *J Histochem Cytochem*. 1969;17:110–124. doi: 10.1177/17.2.110
46. Ducy P, Zhang R, Geoffroy V, Ridall AL, Karsenty G. Osf2/Cbfa1: a transcriptional activator of osteoblast differentiation. *Cell*. 1997;89:747–754. doi: 10.1016/s0092-8674(00)80257-3
47. Speer MY, McKee MD, Guldberg RE, Liaw L, Yang HY, Tung E, Karsenty G, Giachelli CM. Inactivation of the osteopontin gene enhances vascular calcification of matrix Gla protein-deficient mice: evidence for osteopontin as an inducible inhibitor of vascular calcification in vivo. *J Exp Med*. 2002;196:1047–1055. doi: 10.1084/jem.20020911
48. Sellheyer K, Cribier B, Nelson P, Kutzner H, Rütten A. Basaloid tumors in nevus sebaceus revisited: the follicular stem cell marker PHLDA1 (TDAG51) indicates that most are basal cell carcinomas and not trichoblastomas. *J Cutan Pathol*. 2013;40:455–462. doi: 10.1111/cup.12107
49. Janzen J, Vuong PN. Arterial calcifications: morphological aspects and their pathological implications. *Z Kardiol*. 2001;90(Suppl 3):6–11. doi: 10.1007/s003920170044
50. Lanzer P, Boehm M, Sorribas V, Thiriet M, Janzen J, Zeller T, St Hilaire C, Shanahan C. Medial vascular calcification revisited: review and perspectives. *Eur Heart J*. 2014;35:1515–1525. doi: 10.1093/eurheartj/ehu163
51. Hedman K, Kurkinen M, Alitalo K, Vaheri A, Johansson S, Höök M. Isolation of the pericellular matrix of human fibroblast cultures. *J Cell Biol*. 1979;81:83–91. doi: 10.1083/jcb.81.1.83
52. Vimalraj S, Arumugam B, Miranda PJ, Selvamurugan N. Runx2: Structure, function, and phosphorylation in osteoblast differentiation. *Int J Biol Macromol*. 2015;78:202–208. doi: 10.1016/j.ijbiomac.2015.04.008
53. Chavkin NW, Chia JJ, Crouthamel MH, Giachelli CM. Phosphate uptake-independent signaling functions of the type III sodium-dependent phosphate transporter, PiT-1, in vascular smooth muscle cells. *Exp Cell Res*. 2015;333:39–48. doi: 10.1016/j.yexcr.2015.02.002
54. Li X, Giachelli CM. Sodium-dependent phosphate cotransporters and vascular calcification. *Curr Opin Nephrol Hypertens*. 2007;16:325–328. doi: 10.1097/MNH.0b013e3281c55ef1
55. Mizobuchi M, Ogata H, Hatamura I, Koiwa F, Saji F, Shiizaki K, Negi S, Kinugasa E, Ooshima A, Koshikawa S, et al. Up-regulation of Cbfa1 and Pit-1 in calcified artery of uraemic rats with severe hyperphosphataemia and secondary hyperparathyroidism. *Nephrol Dial Transplant*. 2006;21:911–916. doi: 10.1093/ndt/gfk008
56. Carlisle RE, Heffernan A, Brimble E, Liu L, Jerome D, Collins CA, Mohammed-Ali Z, Margetts PJ, Austin RC, Dickhout JG. TDAG51 mediates epithelial-to-mesenchymal transition in human proximal tubular epithelium. *Am J Physiol Renal Physiol*. 2012;303:F467–F481. doi: 10.1152/ajprenal.00481.2011
57. Joo JH, Liao G, Collins JB, Grissom SF, Jetten AM. Farnesol-induced apoptosis in human lung carcinoma cells is coupled to the endoplasmic reticulum stress response. *Cancer Res*. 2007;67:7929–7936. doi: 10.1158/0008-5472.CAN-07-0931
58. Wang J, Wang F, Zhu J, Song M, An J, Li W. Transcriptome Profiling Reveals PHLDA1 as a Novel Molecular Marker for Ischemic Cardiomyopathy. *J Mol Neurosci*. 2018;65:102–109. doi: 10.1007/s12031-018-1066-6
59. Zhang S, Xiao Z, Luo J, He N, Mahlios J, Quarles LD. Dose-dependent effects of Runx2 on bone development. *J Bone Miner Res*. 2009;24:1889–1904. doi: 10.1359/jbmr.090502
60. Ko FC, Martins JS, Reddy P, Bragdon B, Hussein AI, Gerstenfeld LC, Demay MB. Acute Phosphate Restriction Impairs Bone Formation and Increases Marrow Adipose Tissue in Growing Mice. *J Bone Miner Res*. 2016;31:2204–2214. doi: 10.1002/jbmr.2891
61. Liu Z, Yao X, Yan G, Xu Y, Yan J, Zou W, Wang G. Mediator MED23 cooperates with RUNX2 to drive osteoblast differentiation and bone development. *Nat Commun*. 2016;7:11149. doi: 10.1038/ncomms11149
62. Cheng SL, Shao JS, Charlton-Kachigian N, Loewy AP, Towler DA. MSX2 promotes osteogenesis and suppresses adipogenic differentiation of multipotent mesenchymal progenitors. *J Biol Chem*. 2003;278:45969–45977. doi: 10.1074/jbc.M306972200
63. Chertow GM, Burke SK, Raggi P; Treat to Goal Working Group. Sevelamer attenuates the progression of coronary and aortic calcification in hemodialysis patients. *Kidney Int*. 2002;62:245–252. doi: 10.1046/j.1523-1755.2002.00434.x
64. Russo D, Miranda I, Ruocco C, Battaglia Y, Buonanno E, Manzi S, Russo L, Scafarto A, Andreucci VE. The progression of coronary artery calcification in predialysis patients on calcium carbonate or sevelamer. *Kidney Int*. 2007;72:1255–1261. doi: 10.1038/sj.ki.5002518

Downloaded from http://ahajournals.org by on July 22, 2020

SUPPLEMENTAL MATERIALS

TDAG51 is a key modulator of vascular calcification and osteogenic transdifferentiation of arterial smooth muscle cells

Khrystyna Platko[§], Paul F. Lebeau[§], Gabriel Gyulay[§], Šárka Lhoták[§], Melissa E. MacDonald[§], Giusepina Pacher[§], Jae Hyun Byun[§], Felix J. Boivin[¶],Suleiman A. Igdoura[¶,#], Jean-Claude Cutz[‡] *Darren Bridgewater[2], Alistair J. Ingram[§], Joan C. Krepinsky[§*], Richard C. Austin[§*,†]*

Authors Affiliations: [§]Department of Medicine, Division of Nephrology and [‡]Department of Pathology and Molecular Medicine, McMaster University, and The Research Institute of St. Joseph's Hamilton, Hamilton, Ontario L8N 4A6, Canada. The [¶]Department of Pathology and Molecular Medicine and [#]Biology, McMaster University Medical Centre, Hamilton, Ontario, L8N 3Z5, Canada.

* Contributed equally to this work

[†] **Corresponding Author:** To whom correspondence should be addressed: Dr. Richard C. Austin, 50 Charlton Ave East, Room T-3313, Hamilton, Ontario, L8N 4A6. Phone: 905-522-1155 x35175; Fax: 905-540-6589; E-mail: austinr@taari.ca

Materials and Methods

Immunoblotting

Whole cell and tissue lysates were prepared using RIPA buffer containing protease inhibitors (Roche). Protein concentrations were measured using a modified Lowry assay (Bio-Rad). The samples were resolved by SDS-PAGE and subsequently transferred to nitrocellulose membranes (Bio-Rad). The membranes were then blocked using 5% w/v skimmed milk, incubated with primary antibodies, followed by horseradish peroxidase-conjugated secondary antibodies. The signal was detected using a Konica Minolta X-ray film processor or ChemiDoc XRS+ (Bio-Rad). Band intensity was measured by densitometry analysis using ImageLab software and normalized to membranes against respective loading control proteins (Bio-Rad). Genotype is indicated as +/+ and -/- for TDAG51$^{+/+}$ and TDAG51$^{-/-}$, respectively. All antibodies and working dilutions are listed in Supplemental Table IV.

Immunohistochemical (IHC) staining

4 µm thick sections were deparaffinized, blocked in 5% v/v serum and subsequently incubated in primary antibodies for 18 h at 4°C. Sections were then exposed to biotin-labeled secondary antibodies (Vector Laboratories). Streptavidin-labeled HRP solution (Vector Laboratories) and the developing solution (Vector Laboratories) were used to visualize the staining. Slides were examined using a Nikon light microscope. All antibodies and working dilutions are listed in Supplemental Table IV.

Immunofluorescence (IF) of cells

VSMCs were fixed for 1 h using 4% w/v PFA and then permeabilized with 0.025% v/v Triton X-100 for 15 min. After blocking with 5% v/v bovine serum albumin (BSA), cells were incubated with primary antibodies for 1 h at room temperature and stained with the appropriate fluorescently labeled secondary antibodies (Invitrogen) and DAPI. Slides were mounted with Permafluor (ThermoFisher Scientific) and visualized using a fluorescent microscope (EVOS-FL, ThermoFisher Scientific). All primary and secondary antibodies and working dilutions are listed in Supplemental Table IV and Supplemental Table VI, respectively.

Quantitative real-time (qRT)-PCR

qRT-PCR was performed as described previously [1]. Briefly, total RNA was isolated using RNA purification kits (ThermoFisher Scientific). A total of 2 µg of RNA was reverse transcribed to produce cDNA using the High-Capacity cDNA Reverse Transcription Kit (ThermoFisher Scientific). PCR amplification was performed using Fast SYBR Green (ThermoFisher Scientific). Transcript levels were determined using the ΔΔCT method and normalized to 18S. All primer sequences are listed in Supplemental Table III.

Extracellular matrix (ECM) isolation

ECM was isolated from TDAG51$^{+/+}$ VSMCs following 5 days of 2.6 mM Pi treatment using sequential extraction with sodium deoxycholate (DOC).[2] Briefly, cells were washed three times with cold PBS and subsequently lysed in DOC lysis buffer (0.5% DOC, 50 mM Tris pH 8.0, 150 mM NaCl, 1% Nonidet P-40) containing protease inhibitors (Roche) for 10 minutes. Lysis buffer was replaced with fresh DOC lysis buffer for additional 10 minutes followed by three PBS washes. The ECM isolates were then used for quantification of Ca^{2+} and HA deposition, which

were normalized to protein content or cell number, respectively. The quality of ECM preparation was examined by nuclear staining using DAPI (Sigma-Aldrich).

LDH Cytotoxicity assay

A Cytotoxicity Detection Kit (Roche) was used to measure cell death by detecting lactate dehydrogenase (LDH) release into the culture medium, indicating cell membrane permeability. Media was removed from cells and LDH activity was measured at 492 nm using a microplate reader (Molecular Devices), where cytotoxicity (%) = [(experimental value−low control)/(high control−low control)] × 100%.

Blood pressure and serum biochemistry

Blood pressure was measured by the noninvasive CODA tail-cuff method (Kent Scientific Corporation). Serum P_i and Ca^{2+} content was measured by the Core Laboratory Facility at St. Joseph's Healthcare Hamilton.

Fluorescent *in situ* hybridization (FISH)

FISH for PHLDA1, a human homologue of TDAG51,[3] and α-SMA was performed using the Affymetrix QuantiGene ViewRNA assay (ThermoFisher Scientific). Briefly, 5 µm sections were deparaffinized, boiled in pre-treatment solution and digested with Proteinase K. Sections were then incubated with a PHLDA1 probe for 2 h at 40°C. The signal was amplified with Pre-Amp and Amp solutions (ThermoFisher Scientific) and then developed with Fast-Red and Fast-Blue Substrates (ThermoFisher Scientific). Slides were counterstained with DAPI (Sigma-Aldrich), mounted with Fluoromount (ThermoFisher Scientific) and photographed on a Nikon 90i-eclipse upright fluorescent microscope.

Major Resources Tables

Table I: Animal (in vivo studies)

Species	Vendor or Source	Background Strain	Sex
TDAG51$^{+/+}$ and $^{-/-}$ Mice	Bred in-house	C57BL/6J	Male

Table II: Breeding of genetically modified animals

	Species	Vendor or Source	Background Strain	Other Information
Parent – Male	TDAG51$^{+/-}$ Mouse	Bred in-house	C57BL/6J	TDAG51$^{-/-}$ mice were generated as previously described.[4]
Parent – Female	TDAG51$^{+/-}$ Mouse	Bred in-house	C57BL/6J	

Table III: List of primers used for quantitative real-time PCR

Gene	Species	Forward	Reverse
PHLDA1	Human	GAAGATGGCCCATTCAAAAGCG	GAGGAGGCTAACACGCAGG
18S	Human	GTAACCCGTTGAACCCCATT	CCATCCAATCGGTAGTAGCG
18S	Mouse	CTTAGAGGGACAAGTGGCG	ACGCTGAGCCAGTCAGTGTA
Pit-1	Mouse	TTTGACAAACTTCCTCTGTGGG	GGACTTTCAGACGGACTAGACTT
mGLA	Mouse	GGCAACCCTGTGCTACGAAT	CCTGGACTCTCTTTTGGGCTTTA
OPG	Mouse	ACCCAGAAACTGGTCATCAGC	CTGCAATACACACACTCATCACT
OPN	Mouse	AGCAAGAAACTCTTCCAAGCAA	GTGAGATTCGTCAGATTCATCCG
OCN	Mouse	GCAATAAGGTAGTGAACAGACTCC	GTTTGTAGGCGGTCTTCAAGC
ALP	Mouse	CCAACTCTTTTGTGCCAGAGA	GGCTACATTGGTGTTGAGCTTTT
BMP-2	Mouse	TCTTCCGGGAACAGATACAGG	TGGTGTCCAATAGTCTGGTCA
Osx	Mouse	ATGGCGTCCTCTCTGCTTG	TGAAAGGTCAGCGTATGGCTT
RUNX2	Mouse	ATGCTTCATTCGCCTCACAAA	GCACTCACTGACTCGGTTGG

Table IV: List of antibodies used for immunoblotting (IB), immunohistochemistry (IHC) and immunofluorescent (IF) staining

Target antigen	Vendor or Source	Catalog #	Working concentration	Persistent ID / URL
CD31	R&D Systems	AF3628	IF: 1 µg/ml	https://www.rndsystems.com/products/mouse-rat-cd31-pecam-1-antibody_af3628
GAPDH	Cell Signaling Technology	5174	IB: 0.34 µg/ml	https://www.cellsignal.com/products/primary-antibodies/gapdh-d16h11-xp-rabbit-mab/5174
Histone H3	Cell Signaling Technology	4499	IB: 0.12 µg/ml	https://www.cellsignal.com/products/primary-antibodies/histone-h3-d1h2-xp-rabbit-mab/4499
Lamin B1	Abcam	ab16048	IB: 1 µg/ml	https://www.abcam.com/lamin-b1-antibody-nuclear-envelope-marker-ab16048.html
MSX2	Novus Biologicals	NBP1-85445	IB: 0.2 µg/ml IF: 0.4 µg/ml IHC: 0.4 µg/ml	https://www.novusbio.com/products/msx2-antibody_nbp1-85445
OCN	Abcam	ab93876	IF: 1.0 µg/ml IHC: 1.0 µg/ml	https://www.abcam.com/osteocalcin-antibody-ab93876.html
PHLDA1	Proteintech	18263-1AP	IP: 2 µg/ml	https://www.ptglab.com/products/PHLDA1-Antibody-18263-1-AP.htm
Pit-1	Abcam	ab177147	IB: 0.094 µg/ml IF: 0.188 µg/ml IHC: 0.188 µg/ml	https://www.abcam.com/slc20a1-antibody-epr114272-ab177147.html
Pit-2	Sant Cruz Biotechnology	SC-377326	IB:0.2 µg/ml	https://www.scbt.com/p/pit2-antibody-b-4
RUNX2	Cell Signaling Technology	8486	IB: 1.82 µg/ml	https://www.cellsignal.com/products/primary-antibodies/runx2-d1h7-rabbit-mab/8486
RUNX2	Abcam	ab192256	IF: 0.548 µg/ml IHC: 0.548 µg/ml	https://www.abcam.com/runx2-antibody-epr14334-ab192256.html
pSer	Abcam	ab9332	IB: 0.5 µg/ml	https://www.abcam.com/phosphoserine-antibody-ab9332.html
TDAG51	Sant Cruz Biotechnology	SC-23866	IB: 0.4 µg/ml IF: 0.2 µg/ml	https://www.scbt.com/p/tdag51-antibody-rn-6e2

α-SMA	Abcam	ab7817	IB: 1.0 µg/ml IF: 1.0 µg/ml	https://www.abcam.com/alpha-smooth-muscle-actin-antibody-1a4-ab7817.html

Table V: RUNX2 promoter binding assay oligonucleotide sequence and primers used for PCR

Primer set	Sequence
RUNX2 promoter oligonucleotide sequence	5'TTCCTCGGGGTGCTCTTTTTAACCACACTGGAATCAATGCAAGTTCGGT3'
PCR Primers	Forward: AAGGAGCCCCACGAGAAAAAT
	Reverse: ACCGAACTTGCATTGATTCCAG

Table VI: List of secondary antibodies used for IF

Antibody	Vendor	Product #	Working Concentration	URL
Goat anti-Rabbit IgG (H+L) Cross-Absorbed Secondary Antibody, Alexa Flour 488	ThermoFisher Scientific	A11008	1 µg/ml	https://www.thermofisher.com/antibody/product/Goat-anti-Rabbit-IgG-H-L-Cross-Adsorbed-Secondary-Antibody-Polyclonal/A-11008
Goat anti-Mouse IgG (H+L) Highly Cross-Absorbed Secondary Antibody, Alexa Flour 647	ThermoFisher Scientific	A32728	1 µg/ml	https://www.thermofisher.com/antibody/product/Goat-anti-Mouse-IgG-H-L-Highly-Cross-Adsorbed-Secondary-Antibody-Polyclonal/A32728
Donkey anti-Goat IgG (H+L) Highly Cross-Absorbed Secondary Antibody, Alexa Flour 488	ThermoFisher Scientific	A32814	1 µg/ml	https://www.thermofisher.com/antibody/product/Donkey-anti-Goat-IgG-H-L-Highly-Cross-Adsorbed-Secondary-Antibody-Polyclonal/A32814
Donkey anti-Rabbit IgG (H+L) Highly Cross-Absorbed Secondary Antibody, Alexa Flour 594	ThermoFisher Scientific	A21207	1 µg/ml	https://www.thermofisher.com/antibody/product/Donkey-anti-Rabbit-IgG-H-L-Highly-Cross-Adsorbed-Secondary-

				Antibody-Polyclonal/A-21207
Goat anti-Mouse IgG (H+L) Highly Cross-Absorbed Secondary Antibody, Alexa Flour 488	ThermoFisher Scientific	A32723	1 µg/ml	https://www.thermofisher.com/antibody/product/Goat-anti-Mouse-IgG-H-L-Highly-Cross-Adsorbed-Secondary-Antibody-Polyclonal/A32723

REFERENCES

1. Hossain GS, Lynn EG, Maclean KN, Zhou J, Dickhout JG, Lhotak S, Trigatti B, Capone J, Rho J, Tang D, McCulloch CA, Al-Bondokji I, Malloy MJ, Pullinger CR, Kane JP, Li Y, Shiffman D, Austin RC. Deficiency of tdag51 protects against atherosclerosis by modulating apoptosis, cholesterol efflux, and peroxiredoxin-1 expression. *J Am Heart Assoc*. 2013;2:e000134
2. Hedman K, Kurkinen M, Alitalo K, Vaheri A, Johansson S, Hook M. Isolation of the pericellular matrix of human fibroblast cultures. *The Journal of cell biology*. 1979;81:83-91
3. Nagai MA. Pleckstrin homology-like domain, family a, member 1 (phlda1) and cancer. *Biomed Rep*. 2016;4:275-281
4. Rho J, Gong S, Kim N, Choi Y. Tdag51 is not essential for fas/cd95 regulation and apoptosis in vivo. *Molecular and cellular biology*. 2001;21:8365-8370

SUPPLEMENTAL FIGURES AND FIGURE LEGENDS

Supplemental Figure I

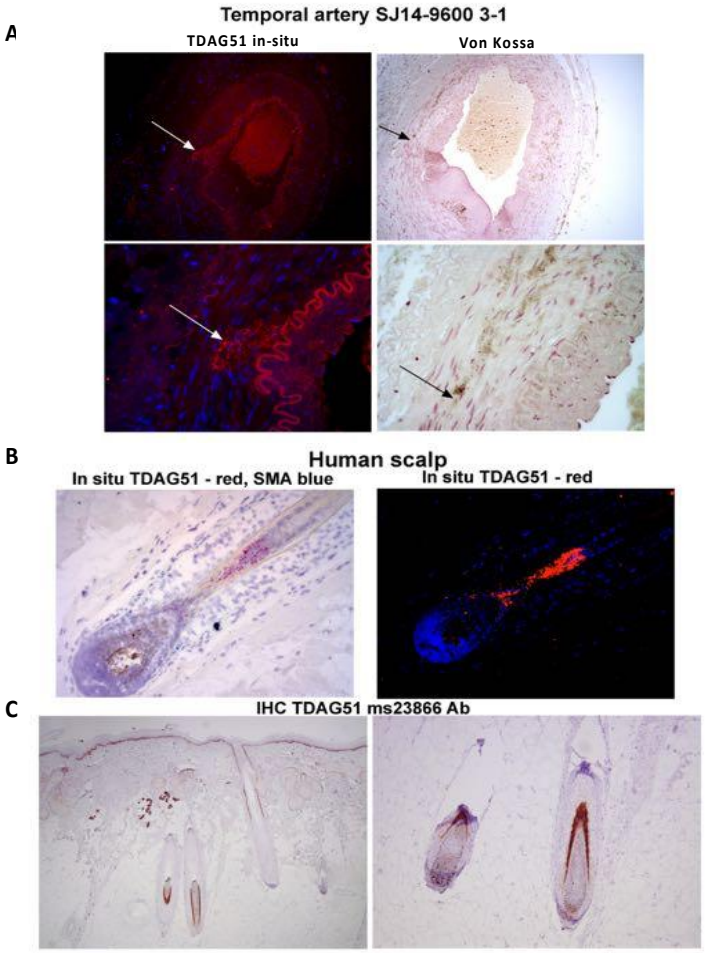

Supplemental Figure I. TDAG51 expression in human temporal arteries and FISH probe validation. (**A**) Representative micrograph of PHLDA1 (human homologue) FISH and von Kossa staining in serial sections of a human temporal artery. (**B**) TDAG51 and α-SMA *in situ* hybridization in human scalp tissue. (**C**) IHC staining of TDAG51 in human scalp tissue.

Supplemental Figure II

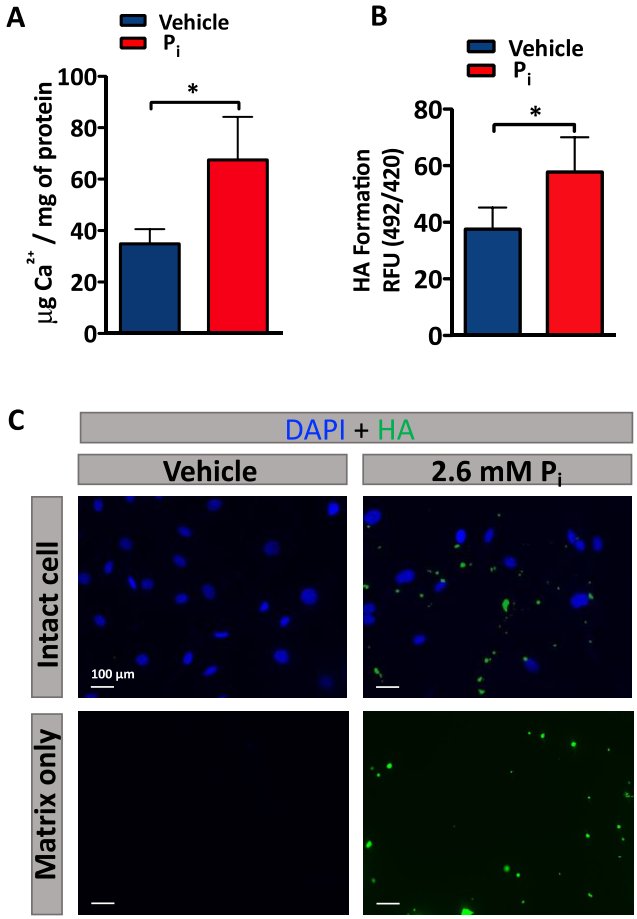

Supplemental Figure II. Quantification of mineral deposition in the extracellular matrix in TDAG51$^{+/+}$ VSMCs. (**A,B**) Quantification of Ca^{2+} and HA deposition in the extracellular matrix of TDAG51$^{+/+}$ VSMCs following 5 days of 2,6 mM P_i treatment (n=8 and n=8). (**C**) Nuclei (DAPI) and HA staining in the intact TDAG51$^{+/+}$ VSMCs as well as ECM matrix isolates.

Supplemental Figure II

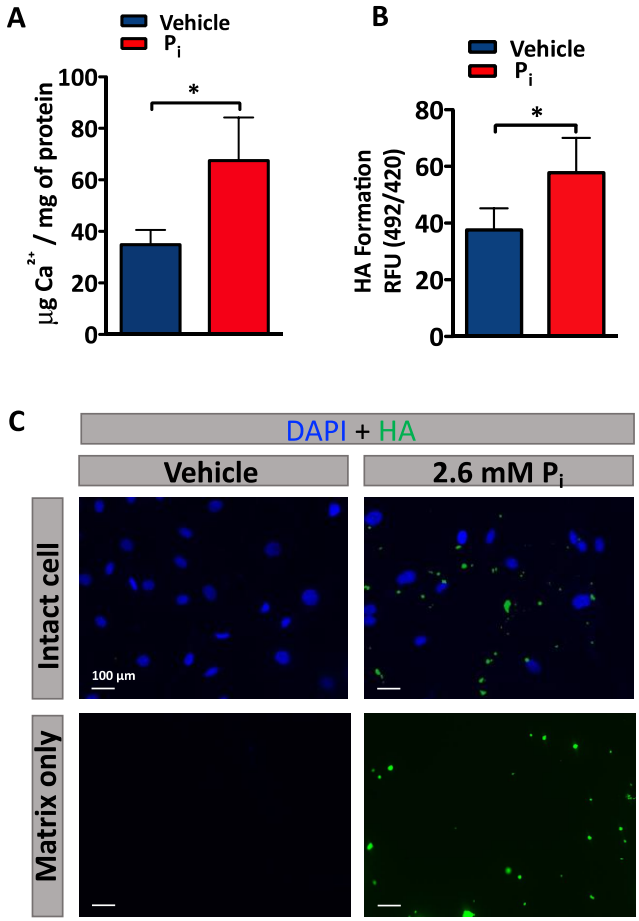

Supplemental Figure II. Quantification of mineral deposition in the extracellular matrix in TDAG51$^{+/+}$ VSMCs. (**A,B**) Quantification of Ca^{2+} and HA deposition in the extracellular matrix of TDAG51$^{+/+}$ VSMCs following 5 days of 2,6 mM P_i treatment (n=8 and n=8). (**C**) Nuclei (DAPI) and HA staining in the intact TDAG51$^{+/+}$ VSMCs as well as ECM matrix isolates.

Supplemental Figure III

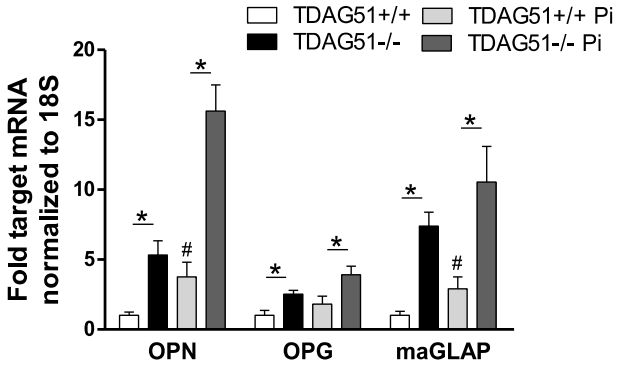

Supplemental Figure III. Expression of inhibitors of osteogenesis in TDAG51$^{+/+}$ and TDAG51$^{-/-}$ VSMCs. Quantitative real-time PCR of mRNA expression of the calcification inhibitors Osteopontin (OPN), Osteoprotegerin (OPG) and matrix Gla Protein (maGLAP) following 2 days of 2.6 mM P_i treatment. *p<0.05 compared to respective TDAG51$^{+/+}$ controls. # p<0.05 compared to TDAG51$^{+/+}$ untreated (n=4 per group).

Supplemental Figure IV

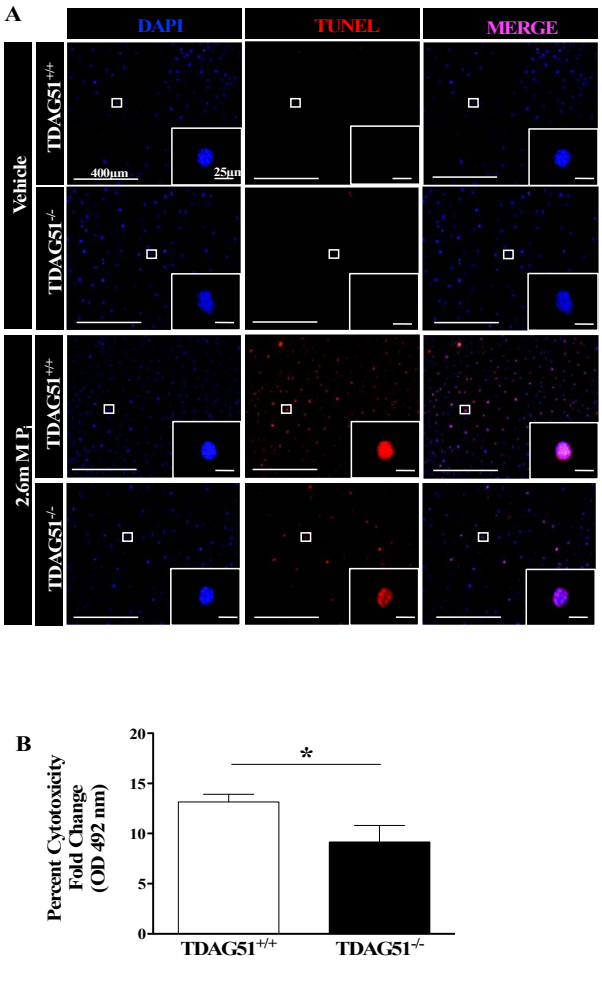

Supplemental Figure IV. TDAG51$^{-/-}$ VSMCs exhibit reduced Pi-mediated apoptotic cell death. TDAG51$^{+/+}$ and TDAG51$^{-/-}$ **VSMCs** were treated with 2.6 mM phosphate for 3 days. (**A**) Detection of DNA fragmentation indicative of apoptotic cell death using the TUNEL labeling method. (**B**) Lactase Dehydrogenase (LDH) cytotoxicity assay in cells treated with P_i. * $p<0.05$ (n=4 per group).

Supplemental Figure V

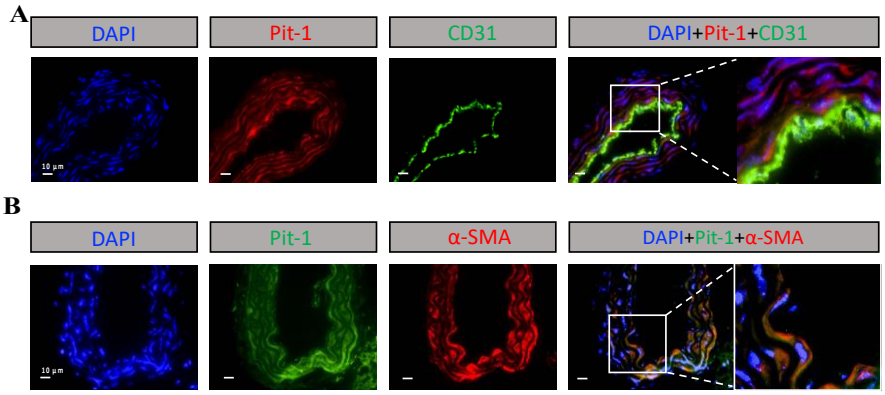

Supplemental Figure V. Colocalization of Pit-1 with endothelial and VSMC markers. (**A**) Immunofluorescence co-staining of Pit-1 (red), endothelial cell marker CD31 (green) and nuclei using DAPI (blue). (**B**) Immunofluorescence co-staining of Pit-1 (green), smooth muscle cell marker α-SMA (red) and nuclei using DAPI (blue).

Supplemental Figure VI

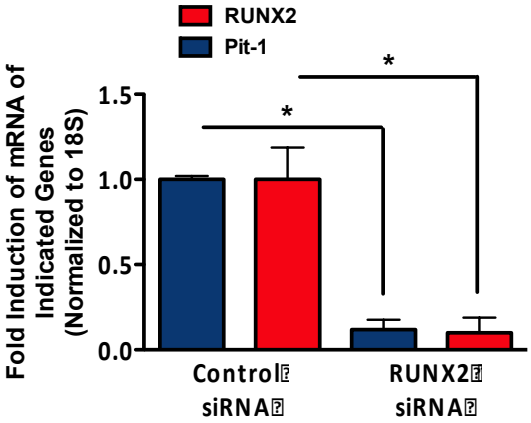

Supplemental Figure VI. Quantitative real-time PCR analysis of Pit-1 and RUNX2 mRNA in cultured mouse VSMCs. * $p<0.05$, n=5 per group

Supplemental Figure VII

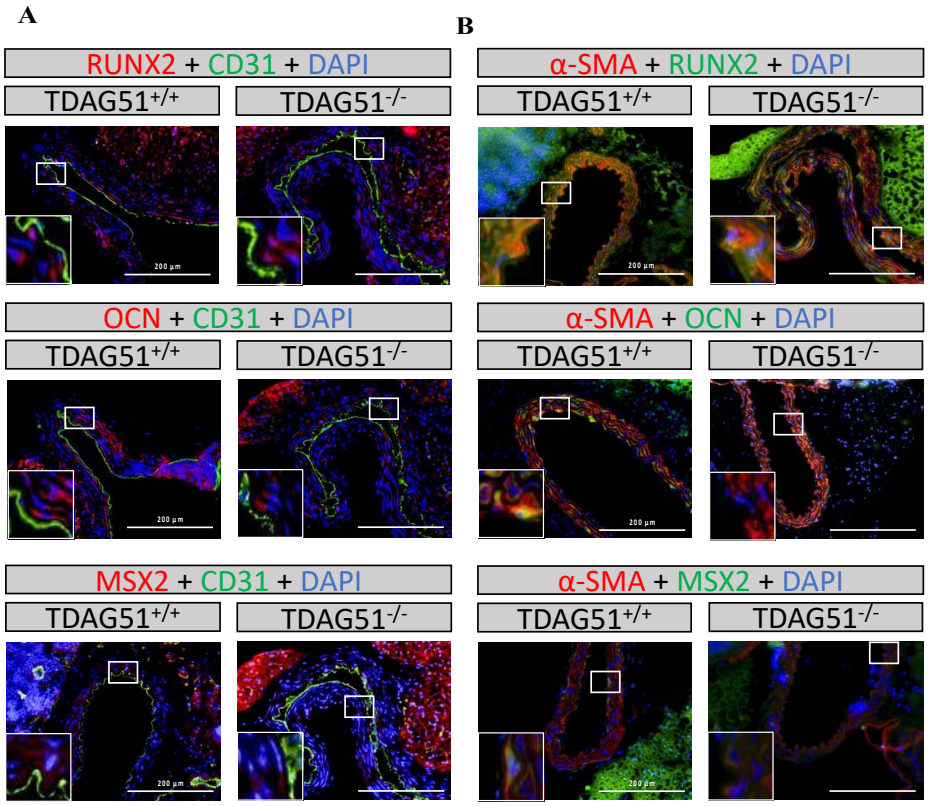

Supplemental Figure VII. Staining of mineral deposition as well as colocalization IF of drivers of osteogenesis with markers of cellular lineage (**A**) Immunofluorecence co-staining of RUNX2/OCN/MSX2 (red), endothelial cell marker CD31 (green) and nuclei using DAPI (blue). (**B**) Immunofluorecence co-staining of α-SMA (red), RUNX2/OCN/MSX2 (green) and nuclei using DAPI (blue).

CHAPTER 3: MANUSCRIPT 2

GDF10 is a negative regulator of vascular calcification of vascular smooth muscle cells.

Khrystyna Platko, Gabriel Gyulay, Paul F. Lebeau, Melissa E. MacDonald, Jae Hyun Byun, Suleiman A. Igdoura, Rachel M. Holden, Anna Roubtsova, Nabil G. Seidah, Joan C. Krepinsky, Richard C. Austin

Manuscript being prepared for submission to the *Journal of Biological Chemistry*

Chapter link: *GDF10 is a novel systemic inhibitor of vascular mineralization*. Follow-up studies aimed at elucidating additional mechanisms by which TDAG51 regulates VC identified GDF10 to be significantly up-regulated in *TDAG51*$^{-/-}$ VSMCs. Although its role in VC has been previously unknown, GDF10 inhibits osteoblast differentiation, a process that is very similar to osteogenic transdifferentiation of VSMCs. This manuscript demonstrates that similar to its anti-osteogenic role in rat calvarial osteoblasts, recombinant human (rh)GDF10 inhibits mineralization of VSMCs and *ex vivo* aortic ring cultures. Mechanistically, treatment with rhGDF10 inhibits P_i-induced Runx2 transcriptional activity and expression in VSMCs.

Author's contribution: K. Platko, G. Gyulay, R. C. Austin, and J.C. Krepinsky designed the study. K. Platko and G. Gyulay performed cell culture experiments, western blotting, immunofluorescence staining, alizarin red staining and ALP activity assay, as well as related analysis with help of P.F. Lebeau and J. Hyun Byun. Analysis of hydroxyapatite deposition in the *ex vivo* aortic rings and VSMCs were performed by G. Gyulay. Anna Roubtsova performed GDF10 *in situ* hybridazation analysis. Human serum samples for analysis of GDF10 abundance were provided by R. M. Holden. Animal experiments were conducted by K. Platko with help of M.E. MacDonald. K. Platko curated the data and wrote the manuscript. G. Gyulay and P.F. Lebeau helped revise the manuscript. K. Platko, R.C. Austin, J.C. Krepinsky, S.A. Igdoura, R.M. Holden and N.G. Seidah reviewed and edited the manuscript. All authors approved the final submission.

Gdf10 is a negative regulator of vascular calcification of vascular smooth muscle cells

*Khrystyna Platko[§], Gabriel Gyulay[§], Paul F. Lebeau[§], Melissa E. MacDonald[§], Jae Hyun Byun[§], Suleiman A. Igdoura[‡,**],Rachel M. Holden[†], Anna Roubtsova[¶], Nabil G. Seidah[¶], Joan C. Krepinsky[§*,†], Richard C. Austin[§*,†]*

Authors Affiliations: The [§]Department of Medicine, Division of Nephrology, McMaster University, and The Research Institute of St. Joseph's Hamilton, Hamilton, Ontario, Canada. The [**]Department of Pathology and Molecular Medicine and [‡]Biology, McMaster University Medical Centre, Hamilton, Ontario, Canada. The [†]Department of Medicine, Queen's University, Kingston, Ontario, Canada. The [¶]Institut de Recherches Cliniques de Montréal (IRCM), Affiliated with Université de Montréal, Montréal, Quebec, Canada

* Contributed equally to this work

[†] **Corresponding Authors:** To whom correspondence should be addressed: Dr. Richard C. Austin, 50 Charlton Ave East, Room T-3313, Hamilton, Ontario, L8N 4A6. Phone: 905-522-1155 x35175; Fax: 905-540-6589; E-mail: rick.austin@taari.ca.

Dr. Joan C. Krepinsky, 50 Charlton Ave East, Room T-3311, Hamilton, Ontario, L8N 4A6. Phone: 905-522-1155 x34991; Fax: 905-540-6589; E-mail: krepinj@mcmaster.ca

Key Words: chronic kidney disease, bone morphogenic proteins, vascular calcification, response to injury

Conflict of Interest: The authors declare that they do not have anything to disclose regarding funding or conflict of interest regarding this manuscript.

Sources of Funding: This work was supported in part by research grants to Richard C. Austin from the Heart and Stroke Foundation of Canada (G-13-0003064 and G-15-0009389) and the Canadian Institutes of Health Research (148539, 111239), to Richard C. Austin and Joan C. Krepinsky from the CIHR (148539) and to Nabil G Seidah from the CIHR foundation grant (148363). Financial support from the Research Institute of St. Joseph's Healthcare Hamilton is acknowledged. Richard C. Austin is a Career Investigator of the Heart and Stroke Foundation of Ontario and holds the Amgen Canada Research Chair in the Division of Nephrology at St. Joseph's Healthcare and McMaster University.

Author Contributions: KP, GG, JCK and RCA conceived the studies and wrote the manuscript. KP, GG, PFL, MEM and JHB performed all of the *in vitro* and *in vivo* studies. The manuscript was revised by SAI, RMH and NGS.

Acknowledgements: We thank Gurbaksh Basi from the Princess Margaret GenomicCentre for his assistance with micro-array analysis.

Abstract

Due to the negative impact of vascular calcification (VC) on vascular compliance, the occurrence of cardiovascular mortality in patients with end-stage renal disease is steadily on the rise. VC is a highly regulated biological process similar to bone formation involving osteogenic transdifferentiation of vascular smooth muscle cells (VSMCs). We have previously demonstrated that loss of T-cell death associated gene 51 (Tdag51) expression leads to an attenuation of medial VC. We now show a significant induction of circulating levels of growth differentiation factor 10 (Gdf10) in *Tdag51*$^{-/-}$ mice, which was of interest due to its established role as an inhibitor osteoblast differentiation. The objective of this study was to examine the role of Gdf10 in the osteogenic transdifferentiation of VSMCs. Using primary mouse and human VSMCs, as well as *ex vivo* aortic ring cultures, we demonstrated that treatment with recombinant human (rh) GDF10 reduced phosphate-mediated hydroxyapatite (HA) mineral deposition. Furthermore, *ex vivo* aortic rings from *Gdf10*$^{-/-}$ mice exhibited increased HA deposition compared to C57BL/6J controls. To explain our observations, we identified that rhGDF10 treatment reduced protein expression of runt-related transcription factor 2, a well-established driver of osteogenic transdifferentiation of VSMCs and VC. Furthermore, we demonstrated an increase in circulating GDF10 in patients with chronic kidney disease with clinically defined severe VC, as assessed by coronary artery calcium score. Thus, our studies identify Gdf10 as a novel inhibitor of mineral deposition and as such, may represent a potential novel biomarker and a therapeutic avenue for detection and management of VC.

Abbreviations

ALP, alkaline phosphatase; α-SMA, α-smooth muscle actin; CVD, cardiovascular disease; CKD, chronic kidney disease; CAC, coronary artery calcium; BMP, bone morphogenic protein; BSA, bovine serum albumin; FBS, fetal bovine serum; Gdf10, mouse growth differentiation factor 10; GDF10, human growth differentiation factor 10; HA, hydroxyapatite; HRP, horseradish peroxidase; IHC, immunohistochemistry; Runx2, runt-related transcription factor 2; rh, recombinant human; Tdag51,T-cell death associated gene 51; P_i, inorganic phosphate; PFA, paraformaldehyde; T-cell death associated gene 51; TGF-β, transforming growth factor-β; VC, vascular calcification; VSMCs, vascular smooth muscle cells; VD_3, vitamin D3

Introduction

Cardiovascular disease (CVD) is the leading cause of mortality in patients with chronic kidney disease (CKD) (1). Vascular calcification (VC) in the medial layer of the vessel wall due to hydroxyapatite (HA) mineral deposition, which subsequently leads to reduced vascular elasticity, is the predominant driver of this mortality (2). The prevalence of VC in patients with CKD ranges from 40% in those with stage 3 CKD to 80-90% in patients with stage 5 CKD (3). Furthermore, VC has been found to be an independent risk factor for sudden cardiac death in patients with CKD (4–6). Despite the growing prevalence of CKD in the aging population (7), there is limited understanding of the molecular mechanisms that modulate the development of VC.

Although previously considered to be passive, VC is now recognized as a highly regulated pathological process that shares many features with bone formation (8). Bone

morphogenic proteins (BMPs) are members of the transforming growth factor-β (TGF-β) superfamily that have long been shown to be crucial modulators of bone formation and are now recognized as drivers of VC (8, 9). Studies demonstrate that BMP2 and Bmp4 are inducers of osteogenic differentiation and HA deposition in osteoblasts and vascular smooth muscle cells (VSMCs) (10–12). In contrast, BMP7 promotes a VSMC-specific phenotype by upregulating the expression of α-smooth muscle actin (α-SMA). BMP3 is another negative regulator of osteoblast differentiation (13). Mice lacking the *Bmp3* gene display increased bone mass (13), whereas transgenic mice overexpressing *BMP3* develop spontaneous rib fractures due to altered endochondral bone formation (14). BMP-3b, also known as growth differentiation factor 10 (GDF10), is a divergent member of the TGF-β superfamily that is closely related to BMP3 (15) and signals through TGF-β receptors (16–18). Gdf10 expression correlates with osteoblast differentiation (19) and in a manner similar to BMP3, is able to inhibit this process (20).

Runt-related transcription factor 2 (Runx2) is a key transcription factor necessary for osteoblast development and maturation (21). Transcriptional regulation of Runx2 by BMPs plays an important role in osteoblast differentiation, as well as mineralization of soft tissues (22–28) Combined treatment of fibroblast-like ligamentum flavum cells and primary skeletal myoblasts with adenoviruses to overexpress Runx2 and Bmp2 revealed a synergistic effect on the expression of osteogenic genes (28). Furthermore, overexpression of Runx2 in VSMCs and adipose-derived stem cells promoted the expression of drivers of osteogenesis and a subsequent phenotypic switch (29–31). In VSMCs, phosphate-mediated increase in Runx2 expression and activation lead to an increase in the expression of type

III sodium-dependent phosphate transporter, Pit-1 (32), a well-established mediator of VC (33–35). Additionally, an increase in Runx2 and Pit-1 expression was observed in calcified aortas (29, 36). Interestingly, Tandon and colleagues (37) demonstrated that there also exists an inverse relationship between Runx2 and Gdf10 expression in lung cancer cells and mesenchymal stem cells from functionally deficient Runx2 mice. Runx2 overexpression and knockdown studies show that Runx2 downregulates Gdf10 expression by increasing its methylation status (37).

We have recently demonstrated that loss of T-cell death-associated gene 51 (Tdag51) expression reduced Runx2 transcriptional activity, Pit-1 expression and subsequently blocked the development of VC (32). Interestingly, our recent microarray analysis revealed that *Gdf10* expression in VSMCs from Tdag51$^{-/-}$ mice was significantly upregulated compared to the VSMCs from littermate controls. To shed light on this critical observation, we now demonstrate that treatment with recombinant human (rh) GDF10 decreases phosphate (P_i)-mediated Runx2 expression and mineral deposition in VSMCs and *ex vivo* aortic ring cultures. Furthermore, we also demonstrate an increase in circulating GDF10 in patients with CKD and clinically defined VC. Therefore, our studies identify Gdf10 as a novel regulator of VC, serving as a potential therapeutic target for the management of VC and as a potential marker for its detection.

Methods

Animals

Tdag51$^{-/-}$ mice were generated as previously described (38) and backcrossed to C57BL/6J (*Tdag51*$^{+/+}$) mice for at least 9 generations. *Gdf10*$^{-/-}$ mice were generously provided by Dr.

Se-Jin Lee (39) and were also backcrossed onto the C57BL/6J background for at least 9 generations. Wild-type (C57BL/6J) mice were purchased from Jackson Laboratory (Stock No: 000664). All mice were housed in a 12h light-dark cycle with free access to regular control diet. For studies examining VC using a vitamin D3 (VD_3) model of hyperphosphatemia-induced rapid VC, 8-week-old male *Gdf10*$^{-/-}$ mice and *Gdf10*$^{+/+}$ littermate controls were used. Mice were subcutaneously injected with 5.55 X 10^5 IU/kg/day of active VD_3 (Sigma-Aldrich) daily for 3 consecutive days (40) and were sacrificed 4 days posttreatment. All animal procedures were approved by the McMaster University Animal Research Ethics Board.

VSMC and *ex vivo* aortic rings cultures

All VSMCs were isolated from the aortas of 6 to 10-week-old male mice by the explant method (41) and cultured in Dulbecco's Modified Eagle's Medium (GIBCO GlutaMAX 10567-014 + 1 g/L D-glucose + 110 mg/mL Sodium Pyruvate) supplemented with 10% v/v fetal bovine serum (FBS) (Sigma-Aldrich), 100 IU/ml penicillin and 100 µg/ml streptomycin (Gibco). Primary human aortic VSMCs were purchased from Lonza (CC-2571) and cultured in SmGM-2 BulletKit medium (Lonza). Cells were plated at a confluence of 50-70% and used at passage 4-8. Aortic rings for *ex vivo* studies were isolated in a similar manner. Briefly, thoracic aortas were removed, washed in PBS-antibiotic-antimycotic solution (Gibco) 6 times while the adventitia and adipose layers were carefully removed. Clean aortas were cut into 5-10 mm segments (~4-5 per animal) and cultured in suspension (42). All VSMCs and *ex vivo* aortic rings were maintained in 5% CO_2 at 37°C.

To induce osteogenic transdifferentiation and calcification of the VSMCs, medium was supplemented with additional P_i to achieve a concentration of 2.6 mM. The addition of cleaved or full length (FL) rhGDF10 (R&D and AbNova) at increasing doses (100-1000 ng/ml) was added to calcification medium.

Calcium quantification assay

After decalcification of cells or tissue with 0.6N HCl for 48-72 hours, calcium deposition was quantified using a colorimetric calcium kit using the o-cresolphthalein method according to the manufacturer's instructions (Sigma-Aldrich). Measurements were normalized to protein content or dry tissue weight.

OsteoImage HA crystal quantification assay

HA deposition was quantified using the OsteoImage fluorescent assay kit (Lonza) according to the manufacturer's instructions. Briefly, cells were plated in a black clear bottom 96-well plate and cultured in calcification medium for 5-6 days. Cells were washed, fixed with 3.7% w/v paraformaldehyde (PFA) and stained with the fluorescent reagent. HA deposition was quantitatively assessed using a fluorescent microplate reader (Molecular Devices) at 492/520 nm wavelengths (32).

Immunoblotting

Immunoblot analysis was performed as previously described (43). Briefly, whole cell and tissue lysates were prepared using RIPA lysis buffer containing a protease inhibitor cocktail

(Roche). Protein concentrations were determined using a modified Lowry assay (Bio-Rad). Equal amount of protein samples were resolved by SDS-PAGE and subsequently transferred to nitrocellulose membranes (Bio-Rad). The membranes were then blocked in 5% w/v skimmed milk, incubated with primary antibodies for 18 h at 4°C, followed by horseradish peroxidase (HRP)-conjugates secondary antibodies. Secondary antibodies were detected using enhanced chemiluminescence reagent (Amersham) and exposed using Konica Minolta X-ray film processor. Band intensity was measured by densitometry analysis using ImageLab software (Bio-Rad) and normalized to membranes reported loading control. All antibodies and working dilutions are listed in **Supplemental Table 1**.

Immunohistochemical (IHC) and histological staining

Paraffin blocks were cut into 4 μm thick sections, deparaffinized and dehydrated in 3 changes of xylene and 100% v/v ethanol respectively. Following an endogenous peroxidase block, sections were then blocked in 5% v/v serum and subsequently incubated in primary antibodies for 18 h at 4 °C. Sections were then exposed to biotin-labeled secondary antibodies (Vector Laboratories). Streptavidin-labeled HRP solution (Vector Laboratories) and the developing solution (Vector Laboratories) were used to visualize the staining. Calcium deposition in mouse tissue sections was visualized using Alizarin Red S stain. Following deparaffinization, sections were stained with 2% w/v Alizarin Red (Sigma-Aldrich) solution at a pH of 4.2 for 2 min, dehydrated and mounted in synthetic mounting medium. Slides were examined using a Nikon light microscope. All antibodies and working dilutions are listed in **Supplemental Table 1**.

In situ hybridization

Glass slides containing 12 μm thick frozen sections of whole body mice at embryonic day 12 (E12) and postnatal day 5 (p5) mice, as well as 30 tissues of adult mice were fixed using 4% formaldehyde. The [^{35}S]-labeled (PerkinElmer) cRNA probes were synthesized *in vitro* and corresponded to mouse while coding region of Gdf10. RNA sense and antisense probes were synthesized and tested by in situ hybridization as reported.

Immunofluorescence (IF)

IF staining was performed as described previously (44). Briefly, 10 μm thick cryosections of thoracic aortas were fixed for 1 h using 4% w/v PFA, permeabilized for 15 min with 0.025% v/v Triton X-100 and subsequently blocked with 5% w/v bovine serum albumin (BSA). Slides were then incubated with primary antibody overnight at 4ºC and stained with appropriate Alexa Fluor-labeled (ThermoFisher Scientific) secondary antibodies and DAPI (Sigma-Aldrich). Slides were mounted with Permafluor (ThermoFisher Scientific) and visualized using a fluorescent microscope (EVOS-FL, ThermoFisher Scientific). All antibodies and working dilutions are listed in **Supplemental Table 1**.

ELISAs

Commercially available ELISA kits were used to measure serum levels of mouse Gdf10 (Elabscience) and Bmp3 (MyBioSource) according to the manufacturer's instructions.

Microarray analysis

Total RNA was isolated from *Tdag51*$^{+/+}$ and *Tdag51*$^{-/-}$ VSMCs (n=3 per group) using the RNA purification kit (Qiagen) according to the manufacturer's instructions. 300 ng of total RNA for each sample was used as input RNA in Ambion® WT Expression Kit (ThermoFisher Scientific) and 2.75 µg of cDNA for each sample was fragmented and labelled according to Affymetrix WT labeling and fragmentation protocol. Mouse 1.0 ST Gene Arrays v1 arrays were hybridized for 18hrs at 45ºC at 60 RPM. Arrays were washed using GeneChip Fluidics Station P450 and were scanned with Affymetrix GeneChip Scanner 7G. The relevant data are represented as the log fold change relative to *Tdag51*$^{+/+}$ VSMCs.

siRNA transfection

To block pleckstrin homology-like domain family A, member 1 (PHLDA1) expression in human VSMCs, targeting siRNA (M-012389-01-0005) and non-targeting control siRNA (D-001210-01-05) were purchased from Dharmacon. Dharmafect 1 (GE Dharmacon) transfection reagent was used according to the manufacturer's instructions (32).

Quantitative real-time (qRT)-PCR

Total RNA was isolated using RNA purification kit (ThermoFisher Scientific) according to the manufacturer's instructions. A total of 2 µg of RNA was reverse transcribed using a High-Capacity cDNA Reverse Transcription Kit (ThermoFisher Scientific). PCR amplification was performed using fast SYBR Green (Applied Biosystems). Relative

transcript expression levels were calculated using the ΔΔCT method and normalized to 18S. All primer sequences are listed in **Supplemental Table 2**.

Human serum samples

Serum from nondiabetic patients with CKD (eGFR 8-45ml/min) and associated severe VC, or no significant calcification as assessed by coronary artery calcium (CAC) score (45) as described in (46) were assessed for GDF10 by ELISA. The study cohort included both males and females and was not stratified by other co-morbidities or biochemical or clinical parameters.

Statistical analysis

Data were analyzed using the unpaired Student's *t*-test and are presented as mean ± standard deviation, with $p<0.05$ considered significant between two groups. Details of biological replicates are listed in figure legends.

Results

Tdag51$^{-/-}$ VSMCs and mice exhibit increased expression of the inhibitor of osteogenesis, Gdf10

Osteogenic transdifferentiation of VSMCs is a major contributor to the development of VC in conditions of hyperphosphatemia (8). Our previous findings demonstrated that *Tdag51*$^{-/-}$ VSMCs and mice exhibit an attenuation of HA deposition due to (i) reduced expression of type III sodium-dependent P_i transporter and (ii) diminished Runx2 activity (32). To further define additional modulators of VC, microarray analysis of *Tdag51*$^{+/+}$ and *Tdag51*$^{-}$

$^{/-}$ VSMCs identified 622 up-regulated and 363 down-regulated genes in *Tdag51*$^{-/-}$ VSMCs. Identified genes were classified according to their molecular function, biological process, cellular component and protein class (Fig. S1 A-D). Further analysis determined 49 genes, with log-fold change cut-off of +/- 1.5 compared to *Tdag51*$^{+/+}$ VSMCs, that have previously been demonstrated to be involved in the regulation of mineral deposition in either soft tissues or bone (Fig. 1A). Among the identified genes was *Gdf10*, which was of interest because it is a circulating factor that is easily detected in the medium from primary mouse VSMCs (data not shown) and has previously been shown to inhibit osteoblast differentiation, a process that draws many parallels with VC (8, 20). Consistent with the notion that Gdf10 plays a role in bone formation and vascular mineral deposition (19, 20), *in situ* hybridization studies reveal that at embryonic day 12 (E12) and post-natal day 5 (p5), *Gdf10* mRNA was abundantly expressed in the vasculature such as the aorta, as well as in bone, such as the vertebrae, skull and cartilage (Fig 1B,C and S2).

Consistent with the microarray data, quantitative real-time PCR and immunoblot analysis demonstrated an increase in *Gdf10* mRNA and protein expression in *Tdag51*$^{-/-}$ VSMCs (Fig. 2A). Similarly, IHC staining of Gdf10 (Fig. 2B) as well as circulating levels of Gdf10 (Fig. 1C) were increased in *Tdag51*$^{-/-}$ mice compared to controls. In support of these findings, siRNA-mediated knockdown of *PHLDA1* (human homologue of Tdag51) in human VSMCs resulted in increased *GDF10* expression (Fig. 2D), thus suggesting that Tdag51 regulates Gdf10 expression. Given that *Tdag51*$^{-/-}$ leads to (i) elevated expression of Gdf10 as well as (ii) an attenuation of HA deposition, our findings suggest that similar

to its role in osteoblast differentiation, Gdf10 is likely an inhibitor of mineral deposition in VSMCs.

Recombinant human GDF10 treatment attenuates P_i-mediated mineral deposition

Given that GDF10 signals through TGFβ receptors (16–18), we first confirmed that treatment with rhGDF10 induces Smad3 phosphorylation in a TGFβ receptor-dependent manner (Fig. S3A). We next examined the effect of rhGDF10 on mineral deposition in primary mouse VSMCs (Fig. 3A) and *ex vivo* aortic ring cultures (Fig. 3B), as well as primary human VSMCs (Fig. 3C). The effect of rhGDF10 treatment on alkaline phosphatase (ALP) activity in VSMCs (Fig. 3D) and the pattern of mineral accumulation in *ex vivo* aortic rings (Fig. 3E) was also examined. Consistent with its previously established role as an inhibitor of osteoblast differentiation (20), rhGDF10 attenuated P_i-mediated mineral deposition in VSMCs and *ex vivo* aortic ring cultures, as well as ALP activity. Furthermore, *ex vivo* aortic rings from *Gdf10*$^{-/-}$ mice exhibited increased mineral deposition compared to *C57BL/6J* controls (Fig. 3F). Collectively, these data indicate that Gdf10 is a negative regulator of P_i-mediated mineral deposition in VSMCs.

Similar to other TGFβ family members, active Gdf10 is generated by proteolytic cleavage of the precursor protein at the putative furin cleavage site (RXXR)(47–49). In order to confirm that active Gdf10 is necessary for the observed anti-osteogenic phenotype, human and mouse VSMCs were treated with either cleaved/active (Gln369-Arg478) or FL rhGDF10 in the presence or absence of an established furin inhibitor, decanoyl-RVKR-CMK (Fig. S3A and S3B) (50). Both FL and active peptide forms of rhGDF10 significantly

reduced calcification, while decanoyl blocked the inhibitory effect of the FL rhGDF10. A control peptide was also used as an additional control and had no effect on HA deposition. Thus, suggesting that only active GDF10 acts as an inhibitor of HA deposition and VC. Given that the decanoyl-RVKR-CMK inhibited the anti-calcific effect of GDF10, these observations also suggest that Gdf10 is processed at the cell surface by furin.

To investigate the role of Gdf10 in VC, a model of VD_3-induced VC was employed. Mineral deposition within the vessel wall was examined by quantification of Ca^{2+} content (Fig. S4A) and Alizarin Red calcium stain (Fig. S4B). To our surprise, no difference in mineral deposition was observed between *Gdf10*$^{-/-}$ and *Gdf10*$^{+/+}$ littermate controls. To interrogate the possibility of compensatory increase in a closely related family member and a known negative regulator of osteogenesis, Bmp3 (13, 14), its circulating levels were measured using ELISAs (Fig. S4C). These data revealed a substantial increase in circulating Bmp3 in *Gdf10*$^{-/-}$ mice, likely compensating for the absence of Gdf10, which may explain inconsistencies between our *in vivo* and *in vitro* observations.

Recombinant human GDF10 treatment inhibits Runx2 expression and activity

Osteogenic transdifferentiation of the medial layer of the vessel wall leading to VC draws many similarities to growth and maturation of osteoblasts (8). We next examined the effect of rhGDF10 on the expression of well-established drivers of osteogenic transdifferention of VSMCs (24, 25, 31, 34). Immunoblot analysis demonstrated that rhGDF10 attenuated P_i and TGF-β-mediated upregulation of Runx2 and its transcriptional cofactor Msh homeobox 2 (Msx2), while Pit-1 levels remained unchanged (Fig. 4A). Because the

expression of Runx2 and its co-factor Msx2 is associated with Runx2-mediated transcriptional activity and pro-osteogenic phenotype (24, 51), Runx2 transciptional activation was also examined using 6XOSE2-Luc. Runx2-dependent activation was inhibited by rhGDF10 (Fig. 4B). In line with these findings, the mRNA expression of established markers of osteogenesis, including Runx2, Msx2, and ALP were also reduced (Fig. 4C). Additionally, rhGDF10 treatment decreased the expression of Runx2 and its downstream target osteocalcin (OCN) in the *ex vivo* aortic ring cultures following 7 days of treatment (Fig. 4D). Thus, these observations reveal that GDF10 may in part inhibit arterial mineral deposition by regulating the expression of key drivers of VC, such as Runx2 and its downstream targets.

Circulating GDF10 levels are elevated in patients with coronary artery calcification

Given the established role of circulating osteogenic proteins in the development of arterial calcification (52–54), we next examined circulating GDF10 levels in a cohort of patients with CKD who were also determined to have severe VC, as assessed by CAC score of >200 (Fig. 5). Similar to other established inhibitors of medial arterial mineral deposition (8, 52–54), we observed an increase in serum GDF10 in patients with severe VC. These data suggest that circulating levels of GDF10 increase in response to vascular injury in calcified regions, likely in an attempt to prevent this process.

Discussion

The relationship between TGF-β signaling and VC has been known for decades, and has predominantly focused on the effect of well-characterized members of this diverse

superfamily, such as TGF-β, BMP-2 and BMP-7 (22–26, 28). Our studies begin to characterize the relationship between a divergent member of the of the TGF-β superfamily, GDF10, and osteogenic transdifferentiation of VSMCs. Using a combination of *in vivo* and *ex vivo* studies, we demonstrated that rhGDF10 attenuated VC. To explain these observations, we also demonstrated that rhGDF10 reduced the expression of well-established drivers of osteogenic transdifferentiation in VSMCs.

Osteogenic transdifferentiaiton of VSMCs is a highly regulated process that shares many similarities with osteoblast differentiation and bone mineralization (8). Runx2 is an indispensable transcription factor necessary for both of these processes to occur (55, 56). Studies demonstrate that Runx2 is essential for osteogenic transdifferentiation of VSMCs and adipose-derived mesenchymal stem cells (30, 56). Importantly, accumulating evidence demonstrates that several members of the BMP family are key regulators of Runx2 transcriptional activity and expression in the context of osteoblast differentiation, as well as mineralization of soft tissues (25–28, 57). We have recently demonstrated that VSMCs derived from *Tdag51*$^{-/-}$ mice exhibit reduced expression of the type III sodium-dependent P_i transporter and Runx2 transcriptional activity, leading to diminished VC (32). Here we illustrate that reduced VC in *Tdag51*$^{-/-}$ mice is also accompanied by an increase in *Gdf10* expression. Evidence also suggests that there exists an inverse relationship whereby Runx2 can regulate a divergent member of the BMP family, Gdf10, in lung carcinoma, and mesenchymal stem cells (37). These findings provide a potential additional mechanism to explain the protective phenotype observed in *Tdag51*$^{-/-}$ mice (32) In the present study, we demonstrate that rhGDF10 treatment inhibits P_i-mediate HA mineral deposition in cultured

mouse and human VSMCs, as well as *ex vivo* aortic ring cultures. Additionally, rhGDF10 treatment attenuated Runx2 expression and transcriptional activity in wild-type VSMCs. Thus, our findings support a role for Gdf10 as a novel negative modulator of Runx2 thus of VC.

GDF10 is a member of the TGF-β superfamily that also shares an 83% amino acid sequence homology with BMP3 (15). Daluiski and colleagues (13) have demonstrated that BMP3 is a powerful negative modulator of osteogenic differentiation and mineralization in mouse myoblast cells, however no skeletal defects were observed in *Bmp3*$^{-/-}$ embryos and newborns. Additionally, the authors observed no obvious skeletal phenotype in adult *Bmp3*$^{-/-}$ mice other than an increase in total trabecular bone volume, which was accompanied by a considerable amount of variation between mice (13). Consistent with the role of BMP3 as an inhibitor of osteogenesis, transgenic mice overexpressing *BMP3* develop spontaneous rib fractures due to defects in bone formation (14). Due to the homology between these two proteins, in a manner similar to BMP3, Gdf10 expression also correlates with periods of osteoblast differentiation in rat calvarial osteoblasts (19, 20). To our surprise, however, we observed no difference in HA mineral deposition between VD_3-treated *Gdf10*$^{-/-}$ and *Gdf10*$^{+/+}$ mice. Similar to the studies conducted in *Bmp3*$^{-/-}$ mice (13), the absence of a VC phenotype observed in *Gdf10*$^{-/-}$ mice from our study may be due to its functional redundancy with its closely related family member, Bmp3.

Our understanding of BMPs is expanding beyond that of bone growth and cartilage formation. Several studies have now demonstrated that BMPs act as *response to injury* factors, mitigating disease progression (17, 18, 58–62). Clinical and pre-clinical studies

demonstrate an increase in circulating BMP9 levels in patients with liver fibrosis as well as an increase in perivascular hepatic fibrosis in *Bmp9* knockout mice (58, 59). Exposure of primary liver sinusoidal endothelial cells to exogenous BMP9 led to an attenuation of the fibrotic response (59). In a similar manner, BMP7 treatment can prevent tubulointerstitial fibrosis and preserve renal function in a rodent model of renal injury (61, 62). Consistent with these findings, exogenous BMP7 also ameliorates the expression of profibrotic genes in the aortas of uremic rats (60). On the other hand, *Gdf15* expression dramatically increases following liver injury (63), while its overexpression ameliorates ischemia reperfusion injury (64) and leads to improved functional recovery following a traumatic spinal cord injury (65). Recent evidence also suggests that GDF10 plays a role in injury prevention and wound healing, as Li and colleagues (18) demonstrate an increase in GDF10 expression in rodent and non-human primate models of stroke, as well as in autopsy samples from patients who presented with a clinically diagnosed stroke event. Furthermore, exogenous treatment with rhGDF10 promoted axonal sprouting and functional recovery after stroke in rodents (18). In line with these findings, we and others demonstrated that *Gdf10*$^{-/-}$ mice develop severe hepatic fibrosis and lipid accumulation, whereas mice with adipose-specific overexpression of BMP-3b were protected against diet-induced obesity (17, 66). In our present study, we demonstrate an increase in serum GDF10 in CKD patients with established VC. Similar to other BMP family members, GDF10 may potentially act as an inhibitor of VC and a circulating *response to injury* protective factor.

The present study identifies GDF10 as a novel mediator of osteogenic transdifferentiation of the VSMCs and HA mineral deposition. Mechanistically, rhGDF10

treatment inhibited P_i-induced Runx2 expression and activity. Our results also show that patients with CKD and established severe VC exhibit elevated circulating levels of GDF10. Thus our findings identify GDF10 as an important circulating factor regulating osteogenic transdifferentiation and subsequent VC of VSMCs and that patients with CKD may benefit from increased circulating levels of this protein.

References

1. Sarnak, M. J., Levey, A. S., Schoolwerth, A. C., Coresh, J., Culleton, B., Hamm, L. L., McCullough, P. A., Kasiske, B. L., Kelepouris, E., Klag, M. J., Parfrey, P., Pfeffer, M., Raij, L., Spinosa, D. J., Wilson, P. W., and Prevention, A. H. A. C. on K. in C. D., High Blood Pressure Research, Clinical Cardiology, and Epidemiology and (2003) Kidney Disease as a Risk Factor for Development of Cardiovascular Disease. *Circulation*. **108**, 2154–2169

2. Noordzij, M., Cranenburg, E. M., Engelsman, L. F., Hermans, M. M., Boeschoten, E. W., Brandenburg, V. M., Bos, W. J. W., Kooman, J. P., Dekker, F. W., Ketteler, M., Schurgers, L. J., Krediet, R. T., Korevaar, J. C., and Group, N. S. (2010) Progression of aortic calcification is associated with disorders of mineral metabolism and mortality in chronic dialysis patients. *Nephrol Dialysis Transplant Official Publ European Dialysis Transpl Assoc - European Ren Assoc*. **26**, 1662–9

3. Liu, Z.-H., and Group, C. D. C. S. (CDCS) (2015) Vascular calcification burden of Chinese patients with chronic kidney disease: methodology of a cohort study. *Bmc Nephrol*. **16**, 129

4. Block, G., Hulbert-Shearon, T., Levin, N., and Port, F. (1998) Association of serum phosphorus and calcium x phosphate product with mortality risk in chronic hemodialysis patients: A national study. *Am J Kidney Dis*. **31**, 607–617

5. Sigrist, M. K., Taal, M. W., Bungay, P., and McIntyre, C. W. (2007) Progressive Vascular Calcification over 2 Years Is Associated with Arterial Stiffening and Increased Mortality in Patients with Stages 4 and 5 Chronic Kidney Disease. *Clin J Am Soc Nephro*. **2**, 1241–1248

6. McCullough, P. A., Agrawal, V., Danielewicz, E., and Abela, G. S. (2008) Accelerated Atherosclerotic Calcification and Mönckeberg's Sclerosis: A Continuum of Advanced Vascular Pathology in Chronic Kidney Disease. *Clin J Am Soc Nephro*. **3**, 1585–1598

7. Arora, P., Vasa, P., Brenner, D., Iglar, K., McFarlane, P., Morrison, H., and Badawi, A. (2013) Prevalence estimates of chronic kidney disease in Canada: results of a nationally representative survey. *Cmaj Can Medical Assoc J J De L'association Medicale Can*. **185**, E417-23

8. Johnson, R. C., Leopold, J. A., and Loscalzo, J. (2006) Vascular Calcification: Pathobiological Mechanisms and Clinical Implications. *Circ Res*. **99**, 1044–1059

9. Wu, M., Chen, G., and Li, Y.-P. (2016) TGF-β and BMP signaling in osteoblast, skeletal development, and bone formation, homeostasis and disease. *Bone Res*. **4**, 16009

10. Li, X., Yang, H.-Y., and Giachelli, C. M. (2008) BMP-2 promotes phosphate uptake, phenotypic modulation, and calcification of human vascular smooth muscle cells. *Atherosclerosis*. **199**, 271–7

11. Liu, T., Gao, Y., Sakamoto, K., Minamizato, T., Furukawa, K., Tsukazaki, T., Shibata, Y., Bessho, K., Komori, T., and Yamaguchi, A. (2007) BMP-2 promotes differentiation of osteoblasts and chondroblasts in Runx2-deficient cell lines. *J Cell Physiol*. **211**, 728–735

12. Wei, X., Wu, W., Li, L., Lin, J., Liu, Q., Gan, L., and Ou, S. (2018) Bone Morphogenetic Proteins 2/4 Are Upregulated during the Early Development of Vascular Calcification in Chronic Kidney Disease. *Biomed Res Int*. **2018**, 8371604

13. Daluiski, A., Engstrand, T., Bahamonde, M. E., Gamer, L. W., Agius, E., Stevenson, S. L., Cox, K., Rosen, V., and Lyons, K. M. (2001) Bone morphogenetic protein-3 is a negative regulator of bone density. *Nat Genet*. **27**, 84–88

14. Gamer, L. W., Cox, K., Carlo, J. M., and Rosen, V. (2009) Overexpression of BMP3 in the developing skeleton alters endochondral bone formation resulting in spontaneous rib fractures. *Dev Dyn Official Publ Am Assoc Anatomists*. **238**, 2374–81

15. Cunningham, N. S., Jenkins, N. A., Gilbert, D. J., Copeland, N. G., Reddi, A. H., and Lee, S.-J. (1995) Growth/Differentiation Factor-10: A New Member of the Transforming Growth Factor-β Superfamily Related to Bone Morphogenetic Protein-3. *Growth Factors*. **12**, 99–109

16. Upadhyay, G., Yin, Y., Yuan, H., Li, X., Derynck, R., and Glazer, R. I. (2011) Stem cell antigen-1 enhances tumorigenicity by disruption of growth differentiation factor-10 (GDF10)-dependent TGF-beta signaling. *P Natl Acad Sci Usa*. **108**, 7820–5

17. Platko, K., Lebeau, P. F., Byun, J. H., Poon, S. V., Day, E. A., MacDonald, M. E., Holzapfel, N., Mejia-Benitez, A., Maclean, K. N., Krepinsky, J. C., and Austin, R. C. (2019) GDF10 blocks hepatic PPARγ activation to protect against diet-induced liver injury. *Mol Metab*. **27**, 62–74

18. Li, S., Nie, E. H., Yin, Y., Benowitz, L. I., Tung, S., Vinters, H. V., Bahjat, F. R., Stenzel-Poore, M. P., Kawaguchi, R., Coppola, G., and Carmichael, S. T. (2015) GDF10 is a signal for axonal sprouting and functional recovery after stroke. *Nat Neurosci*. **18**, 1737–45

19. Hino, J., Matsuo, H., and Kangawa, K. (1999) Bone Morphogenetic Protein-3b (BMP-3b) Gene Expression Is Correlated with Differentiation in Rat Calvarial Osteoblasts. *Biochem Bioph Res Co*. **256**, 419–424

20. Matsumoto, Y., Otsuka, F., Hino, J., Miyoshi, T., Takano, M., Miyazato, M., Makino, H., and Kangawa, K. (2011) Bone morphogenetic protein-3b (BMP-3b) inhibits osteoblast differentiation via Smad2/3 pathway by counteracting Smad1/5/8 signaling. *Mol Cell Endocrinol*. **350**, 78–86

21. Liu, T. M., and Lee, E. H. (2013) Transcriptional Regulatory Cascades in Runx2-Dependent Bone Development. *Tissue Eng Part B Rev*. **19**, 254–263

22. Jang, W.-G., Kim, E.-J., Kim, D.-K., Ryoo, H.-M., Lee, K.-B., Kim, S.-H., Choi, H.-S., and Koh, J.-T. (2011) BMP2 protein regulates osteocalcin expression via Runx2-mediated Atf6 gene transcription. *J Biological Chem*. **287**, 905–15

23. Javed, A., Afzal, F., Bae, J.-S., Gutierrez, S., Zaidi, K., Pratap, J., Wijnen, A. J. van, Stein, J. L., Stein, G. S., and Lian, J. B. (2008) Specific residues of RUNX2 are obligatory for formation of BMP2-induced RUNX2-SMAD complex to promote osteoblast differentiation. *Cells Tissues Organs*. **189**, 133–7

24. Matsubara, T., Kida, K., Yamaguchi, A., Hata, K., Ichida, F., Meguro, H., Aburatani, H., Nishimura, R., and Yoneda, T. (2008) BMP2 regulates Osterix through Msx2 and Runx2 during osteoblast differentiation. *J Biological Chem*. **283**, 29119–25

25. Yang, S., Wei, D., Wang, D., Phimphilai, M., Krebsbach, P. H., and Franceschi, R. T. (2003) In Vitro and In Vivo Synergistic Interactions Between the Runx2/Cbfa1 Transcription Factor and Bone Morphogenetic Protein-2 in Stimulating Osteoblast Differentiation. *J Bone Miner Res*. **18**, 705–715

26. Tou, L., Quibria, N., and Alexander, J. M. (2003) Transcriptional regulation of the human Runx2/Cbfa1 gene promoter by bone morphogenetic protein-7. *Mol Cell Endocrinol*. **205**, 121–129

27. Gersbach, C. A., Byers, B. A., Pavlath, G. K., and García, A. J. (2004) Runx2/Cbfa1 stimulates transdifferentiation of primary skeletal myoblasts into a mineralizing osteoblastic phenotype. *Exp Cell Res*. **300**, 406–417

28. Kim, H.-N., Min, W.-K., Jeong, J.-H., Kim, S.-G., Kim, J.-R., Kim, S.-Y., Choi, J.-Y., and Park, B.-C. (2011) Combination of Runx2 and BMP2 increases conversion of human ligamentum flavum cells into osteoblastic cells. *Bmb Rep*. **44**, 446–451

29. Steitz, S. A., Speer, M. Y., Curinga, G., Yang, H. Y., Haynes, P., Aebersold, R., Schinke, T., Karsenty, G., and Giachelli, C. M. (2001) Smooth muscle cell phenotypic transition associated with calcification: upregulation of Cbfa1 and downregulation of smooth muscle lineage markers. *Circ Res*. **89**, 1147–54

30. Zhang, X., Yang, M., Lin, L., Chen, P., Ma, K. T., Zhou, C. Y., and Ao, Y. F. (2006) Runx2 Overexpression Enhances Osteoblastic Differentiation and Mineralization in Adipose - Derived Stem Cells in vitro and in vivo. *Calcified Tissue Int*. **79**, 169–178

31. Lin, M.-E., Chen, T., Leaf, E. M., Speer, M. Y., and Giachelli, C. M. (2015) Runx2 Expression in Smooth Muscle Cells Is Required for Arterial Medial Calcification in Mice. *Am J Pathology*. **185**, 1958–69

32. Platko, K., Lebeau, P. F., Gyulay, G., Lhoták, Š., MacDonald, M. E., Pacher, G., Byun, J. H., Boivin, F. J., Igdoura, S. A., Cutz, J.-C., Bridgewater, D., Ingram, A. J., Krepinsky, J. C., and Austin, R. C. (2020) TDAG51 (T-Cell Death-Associated Gene 51) Is a Key Modulator of Vascular Calcification and Osteogenic Transdifferentiation of Arterial Smooth Muscle Cells. *Arteriosclerosis Thrombosis Vasc Biology*. 10.1161/atvbaha.119.313779

33. Giachelli, C. M. (2009) The emerging role of phosphate in vascular calcification. *Kidney Int*. **75**, 890–7

34. Li, X., and Giachelli, C. M. (2007) Sodium-dependent phosphate cotransporters and vascular calcification. *Curr Opin Nephrol Hy*. **16**, 325–328

35. Li, X., Yang, H.-Y., and Giachelli, C. M. (2006) Role of the Sodium-Dependent Phosphate Cotransporter, Pit-1, in Vascular Smooth Muscle Cell Calcification. *Circ Res*. **98**, 905–912

36. Koleganova, N., Piecha, G., Ritz, E., Schirmacher, P., Muller, A., Meyer, H.-P., and Gross, M.-L. (2009) Arterial calcification in patients with chronic kidney disease. *Nephrol Dial Transpl*. **24**, 2488–2496

37. Tandon, M., Gokul, K., Ali, S. A., Chen, Z., Lian, J., Stein, G. S., and Pratap, J. (2012) Runx2 mediates epigenetic silencing of the bone morphogenetic protein-3B (BMP-3B/GDF10) in lung cancer cells. *Mol Cancer*. **11**, 27

38. Rho, J., Gong, S., Kim, N., and Choi, Y. (2001) TDAG51 Is Not Essential for Fas/CD95 Regulation and Apoptosis In Vivo. *Mol Cell Biol*. **21**, 8365–8370

39. Zhao, R., Lawler, A. M., and Lee, S.-J. (1999) Characterization of GDF-10 Expression Patterns and Null Mice. *Dev Biol*. **212**, 68–79

40. Kang, Y. H., Jin, J. S., Yi, D. W., and Son, S. M. (2010) Bone Morphogenetic Protein-7 Inhibits Vascular Calcification Induced by High Vitamin D in Mice. *Tohoku J Exp Medicine*. **221**, 299–307

41. Metz, R. P., Patterson, J. L., and Wilson, E. (2011) Methods in Molecular Biology. *Methods Mol Biology Clifton N J*. **843**, 169–176

42. Akiyoshi, T., Ota, H., Iijima, K., Son, B.-K., Kahyo, T., Setou, M., Ogawa, S., Ouchi, Y., and Akishita, M. (2015) A novel organ culture model of aorta for vascular calcification. *Atherosclerosis*. **244**, 51–8

43. Lebeau, P. F., Byun, J. H., Platko, K., Al-Hashimi, A. A., Lhoták, Š., MacDonald, M. E., Mejia-Benitez, A., Prat, A., Igdoura, S. A., Trigatti, B., Maclean, K. N., Seidah, N. G., and Austin, R. C. (2019) Pcsk9 knockout exacerbates diet-induced non-alcoholic steatohepatitis, fibrosis and liver injury in mice. *Jhep Reports*. **1**, 418–429

44. Lebeau, P. F., Byun, J. H., Platko, K., MacDonald, M. E., Poon, S. V., Faiyaz, M., Seidah, N. G., and Austin, R. C. (2019) Diet-induced hepatic steatosis abrogates cell-surface LDLR by inducing de novo PCSK9 expression in mice. *J Biological Chem*. **294**, 9037–9047

45. Koukoulaki, M., Papachristou, E., Kalogeropoulou, C., Papathanasiou, M., Zampakis, P., Vardoulaki, M., Alexopoulos, D., and Goumenos, D. S. (2012) Increased Prevalence and Severity of Coronary Artery Calcification in Patients with Chronic Kidney Disease Stage III and IV. *Nephron Extra*. **2**, 192–204

46. Holden, R. M., Beseau, D., Booth, S. L., Adams, M. A., Garland, J. S., Morton, R. A., Collier, C. P., and Foley, R. N. (2011) FGF-23 is associated with cardiac troponin T and mortality in hemodialysis patients: FGF-23, troponin and mortality. *Hemodial Int*. **16**, n/a-n/a

47. Morikawa, M., Derynck, R., and Miyazono, K. (2016) TGF-β and the TGF-β Family: Context-Dependent Roles in Cell and Tissue Physiology. *Csh Perspect Biol*. **8**, a021873

48. Hino, J., Nishimatsu, S., Nagai, T., Matsuo, H., Kangawa, K., and Nohno, T. (2003) Coordination of BMP-3b and cerberus is required for head formation of Xenopus embryos. *Dev Biol*. **260**, 138–157

49. Hino, J., Kangawa, K., Matsuo, H., Nohno, T., and Nishimatsu, S. (2004) Bone morphogenetic protein-3 family members and their biological functions. *Front Biosci*. **9**, 1520

50. Remacle, A. G., Gawlik, K., Golubkov, V. S., Cadwell, G. W., Liddington, R. C., Cieplak, P., Millis, S. Z., Desjardins, R., Routhier, S., Yuan, X. W., Neugebauer, W. A., Day, R., and Strongin, A. Y. (2010) Selective and potent furin inhibitors protect cells from anthrax without significant toxicity. *Int J Biochem Cell Biology*. **42**, 987–95

51. Sierra, O. L., and Towler, D. A. (2010) Runx2 trans-activation mediated by the MSX2-interacting nuclear target requires homeodomain interacting protein kinase-3. *Mol Endocrinol Baltim Md*. **24**, 1478–97

52. Pesaro, A. E., Katz, M., Liberman, M., Pereira, C., Mangueira, C. L. P., Carvalho, A. E. Z. de, Carvalho, K. S., Nomura, C. H., Franken, M., and Serrano, C. V. (2018) Circulating osteogenic proteins are associated with coronary artery calcification and increase after myocardial infarction. *Plos One*. **13**, e0202738

53. Schurgers, L. J., Barreto, D. V., Barreto, F. C., Liabeuf, S., Renard, C., Magdeleyns, E. J., Vermeer, C., Choukroun, G., and Massy, Z. A. (2010) The circulating inactive form of matrix gla protein is a surrogate marker for vascular calcification in chronic kidney disease: a preliminary report. *Clin J Am Soc Nephrol Cjasn*. **5**, 568–75

54. Ford, M. L., Tomlinson, L. A., Smith, E. R., Rajkumar, C., and Holt, S. G. (2010) Fetuin-A is an independent determinant of change of aortic stiffness over 1 year in non-diabetic patients with CKD stages 3 and 4. *Nephrol Dialysis Transplant Official Publ European Dialysis Transpl Assoc - European Ren Assoc*. **25**, 1853–8

55. Komori, T., Yagi, H., Nomura, S., Yamaguchi, A., Sasaki, K., Deguchi, K., Shimizu, Y., Bronson, R. T., Gao, Y.-H., Inada, M., Sato, M., Okamoto, R., Kitamura, Y., Yoshiki, S., and Kishimoto, T. (1997) Targeted Disruption of Cbfa1 Results in a Complete Lack of Bone Formation owing to Maturational Arrest of Osteoblasts. *Cell*. **89**, 755–764

56. Sun, Y., Byon, C. H., Yuan, K., Chen, J., Mao, X., Heath, J. M., Javed, A., Zhang, K., Anderson, P. G., and Chen, Y. (2012) Smooth muscle cell-specific runx2 deficiency inhibits vascular calcification. *Circ Res*. **111**, 543–52

57. Phimphilai, M., Zhao, Z., Boules, H., Roca, H., and Franceschi, R. T. (2006) BMP Signaling Is Required for RUNX2-Dependent Induction of the Osteoblast Phenotype. *J Bone Miner Res*. **21**, 637–646

58. Li, P., Li, Y., Zhu, L., Yang, Z., He, J., Wang, L., Shang, Q., Pan, H., Wang, H., Ma, X., Li, B., Fan, X., Ge, S., Jia, R., and Zhang, H. (2017) Targeting secreted cytokine BMP9 gates the attenuation of hepatic fibrosis. *Biochim Biophys Acta*. **1864**, 709–720

59. Desroches-Castan, A., Tillet, E., Ricard, N., Ouarné, M., Mallet, C., Belmudes, L., Couté, Y., Boillot, O., Scoazec, J.-Y., Bailly, S., and Feige, J.-J. (2019) BMP9 is a paracrine factor controlling liver sinusoidal endothelial cell fenestration and protecting from hepatic fibrosis. *Hepatology Baltim Md*. **70**, 1392–1408

60. Gravesen, E., Mace, M. L., Nordholm, A., Hofman-Bang, J., Hruska, K., Nielsen, C. H., Kjær, A., Olgaard, K., and Lewin, E. (2018) Exogenous BMP7 in aortae of rats with

chronic uremia ameliorates expression of profibrotic genes, but does not reverse established vascular calcification. *Plos One*. **13**, e0190820

61. Vukicevic, S., Basic, V., Rogic, D., Basic, N., Shih, M. S., Shepard, A., Jin, D., Dattatreyamurty, B., Jones, W., Dorai, H., Ryan, S., Griffiths, D., Maliakal, J., Jelic, M., Pastorcic, M., Stavljenic, A., and Sampath, T. K. (1998) Osteogenic protein-1 (bone morphogenetic protein-7) reduces severity of injury after ischemic acute renal failure in rat. *J Clin Invest*. **102**, 202–214

62. Li, T., Surendran, K., Zawaideh, M. A., Mathew, S., and Hruska, K. A. (2004) Bone morphogenetic protein 7: a novel treatment for chronic renal and bone disease. *Curr Opin Nephrol Hy*. **13**, 417–422

63. Hsiao, E. C., Koniaris, L. G., Zimmers-Koniaris, T., Sebald, S. M., Huynh, T. V., and Lee, S.-J. (2000) Characterization of Growth-Differentiation Factor 15, a Transforming Growth Factor β Superfamily Member Induced following Liver Injury. *Mol Cell Biol*. **20**, 3742–3751

64. Zhang, Y., Moszczynski, L. A., Liu, Q., Jiang, J., Zhao, D., Quan, D., Mele, T., McAlister, V., Jevnikar, A., Baek, S. J., Liu, K., and Zheng, X. (2017) Over-expression of growth differentiation factor 15 (GDF15) preventing cold ischemia reperfusion (I/R) injury in heart Transplantation through Foxo3a signaling. *Oncotarget*. 10.18632/oncotarget.16607

65. Golakani, M. H., Mohammad, M. G., Li, H., Gamble, J., Breit, S. N., Ruitenberg, M. J., and Brown, D. A. (2019) MIC-1/GDF15 Overexpression Is Associated with Increased Functional Recovery in Traumatic Spinal Cord Injury. *J Neurotraum*. **36**, 3410–3421

66. Hino, J., Nakatani, M., Arai, Y., Tsuchida, K., Shirai, M., Miyazato, M., and Kangawa, K. (2017) Overexpression of bone morphogenetic protein-3b (BMP-3b) in adipose tissues protects against high-fat diet-induced obesity. *Int J Obes 2005*. **41**, 483–488

Figures and figure legends

Figure 1.

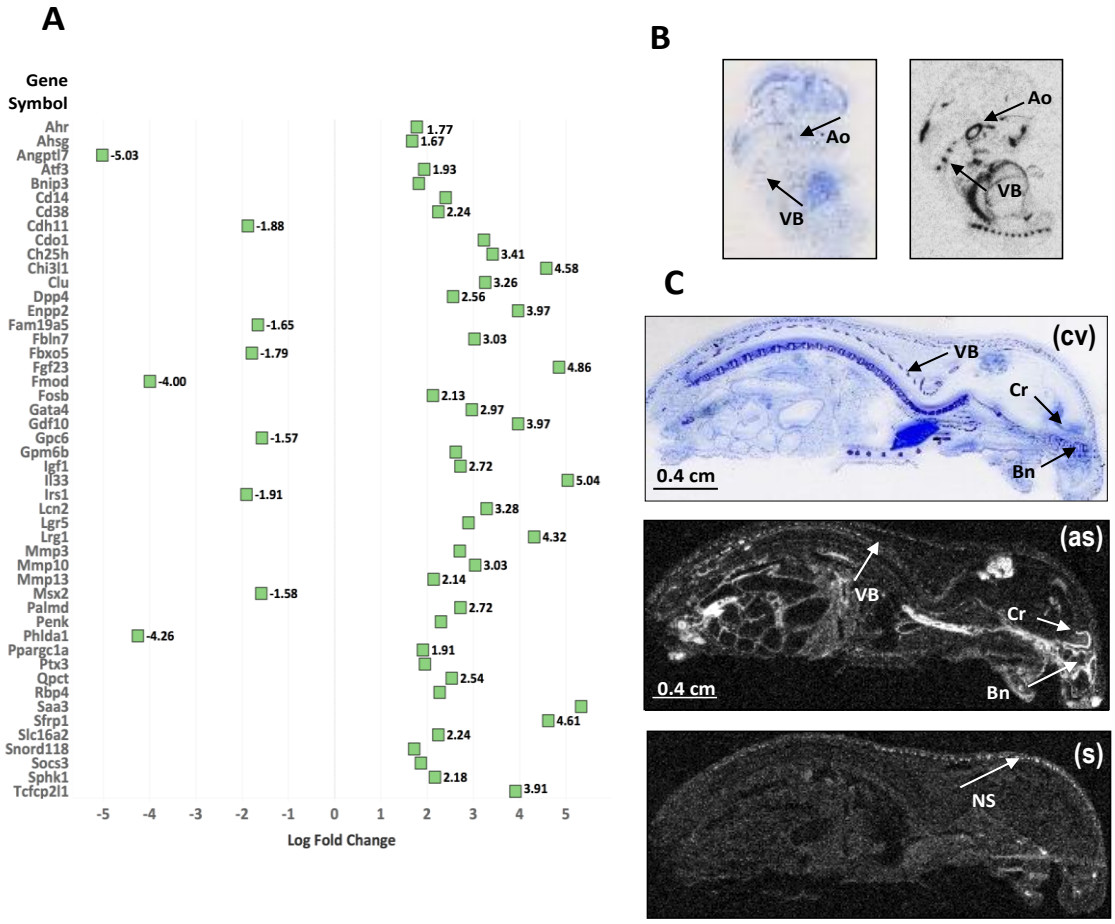

Figure 1. Gdf10 is highly expressed in the vasculature, bone and cartilage, and is upregulated in *Tdag51*$^{-/-}$ mice. (A**)** Representation of the log fold change of genes that have previously been demonstrated to be involved in the regulation of mineral deposition in either soft tissues or bone in VSMCs from *Tdag51*$^{-/-}$ mice compared to littermate controls. (**B** and **C**). *Gdf10* mRNA distribution in whole body sections of mice at embryonic day 12 (E12) and postnatal day 5 (p5). All data are shown as mean and error bars as S.D. *, $p<0.05$ by unpaired two-tailed Student's *t*-test. As, antisense; Ao, aorta; Bn, bone; CV, thionin staining; Cr, cartilage; NS, non-specific staining; S, control sense; Tdag51, T-cell death associated gene 51; VB, vertebrae.

Figure 2.

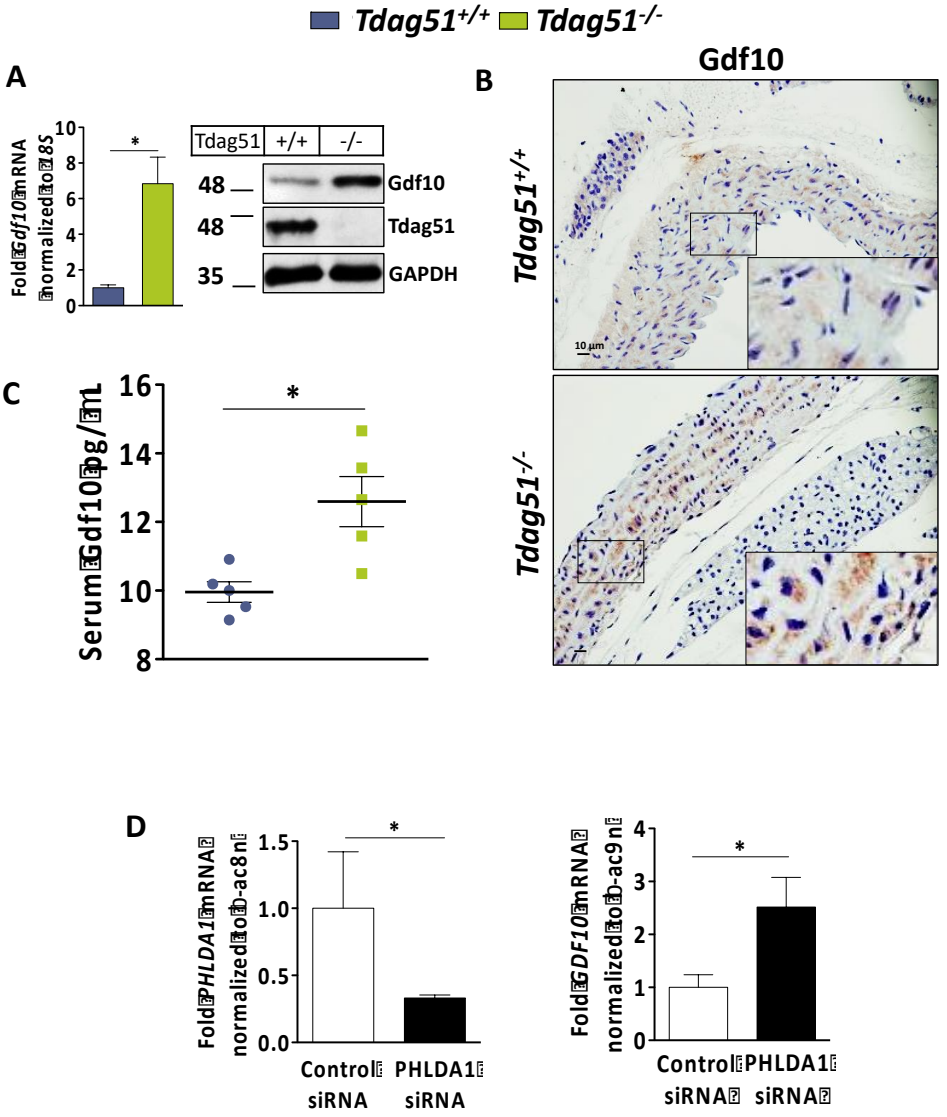

Figure 2. *Tdag51*$^{-/-}$ VSMCs and mice exhibit increased expression of Gdf10. (A) Quantitative real-time PCR and immunoblot analysis of Gdf10 expression in *Tdag51*$^{+/+}$ and *Tdag51*$^{-/-}$ VSMCs (n=3). **(B)** IHC staining of Gdf10 in *Tdag51*$^{+/+}$ and *Tdag51*$^{-/-}$ mouse aortas. **(C)** Plasma levels of Gdf10 protein in male *Tdag51*$^{+/+}$ and *Tdag51*$^{-/-}$ mice (n=5). **(D)** Quantitative real-time PCR analysis of *PHLDA1* and *GDF10* expression in human VSMCs transfected with either control siRNA or siRNA targeted against *PHLDA1* (n=3). All data are shown as mean and error bars as S.D. *, $p<0.05$ by unpaired two-tailed Student's *t*-test. GAPDH, Glyceraldehyde 3-phosphate dehydrogenase; Gdf10, growth differentiation factor 10; PHLDA1, pleckstrin homology like domain family A member 1; Tdag51, T-cell death associated gene 51; VSMCs, vascular smooth muscle cells.

Figure 3.

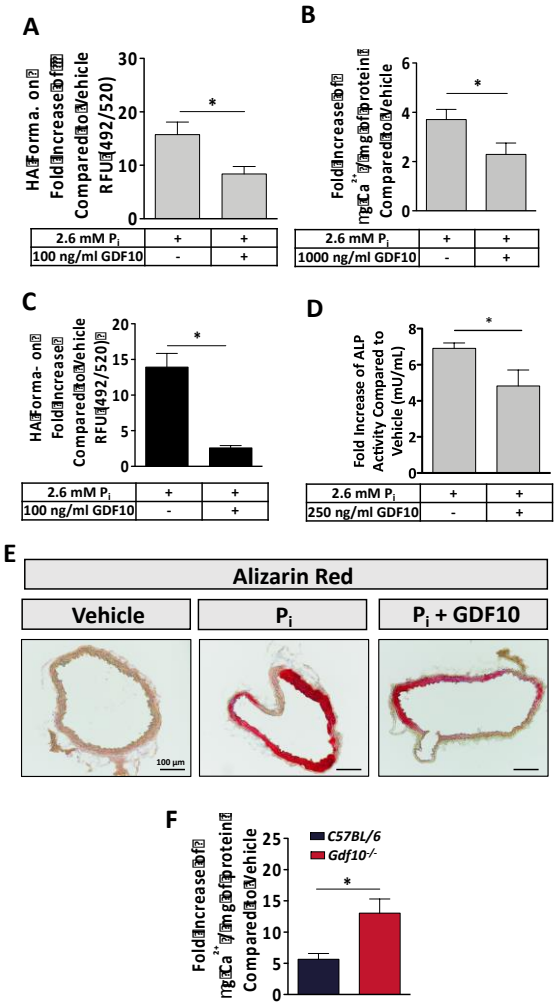

Figure 3. rhGDF10 treatment inhibits P_i-mediated mineral deposition. (A, B) Quantification of P_i-induced HA crystal formation and calcium deposition in wild-type (C57BL/6J) mouse VSMCs (n=5-10) and *ex vivo* aortic ring cultures (n=4) following P_i (2.6 mM) treatment for 5 and 7 days, respectively, in the presence or absence of rhGDF10 (100 ng/ml or 1000 ng/ml). **(C)** Quantification of P_i-induced HA crystal formation in human VSMCs following 5 days of P_i (2.6 mM) treatment in the presence or absence of rhGDF10 (100 ng/ml; n=8-11). **(D)** Quantification of alkaline phosphatase activity in wild-type VSMCs following 4 days of P_i (2.6 mM) and rhGDF10 (250 ng/ml) treatment. **(E)** Alizarin red calcium stain in wild-type *ex vivo* aortic rings following 7 days of Pi (2.6 mM) and rhGDF10 (1000 ng/ml) treatment. **(F)** Quantification of calcium deposition in C57BL/6J and *Gdf10*$^{-/-}$ mouse *ex vivo* aortic ring cultures following 7 days of P_i (2.6 mM) treatment (n=4). All data are shown as means and error bars as S.D. *, $p<0.05$ by unpaired two-tailed Student's *t*-test. ALP, alkaline phosphatase; Gdf10, growth differentiation factor 10; HA, hydroxyapatite; P_i, inorganic phosphate; rh, recombinant human.

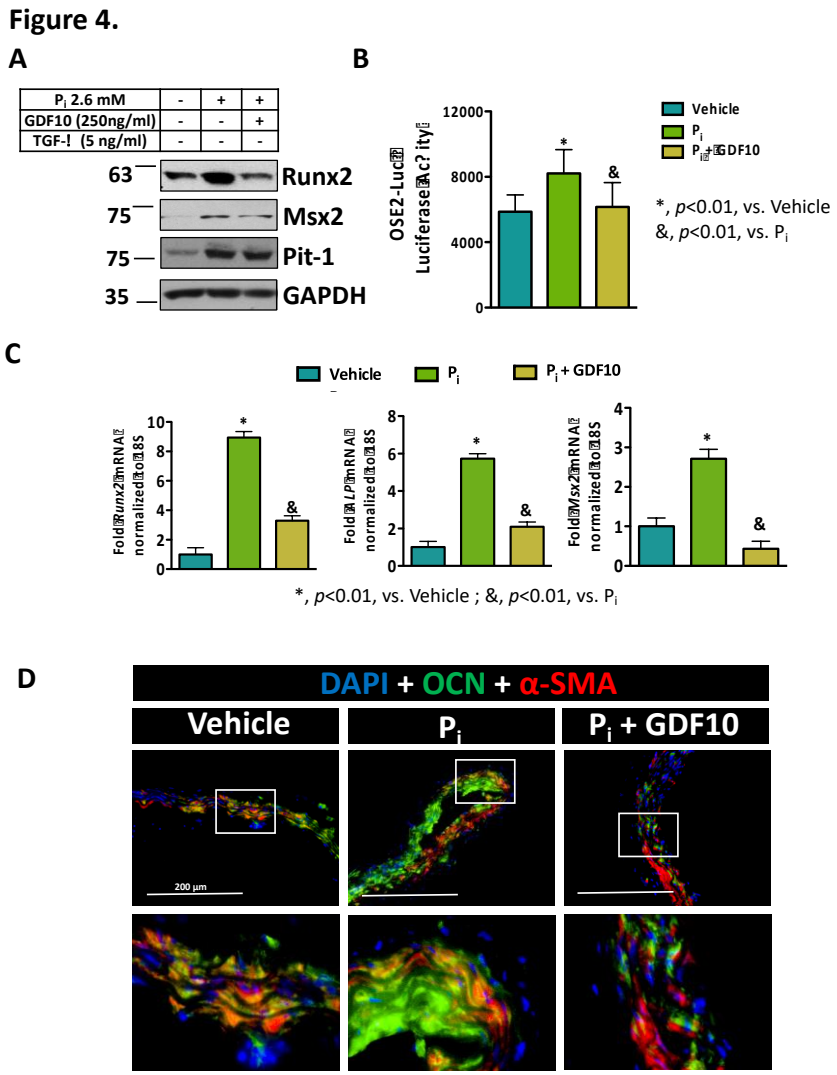

Figure 4. rhGDF10 treatment inhibits P_i-induced Runx2 protein expression in C57BL/6J VSMCs. (A) Immunoblot analysis of Runx2, Msx2, Pit-1 and GAPDH expression in VSMCs from C57BL/6J mice following 4 day treatment of P_i (2.6 mM) in the presence or absence rhGDF10 (250 ng/ml). **(B)** Runx2 luciferase reporter assay following 2 days of 2.6 mM P_i treatment (n=6-13 per group). **(C)** Quantitative real time polymerase chain reaction of Runx2, Msx2, and ALP mRNA expression (n=3). **(D)** Representative micrograph of immunofluorescence staining in wild-type ex vivo aortic rings following 7 days of Pi (2.6 mM) and rhGDF10 (1000 ng/ml) treatment, OCN (green), α-SMA (red) and DAPI (blue). All data are shown as means and error bars as S.D. *, $p<0.05$ by 1-way ANOVA with Tukey multiple comparison testing. ALP, alkaline phosphatase; GAPDH, Glyceraldehyde 3-phosphate dehydrogenase; Msx2, Msh homeobox 2; rh, recombinant human; Pit-1, type III sodium-dependent phosphate transporter; Runx2, runt-related transcription factor 2.

Figure 5.

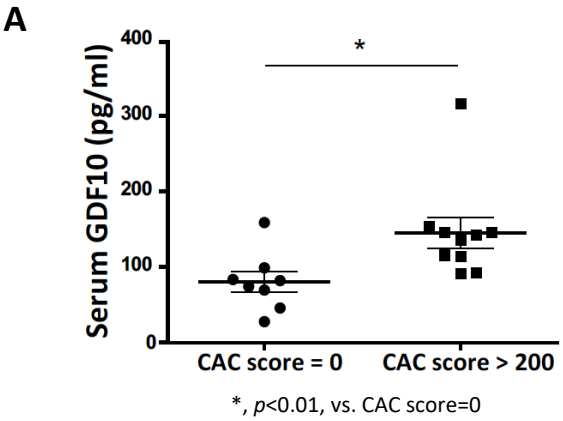

Figure 5. Serum GDF10 levels are elevated in patients with CKD and established VC. (A) Quantification of serum GDF10 levels in patients with CKD (n=8-9). All data are shown as means and error bars as S.D. *, $p<0.05$ by unpaired two-tailed Student's *t*-test. CAC, coronary artery calcium; CKD, chronic kidney disease; GDF10, growth differentiation factor 10.

SUPPLEMENTAL MATERIALS

Gdf10 is a negative regulator of hydroxyapatite mineral deposition in VSMCs

*Khrystyna Platko[§], Gabriel Gyulay[§], Paul F. Lebeau[§], Melissa E. MacDonald[§], Jae Hyun Byun[§], Suleiman A. Igdoura[‡,**],Rachel M. Holden[†], Anna Roubtsova[¶], Nabil G. Seidah[¶], Joan C. Krepinsky[§*,†], Richard C. Austin[§*,†]*

Authors Affiliations: The [§]Department of Medicine, Division of Nephrology, McMaster University, and The Research Institute of St. Joseph's Hamilton, Hamilton, Ontario, Canada. The [**]Department of Pathology and Molecular Medicine and [‡]Biology, McMaster University Medical Centre, Hamilton, Ontario, Canada. The [†]Department of Medicine, Queen's University, Kingston, Ontario, Canada. The [¶]Institut de Recherches Cliniques de Montréal (IRCM), Affiliated with Université de Montréal, Montréal, Quebec, Canada

* Contributed equally to this work

[†] **Corresponding Author:** To whom correspondence should be addressed: Dr. Richard C. Austin, 50 Charlton Ave East, Room T-3313, Hamilton, Ontario, L8N 4A6. Phone: 905-522-1155 x35175; Fax: 905-540-6589; E-mail: austinr@taari.ca

Supplemental Table 1: List of antibodies used for immunoblotting (IB), immunohistochemistry (IHC) and immunofluorescence (IF)

Target antigen	Vendor or Source	Catalog #	Working concentration	Persistent ID / URL
GAPDH	Cell Signaling Technology	5174	IB: 0.34 µg/ml	https://www.cellsignal.com/products/primary-antibodies/gapdh-d16h11-xp-rabbit-mab/5174
OCN	Abcam	ab93876	IF: 1.0 µg/ml	https://www.abcam.com/osteocalcin-antibody-ab93876.html
RUNX2	Cell Signaling Technology	8486	IB: 1.82 µg/ml	https://www.cellsignal.com/products/primary-antibodies/runx2-d1h7-rabbit-mab/8486
Msx2	Novus Biologicals	NBP1-85445	IB: 0.548 µg/ml	https://www.novusbio.com/products/msx2-antibody_nbp1-85445
TDAG51	Sant Cruz Biotechnology	SC-23866	IB: 0.4 µg/ml	https://www.scbt.com/p/tdag51-antibody-rn-6e2
GDF10	Novus Biologicals	H00002662-B01P	IB:0.5 µg/ml IHC: 2 µg/ml	https://www.novusbio.com/products/bmp-3b-gdf-10-antibody_h00002662-b01p

Supplemental Table 2: List of Primers Used for Quantitative Real-Time PCR

Gene	Species	Forward	Reverse
PHLDA1	Human	GAAGATGGCCCATTCAAAAGCG	GAGGAGGCTAACACGCAGG
18S	Human	GTAACCCGTTGAACCCCATT	CCATCCAATCGGTAGTAGCG
18s	Mouse	CTTAGAGGGACAAGTGGCG	ACGCTGAGCCAGTCAGTGTA
Gdf10	Mouse	AATGATCGACCAAAAGCCTGT	CTTGCAGAATACCTCACGAGC
Runx2	Mouse	ATGCTTCATTCGCCTCACAAA	GCACTCACTGACTCGGTTGG
ALP	Mouse	CCAACTCTTTTGTGCCAGAGA	GGCTACATTGGTGTTGAGCTTTT
Msx2	Mouse	GGCAACCCTGTGCTACGAAT	CCTGGACTCTCTTTTGGGCTTTA

Supplemental figures and figure legends

Fig. S1

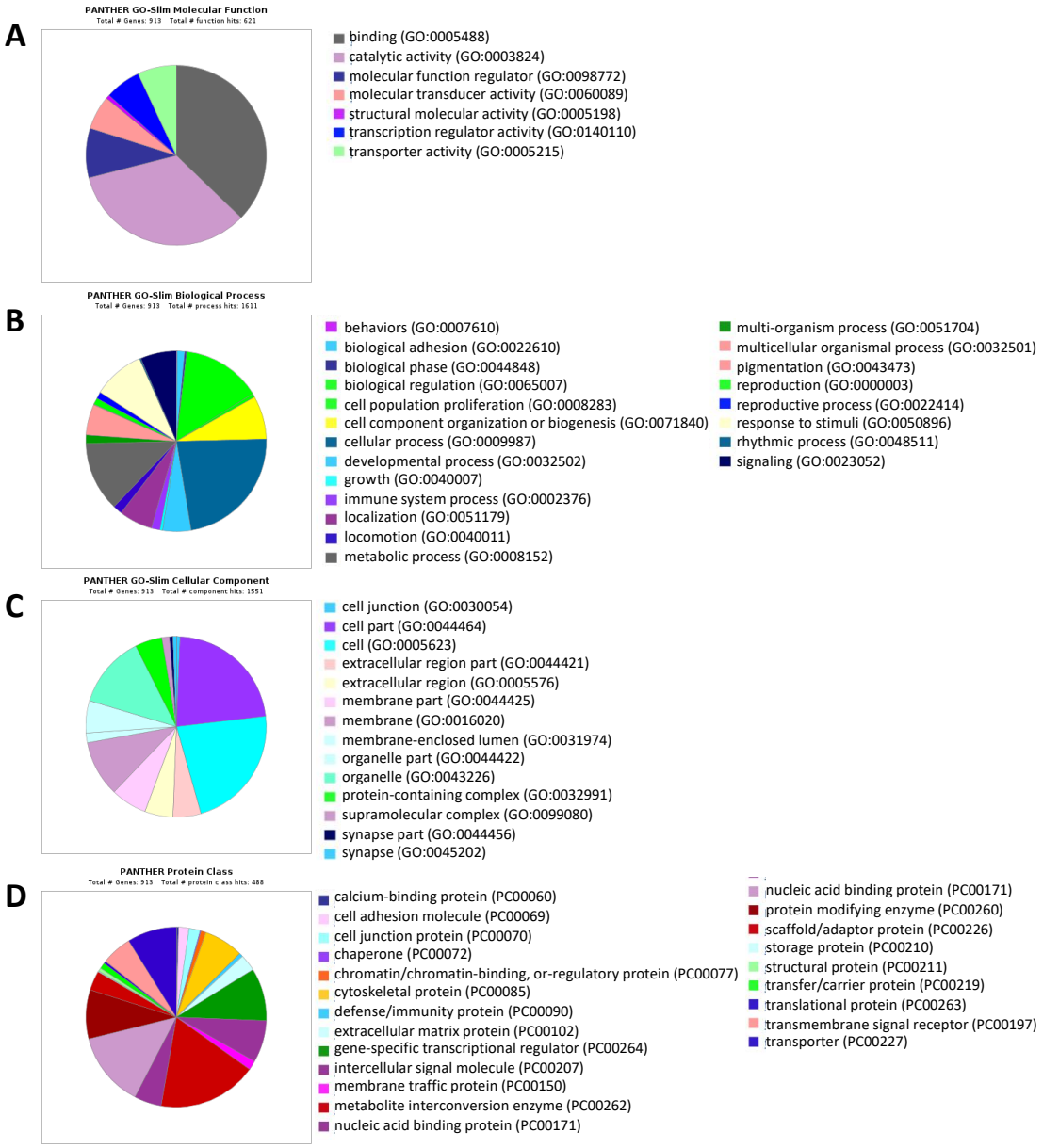

Figure S1. Gene ontology classification of targets identified by the microarray analysis. (A) Molecular function. **(B)** Biological process. **(C)** Cellular component. **(D)** Protein class.

Fig. S2

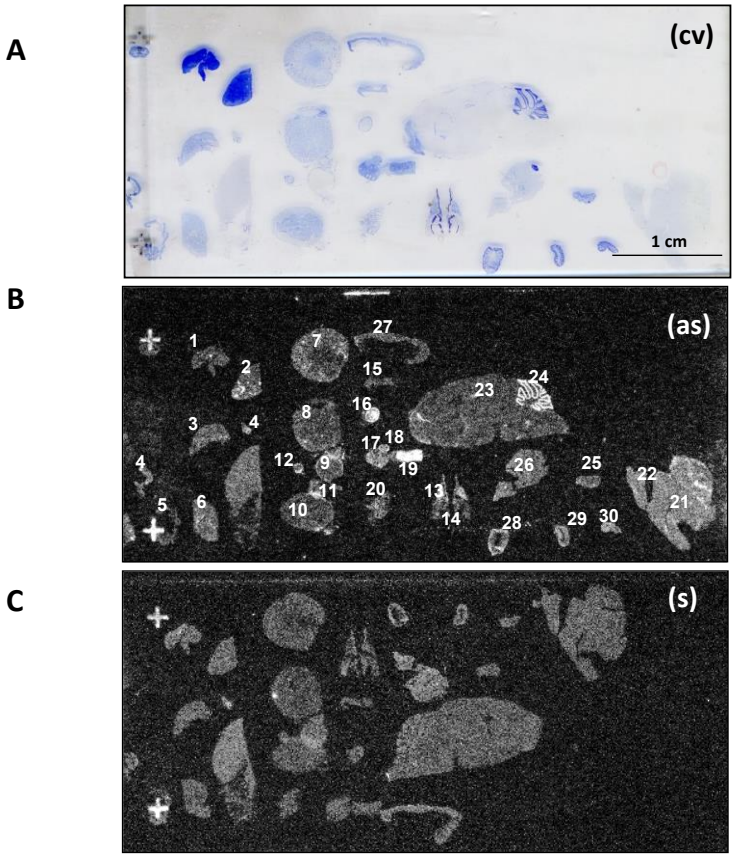

Tissues:

1 – thymus	11 – epididymis	21 – liver
2 – spleen	12 – esophagus	22 – gallbladder
3 – lung	13 – parathyroid gland	23 – brain
4 – aorta	14 – thyroid gland	24 - cerebellum
5 – submaxillary gland	15 – pituitary gland	25 – colon
6 – heart	16 – adrenal gland	26 – pancreas
7 – testis	17 – ovary (estrus)	27 – stomach
8 – kidney	18 – oviducts	28 – duodenum
9 – coagulating gland	19 – uterus	29 – jejunum
10 – urinary bladder	20 – prostate	30 – ileum

Figure S2. Local distribution of Gdf10 mRNA expression in 30 tissues of adult mice, following antisense and sense hybridization. (**A**) Frozen tissue cryostat sections in 30 mouse tissues array after thionin staining. (**B**) X-ray film autoradiography with frozen tissue cryostat sections following antisense hybridization and 5 days exposure (same slide as in A). (**C**) Control (sense) hybridization in adjacent cryostat sections showing a level of non-specific labelling (same slide as in A). As, antisense; CV, thionin staining; Gdf10, growth differentiation factor 10; S, control sense.

Fig. S3

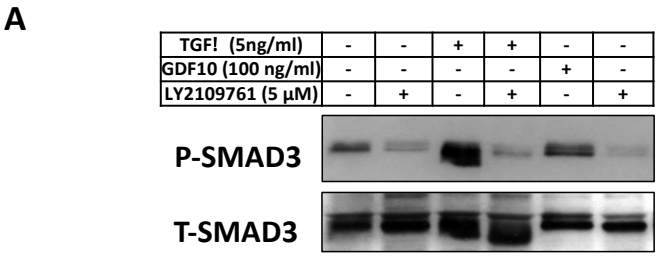

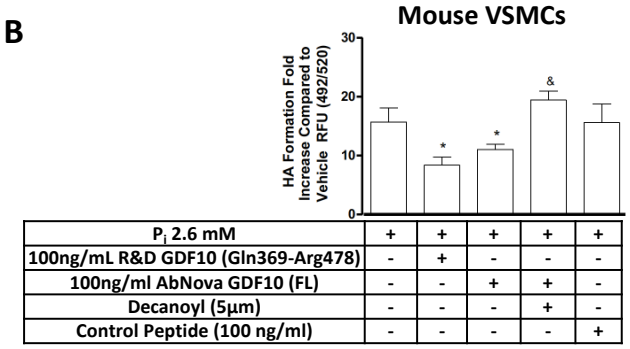

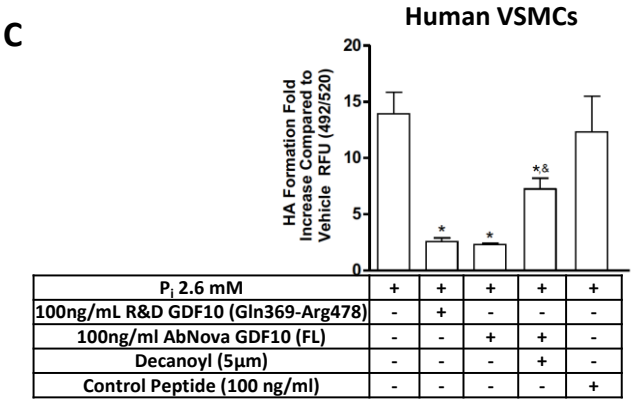

Figure S3. rhGDF10 treatment induces SMAD3 phosphorylation in TGFβ receptor-dependent manner. (A) Immunoblot analysis of P-SMAD3 and T-SMAD3 expression in VSMCs from C57BL6/J mice treated with rhGDF10 (100 ng/ml) in the presence or absence of TGFβ receptor inhibitor (5 µm). Recombinant TGFβ used as a positive control (5 ng/ml). (B and C) Quantification of P_i-induced HA crystal formation and calcium deposition in mouse and human *ex vivo* aortic ring cultures (n=8) following 5 days of P_i (2.6 mM) treatment in the presence or absence of cleaved/active or full length rhGDF10 (100 ng/ml) as well as decanoyl (5 µm) and control peptide (100 ng/ml). All data are shown as means and error bars as S.D. *, $p<0.05$ by 1-way ANOVA with Tukey multiple comparison testing. GDF10, growth differentiation factor 10; TGFβ, transforming growth factor beta.

Fig. S4

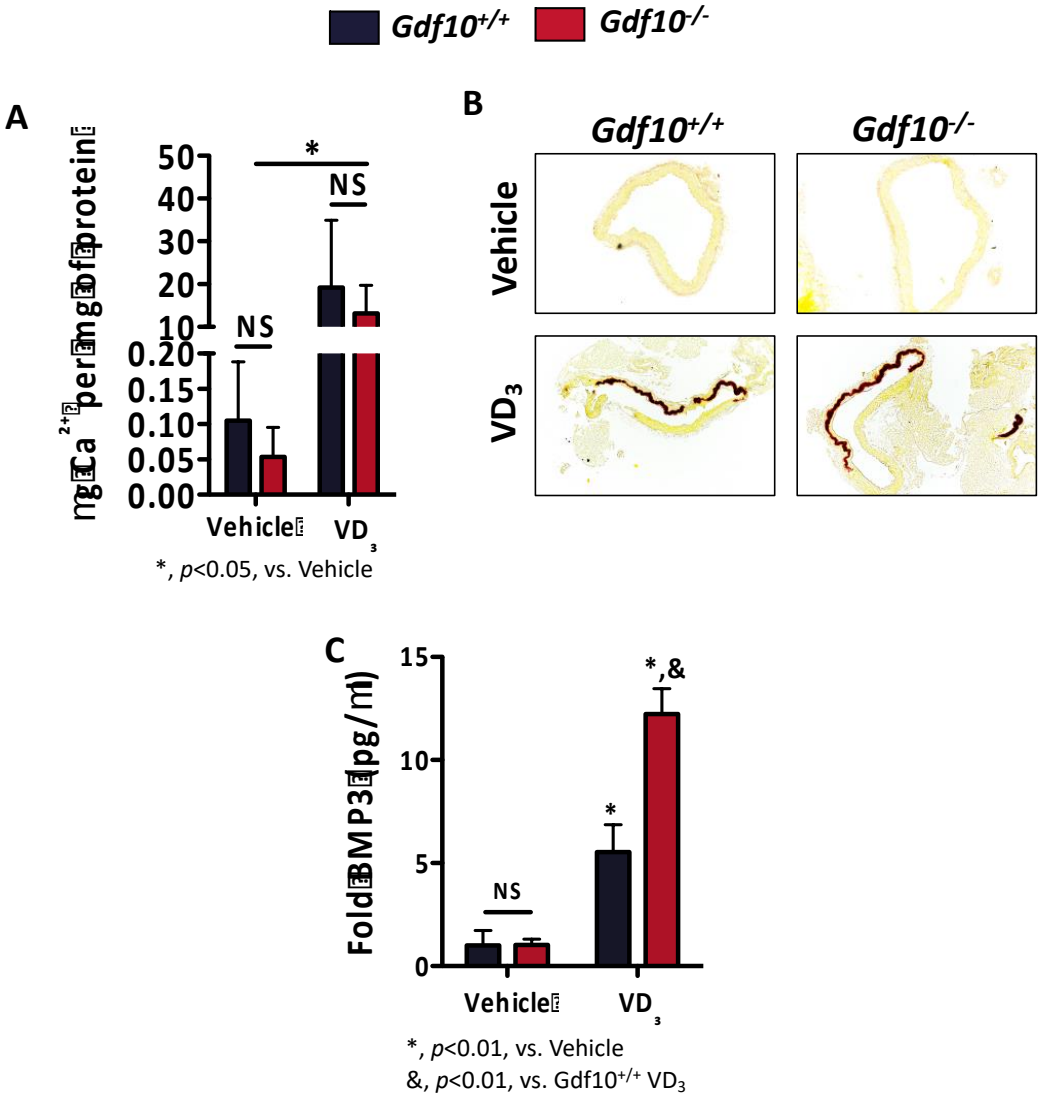

Figure S4. Gdf10$^{-/-}$ mice develop similar degree of VD3-induced mineral deposition compared to Gdf10$^{+/+}$ littermate controls. (**A, B**) Calcium quantification and Alizarin Red calcium stain in the abdominal aortas (n=5-8). **(C)** BMP3 ELISAs (n=6). All data are shown as mean and error bars as S.D. *, $p<0.05$ by unpaired two-tailed Student's *t*-test. BMP3, bone morphogenic protein 3; Gdf10 growth differentiation factor 10; VD3, vitamin G3.

CHAPTER 4: MANUSCRIPT 3

GDF10 blocks hepatic PPARγ activation to protect against diet-induced liver injury.

Khrystyna Platko*, Paul F. Lebeau*, Jae Hyun Byun, Samantha V. Poon, Emily A. Day, Melissa E. MacDonald, Nicholas Holzapfel, Aurora Mejia-Benitez, Kenneth N. Maclean, Joan C. Krepinsky, Richard C. Austin

* Authors contributed equally to this work.

Molecular Metabolism (2019). 27(9):62-74. doi: 10.1016/j.molmet.2019.06.021
.

Chapter link: *GDF10 blocks hepatic lipid accumulation and injury*. While examining the role of GDF10 in VC, we observed that GDF10 KO mice develop increased body weight, adiposity, and hepatic lipid accumulation when fed normal control diet. In line with our preliminary observations, mice overexpressing GDF10 are protected against HFD-induced obesity[196]. This journal article further characterizes GDF10 as modulator of metabolic homeostasis. More specifically, recombinant human GDF10 attenuated hepatic lipid accumulation and subsequent injury by antagonizing PPARγ activation and expression in cultured hepatocyte cells and liver tissue. Consistent with these observations, GDF10 KO developed severe diet-induced hepatic steatosis and fibrosis.

Author's contribution: K. Platko, P.F. Lebeau and R. C. Austin designed the study. K. Platko and P.F. Lebeau performed cell culture experiments, western blotting, immunohistochemistry staining, immunofluorescence staining, morphological staining (H&E, Masson's Trichrome), as well as related analysis with help of, J. Hyun Byun, S. V. Poon, and N. Holzapfel. Analysis of fatty acid oxidation was performed by E.A. Day. Animal experiments were conducted by K. Platko with help of M.E. MacDonald. K. Platko and P.F. Lebeau curated the data and wrote the manuscript. K. Platko, P.F. Lebeau, R.C. Austin, J.C. Krepinsky, K.N. Maclean and A. Mejia-Benitez reviewed and edited the manuscript. All authors approved the final submission

Original Article

MOLECULAR METABOLISM

GDF10 blocks hepatic PPARγ activation to protect against diet-induced liver injury

Khrystyna Platko [1,4], Paul F. Lebeau [1,4], Jae Hyun Byun [1], Samantha V. Poon [1], Emily A. Day [2], Melissa E. MacDonald [1], Nicholas Holzapfel [1], Aurora Mejia-Benitez [1], Kenneth N. Maclean [3], Joan C. Krepinsky [1], Richard C. Austin [1,*]

ABSTRACT

Objective: Growth differentiation factors (GDFs) and bone-morphogenic proteins (BMPs) are members of the transforming growth factor β (TGFβ) superfamily and are known to play a central role in the growth and differentiation of developing tissues. Accumulating evidence, however, demonstrates that many of these factors, such as BMP-2 and -4, as well as GDF15, also regulate lipid metabolism. GDF10 is a divergent member of the TGFβ superfamily with a unique structure and is abundantly expressed in brain and adipose tissue; it is also secreted by the latter into the circulation. Although previous studies have demonstrated that overexpression of GDF10 reduces adiposity in mice, the role of circulating GDF10 on other tissues known to regulate lipid, like the liver, has not yet been examined.

Methods: Accordingly, GDF10$^{-/-}$ mice and age-matched GDF10$^{+/+}$ control mice were fed either normal control diet (NCD) or high-fat diet (HFD) for 12 weeks and examined for changes in liver lipid homeostasis. Additional studies were also carried out in primary and immortalized human hepatocytes treated with recombinant human (rh)GDF10.

Results: Here, we show that circulating GDF10 levels are increased in conditions of diet-induced hepatic steatosis and, in turn, that secreted GDF10 can prevent excessive lipid accumulation in hepatocytes. We also report that GDF10$^{-/-}$ mice develop an obese phenotype as well as increased liver triglyceride accumulation when fed a NCD. Furthermore, HFD-fed GDF10$^{-/-}$ mice develop increased steatosis, endoplasmic reticulum (ER) stress, fibrosis, and injury of the liver compared to HFD-fed GDF10$^{+/+}$ mice. To explain these observations, studies in cultured hepatocytes led to the observation that GDF10 attenuates nuclear peroxisome proliferator-activated receptor γ (PPARγ) activity; a transcription factor known to induce *de novo* lipogenesis.

Conclusion: Our work delineates a hepatoprotective role of GDF10 as an adipokine capable of regulating hepatic lipid levels by blocking *de novo* lipogenesis to protect against ER stress and liver injury.

© 2019 The Authors. Published by Elsevier GmbH. This is an open access article under the CC BY-NC-ND license (http://creativecommons.org/licenses/by-nc-nd/4.0/).

Keywords BMP-3b; ER stress; Hepatic steatosis; HFD; NAFLD; NASH; TGFβ

1. INTRODUCTION

Obesity is considered by many as the epidemic of the 21st century, affecting over 2 billion individuals worldwide and still increasing in frequency [1]. Although obesity is commonly thought of as a disease characterized by excess adipose tissue, other hallmark characteristics are also common in obese individuals. Non-alcoholic fatty liver disease (NAFLD) affects approximately 75% of obese individuals and contributes to other comorbidities associated with obesity, such as type 2 diabetes mellitus, hypertension, heart disease and ischemic stroke [2,3]. NAFLD is defined as an accumulation of triglyceride in the liver in excess of 5% of total liver weight and is commonly referred to as steatosis. Simple steatosis is largely benign; however, NAFLD can progress to life-threatening non-alcoholic steatohepatitis (NASH) or liver cirrhosis. Although the precise mechanism of progression remains poorly understood, the well-accepted *multiple-hits hypothesis* suggests that cellular events including oxidative stress, lipid peroxidation, Kupffer cell activation, and adipocytokine alterations play a central role [1,4]. Numerous studies have also demonstrated that ER stress plays a key role in the development of NAFLD and NASH by promoting Kupffer cell activation, oxidative stress and mitochondrial dysfunction [5—7]. Given that secretory cells like adipocytes and hepatocytes are rich in ER, the role of ER stress has become a topic of considerable interest in the development of metabolic diseases. ER stress is characterized by an overwhelming of ER-resident chaperones by misfolded *de novo* polypeptides in the ER lumen. This event triggers the unfolded protein response (UPR) in order to increase ER protein folding capacity and restore homeostatic conditions. The signaling cascades of the UPR are comprised of (a) the activating transcription factor 6 (ATF6) pathway, which modulates sterol regulatory element-binding protein (SREBP)-2

[1]Department of Medicine, McMaster University, The Research Institute of St. Joe's Hamilton, Hamilton Centre for Kidney Research, Hamilton, Ontario, L8N 4A6, Canada [2]The Division of Endocrinology and Metabolism, Department of Medicine, McMaster University, 1280 Main Street West, Hamilton, Ontario, L8N 4A6, Canada [3]The Department of Pediatrics, University of Colorado School of Medicine, Aurora, CO, 80045, USA

[4] Khrystyna Platko and Paul F. Lebeau contributed equally to this work.

*Corresponding author. 50 Charlton Ave East, Room T-3313, Hamilton, Ontario, L8N 4A6, Canada. Fax: +905 540 6589. E-mail: austinr@taari.ca (R.C. Austin).

Received April 9, 2019 • Revision received June 14, 2019 • Accepted June 24, 2019 • Available online 28 June 2019

https://doi.org/10.1016/j.molmet.2019.06.021

 © 2019 The Authors. Published by Elsevier GmbH. This is an open access article under the CC BY-NC-ND license (http://creativecommons.org/licenses/by-nc-nd/4.0/).

MOLECULAR METABOLISM

Abbreviations

ANGPTL4	angiopoietin-like 4
ACOX1	acyl-coenzyme A oxidase 1
ACOT2	acyl-coenzyme A thioesterase 2
ACADM	acyl-coenzyme A dehydrogenase, C-4 to C-12 straight chain
ATF4	activating transcription factor 4
ATF6	activating transcription factor 6
ALT	alanine-L transaminase
BMP	bone morphogenic protein
BAT	brown adipose tissue
BSA	bovine-serum albumin
C/EBPα	CCAAT-enhancer-binding protein α
CD36	cluster of differentiation 36
CGTZ	ciglitizone
CLAMS	Columbus Instruments Comprehensive Lab Animal Monitoring System
CRTC2	CREB-regulated transcription cofactor 2
CHOP	C/EBP homologous protein
DMEM	Dulbecco's Modified Eagle's Medium
ER	endoplasmic reticulum
FBS	fetal bovine serum
FATP5	fatty acid transport protein 5
FSP27	fat-specific protein 27
FOXO1	forkhead box protein O1
FN1	fibronectin 1
FFPE	formalin-fixed paraffin-embedded
GDF10	growth differentiation factor 10
GAT	gonadal adipose tissue
GRP78	glucose-regulated protein of 78 kDa
GRP94	glucose-regulated protein of 94 kDa
β-HB	β-hydroxybutyrate
HFD	high-fat diet
IHC	immunohistochemistry
IAT	inguinal adipose tissue
IRE1α	inositol-requiring 1α
LPL	lipoprotein lipase
IL1β	interleukin 1β
LDH	lactate dehydrogenase
NAFLD	non-alcoholic fatty liver disease
NASH	non-alcoholic steatohepatitis
NCD	normal control diet
ORO	Oil Red O
OA	oleate
PFA	paraformaldehyde
PPARγ/α	peroxisome proliferator-activated receptor γ/α
PGC1β	peroxisome proliferator-activated receptor gamma coactivator 1-β
PPRE	peroxisome proliferator response element
PSR	Picrosirius red
PDK4	pyruvate dehydrogenase lipoamide kinase isozyme 4
PERK	protein kinase RNA (PKR)-like ER kinase
PA	palmitate
PCK1	phosphoenolpyruvate carboxykinase 1
PBS	phosphate-buffered saline
rhGDF10	recombinant human growth differentiation factor 10
si	small interfering
STAT3	signal transducer and activator of transcription 3
SREBP-1/-2	sterol regulatory element-binding protein-1/-2
TGFβ	transforming growth factor β
TGFβR1	TGFβ receptor subtype-1
TG	thapsigargin
TM	tunicamycin
TNFα	tumor necrosis factor alpha
UPR	unfolded protein response
XBP1	X-box-binding protein 1

mediated *de novo* lipogenesis [8]; (b) the highly conserved inositol-requiring 1α (IRE1α) - X-box-binding protein 1 (XBP1) pathway, which is required for the regulation of hepatic lipids during conditions of stress [9]; as well as (c) the protein kinase RNA (PKR)-like ER kinase (PERK) - activating transcription factor 4 (ATF4) pathway capable of regulating *de novo* lipogenesis via fatty acid synthase and SREBP-1 [10]. Previous studies have also demonstrated that ATF4 can induce the expression and activation of PPARγ, a transcription factor known to promote the expression of pro-adipogenic mediators including fatty acid transport protein 5 (*FATP5*), angiopoietin-like 4 (*ANGPTL4*), lipoprotein lipase *(LPL), Perilipin,* cluster of differentiation 36 (*CD36*) and fat-specific protein 27 (*FSP27*) [11,12]. Clinical studies have also characterized increased PPARγ expression in the livers of patients with NAFLD [13]. Although pro-survival at its core, chronic or severe ER stress can induce the expression of lipid-regulatory genes that promote *de novo* lipogenesis, as well as drive inflammation, fibrosis, and apoptosis in the liver [14].

GDF10, also known as BMP-3b, is an atypical member of the TGFβ superfamily capable of inhibiting osteoblast differentiation by antagonizing BMP-2 and -4 -mediated osteogenesis [15]. To date, over 30 members of the superfamily have been described, and all share common features. They are synthesized as precursor proteins containing N-terminal signal peptide sequences and pro-regions. Once secreted, the mature, biologically active molecule is believed to consist of a homodimer originating from proteolytically-cleaved precursors [16]. In recent years, accumulating evidence has shown that these factors play a central role in the regulation of energy balance and homeostasis. BMP-2 and -4 promote white adipogenesis while BMP-7 promotes brown adipogenesis [17—19]. Studies have also demonstrated that *in vitro* knockdown of GDF10 enhances adipogenesis and that transgenic mice overexpressing GDF10 are protected against diet-induced obesity and insulin resistance [20,21]. GDF15 has also been shown to regulate feeding and fatty acid oxidation and to protect against steatosis, insulin resistance, obesity, and ER stress in the livers of mice fed a HFD [22—24].

It is well-established that adipokines can modulate obesity and a variety of its comorbidities, including NAFLD [25]. However, little is known about the role of circulating GDF10 on liver health/function and injury in the face of diet-induced obesity. Here, we report that pharmacologic and diet-induced ER stress increases the expression of GDF10 in cultured pre-adipocytes and in white adipose tissue. We also show that GDF10$^{-/-}$ mice exhibit increased nuclear PPARγ expression and activity coupled with hepatic steatosis on the NCD and develop a severe NASH-like phenotype on the HFD. Collectively, our findings suggest that circulating GDF10 plays a critical role as a regulator of hepatic PPARγ during conditions of dietary stress and that GDF10 is capable of attenuating the progression of steatosis to NASH.

 © 2019 The Authors. Published by Elsevier GmbH. This is an open access article under the CC BY-NC-ND license (http://creativecommons.org/licenses/by-nc-nd/4.0/).

2. MATERIALS AND METHODS

2.1. Animal studies

GDF10$^{-/-}$ mice were a generous gift from Dr. Se-Jin Lee (Johns Hopkins University) [16]. Animals were housed in 12 h light cycles and controlled temperature and humidity conditions and had access to standard NCD (2918, Envigo) and water *ad libitum* (n = 10). In experiments designed to study diet-induced hepatic steatosis, male GDF10$^{-/-}$ mice and age-matched GDF10$^{+/+}$ controls were provided with HFD (60% Kcal; TD.06414, Envigo) *ad libitum* starting at 6 weeks of age for an additional 12 weeks prior to sacrifice (n = 5). Measurements of metabolic parameters were performed using the Columbus Instruments Comprehensive Lab Animal Monitoring System (CLAMS) one week prior to sacrifice. A cohort of 12-week-old male C57BL/6J mice were also treated with phosphate-buffered saline (PBS) vehicle control or with the ER stress-inducing agent, tunicamycin (TM; 500 μg/kg), for 24 h via intraperitoneal injection in the left flank (n = 5). All mice were fasted for 6 h and anesthetized using isoflurane prior to sacrifice. Experimental procedures were approved by the McMaster University Animal Research Ethics Board.

2.2. Cell culture and treatment

Huh7 and HepG2 immortalized human hepatocyte cell lines as well as primary human hepatocytes were maintained in 5% CO_2 at 37 °C and cultured in Dulbecco's Modified Eagle's Medium (DMEM) or Willams' E medium, supplemented with 10% v/v fetal bovine serum (FBS), 100 IU/ml penicillin and 100 μg/ml streptomycin. For experimental procedures designed to examine the effect of GDF10 on lipid accumulation, cells were pre-treated with rhGDF10 (250 ng/mL, R&D Systems) for 24 h and then treated with agents known to stimulate lipid droplet accumulation, such as oleate (OA; 200 μM, Sigma—Aldrich), palmitate (PA; 200 μM, Sigma—Aldrich), thapsigargin (TG; 100 nM, Sigma—Aldrich) and TM (2 μg/mL, Sigma—Aldrich) for an additional 24 h. Similarly, for studies examining the effect of GDF10 on PPARγ-mediated lipid accumulation, hepatocytes were pre-treated with rhGDF10 and then treated with PPARγ agonist, ciglitizone (CGTZ; 10 μM, Tocris Bioscience), for 24 h prior to analysis. For experiments designed to examine the effect of GDF10 on PPARγ cellular localization and promoter binding, cells were pre-treated with rhGDF10 for 24 h, and subsequently treated with CGTZ for 1 h prior to analysis. All cell culture experiments were repeated a minimum of 3 times. To block Smad3 expression, siGENOME SMARTpool siRNA targeted against Smad3 (UCAAGAGCCUGGUCAAGAA, GAGUUCGCCUUCAAUAUGA, GGACGCAGGUUCUC-CAAAC, GGACGAGGUCUGCGUGAAU) was purchased from Dharmacon (SO-2782081G). 100 nM of siRNA targeted against Smad3 or scrambled siRNA control was transfected using RNAiMAX (ThermoFisher Scientific) as described previously [26].

2.3. Cell fractionation and transcriptional activity studies

Huh7 and HepG2 cells were seeded into 100 mm dishes and allowed to grow to confluency of 80%. Following treatment, nuclear and cytosolic fractions were isolated using an extraction kit (Abcam) according to the manufacturer's instructions. For experiments designed to examine the effect of GDF10 on PPARγ transcriptional activity, HepG2 cells were pre-treated with rhGDF10 for 24 h, and subsequently treated with CGTZ for 1 h prior to cellular fractionation. PPARγ transcription factor assay kit (Abcam) was carried out according to manufacturer's instructions. Briefly, 120 μg of protein isolated from nuclear extracts was added to each well of a 96-well plate coated with a double-stranded DNA sequence containing peroxisome proliferator response element (PPRE). Following an over-night incubation, anti-PPARγ primary antibody was added, followed by an HRP-conjugated secondary antibody. PPARγ binding to the PPRE was detected using a spectrophotometer at a wavelength of 450 nm.

2.4. Histological and immunohistochemical staining

Histological analysis was carried out in formalin-fixed paraffin-embedded (FFPE) tissues that were cut into 4 μm thick sections. Gross pathological changes were first examined with hematoxylin and eosin (H&E) and collagen accumulation was examined using Mason's Trichrome (Sigma—Aldrich). Analysis of intracellular triglyceride accumulation was carried out in OCT-embedded liver sections (10 μm) and in cultured cells fixed in 4% paraformaldehyde (PFA) using Oil Red O (ORO). The ORO content of isopropanol extracts was measured using a spectrophotometer (Molecular Devices) at a wavelength of 520 nm [27]. Immunohistochemical (IHC) staining was also carried out in 4 μm thick FFPE sections. Briefly, deparaffinized sections were blocked in 5% serum, incubated in primary antibody for 18 h at 4 °C, and exposed to biotin-labeled secondary antibody (Vector Laboratories; for a complete list of antibodies and working dilutions, please refer to Supplemental Table 1). Streptavidin-labeled HRP solution (Vector Laboratories) and the developing solution (Vector Laboratories) were used to visualize staining. Slides were examined using a Nikon microscope and images were quantified using ImageJ Software (NIH).

2.5. Quantitative real time PCR

Total RNA was isolated using RNA purification kits (ThermoFisher Scientific). A total of 2 μg of RNA was reverse transcribed to cDNA using the High-Capacity cDNA Reverse Transcription Kit (Applied Biosystems). PCR amplification was performed using the Fast SYBRGreen PCR master mix (Applied Biosystems) according to the manufacturer's instructions. All primer sequences are listed in Supplemental Table 2.

2.6. Immunoblots

Whole cell and tissue lysates were prepared using SDS lysis buffer containing a protease inhibitor cocktail (Roche), and protein concentration was measured as described previously [26]. The samples were resolved using SDS-PAGE and subsequently transferred to nitrocellulose membranes. Nitrocellulose membranes were then incubated in 5% w/v skimmed milk and primary antibody followed by the respective secondary antibody. The signal was detected using a Konica Minolta X-Ray film processor.

2.7. Immunofluorescent staining

Following treatment, Huh7 and primary human hepatocytes were fixed in 4% PFA and permeabilized in 0.025% Triton X-100 for 15 min. After blocking in 5% bovine-serum albumin (BSA), cells were stained with primary antibody, washed, and subsequently stained with fluorescently-labeled secondary antibodies and DAPI nuclear stain. Slides were then mounted using an aqueous mounting medium (ThermoFisher Scientific) and visualized using the EVOS FL (ThermoFisher Scientific) imaging system.

2.8. Plasma β-hydroxybutyrate (β-HB), ELISA, lactate dehydrogenase (LDH) and alanine-L transaminase (ALT) assays

Plasma levels of the ketone body β-HB were measured using a colorimetric assay (Cayman). Circulating GDF10 levels were measured using a mouse GDF10 ELISA kit (Elabscience). Plasma ALT was measured using a commercially available colorimetric assay (Abcam). Cytotoxicity was examined using a LDH colorimetric assay kit (Roche). All assays were performed according to the manufacturer's instructions.

 © 2019 The Authors. Published by Elsevier GmbH. This is an open access article under the CC BY-NC-ND license (http://creativecommons.org/licenses/by-nc-nd/4.0/).

MOLECULAR METABOLISM

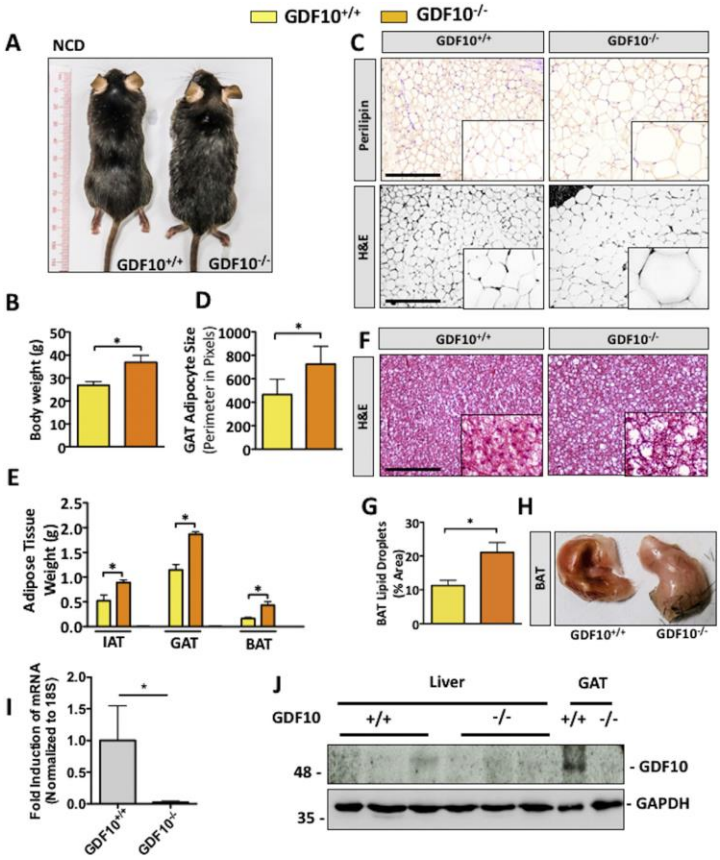

Figure 1: GDF10$^{-/-}$ mice have increased body weight and adiposity. (A) Macroscopic appearance and (B) body weights of 30 week old GDF10$^{+/+}$ and GDF10$^{-/-}$ mice fed NCD (n = 5). (C) IHC staining of the adipocyte marker perilipin and H&E staining of the GAT. (D) Average adipocyte size in GAT. (E) Weights of the IAT, GAT, and BAT. (F) H&E staining of the BAT. (G) Quantification of lipid droplets in BAT using ImageJ software. (H) Macroscopic appearance of the BAT from GDF10$^{+/+}$ and GDF10$^{-/-}$ mice at 30 weeks of age. (I) Real time PCR analysis of mRNA abundance of GDF10 in the GAT to confirm knockout (n = 5). (J) Immunoblots of the liver and GAT from GDF10$^{+/+}$ and GDF10$^{-/-}$ mice. Scale bars, 100 μm. All data are shown as the mean ± S.D. *, $p < 0.05$ by unpaired two-tailed Student's *t*-test.

2.9. Quantification of plasma, hepatic, and fecal lipid

Equal amounts of liver tissues were lysed in a mixture of hexane/2-propanol and incubated on an orbital shaker at 37 °C for 5 h. Samples were then subjected to centrifugation for 5 min (12,000 rpm) in order to isolate the lipid-containing liquid phase. Lipid content was quantified using a colorimetric triglyceride assay (Wako Diagnostics) according to the manufacturer's instructions. In a similar manner, fecal cholesterol content was measured directly from feces normalized to dry weight. Hepatic cholesterol content was measured using a commercially available colorimetric kit (Abcam) according to the manufacturer's instructions.

2.10. Statistical analysis

Data are reported as the mean ± SD. Statistical analysis was performed using GraphPad Prism. For comparison between two groups, an unpaired two-tailed Student's *t*-test was used. For analysis of three or more groups, a one-way ANOVA followed by Tukey's HSD multiple comparison test was performed. Differences between groups were considered statistically significant when $p < 0.05$.

3. RESULTS

3.1. GDF10$^{-/-}$ mice exhibit increased body weight gain and adiposity

Increased body weight gain in our GDF10$^{-/-}$ mouse colony was among our initial observations and was consistently observed in mice fed NCD (Figure 1A,B; *, $p < 0.05$, n = 5). Following this observation, adiposity was examined via IHC staining for the adipocyte marker, perilipin, as well as H&E of the gonadal adipose tissue (GAT). Consistent with gross morphological observations, GDF10$^{-/-}$ mice had increased mean adipocyte size (Figure 1C,D; *, $p < 0.05$, n = 5) and weight of the inguinal adipose tissue (IAT), GAT and brown adipose tissue (BAT) (Figure 1E; *, $p < 0.05$, n = 5). BAT from GDF10$^{-/-}$ mice also appeared lighter in color and revealed increased lipid droplets

 © 2019 The Authors. Published by Elsevier GmbH. This is an open access article under the CC BY-NC-ND license (http://creativecommons.org/licenses/by-nc-nd/4.0/).

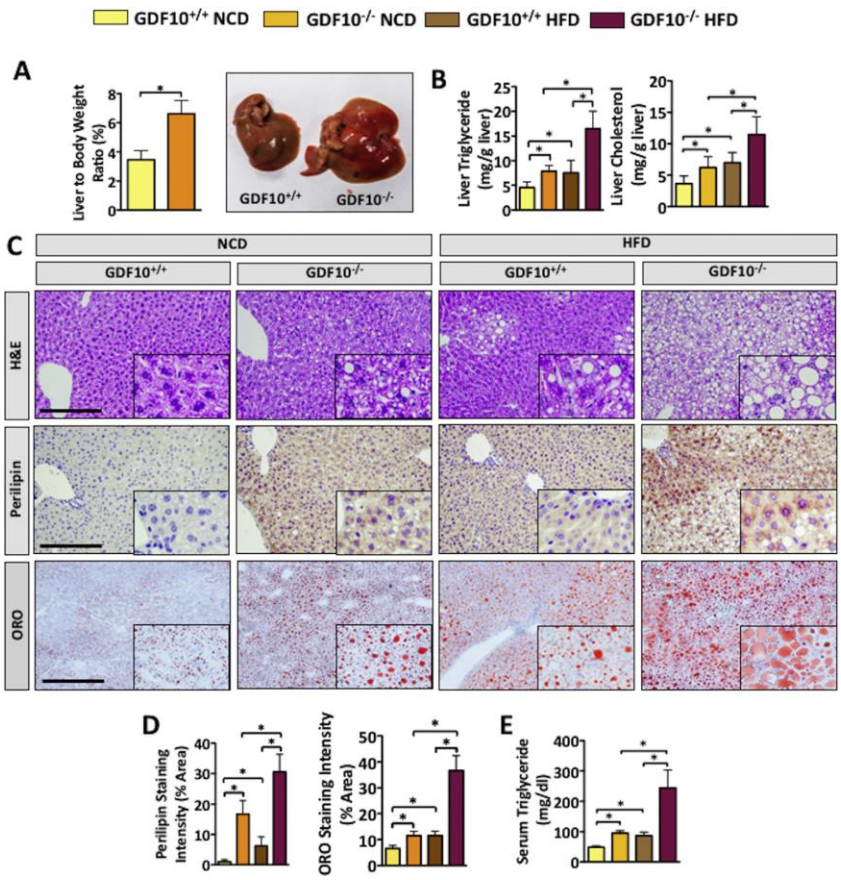

Figure 2: GDF10 deficiency leads to hepatic lipid accumulation. (A) Weights and macroscopic appearance of the livers from NCD-fed GDF10$^{+/+}$ and GDF10$^{-/-}$ mice (n = 5). (B) Hepatic triglyceride and cholesterol content (n = 5). (C) H&E, perilipin and ORO staining of livers from GDF10$^{+/+}$ and GDF10$^{-/-}$ mice fed NCD or HFD. (D) Quantification of perilipin and ORO staining using ImageJ Software (n = 5). (E) Serum triglyceride content. Scale bar, 100 μm. All data are shown as the mean ± S.D. *, $p < 0.05$ by unpaired two-tailed Student's *t*-test or one-way ANOVA.

compared to BAT from control mice (Figure 1F,G and H; *, $p < 0.05$, n = 5). GDF10 knockout was confirmed in these mice via real time PCR in GAT (Figure 1I; *, $p < 0.05$) and immunoblot (Figure 1J). Immunoblot analysis also revealed that GDF10 is expressed in GAT, but not in the livers of healthy wild-type mice (Figure 1J).

3.2. GDF10$^{-/-}$ mice exhibit hepatic lipid accumulation

Given that steatosis is commonly observed in obese patients as well as in rodent models of obesity [1,4], we next examined the livers of GDF10$^{-/-}$ mice fed NCD and HFD. Consistent with our observations in adipose tissue, liver weight was increased in GDF10$^{-/-}$ mice compared to controls on the NCD (Figure 2A; *, $p < 0.05$, n = 5). Analysis of hepatic triglyceride and cholesterol content yielded findings that were consistent with liver weights (Figure 2B; *, $p < 0.05$, n = 5). Similarly, H&E, perilipin and ORO staining also revealed increased lipid accumulation in the livers of NCD- and HFD-fed GDF10$^{-/-}$ mice compared to wild-type counterparts (Figure 2C). To confirm our visual observations, perilipin and ORO staining was quantified using ImageJ software (Figure 2D; *, $p < 0.05$, n = 5). In line with increased hepatic lipid accumulation, an increase in plasma triglyceride content was also observed in GDF10$^{-/-}$ compared to GDF10$^{+/+}$ mice (Figure 2E; *, $p < 0.05$). The ability of GDF10 to modulate lipid droplet accumulation was then examined in immortalized human HepG2 cells. Consistent with *in vivo* findings, exogenously added rhGDF10 markedly reduced lipid accumulation in hepatocytes, resulting from exposure to the fatty acid, PA, and to the ER stress-inducing agent, TG (Fig. S1A; *, $p < 0.05$). Exogenously added rhGDF10 also reduced cytotoxicity resulting from the treatment of cells with ER stress-inducing agents known to cause *de novo* lipogenesis [28], TG and TM (Fig. S1B; *, $p < 0.05$).

 © 2019 The Authors. Published by Elsevier GmbH. This is an open access article under the CC BY-NC-ND license (http://creativecommons.org/licenses/by-nc-nd/4.0/).

MOLECULAR METABOLISM

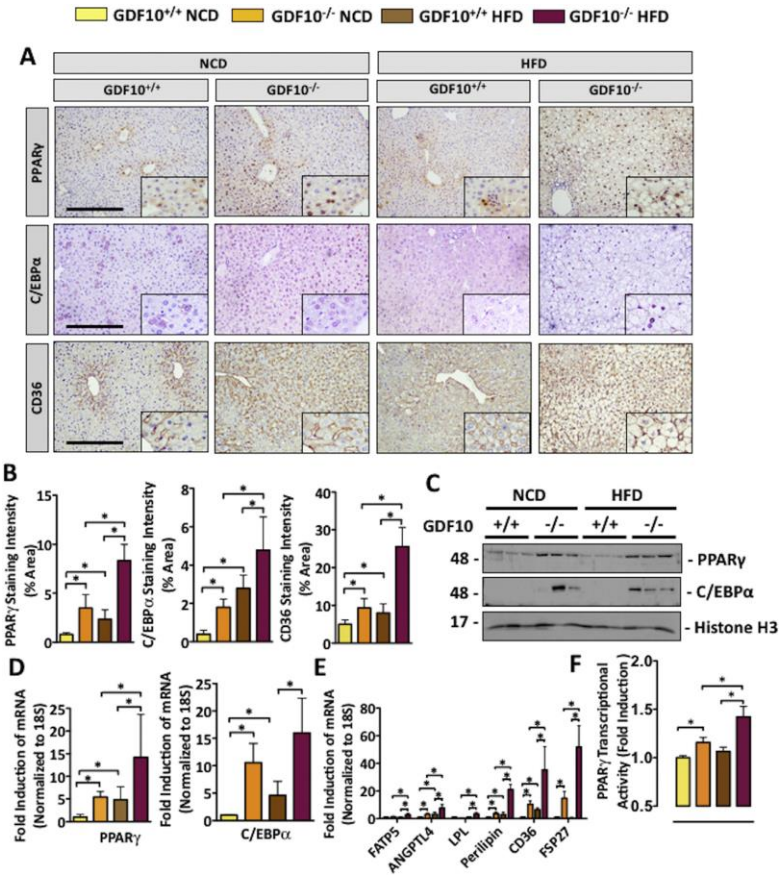

Figure 3: GDF10 deficiency increases the nuclear abundance of hepatic PPARγ and C/EBPα. (A) IHC staining of PPARγ, C/EBPα and CD36 in the livers of mice fed NCD or HFD. (B) Quantification of indicated histological staining. (C) Immunoblots of the nuclear subcellular fraction from livers of the mice fed NCD or HFD. (D) Real time PCR analysis of hepatic mRNA abundance of PPARγ, C/EBPα and (E) mRNA abundance of PPARγ-regulated genes. (F) PPARγ transcription factor activity assay. Scale bar, 100 μm. All data are shown as the mean ± S.D. *, $p < 0.05$ by one-way ANOVA.

3.3. GDF10 reduces PPARγ expression via the TGFβR1-Smad3 pathway in hepatocytes

Given the abundance of triglyceride observed in the livers of GDF10$^{-/-}$ mice, we next assessed the expression of established modulators of *de novo* lipogenesis and lipid uptake.

Previous studies have demonstrated that mouse models of steatosis exhibit increased PPARγ expression and activity [29]; thus, it was among the first markers examined. It is also well-known that naturally occurring derivatives of long-chain polyunsaturated fatty acids, including palmitic, linoleic, linolenic, and arachidonic acids, can activate PPAR receptor transcriptional activity [30,31]. Upon assessment of these mice, IHC staining revealed an increase in PPARγ expression in the livers of NCD- and HFD-fed GDF10$^{-/-}$ mice compared to controls. The expression of pro-adipogenic PPARγ-responsive proteins, including C/EBPα and CD36, were also increased (Figure 3A,B; *, $p < 0.05$, n = 5). Immunoblot analysis of nuclear fractions from the livers of NCD- and HFD-fed mice revealed consistent findings, whereby an increase in PPARγ and C/EBPα was observed in GDF10$^{-/-}$ compared to GDF10$^{+/+}$ mice (Figure 3C; n = 3). The mRNA transcript abundance of PPARγ and C/EBPα was also increased in the livers of NCD- and HFD-fed GDF10$^{-/-}$ (Figure 3D; *, $p < 0.05$, n = 5), as was the expression of CD36 and other PPARγ-responsive targets including FATP5, ANGPTL4, LPL, Perilipin and FSP27 (Figure 3E; *, $p < 0.05$, n = 5). Further examination of PPARγ using an ELISA-based transcription factor assay [32,33] revealed a concomitant increase in the binding of PPARγ to its PPRE, indicative of increased transcriptional activity in the livers of GDF10$^{-/-}$ mice compared to controls (Figure 3F; *, $p < 0.05$, n = 5). Given its established role in the regulation of feeding and metabolism, circulating leptin was also examined in a cohort of 30 week old NCD-fed GDF10$^{-/-}$ mice and age-matched controls. Consistent with previous reports in which PPARγ activation was inversely correlated with leptin, we observed leptin levels to be approximately 2-fold lower in GDF10$^{-/-}$ mice (Fig. S2; *, $p < 0.05$; n = 7) [34].

 © 2019 The Authors. Published by Elsevier GmbH. This is an open access article under the CC BY-NC-ND license (http://creativecommons.org/licenses/by-nc-nd/4.0/).

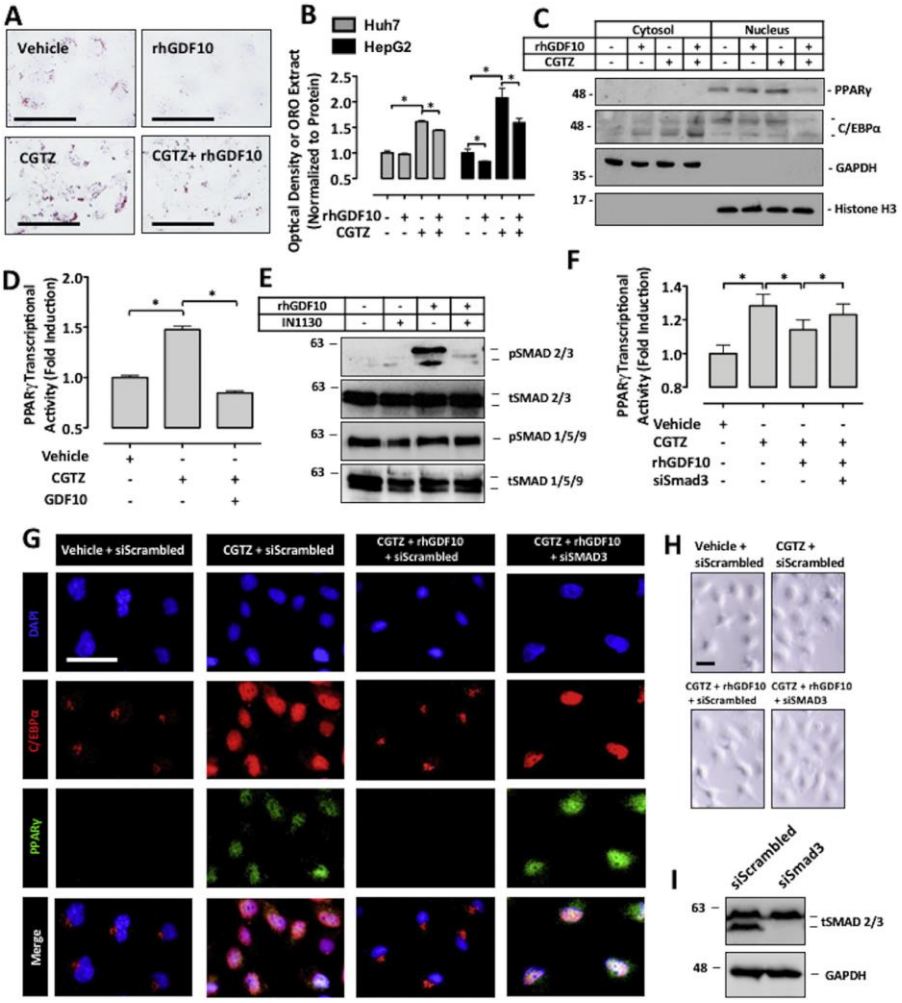

Figure 4: GDF10 modulates PPARγ nuclear abundance and transcriptional activity. (A) ORO staining and (B) extract quantification of HepG2 cells treated with PPARγ agonist, CGTZ (10 μM), or rhGDF10 (250 ng/mL) for 24 h. (C) Immunoblots of the nuclear and cytosolic subcellular fractions of Huh7 cells treated with CGTZ or rhGDF10. (D) PPARγ transcription factor activity assay after treatment with rhGDF10 or CGTZ for 1 h. (E) Immunoblots of HepG2 cells treated with IN1130 (100 nM) or rhGDF10. (F) PPARγ transcription factor activity assay in HepG2 cells transfected with either siRNA targeted against Smad3 or scrambled control siRNA and subsequently treated with CGTZ or rhGDF10. (G) Immunofluorescent staining of PPARγ and C/EBPα in Huh7 cells transfected with siRNA targeted against Smad3 and treated with rhGDF10 or CGTZ. (H) Morphology of the Huh7 cells was examined using a light microscope. (I) Immunoblots of HepG2 cells transfected with either siRNA targeted against Smad3 or scrambled control siRNA to confirm knockdown. Scale bars, 50 μm. All data are shown as the mean ± S.D. *, $p < 0.05$ by one-way ANOVA.

To substantiate our findings on the inhibitory effect of GDF10 on PPARγ-mediated lipid droplet accumulation, cultured HepG2 and Huh7 immortalized human hepatocytes were pre-treated with rhGDF10 and exposed to CGTZ, an established glitazone agonist of PPARγ. Representative images of HepG2 cells, as well as quantification of ORO isopropanol extracts of HepG2 and Huh7 cells, demonstrate that GDF10 reduced cellular lipid content in response to CGTZ treatment (Figure 4A,B; *, $p < 0.05$).

To follow up with our *in vivo* observations, we next examined the ability of GDF10 to modulate the nuclear abundance of C/EBPα as well as PPARγ in Huh7 cells. Consistent with the livers of GDF10$^{-/-}$ mice, immunoblot analysis of subcellular fractions in cultured hepatocytes revealed that GDF10 blocked the CGTZ-mediated nuclear localization of C/EBPα, and abundance of PPARγ (Figure 4C). In line with subcellular fraction data, immunofluorescent staining of HepG2 and primary human hepatocytes also demonstrated that GDF10 blocked the

 © 2019 The Authors. Published by Elsevier GmbH. This is an open access article under the CC BY-NC-ND license (http://creativecommons.org/licenses/by-nc-nd/4.0/).

MOLECULAR METABOLISM

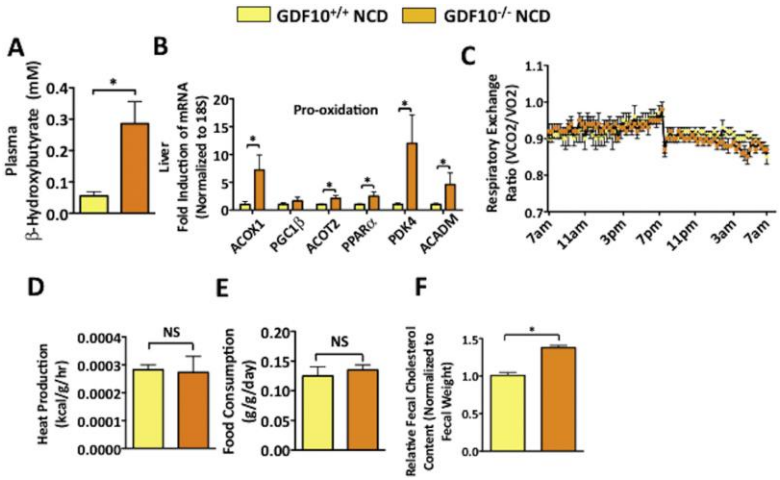

Figure 5: GDF10$^{-/-}$ mice exhibit compensatory changes in lipid homeostasis. (A) Plasma β-HB content (n = 5). (B) Real time PCR analysis of hepatic mRNA abundance of the indicated genes. (C) Respiratory exchange ratio (D) heat production and (E) food consumption in GDF10$^{+/+}$ and GDF10$^{-/-}$ mice fed NCD (n = 5). (F) Biliary cholesterol excretion in GDF10$^{+/+}$ and GDF10$^{-/-}$ mice fed NCD. All data are shown as the mean ± S.D. *, $p < 0.05$ by unpaired two-tailed Student's *t*-test.

CGTZ-mediated nuclear localization of these transcription factors (Fig. S3A,S3B). Finally, the antagonistic effect of GDF10 on PPARγ transcriptional activity was also confirmed in HepG2 cells using the transcription factor activity assay (Figure 4D; *, $p < 0.05$).

We next utilized this cultured hepatocyte model to determine the mechanism by which GDF10 affects PPARγ expression and activity. Importantly, previous studies have demonstrated that (a) signaling of TGFβ through TGFβ receptor subtype-1 (TGFβR1) induces the phosphorylation of Smad3, which (b) leads to the suppression of PPARγ expression and activity [35,36]. Furthermore, recent studies have also shown that (c) in a manner similar to TGFβ, GDF10 induces the phosphorylation of Smad3 [35]. Similar to previous studies, we observed that exogenously-added rhGDF10 induced the phosphorylation of Smad3, but only in the absence of the TGFβR1 antagonist, IN1130. Also consistent with previous studies, rhGDF10 and/or IN1130 did not affect the phosphorylation of Smad1/5/9 (Figure 4E). Using the PPARγ transcription factor assay, we next observed that rhGDF10 failed to antagonize CGTZ-mediated PPARγ activity in cells transfected with small interfering (si)RNA targeted against Smad3 (siSmad3; Figure 4F; *, $p < 0.05$). This observation was also confirmed via immunofluorescent staining of PPARγ and C/EBPα in Huh7 cells (Figure 4G). No marked change in cytotoxicity or cell morphology was observed in these cells (Figure 4H) and effective knockdown of Smad3 was confirmed via immunoblotting (Figure 4I). Finally, in line with these findings, we also observed that IN1130 attenuated the lipid-lowering effect of rhGDF10 in the presence of CGTZ (Fig. S4). Taken together, our results indicate that GDF10 acts to oppose PPARγ-mediated lipid accumulation in cultured hepatocyte models via TGFβR1-induced Smad3 phosphorylation.

3.4. GDF10$^{-/-}$ mice exhibit compensatory changes in fatty acid oxidation

Other parameters known to contribute to fatty liver and/or obesity, such as changes in lipid oxidation, biliary cholesterol excretion, energy expenditure and food consumption were also examined in GDF10$^{-/-}$ mice. To examine the possibility of lipid accumulation occurring as a result of reduced fatty acid oxidation, the ketogenic marker β-HB, was measured in the plasma. Interestingly, the elevated levels of β-HB observed in NCD-fed GDF10$^{-/-}$ mice are indicative of increased global fatty acid oxidation (Figure 5A; *, $p < 0.05$), likely working as a compensatory mechanism to oppose further lipid accumulation. Consistent with this result, increased hepatic mRNA transcript levels of a number of known drivers of fatty acid oxidation, including acyl-coenzyme A oxidase (ACOX1), peroxisome proliferator-activated receptor gamma coactivator 1- β (PGC1β), acyl-coenzyme A thioesterase 2 (ACOT2), peroxisome proliferator-activated receptor α (PPARα), pyruvate dehydrogenase lipoamide kinase isozyme 4 (PDK4) and acyl-coenzyme A dehydrogenase, C-4 to C-12 straight chain (ACADM) were also observed in the livers of NCD-fed GDF10$^{-/-}$ mice (Figure 5B; *, $p < 0.05$). However, no difference in respiratory exchange ratio and heat production was detected between GDF10$^{+/+}$ and GDF10$^{-/-}$ mice (Figure 5C,D. *, $p < 0.05$). In addition, no difference in food consumption was observed between GDF10$^{+/+}$ and GDF10$^{-/-}$ mice (Figure 5E. *, $p < 0.05$). Increased fecal cholesterol content was also observed in the GDF10$^{-/-}$ mice, suggesting heightened biliary cholesterol excretion (Figure 5F; *, $p < 0.05$). Collectively, these data suggest that despite increased liver fat content observed in GDF10$^{-/-}$ mice, a variety of compensatory mechanisms act in tandem to attenuate further lipid accumulation.

3.5. GDF10$^{-/-}$ mice exhibit increased UPR activation, fibrosis and liver injury

ER stress is a well-established early initiator of hepatic steatosis and is known to contribute to the progression of liver disease [7,37,38]. Therefore, our next aim was to assess the expression of ER stress markers in the livers of NCD- and HFD-fed GDF10$^{-/-}$ mice. Consistent with the observed increase in hepatic triglyceride levels, histological analysis revealed increased expression of ER stress markers, glucose regulated protein of 78 and 94 kDa (GRP78, GRP94) as well as phosphorylated (p)PERK in response to a HFD in the livers GDF10$^{-/-}$

 © 2019 The Authors. Published by Elsevier GmbH. This is an open access article under the CC BY-NC-ND license (http://creativecommons.org/licenses/by-nc-nd/4.0/).

Original Article

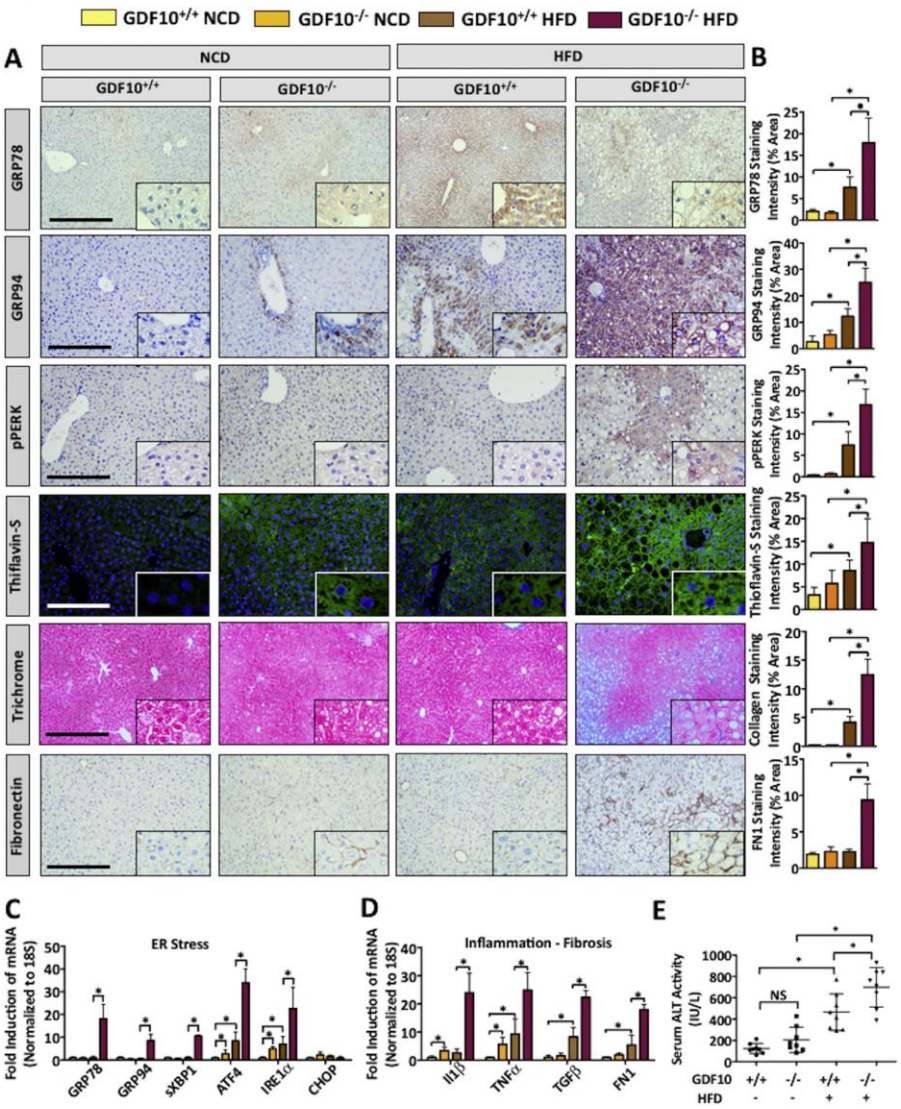

Figure 6: Livers from GDF10$^{-/-}$ mice exhibit increased UPR activation, fibrosis, and inflammation. (A) IHC staining of GRP78, GRP94, pPERK and fibronectin, as well as Masson's Trichrome and Thioflavin-S in the livers of NCD- and HFD-fed mice. (B) Quantification of indicated histological staining (n = 5). Real time PCR analysis of hepatic mRNA abundance of the indicated genes involved in (C) ER stress, (D) inflammation, and fibrosis. (E) Analysis of serum ALT activity, a marker of liver injury (n = 8). Scale bars, 100 μm. All data are shown as the mean ± S.D. *, $p < 0.05$ by one-way ANOVA.

mice (Figure 6A,B; *, $p < 0.05$). Thioflavin-S staining of misfolded protein amyloid, known to occur as a result of prolonged ER stress [9] was also increased in HFD-fed GDF10$^{-/-}$ mice compared to controls. Further assessment of the livers via IHC staining of fibronectin and Masson's Trichrome also revealed increased fibrosis in HFD-fed GDF10$^{-/-}$ mice (Figure 6A,B; *, $p < 0.05$, n = 5). Increased fibrosis in the livers of HFD-fed GDF10$^{-/-}$ mice was also independently confirmed via Picrosirius red (PSR) staining of fibrotic collagen deposition (Fig. S5A). Although a marked increase in ER stress and fibrosis markers was observed in the livers of HFD-fed GDF10$^{-/-}$ mice, no substantial difference was observed in the NCD-fed cohort. mRNA transcript abundance of ER stress, fibrotic, inflammatory, and

 © 2019 The Authors. Published by Elsevier GmbH. This is an open access article under the CC BY-NC-ND license (http://creativecommons.org/licenses/by-nc-nd/4.0/).

MOLECULAR METABOLISM

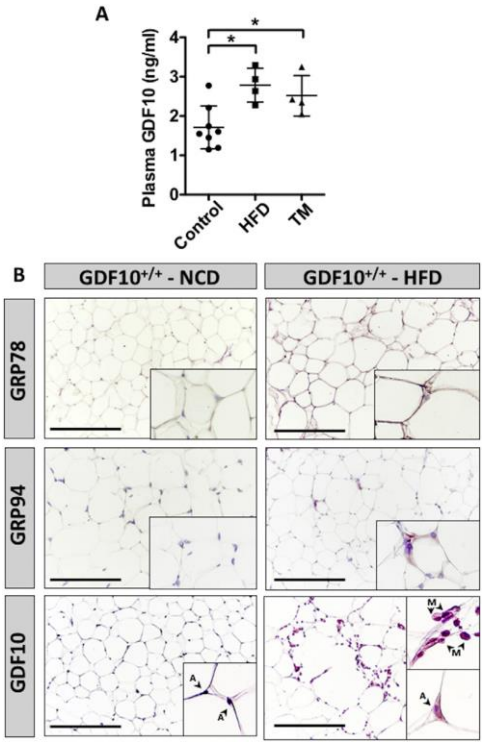

Figure 7: ER stress increases GDF10 abundance in GAT and in circulation. (A) Plasma content of circulating GDF10 in mice fed NCD or HFD for 12 weeks (n = 5), and mice treated with a bolus injection of TM (250 μg/kg - 24 h; n = 5). (B) IHC staining of GRP78, GRP94 and GDF10 in the GAT of mice fed NCD or HFD. Scale bars, 100 μm. A and M indicate adipocytes and macrophages, respectively. All data are shown as the mean ± S.D. *, $p < 0.05$ by one-way ANOVA.

apoptotic markers was also examined by real time PCR and yielded consistent findings with histological analysis (Figure 6C, D and Fig. S5B; *, $p < 0.05$, n = 5).

Hepatic insulin resistance represents another hallmark feature of liver disease. Thus, markers of hepatic gluconeogenesis were assessed via real time PCR. Interestingly, the gluconeogenic markers induced in the livers GDF10$^{-/-}$ mice, including signal transducer and activator of transcription 3 (STAT3), CREB-regulated transcription cofactor 2 (CRTC2), forkhead box protein O1 (FOXO1) and phosphoenolpyruvate carboxykinase 1 (PCK1) are also known to be upregulated by conditions of ER stress (Fig. S5C; *, $p < 0.05$) [39]. Finally, the enzymatic activity of circulating ALT was increased in the HFD-fed GDF10$^{-/-}$ mice compared to NCD-fed controls, which is indicative of liver injury (Figure 6E; *, $p < 0.05$). Collectively, these data provide compelling evidence of heightened ER stress in the livers GDF10$^{-/-}$ mice and highlight the ability of GDF10 to attenuate diet-induced liver injury.

3.6. ER stress increases circulating and adipose GDF10 levels

Given the role of GDF10 in the regulation of hepatic triglyceride levels and injury, our final aim was to assess the effect of diet-induced stress on GDF10 expression in GDF10$^{+/+}$ mice. Similar to findings demonstrating a positive correlation between circulating GDF15 levels and hepatic ER stress [24], we also observed increased plasma GDF10 levels in HFD-fed GDF10$^{+/+}$ and in wild-type mice injected with the ER stress-inducing agent, TM (Figure 7A; *, $p < 0.05$, n = 7). Because GDF10 is primarily expressed in adipose tissue, we also examined whether TM affects GDF10 expression in 3T3-L1 adipocytes at day 10 of differentiation (Fig. S6; *, $p < 0.05$, n = 5) and in GAT from HFD-fed mice (Figure 7B; n = 7). Similar to secreted levels, an increase in GDF10 expression was observed in response to TM in 3T3-L1 adipocytes and in the GAT from HFD-fed GDF10$^{+/+}$ mice. We also report the surprising finding that GAT-resident macrophages in HFD-fed mice express abundant levels of GDF10 (Figure 7B); an observation that was not present in GAT from NCD-fed mice. Collectively, these data suggest that during conditions of diet-induced stress, adipose tissue promotes the expression of GDF10 to attenuate further triglyceride accumulation in the liver as a response to injury.

4. DISCUSSION

A growing body of evidence suggests that GDF10, in addition to being a key modulator of osteogenesis, also plays a critical role in adipose lipid metabolism [20,21]. To the best of our knowledge, however, the functional importance of GDF10 in liver lipid metabolism has not yet been evaluated. Here, we demonstrate that GDF10$^{-/-}$ mice exhibit increased adiposity, as well as increased body weight and hepatic triglyceride and cholesterol levels; an early feature in the development of diet-induced liver disease [3]. We also observed that severe lipid accumulation in the livers of HFD-fed GDF10$^{-/-}$ mice was associated with a substantial induction of a variety of ER stress markers and concomitant liver injury. Additional hallmark characteristics of liver disease, such as apoptosis, inflammation, fibrosis and changes in gluconeogenic gene expression, were also observed in the livers of HFD-fed GDF10$^{-/-}$ mice.

To explain these findings, we examined a number of metabolic parameters and expression of genes known to alter lipid metabolism. Despite elevated body weight and adiposity, an increase in global fatty acid oxidation was observed in GDF10$^{-/-}$ mice. Given that this finding is in mechanistic contrast to the obese phenotype in the mice, these findings suggest that heightened fatty acid oxidation likely occurred as a compensatory response to attenuate further fat accumulation. In line with these data, an increase in biliary cholesterol excretion was also identified. To this end, we observed an increase in the expression of key modulators of adipogenesis and well-known drivers of NAFLD, such as PPARγ and C/EBPα, in the livers of GDF10$^{-/-}$ mice. Upon further analysis using cultured hepatocytes, exogenously added rhGDF10 reduced the abundance and transcriptional activity of PPARγ, and also blocked PPARγ agonist-driven lipid accumulation. Lastly, we have also demonstrated that GDF10 inhibits PPARγ transcriptional activity via the conventional TGFβR1-Smad3 signaling cascade. Collectively, these data suggest that GDF10 is a potent antagonist of PPARγ and can protect from diet-induced hepatic steatosis.

Several groups have recently demonstrated the involvement of multiple TGFβ superfamily members in the pathogenesis of obesity-related diseases such as type 2 diabetes and NAFLD [40–42]. In clinical studies, GDF15 expression correlates with a variety of metabolic disorders, including obesity, insulin resistance and the risk of cardiovascular events [43]. GDF15$^{-/-}$ mice also exhibit increased body weight and peripheral lipid accumulation following a metabolic challenge, whereas overexpression of this protein led to reduced body weight and improved metabolic parameters [44,45]. Similar to GDF15$^{-/-}$ mice, GDF10$^{-/-}$ mice have increased body weight and

 © 2019 The Authors. Published by Elsevier GmbH. This is an open access article under the CC BY-NC-ND license (http://creativecommons.org/licenses/by-nc-nd/4.0/).

adiposity, a phenotype that unlike GDF15$^{-/-}$ mice, does not require a metabolic stimulus such as a HFD. Our findings are also consistent with studies in which overexpression of GDF10 in mice led to a reduction in adiposity and improved metabolic outcomes [21].

Activation of the TGFβ signaling cascade has been shown to differentially modulate the expression of lipogenic markers, based on tissue/cell-specific expression, and unique molecular interactions with a variety of inhibitory molecules and receptor—ligand complexes. TGFβ signaling has been shown to induce lipogenesis, inflammation and cell death via Smad2/3 [42], while also blocking PPARγ expression, activity and lipogenesis in a manner dependent on β-catenin [46]. Overexpression of Smad3 and its partner Smad4 has been shown to reduce PPARγ promoter activity in aortic smooth muscle cells [47]. Furthermore, TGFβ suppresses PPARγ expression and activity via Smad3/4 binding to the inhibitory element in the PPAR promoter region in lung fibroblasts [36]. Given that GDF10 can induce the phosphorylation and activation of Smad3, but also block the transcriptional activation of PPARγ, our data suggest that in a manner similar to TGFβ, GDF10 reduces PPARγ activity in a Smad3-dependent manner.

PPARγ activation is necessary and sufficient to induce adipocyte differentiation. Studies have demonstrated that (a) selective ablation of PPARγ, using a tamoxifen-dependent recombination system in mice, led to the death of adipocytes only a few days following treatment [48], and (b) AAV-mediated hepatic overexpression of PPARγ_2 in mice promoted an adipose-like phenotype in hepatocytes by inducing the expression of pro-adipogenic mediators, such as adipsin, adiponectin, and aP2, which resulted in severe steatosis [49]. Moreover, previous studies have also demonstrated that hepatic PPARγ is robustly induced in the livers of patients, as well as in pre-clinical models of NAFLD [13,49]. Conversely, PPARγ deletion in mouse hepatocytes has been shown to attenuate intracellular lipid accumulation [50]. Consistent with our studies, it is also well-established that exposure of mice to a HFD promotes the expression of hepatic PPARγ and a variety of its downstream targets [51]. In addition to PPARγ, we also observed increased expression and nuclear localization of C/EBPα in the livers of GDF10$^{-/-}$ mice compared to the GDF10$^{+/+}$ controls. C/EBPα is also known to play a crucial role in adipocyte differentiation, and similar to PPARγ, its expression is both necessary and sufficient for adipogenesis [52]. Studies also demonstrate that C/EBPα can directly regulate PPARγ promoter activity [53] and has been described as a critical and obligate regulator of PPARγ expression [54]. Furthermore, PPARγ and C/EBPα mutually induce each other's expression in order to promote adipogenesis [53,55,56] Given the cross-talk that occurs between these two master regulators of adipogenesis, it remains unclear which of the two, or whether both are directly affected by GDF10.

In summary, we demonstrate that GDF10 is an essential modulator of hepatic lipid homeostasis and is crucial for the maintenance of hepatic lipid turnover. GDF10 knockout leads to hepatic steatosis in NCD-fed mice, as well as severe steatosis, inflammation, fibrosis, and ER stress in response to a HFD. Given that most diet-induced models of liver disease fail to recapitulate fibrosis, a key marker of NASH, in this report we also describe a new genetic model for the study of liver disease. Furthermore, conditions that cause hepatic and/or adipocyte lipid accumulation also induced a compensatory increase in circulating GDF10 levels in GDF10-expressing control mice. Additional tissue-specific knockdown studies, however, are required to confirm the origin of circulating GDF10 in the context of diet-induced NAFLD. Future studies examining the correlation between polymorphisms in the *GDF10* gene and the prevalence of obesity and/or NAFLD may also yield interesting findings. Overall, we identify circulating GDF10 as a novel regulator of liver lipid metabolism and demonstrate that in a manner similar to GDF15, this adipokine could be utilized for the management of metabolic disorders.

FINANCIAL SUPPORT

This work was supported in part by research grants to Richard C. Austin from the Heart and Stroke Foundation of Canada (G-13-0003064 and G-15-0009389) and the Canadian Institutes of Health Research (74477, 111239). Financial support from the Research Institute of St. Joe's Hamilton is acknowledged. Richard C. Austin is a Career Investigator of the Heart and Stroke Foundation of Ontario and holds the Amgen Canada Research Chair in the Division of Nephrology at St. Joseph's Healthcare Hamilton and McMaster University. Kenneth N. Maclean gratefully acknowledges financial support from the William R. Hummel Homocystinuria Research Fund and holds the Ehst-Hummel-Kaufmann Family Endowed Chair in Inherited Metabolic Disease.

AUTHOR CONTRIBUTIONS

KP, PL, and RCA conceived the studies and wrote the manuscript. KP, PL, JHB, SVP, EAD, MEM, and AMB performed all of the *in vitro* and *in vivo* studies. The manuscript was revised by KNM and JCK.

CONFLICT OF INTEREST

The authors declare that they have no conflicts of interest with the contents of this article.

APPENDIX A. SUPPLEMENTARY DATA

Supplementary data to this article can be found online at https://doi.org/10.1016/j.molmet.2019.06.021.

REFERENCES

[1] Gonzalez-Muniesa, P., Martinez-Gonzalez, M.A., Hu, F.B., Despres, J.P., Matsuzawa, Y., Loos, R.J.F., et al., 2017. Obesity. Nature Reviews Disease Primers 3:17034.

[2] Perry, R.J., Samuel, V.T., Petersen, K.F., Shulman, G.I., 2014. The role of hepatic lipids in hepatic insulin resistance and type 2 diabetes. Nature 510: 84—91.

[3] Brunt, E.M., Wong, V.W., Nobili, V., Day, C.P., Sookoian, S., Maher, J.J., et al., 2015. Nonalcoholic fatty liver disease. Nature reviews Disease primers 1: 15080.

[4] Angulo, P., 2002. Nonalcoholic fatty liver disease. New England Journal of Medicine 346:1221—1231.

[5] Kim, J.Y., Garcia-Carbonell, R., Yamachika, S., Zhao, P., Dhar, D., Loomba, R., et al., 2018. ER stress drives lipogenesis and steatohepatitis via caspase-2 activation of S1P. Cell 75:133—145 e115.

[6] Ashraf, N.U., Sheikh, T.A., 2015. Endoplasmic reticulum stress and oxidative stress in the pathogenesis of non-alcoholic fatty liver disease. Free Radical Research 49:1405—1418.

[7] Puri, P., Mirshahi, F., Cheung, O., Natarajan, R., Maher, J.W., Kellum, J.M., et al., 2008. Activation and dysregulation of the unfolded protein response in nonalcoholic fatty liver disease. Gastroenterology 134:568—576.

[8] Zeng, L., Lu, M., Mori, K., Luo, S., Lee, A.S., Zhu, Y., et al., 2004. ATF6 modulates SREBP2-mediated lipogenesis. The EMBO Journal 23:950—958.

 © 2019 The Authors. Published by Elsevier GmbH. This is an open access article under the CC BY-NC-ND license (http://creativecommons.org/licenses/by-nc-nd/4.0/).

MOLECULAR METABOLISM

[9] Zhou, H., Liu, R., 2014. ER stress and hepatic lipid metabolism. Frontiers in Genetics 5:112.
[10] Bobrovnikova-Marjon, E., Hatzivassiliou, G., Grigoriadou, C., Romero, M., Cavener, D.R., Thompson, C.B., et al., 2008. PERK-dependent regulation of lipogenesis during mouse mammary gland development and adipocyte differentiation. Proceedings of the National Academy of Sciences of the United States of America 105:16314—16319.
[11] Matsusue, K., Kusakabe, T., Noguchi, T., Takiguchi, S., Suzuki, T., Yamano, S., et al., 2008. Hepatic steatosis in leptin-deficient mice is promoted by the PPAR gamma target gene Fsp27. Cell Metabolism 7:302—311.
[12] Lee, Y.J., Ko, E.H., Kim, J.E., Kim, E., Lee, H., Choi, H., et al., 2012. Nuclear receptor PPARγ-regulated monoacylglycerol O-acyltransferase 1 (MGAT1) expression is responsible for the lipid accumulation in diet-induced hepatic steatosis. Proceedings of the National Academy of Sciences of the United States of America 109:13656—13661.
[13] Pettinelli, P., Videla, L.A., 2011. Up-regulation of PPAR-γ mRNA expression in the liver of obese patients: an additional reinforcing lipogenic mechanism to SREBP-1c induction. Journal of Clinical Endocrinology & Metabolism 96: 1424—1430.
[14] Zhang, X.Q., Xu, C.F., Yu, C.H., Chen, W.X., Li, Y.M., 2014. Role of endoplasmic reticulum stress in the pathogenesis of nonalcoholic fatty liver disease. World Journal of Gastroenterology 20:1768—1776.
[15] Matsumoto, Y., Otsuka, F., Hino, J., Miyoshi, T., Takano, M., Miyazato, M., et al., 2012. Bone morphogenetic protein-3b (BMP-3b) inhibits osteoblast differentiation via Smad2/3 pathway by counteracting Smad1/5/8 signaling. Molecular and Cellular Endocrinology 350:78—86.
[16] Zhao, R., Lawler, A.M., Lee, S.J., 1999. Characterization of GDF-10 expression patterns and null mice. Developmental Biology 212:68—79.
[17] Tseng, Y.H., Kokkotou, E., Schulz, T.J., Huang, T.L., Winnay, J.N., Taniguchi, C.M., et al., 2008. New role of bone morphogenetic protein 7 in brown adipogenesis and energy expenditure. Nature 454:1000—1004.
[18] Schulz, T.J., Tseng, Y.H., 2009. Emerging role of bone morphogenetic proteins in adipogenesis and energy metabolism. Cytokine & Growth Factor Reviews 20:523—553.
[19] Zamani, N., Brown, C.W., 2011. Emerging roles for the transforming growth factor-β superfamily in regulating adiposity and energy expenditure. Endocrine Reviews 32:387—403.
[20] Hino, J., Miyazawa, T., Miyazato, M., Kangawa, K., 2012. Bone morphogenetic protein-3b (BMP-3b) is expressed in adipocytes and inhibits adipogenesis as a unique complex. International Journal of Obesity 36:725—734.
[21] Hino, J., Nakatani, M., Arai, Y., Tsuchida, K., Shirai, M., Miyazato, M., et al., 2017. Overexpression of bone morphogenetic protein-3b (BMP-3b) in adipose tissues protects against high-fat diet-induced obesity. International Journal of Obesity 41:483—488.
[22] Chrysovergis, K., Wang, X., Kosak, J., Lee, S.H., Kim, J.S., Foley, J.F., et al., 2014. NAG-1/GDF-15 prevents obesity by increasing thermogenesis, lipolysis and oxidative metabolism. International Journal of Obesity 38:1555—1564.
[23] Li, D., Zhang, H., Zhong, Y., 2018. Hepatic GDF15 is regulated by CHOP of the unfolded protein response and alleviates NAFLD progression in obese mice. Biochemical and Biophysical Research Communications 498:388—394.
[24] Tsai, V.W.W., Husaini, Y., Sainsbury, A., Brown, D.A., Breit, S.N., 2018. The MIC-1/GDF15-GFRAL pathway in energy homeostasis: implications for obesity, cachexia, and other associated diseases. Cell Metabolism 28:353—368.
[25] Polyzos, S.A., Kountouras, J., Mantzoros, C.S., 2016. Adipokines in nonalcoholic fatty liver disease. Metabolism Clinical and Experimental 65:1062—1079.
[26] Lebeau, P., Platko, K., Al-Hashimi, A.A., Byun, J.H., Lhotak, S., Holzapfel, N., et al., 2018. Loss-of-function PCSK9 mutants evade the unfolded protein response sensor GRP78 and fail to induce endoplasmic reticulum stress when retained. Journal of Biological Chemistry 293:7329—7343.
[27] Lebeau, P.F., Byun, J.H., Platko, K., MacDonald, M.E., Poon, S.V., Faiyaz, M., 2019. Diet-induced hepatic steatosis abrogates cell-surface LDLR by inducing de novo PCSK9 expression in mice. Journal of Biological Chemistry 294: 9037—9047.
[28] Lee, J.S., Zheng, Z., Mendez, R., Ha, S.W., Xie, Y., Zhang, K., 2012. Pharmacologic ER stress induces non-alcoholic steatohepatitis in an animal model. Toxicology Letters 211:29—38.
[29] Gross, B., Pawlak, M., Lefebvre, P., Staels, B., 2017. PPARs in obesity-induced T2DM, dyslipidaemia and NAFLD. Nature Reviews Endocrinology 13:36—49.
[30] Bocos, C., Göttlicher, M., Gearing, K., Banner, C., Enmark, E., Teboul, M., et al., 1995. Fatty acid activation of peroxisome proliferator-activated receptor (PPAR). The Journal of Steroid Biochemistry and Molecular Biology 53:467—473.
[31] Krey, G., Braissant, O., L'Horset, F., Kalkhoven, E., Perroud, M., Parker, M.G., et al., 1997. Fatty acids, eicosanoids, and hypolipidemic agents identified as ligands of peroxisome proliferator-activated receptor by coactivator-dependent receptor ligand assay. Molecular Endocrinology 6:779—791.
[32] Ahmad, I., Mui, E., Galbraith, L., Patel, R., Tan, E.H., Salji, M., et al., 2016. Sleeping beauty screen revealed pparg activation in metastatic prostate cancer. Proceedings of the National Academy of Sciences 29:8290—8295.
[33] Jiang, Y., Thakran, S., Bheemreddy, R., Ye, E.A., He, H., Walker, R.J., et al., 2014. Pioglitazone normalizes insulin signaling in the diabetic rat retina through reduction in tumor necrosis factor α and suppressor of cytokine signaling 3. Journal of Biological Chemistry 289:26395—26405.
[34] De Vos, P., Lefebvre, A.M., Miller, S.G., Guerre-Millo, M., Wong, K., Saladin, R., et al., 1996. Thiazolidinediones repress ob gene expression in rodents via activation of peroxisome proliferator-activated receptor gamma. Journal of Clinical Investigation 98:1004—1009.
[35] Upadhyay, G., Yin, Y., Yuan, H., Derynch, R., Glazer, R.I., 2011. Stem cell antigen-1 enhances tumorigenicity by disruption of growth differentiation factor-10 (GDF10)-dependent TGF-β signaling. Proceedings of the National Academy of Sciences of the United States of America 108:7820—7825.
[36] Lakshmi, S.P., Reddy, A.T., Reddy, R.C., 2017. Transforming growth factor β suppresses peroxisome proliferator-activated receptor γ expression via both SMAD binding and novel TGF- β inhibitory elements. Biochemical Journal 474: 1531—1546.
[37] Wang, D., Wei, Y., Pagliassotti, M.J., 2006. Saturated fatty acids promote endoplasmic reticulum stress and liver injury in rats with hepatic steatosis. Endocrinology 147:943—951.
[38] Bashiri, A., Nesan, D., Tavallaee, G., Sue-Chu-Lam, I., Chien, K., Maguire, G.F., et al., 2016. Cellular cholesterol accumulation modulates high fat high sucrose (HFHS) diet-induced ER stress and hepatic inflammasome activation in the development of non-alcoholic steatohepatitis. Biochemica et Biophysica Acta 1861:594—605.
[39] Kim, O.K., Jun, W., Lee, J., 2015. Mechanism of ER Stress and inflammation for hepatic insulin resistance in obesity. Annals of Nutrition & Metabolism 67: 218—227.
[40] Yadav, H., Quijano, C., Kamaraju, A.K., Gavrilova, O., Malek, R., Chen, W., et al., 2011. Protection from obesity and diabetes by blockade of TGF-β/Smad3 signaling. Cell Metabolism 14:67—79.
[41] Margoni, A., Fotis, L., Papavassiliou, A.G., 2012. The transforming growth factor-beta/bone morphogenetic protein signalling pathway in adipogenesis. The International Journal of Biochemistry & Cell Biology 44:475—479.
[42] Yang, L., Roh, Y.S., Song, J., Zhang, B., Liu, C., Loomba, R., et al., 2014. Transforming growth factor beta signaling in hepatocytes participates in steatohepatitis through regulation of cell death and lipid metabolism in mice. Hepatology 59:483—495.
[43] Kempf, T., Guba-Quint, A., Torgerson, J., Magnone, M.C., Haefliger, C., Bobadilla, M., et al., 2012. Growth differentiation factor 15 predicts future insulin resistance and impaired glucose control in obese nondiabetic individuals: results from the XENDOS trial. European Journal of Endocrinology 167:671—678.
[44] Macia, L., Tsai, V.W., Nguyen, A.D., Johnen, H., Kuffner, T., Shi, Y.C., et al., 2012. Macrophage inhibitory cytokine 1 (MIC-1/GDF15) decreases food intake,

 © 2019 The Authors. Published by Elsevier GmbH. This is an open access article under the CC BY-NC-ND license (http://creativecommons.org/licenses/by-nc-nd/4.0/).

body weight and improves glucose tolerance in mice on normal & obesogenic diets. PLoS One 7:e34868.

[45] Kim, J.M., Kosak, J.P., Kim, J.K., Kissling, G., Germolec, D.R., Zeldin, D.C., et al., 2013. NAG-1/GDF15 transgenic mouse has less white adipose tissue and a reduced inflammatory response. Mediators of Inflammation 2013:641851.

[46] Qian, J., Niu, M., Zhai, X., Zhou, Q., Zhou, Y., 2012. Beta-catenin pathway is required for TGF-β1 inhibition of PPARγ expression in cultured hepatic stellate cells. Pharmacological Research 66:219—225.

[47] Fu, M., Zhang, J., Lin, Y., Zhu, X., Zhao, L., Ahmad, M., et al., 2003. Early stimulation and late inhibition of peroxisome proliferator-activated receptor gamma (PPAR gamma) gene expression by transforming growth factor beta in human aortic smooth muscle cell: role of early growth-response factor-1 (Egr-1), activator protein 1 (AP1) and Smads. Biochemical Journal 370:1019—1025.

[48] Imai, T., Takakuwa, R., Marchand, S., Dentz, E., Bornert, J.M., Messaddeq, N., et al., 2004. Peroxisome proliferator-activated receptor gamma is required in mature white and brown adipocytes for their survival in the mouse. Proceedings of the National Academy of Sciences of the United States of America 101:4543—4547.

[49] Yu, S., Matsusue, K., Kashireddy, P., Cao, W.Q., Yeldandi, V., Yeldandi, A.V., et al., 2003. Adipocyte-specific gene expression and adipogenic steatosis in the mouse liver due to peroxisome proliferator-activated receptor γ1 (PPARγ1) overexpression. Journal of Biological Chemistry 278:498—505.

[50] Moran-Salvador, E., Lopez-Parr, M., Garcia-Alonso, V., Titos, E., Martinez-Clemente, M., Gonzalez-Periz, A., et al., 2011. Role of PPARγ in obesity-induced hepatic steatosis as determined by hepatocyte- and macrophage-specific conditional knockouts. Federation of American societies of Experimental Biology 25:2538—2550.

[51] Inoue, M., Ohtake, T., Motomura, W., Takahashi, N., Hosoki, Y., Miyoshi, S., et al., 2005. Increased expression of PPARγ in high fat diet-induced liver steatosis in mice. Biochemical and Biophysical Research Communications 336:215—222.

[52] Lane, M.D., Tang, Q.Q., Jiang, M.S., 1999. Role of the CCAAT enhancer binding proteins (C/EBPs) in adipocyte differentiation. Biochemical and Biophysical Research Communications 3:677—683.

[53] Clarke, S.L., Robinson, C.E., Gimble, J.M., 1997. CAAT/enhancer binding proteins directly modulate transcription from the peroxisome proliferator-activated receptor γ2 promoter. Biochemical and Biophysical Research Communications 1:99—103.

[54] Madsen, M.S., Siersbaek, R., Boergesen, M., Nielsen, R., Mandrup, S., 2014. Peroxisome proliferator-activated receptor gamma and C/EBPalpha synergistically activate key metabolic adipocyte genes by assisted loading. Molecular and Cellular Biology 34:939—954.

[55] Wu, Z., Rosen, E., Brun, R., Hauser, S., Adelmant, G., Troy, A., 1999. Cross regulation of C/EBPα and PPARγ controls the transcriptional pathway of adipogenesis and insulin sensitivity. Molecular Cell 3:151—158.

[56] Elberg, G., Gimble, J., Tsai, S., 2000. Modulation of the murine peroxisome proliferator-activated receptor γ2promoter activity by CCAAT/enhancer-binding proteins. Journal of Biological Chemistry 275:27815—27822.

 © 2019 The Authors. Published by Elsevier GmbH. This is an open access article under the CC BY-NC-ND license (http://creativecommons.org/licenses/by-nc-nd/4.0/).

Supplemental Material

GDF10 blocks hepatic PPARγ activation to protect against diet-induced liver injury

Khrystyna Platko[1], Paul F. Lebeau[1]*, Jae Hyun Byun[1], Samantha V. Poon[1], Emily A. Day[2], Melissa E. MacDonald[1], Nicholas Holzapfel[1], Aurora Mejia-Benitez[1], Kenneth N. Maclean[3], Joan C. Krepinsky[1] and Richard C. Austin[1,†]*

Table 1: List of antibodies used for IHC and immunoblotting.

Antibody	Manufacturer and Product Number	Application	Dilution
C/EBP	sc-7273, Santa Cruz Biotechnology	IHC	1:50, HIER
CD36	NB400-144, Novus Biologicals	IHC	1:100, no retrieval
GRP78	sc-1050, Santa Cruz Biotechnology	IHC	1:40, no retrieval
GRP94	ADI-SPA-850, Enzo Life Sciences	IHC	1:100, HIER
Perilipin	ab3526, Abcam	IHC	1:100, HIER
PPARγ	sc-7273, Santa Cruz Biotechnology	IHC	1:50, HIER
pPERK	ab192591, Abcam	IHC	1:50, HIER
GAPDH	2118, Cell Signaling Technology	IB	1;1000
GDF10	16630, Novus Biologicals	IHC, IB	1:50, 1:1000
Histone H3	9715, Cell Signaling Technology	IB	1:1000
C/EBPα	sc-150, Santa Cruz Biotechnology	IF, IB	1:50, 1:200
PPARγ	sc-7273, Santa Cruz Biotechnology	IF, IB	1:50, 1:200
Smad2/3	3102, Cell Signaling Technology	IB	1:500

Phospho-Smad2/3	8828, Cell Signaling Technology	IB	1:500
Smad1/5/9	12656, Cell Signaling Technology	IB	1:500
Phospho-Smad1/5/9	13820, Cell Signaling Technology	IB	1:500

IB, immunoblot; IHC, immunohistochemical staining; IF, immunofluorescence; HIER, heat-induced epitope retrieval

Table 2: List of primers used for quantitative real time PCR

Gene	Species	Forward	Reverse
ANGPTL4	Mouse	CATCCTGGGACGAGATGAACT	TGACAAGCGTTACCACAGGC
ACOX1	Mouse	GGGAGTGCTACGGGTTACATG	CCGATATCCCCAACAGTGATG
ACOT2	Mouse	GTTGTGCCAACAGGATTGGAA	GCTCAGCGTCGCATTTGTC
Acadm	Mouse	AGGGTTTAGTTTTGAGTTGACGG	CCCCGCTTTTGTCATATTCCG
ATF4	Mouse	ATGGCCGGCTATGGATGAT	CGAAGTCAAACTCTTTCAGATCCATT
BBC3	Mouse	TGTGGAGGAGGAGGAGTGG	TGCTGCTCTTCTTGTCTCCG
CEBPa	Mouse	CAAGAACAGCAACGAGTACCG	GTCACTGGTCAACTCCAGCAC
CD36	Mouse	GATGACGTGGCAAAGAACAG	TCCTCGGGGTCCTGAGTTAT
CHOP	Mouse	CTGCCTTTCACCTTGGAGAC	CGTTTCCTGGGGATGAGATA
Casp3	Mouse	CCTCAGAGAGACATTCATGG	GCAGTAGTCGCCTCTGAAGA
Casp7	Mouse	GGACCGAGGGCCCACTTATC	TCGCTTTGTCGAAGTTCTTGTT
CRCT2	Mouse	ATGAACCCTAACCCCCAAGAC	CGTTCTCCTCAATAGCAGGGA
FOXO1	Mouse	CCCAGGCCGGAGTTTAACC	GTTGCTCATAAAGTCGGTGCT
FGF21	Mouse	AGATCAGGGAGGATGGAACA	TCAAAGTGAGGCGATCCATA
FN1	Mouse	CGAGGTGACAGAGACCACCA	CTGGGAGTCAAGCCAGACACA
FSP27	Mouse	ATGGACTACGCCATGAAGTCT	CGGTGCTAACACGACAGGG
FATP5	Mouse	GAATCGGGAGGCAGAGAACT	AGCGGGTCATACAAGTGAGC
GRP78	Mouse	GTCCTGCATCATCAGCAAAG	GGTAGCCACATACTGAACACC
GRP94	Mouse	GATGGTCTGGCAACATGGAG	CGCCTTGGTGTCTGGTAGAA
GDF10	Mouse	AATGATCGACCAAAAGCCTGT	CTTGCAGAATACCTCACGAGC

IRE1a	Mouse	TGAAACACCCCTTCTTCTGG	CCTCCTTTTCTATTCGGTCACTT
Il1b	Mouse	GCACTACAGGCTCCGAGATGAAC	TTGTCGTTGCTTGGTTCTCCTTGT
LPL	Mouse	GGGCTCTGCCTGAGTTGTAG	AGAAATTTCGAAGGCCTGGT
PPARa	Mouse	GAAGGGCACACGCGTGCGAGTTTTCAG	GAAGGGCACACGCGTGCGAGTTTTCAG
Perilipin	Mouse	CTGTGTGCAATGCCTATGAGA	CTGGAGGGTATTGAAGAGCCG
PGC1b	Mouse	TCCTGTAAAAGCCCGGAGTAT	GCTCTGGTAGGGGCAGTGA
PDK4	Mouse	AGGGAGGTCGAGCTGTTCTC	GGAGTGTTCACTAAGCGGTCA
PARP1	Mouse	GGAAAGGGATCTACTTTGCCG	TCGGGTCTCCCTGAGATGTG
PCK1	Mouse	CTGCATAACGGTCTGGACTTC	CAGCAACTGCCCGTACTCC
sXBP1	Mouse	GAGTCCGCAGCAGGTG	GTGTCAGAGTCCATGGGA
STAT3	Mouse	CACCTTGGATTGAGAGTCAAGAC	AGGAATCGGCTATATTGCTGGT
TNFa	Mouse	CATGAGCACAGAAAGCATGATCCG	AAGCAGGAATGAGAAGAGGCTGAG
TGF beta	Mouse	CAACAATTCCTGGCGTTACCTTGG	GAAAGCCCTGTATTCCGTCTCCTT

Figure legends

Fig. S1 GDF10 treatment reduces cytotoxicity in response to TG and TM. **(A)** ORO staining and isopropanol extract quantification of HepG2 cells treated with TG (100 nM), PA (200 µM) and rhGDF10 (250 ng/mL) for 24 hours. **(B)** LDH release assay in the medium from Huh7 cells treated with TG (100 nM) and TM (2 µg/mL). Scale bar, 50 µm. All data are shown as the mean ± S.D. *, $p<0.05$ by unpaired two-tailed Student's *t*-test or one-way ANOVA.

Fig. S2 GDF10$^{-/-}$ exhibit a reduction in plasma Leptin. Plasma content of circulating Leptin in wild type and GDF10$^{-/-}$ mice fed NCD (n=5). All data are shown as the mean ± S.D. *, $p<0.05$ by unpaired two-tailed Student's *t*-test.

Fig. S3 GDF10 modulates PPARγ and C/EBPα nuclear abundance. Immunofluorescent staining of PPARγ and C/EBPα in **(A)** HepG2 cells and **(B)** primary human hepatocytes treated with rhGDF10 or CGTZ. Scale bars, 50 µm.

Fig. S4 TGFβR1 inhibition reduces CGTZ-mediated lipid droplet accumulation in HepG2 cells. ORO staining in HepG2 cells treated with CGTZ (10 µM), rhGDF10 (250 ng/mL) and IN1130 (100 nM). Scale bar, 50 µm.

Fig. S5 GDF10$^{-/-}$ mice exhibit increased hepatic fibrosis, apoptosis and gluconeogenesis. (A) PSR staining in the livers of mice fed NCD or HFD. Real time PCR analysis of hepatic mRNA abundance of indicated genes involved in **(B)** apoptosis and **(C)** gluconeogenesis (n=5). Scale bars, 200 µm. All data are shown as the mean ± S.D. *, $p<0.05$ by one-way ANOVA.

Fig. S6. ER stress-inducing agent TM induces the expression of GDF10 in 3T3-L1 adipocytes. Real time PCR analysis of GDF10 mRNA transcript levels in 3T3-L1 adipocytes treated with TM (2 µg/ml) for 24 hours. All data are shown as the mean ± S.D. *, $p<0.05$ by unpaired two-tailed Student's *t*-test.

Figure S1. **Platko & Lebeau et al., 2019**

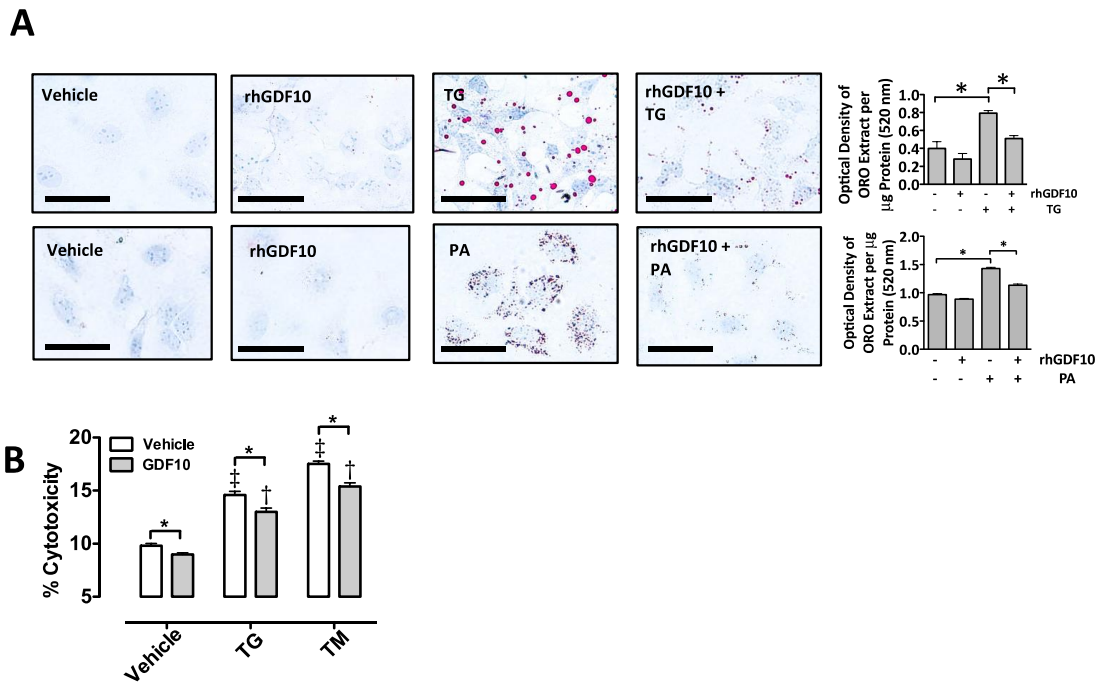

Figure S2. **Platko & Lebeau et al., 2019**

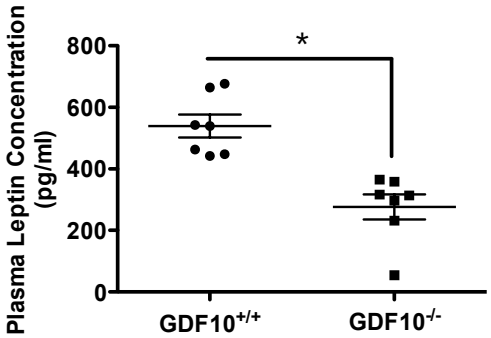

Figure S3. **Platko & Lebeau et al., 2019**

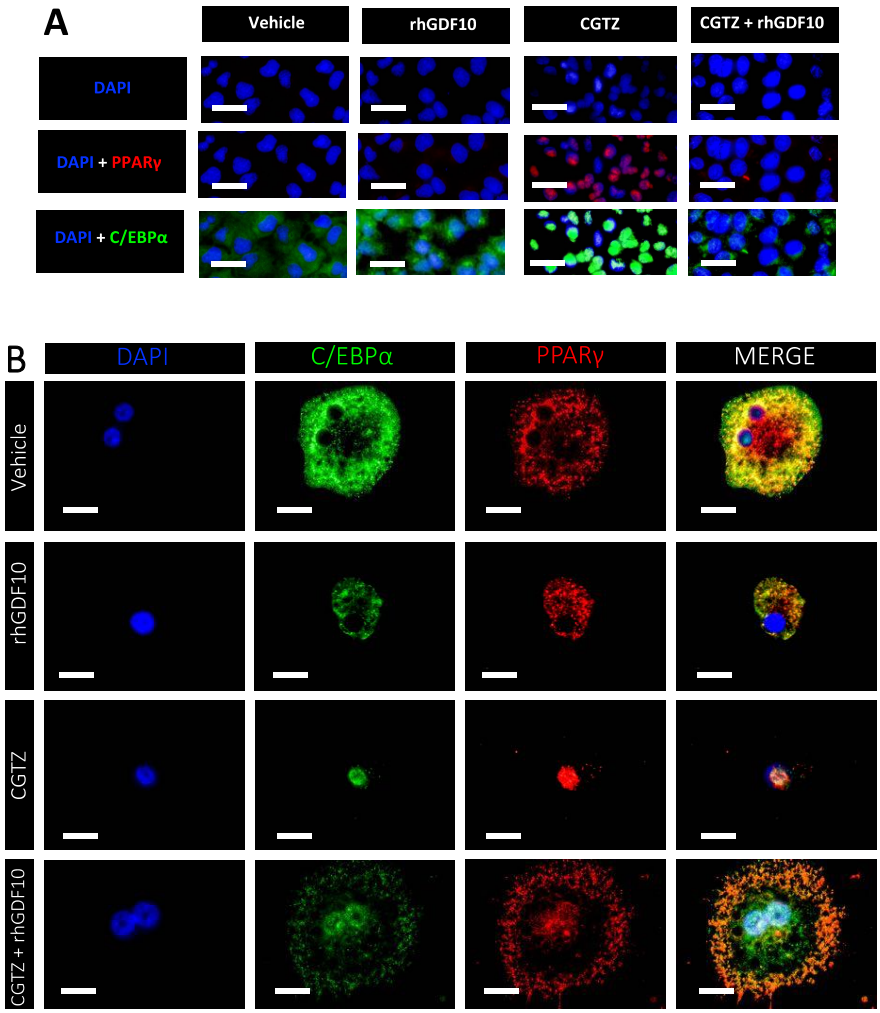

Figure S4.

Platko & Lebeau et al., 2019

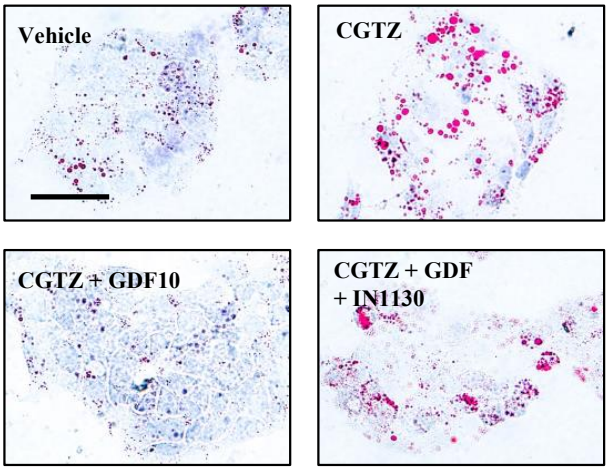

Figure S5.

Platko & Lebeau et al., 2019

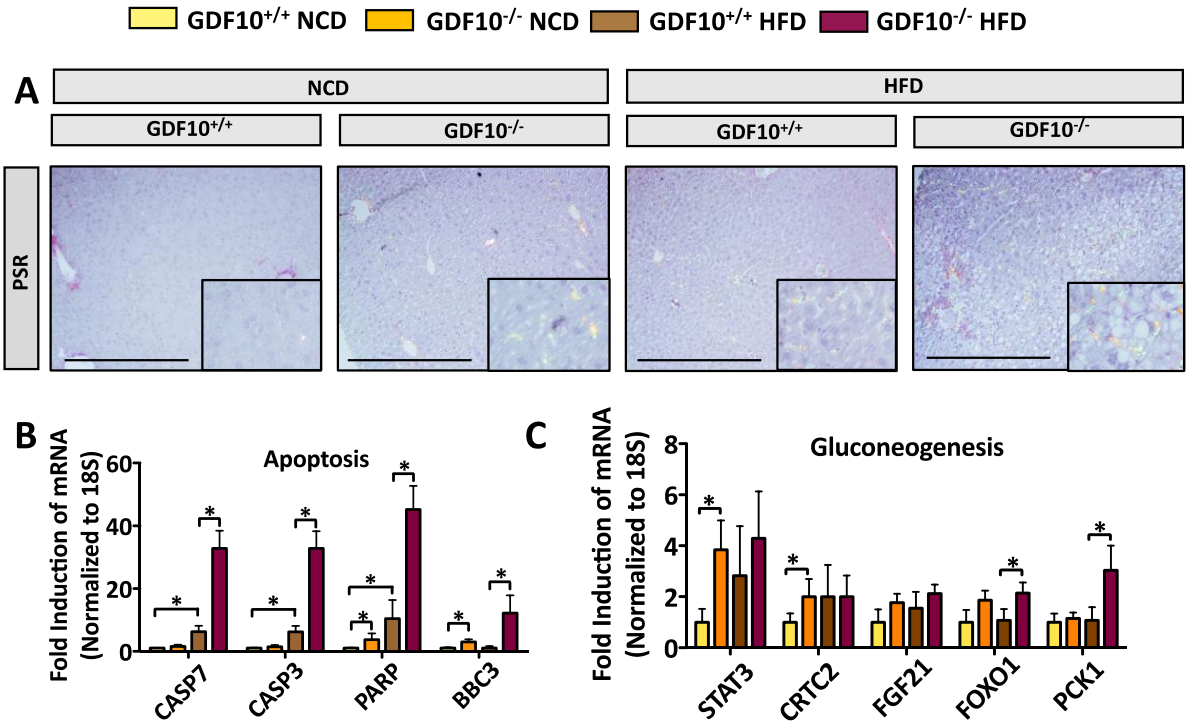

Figure S6. **Platko & Lebeau et al., 2019**

A

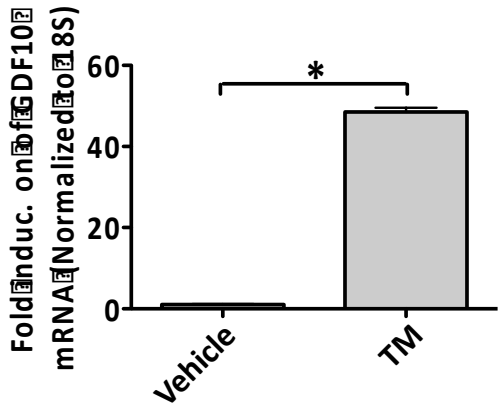

CHAPTER 5: GENERAL DISCUSSION

CVD is the primary cause of mortality in patients with advanced CKD[11,35-37]. Increased arterial stiffness, occurring as a result of VC, is an established predictor and independent risk factor of CVD-associated mortality in patients with impaired renal function[15,17-19]. The data shown in this thesis demonstrate that TDAG51 modulates VC by regulating the expression of Runx2, Pit-1 (*Chapter 2*), as well as GDF10 in the VSMCs (*Chapter 3*). Findings summarized in *Chapter 3* also identify GDF10 as a novel systemic inhibitor of VC, and as such, a potential therapeutic avenue for the management and diagnosis of this disease. In addition to its role as an inhibitor of VC, the results indicated in this thesis also report that GDF10 is a crucial modulator of hepatic lipid homeostasis, and therefore may indirectly affect vascular heath by regulating other metabolic parameters (*Chapter 4*).

5.1 The pathogenesis of VC

The appropriate diagnosis and management of VC among patients with CKD represents a significant unmet need[227]. There are currently no clinically-applicable methods that reliably detect and quantify CKD-associated VC. As a result, most VC is detected unintentionally through imaging that was designed to assess other indications[227]. In the academic setting, however, several imaging-based quantitative methods have been developed and are thought to have prognostic value. Among these, the computed tomography-based quantification of arterial mineral deposition, reflected as CAC score, is the most widely used[227,228]. The ability of imaging-based quantification tools to accurately distinguish between intimal and medial VC, represents a limitation of this technology[227].

In recent years however, this area of research has focused on the identification of systemic biomarkers of VC. These include serum calcioprotein particles and extracellular vesicle-associated mineral quantification approaches[229,230]. Increasing evidence suggests that circulating levels of microRNAs also have a potential prognostic value[231]. Additionally, elevated circulating levels of calcification inhibitors, OPN and OPG, have been associated with VC in DM, and hemodialysis patients, respectively[232,233]. In line with these studies, we report that a novel inhibitor of VC, GDF10, may serve as a potential biomarker of VC. These findings are supported by the observed increase in circulating GDF10 levels in patients with established CAC (*Chapter 3*). Thus similar to other well-established inhibitors of the mineralization process, GDF10 may possess a dual role as an inhibitor and a marker of this disease[232,233].

Although our understanding of biomarkers of VC is rapidly improving, there are currently no established therapeutic intervention for the prevention and reversal of this process. In clinical studies, several lines of evidence demonstrate that lowering of serum P_i can decrease mineral and bone disorder and CV risk in patients with CKD[64]. As a result, P_i binders are regularly used as a treatment modality for the management of hyperphosphatemia in these patients[227]. Additionally, vitamin K and magnesium supplementation both show potential for the management of VC[234,235]. Given that pro-osteogenic differentiation and apoptosis are the two main mechanisms that drive VC of VSMCs, novel therapies aimed directly at these processes in the vasculature are necessary to effectively target VC[12]. In support of this notion, evidence from *in vitro* studies show that inhibition of apoptotic cell death can attenuate VC[128]. To our knowledge, however, no

evidence of reversal of osteogenic transdifferentiation of VSMCs has been documented. Interestingly, one study reports that mature osteoblast can dedifferentiate to osteogenic precursor cells, suggesting that similar to VSMCs, osteoblasts possess some degrees of plasticity[236]. Because mesenchymal stem cells give rise to both osteoblast and VSMCs, these data also suggest that dedifferentiating osteoblast may in some circumstances commit to a VSMC lineage[2]. Given that previous studies from our laboratory, in accordance with the data presented in this thesis, highlight TDAG51 as regulator of cellular differentiation and apoptosis, TDAG51 may serve as an important molecular link for delineating the exact cellular mechanisms involved in the development of VC[114,145,152,226].

Another important consideration for scientists in the field of VC is the question of whether it is safe to reverse/remove VC. VC is a pathophysiological adaptation of the VSMCs that occurs at every spectrum of renal dysfunction and only reaches its maximal size potential after chronic exposure to circulating toxins[12,60]. As a result, substantial VC that is readily detectable using currently available techniques is predominantly present in patients with advanced CKD. The calcified areas in the vasculature consist of HA crystals and osteoblast-like transdifferentiated VSMCs[60,227]. Given the current knowledge of disease aetiology, in the early stages of the disease, dissolution of micro calcification within the arterial wall may have a beneficial effect on vascular compliance and CV risk, with minimal adverse side effects. Importantly, it is well-accepted that dissolution of large HA crystals present in patients with advanced CKD would potentially lead to empty spaces or gaps in the large arteries, likely resulting in serious health consequences primarily affecting the hemodynamic balance and arterial wall integrity in these patients.

5.1.1 TDAG51 is a key modulator of vascular calcification and osteogenic transdifferentiation of arterial smooth muscle cells

In humans, chronic renal insufficiency leads to a persistent state of hyperphosphatemia, which is associated with increased risk of CV mortality due to changes in vessel wall elasticity[17-19]. Consistently, presence of medial VC is a strong predictor of CV and all-cause mortality in patients with CKD[15,17-19]. Experimental studies have identified Runx2 as a crucial mediator of VC, as its expression is upregulated in conditions of hyperphosphatemia[103,104,108]. Pit-1 is the predominant P_i cotransporter found in VSMCs, and is necessary for P_i-mediated mineralization of the VSMCs[69]. Using *in vitro*, *in vivo*, and *ex vivo* models of VC, *Chapter 2* illustrates that TDAG51 modulates hyperphosphatemia-induced VC by regulating (i) Runx2 transcriptional activity and (ii) Pit-1 expression. In line with the regulatory role of TDAG51, its expression is also increased in calcified human arteries and mouse VSMCs, while TDAG51 deficiency confers a protective phenotype.

Although *Chapter 2* predominantly focused on the Pit-1-Runx2-mediated mechanism of TDAG51 regulatory action, other molecular mechanisms may also contribute to the protective phenotype observes in *TDAG51*$^{-/-}$ mice and VSMCs. TDAG51 is traditionally regarded as a transcription factor with pro-apoptotic activity[143]. In line with this notion, antibody-mediated neutralization of its human homologue, PHLDA1, increases while its overexpression decreases cell survival[151]. TDAG51 expression also correlates with apoptotic cell death in atherosclerotic lesions from *ApoE*$^{-/-}$ mice[152]. Cell membrane distortion, resulting in increased permeability of VSMCs, can lead to apoptotic cell death.

We have reported that overexpression of PHLDA1 leads to substantial changes in cellular morphology and adhesion, and promotes detachment-mediate cell death of endothelial cells[152]. Similarly, Carlisle *et. al*[153] found that transient overexpression of TDAG51 promoted changes in cell shape and morphology that exacerbate TGF-β mediated EMT. Given these findings, apoptosis is one of the major mechanisms contributing to VC, the phenotype observed in *TDAG51*$^{-/-}$ may partially occur due to their resistance to apoptotic cell death.

Accumulating evidence also demonstrates that ER stress plays an important role in the development of VC. A variety of well-established inducers of VC, such as BMP2, advanced glycation end products, TGF-β, vitamin D3, as well as calcium and P_i, are also know to induce ER stress[132,169]. Activation of ER stress signaling promotes pro-osteogenic ALP activity in primary human VSMCs[237]. Conversely, inhibition of ER stress attenuates P_i-mediated pro-osteogenic differentiation of fibroblast cells[238]. ER stress also mediates TDAG51 induction and detachment-mediated cell death, while *TDAG51*$^{-/-}$ mice are protected from ER stress-mediated pathological processes in the context of atherosclerosis, and renal disease[153,226]. To this end, additional unpublished observations shown in this thesis demonstrate that aortas from *TDAG51*$^{-/-}$ mice display attenuation of ER chaperones, GRP78 and GRP94 (*Appendix 1*). These data suggest that the phenotype observed in *TDAG51*$^{-/-}$ may partially occur due to an attenuation in ER stress response.

Studies from our laboratory also highlight the existing relationship between TDAG51 and well-established inhibitor of osteogenic transdifferentiation of VSMCs, PPARγ[145]. TDAG51 negatively regulates the expression of PPARγ and its downstream

targets, whereas TDAG51 deficiency enhanced PPARγ activity[145]. Recent evidence also found that PPARγ inhibits Runx2 expression and transcriptional activity by preventing Runx2 interaction with osteoblast-specific element-2 promoter in osteoblasts[223]. There exists a reciprocal relationship between Runx2 and PPARγ via the MAPK pathway[120-122]. Specifically, MAPK-mediated phosphorylation of Runx2 and PPARγ is necessary for the initiation of osteogenic and inhibition of adipogenic program in mouse embryonic fibroblast cells[120]. To this end, reduced VC in *TDAG51*$^{-/-}$ mice may also be observed due to enhanced PPARγ expression that works to oppose Runx2-mediated pro-osteogenic phenotype.

Although the major hypothesis is supported by ample evidence in this thesis, there remains certain key limitations. One of the most evident limitations is the use of the global *TDAG51*$^{-/-}$ mouse model. It is well-established that TDAG51 plays a role in the development of diabetes, obesity, atherosclerosis, and renal impairment, conditions that have all been previously correlated to development of VC[145,152,153]. Thus, the use of smooth muscle cell-specific *TDAG51*$^{-/-}$ would provide a better understanding of the role of TDAG51 in VC. A second limitation of the studies included in this thesis is the use of a non-CKD model of VC. Although the vitamin D3 overload model leads to VC as a result of P_i overload, this model is very rapid and thus may not be representative of the changes in vasculature that occur as a result of chronic hyperphosphatemia observed in patients with advanced CKD. This model was chosen due to the lack of reliable and easily reproducible mouse models of CKD-associated VC. Although studies demonstrate that adenine feeding combined with high P_i feeding is able to induce VC, we were not able to replicate these

studies due to high mortality rate (*Appendix 2*)[239,240]. The last limitation of this study is that only male mice were used for the *in vivo* experiments. Recent studies have found that there may be sex differences associated with development of VC[241,242]. Thus, examining VC in female mice would determine whether the role of TDAG51 as a regulator of VC is dependent on sex.

5.1.2 GDF10 is a negative regulator of vascular calcification of vascular smooth muscle cells

Osteogenic transdifferentiation of VSMCs is a highly regulated process that shares many similarities with osteoblast differentiation and bone mineralization[12,16]. The relationship between TGF-β signaling and pro-osteogenic differentiation of the VSMCs is well-established, and has predominantly focused on the effect of well-characterized members of the superfamily, including TGF-β, BMP2 and BMP7[243-246]. *Chapter 2* of this thesis demonstrates that VSMCs derived from *TDAG51*$^{-/-}$ mice exhibit reduced expression of the type III sodium-dependent P_i transporter and Runx2 transcriptional activity, leading to diminished VC[114]. Building on these observations, *Chapter 3* also shows that reduced VC in *TDAG51*$^{-/-}$ mice is accompanied by an increase in the expression of known inhibitor of osteogenesis, *GDF10*[176-178]. In line with its anti-osteogenic role, recombinant human GDF10 treatment attenuated VC by reducing the expression and activity of Runx2. These findings provide potential additional mechanism to explain the protective phenotype observed in the *TDAG51*$^{-/-}$ mice.

Similar to TGF-β, GDF10 exerts its effect by activating the TGF-β receptor-SMAD2/3 signaling pathway[175,195]. However, TGF-β and GDF10 have opposing effect on VC. While TGF-β promotes pro-osteogenic phenotype in vascular cells, our observations show that GDF10 inhibits this process[247]. The various biological functions controlled by the TGF-β signaling cascade are mediated by the combinations of ligands and type I/II receptors that differ based on the cell type and state[154,248]. For example, BMP2 and BMP4 preferentially bind to ALK3 or ALK6, while BMP6 and BMP7 are more likely to exert their effect through ALK2 or ALK6[249-251]. The closely related family member BMP3 was reported to exert its effect via the ALK4/Actr-IIB-mediated pathway activation[172,252,253]. While, Matsumoto *et al.*[177] demonstrated that GDF10 facilitates its anti-osteogenic effect via ALK4/Actr-IIA. In line with differential effect of TGF-β and GDF10 on VC, TGF-β induces VC via the ALK5-mediated pathway[254]. Additionally, activation of the same ALK receptors may produce differential physiological response dependent on cell type. For instance, activation of ALK3 induced osteogenesis in mesenchymal stem cell, while its downregulation in osteoblast cells can also lead to ectopic mineralization via the upregulation of bone-specific markers, including Runx2 and ALP[255,256]. The observed differential effect may also occur as a result of differences in receptor innervation achieved by the two ligands, occurring because of differences in their structure. GDF10 is a divergent member of the TGF-β superfamily, and as such shares only 40 to 50% sequence homology with TGF-β in the active domain (*Appendix 3*). Because of these differences in protein structure, GDF10 and TGF-β may differentially affect the same receptor, thus resulting in the recruitment of distinct coregulatory partners and contrasting actions of its two ligands.

Chapter 3 of this thesis identifies GDF10 as a novel inhibitor of P_i-mediated Runx2 expression and transcriptional activity, as well as HA deposition in the VSMCs. The work described in *Chapter 2* of thesis showed that there exists a reciprocal relationship between Runx2 and Pit-1, suggesting that Pit-1 may be a downstream target of Runx2 transcriptional activity in the VSMCs. However, no change in Pit-1 expression upon GDF10-mediated downregulation of Runx2 expression and transcriptional activation was observed. Although inconsistent with previous studies, it is not uncharacteristic of a complex transcription factor like Runx2 to promote or repress the expression of varying genes dependent on cellular type and state, as well as stimulus type and duration[257]. In line with this notion, a regulator of Runx2 activity, DLX3 exerts both positive and negative regulation of gene transcription[258]. During proliferation stages, DLX3 directly interacts with Runx2, thorough protein-protein interaction to inhibit Runx2 activation. While during the maturation of osteoblasts, DLX3 acts as an induced of Runx2 transcriptional activity via DNA-protein interaction which stimulates OCN transcription[258]. Runx2 transcriptional activation is also regulated by a variety of post-translational modifications and/or protein-protein interactions[257,259-261]. Moreover, Runx2 contains two activation domains that facilitate coactivator or repressor recruitment and transcriptional activation. As such, its promoter regions are either surrounded by or overlapped with binding sites for a variety of coregulatory molecules, including SMADS[259,262]. Given that GDF10 exerts its effect in SMAD3-dependent manner and that Runx2 activation is also regulated by SMAD3, GDF10 and Runx2 may compete for SMAD3 and well as the co-receptor SMAD4 in VSMCs[175,195,263]. Given that regulation of Runx2 transcriptional activity occurs in multiple

regions, GDF10-mediated downregulation or Runx2 expression may occur through one of several potential mechanisms described above, and thus may only affect some genes.

While this thesis provides considerable evidence in support of an anti-osteogenic role of GDF10 *in vitro*, one of the most evident limitations is that no difference in HA deposition was observed in the *GDF10*$^{-/-}$ mice. Thus, additional studies using GDF10 supplementation *in vivo* are necessary to confirm its role as a novel inhibitor of VC. The data presented in *Chapter 3* also demonstrate a substantial increase in circulating levels of closely related BMP3 in *GDF10*$^{-/-}$ mice, which likely occurred in a compensatory manner due to the absence of GDF10, and may explain inconsistencies between *in vivo* and *in vitro* experiments. For this reason, additional studies using GDF10 and BMP3 double KO mice would further elucidate the role of GDF10 in ectopic mineralization. Future studies are also necessary to examine the mechanisms by which GDF10-mediated downregulation of Runx2 transcriptional activity occurs. Given that hyperphosphatemia-mediated development of osteogenic phenotype in VSMCs is similar to osteoblast differentiation, the potential mechanisms underlying GDF10-mediated inhibition of Runx2 are also likely closely related to inhibitory mechanisms observed in osteoblast. Activation of the TGF-β-SMAD pathway results in the recruitment of histone deacetylases that antagonize Runx2 activity and as such inhibit osteogenesis[99]. Given that *TDAG51*$^{-/-}$ VSMCs exhibit reduced Runx2 activity (*Chapter 2*), coupled with an increase in GDF10 and HDAC3 expression (*Appendix 4*), GDF10 may exert its effect in an HDAC-dependent manner.

5.2 The relationship between CKD and NAFLD

Mounting evidence demonstrates the increased prevalence of metabolic syndrome (MS), characterized by presence of obesity, hypertension, and DM in patients with CKD[264-266]. Epidemiological studies show that NAFLD is an independent risk factor for CKD, where presence and severity of NAFLD correlates with increased risk and severity of CKD[267,268]. Approximately 20% to 50% of patients with NAFLD have impaired renal function[269]. Likewise the prevalence of CKD is increased in patients with NAFLD[270]. Given that NAFLD and CKD are both progressive chronic conditions that occur as feature of MS, they have an independent and likely additive effect on CV risk in patients with impaired renal function.

Similar to the association between CKD and VC, there also exists an association between NAFLD and CAC in patients with and without previous history of CVD[271]. A relationship between presence the of NAFLD and abdominal aortic calcification has been highlighted previsously[272]. In line with these observations the Multi-Ethnic Study of Atherosclerosis defined an association between NAFLD and arterial stiffness–which is frequently used as a surrogate measure of VC[273]. A cross-sectional study of 4123 patients and controls also determined that presence of NAFLD is predictive of an increase in CAC score independent of other CV risk factors[274]. Similarly, in the Framingham Heart Study, hepatic lipid accumulation was associated with increase in the CAC score[275]. Recent epidemiological studies have also reported lower bone mineral density in patients with NAFLD; a condition which is also highly prevalent in patients with advanced CKD and VC[48,276].

Limited mechanistic insight exists to link these symptomatically distinct diseases that occur as a result of MS. In one study, an increase in circulating leptin and metabolic oxidative stress, as a result of NAFLD, was shown to increase renal inflammation and fibrosis in a mouse model of hepatic steatosis and acute renal toxicity[277]. In line with these studies, NAFLD-associated increase in circulating leptin was also demonstrated to cause renal mesangial cell activation and inflammation, subsequently leading to renal fibrosis[278]. However, to date no mechanistic evidence exists to delineate the relationship between NAFLD and an increase in CAC observed in epidemiological studies. Thus, vascular manifestations may occur either as a direct result of NAFLD, or indirectly as a result of renal disease.

5.2.1 GDF10 blocks hepatic PPARγ activation to protect against diet-induced liver injury

The prevalence of MS is quickly rising worldwide[279]. NAFLD is a feature of a MS that affects approximately 25% of the global population, and contributes to other comorbidities associated with MS, such as DM, hypertension, heart disease, and ischemic stroke[280]. *Chapter 4* of this thesis demonstrates that *GDF10*$^{-/-}$ mice develop increased HFD-induced obesity, hepatic steatosis, and liver fibrosis. Using *in vitro* models the data presented in *Chapter 4* show that recombinant human GDF10 can prevent excessive lipid accumulation in hepatocytes by attenuating PPARγ transcriptional activity. These findings are consistent with the previously reported role of GDF10 in adipocyte differentiation[196,207].

While the study described in *Chapter 4* provides insight into the hepatoprotective role of GDF10 via the regulation of *de novo* lipogenesis, the role of GDF10 on liver injury

has not been fully elucidated. A substantial increase in hepatic fibrosis was found in the *GDF10*$^{-/-}$ mice, which is of interest because the observed degree of liver damage does not normally occur as a result of HFD-feeding in mice with C57BL/6J genetic background, and is comparable to established models of hepatic fibrosis[281,282]. This suggests that *GDF10*$^{-/-}$ mice may represent a novel model of diet-induced hepatic injury. However, additional studies using established models of liver injury are necessary to fully elucidate the potential protective effect of GDF10.

Although antagonistic activity of GDF10 against PPARγ in hepatocytes confers a protective phenotype, these findings are in conflict with a previously demonstrated protective effect of GDF10 in other PPARγ-rich cell types, like VSMCs[126]. Given that an increase PPARγ activation in the VSMCs confers a protective phenotype against VC, there exists a possibility that in a manner similar to TGF-β, GDF10-mediated regulation of PPARγ function can occur in a cell- and context-dependent manner[126]. These findings suggest that in contrast to hepatocytes, GDF10 may function as a PPARγ agonist in VSMCs. If this holds true, GDF10-induced downregulation of Runx2 transcriptional activity in VSMCs may occur as a result of heightened PPARγ activation[120,125]. Additionally, the GDF10-mediated response in VSMCs may occur through an alternative regulatory signaling cascade, which could also result in differential response. However, additional studies are necessary to test this hypothesis.

5.3 Conclusion and future directions

One of main findings of this thesis demonstrates that TDAG51 modulates VC by regulating Runx2 transcriptional activity and Pit-1 expression. To this end, *TDAG51*$^{-/-}$ mice and VSMCs exhibit an attenuation of VC[114]. The second main findings is that in addition to the regulatory action of TDAG51 on Runx2 and Pit-1, TDAG51 also modulates the expression of the novel systemic inhibitor of VC, GDF10. This finding provides additional and alternative mechanism to explain diminished mineral deposition that was observed in *TDAG51*$^{-/-}$. Lastly, the results shown in this thesis also demonstrate that GDF10 is a powerful circulating inhibitor of PPARγ activation in hepatocytes, and as such an important modulator of hepatic lipid accumulation[195]. These last two observations are especially exciting because as a circulating protein, GDF10 holds great potential as a therapeutic treatment for VC and NAFLD.

Give that we have previously demonstrated that *TDAG51*$^{-/-}$ mice exhibit a predisposition to conditions that affect renal insufficiency, as well as VC, future studies should focus on examining VSMC-specific role of TDAG51[145,152,153,226]. Studies utilizing VSMC-specific knockout and overexpression of TDAG51 would allow to determine the role TDAG51 in VC independent of other modulators of this disease. This is of interest because *TDAG51*$^{-/-}$ mice exhibit an increase in circulating levels of novel inhibitor of VC, GDF10 (*Chapter 3*). Importantly, GDF10 is predominantly expressed in adipose tissue and is also involved in the regulation of adipocyte differentiation[196,207]. Consistent with these findings, *TDAG51*$^{-/-}$ mice develop increased adiposity characterized by enlarged adipocytes[145]. Because adipose tissue is known to secrete a variety of factors involved in

both paracrine and autocrine regulation, increase in circulating GDF10 in *TDAG51*$^{-/-}$ mice likely occurs as a result of increased GDF10 secretion from adipose tissue as opposed to VSMCs[283]. In turn, adipose-secreted GDF10 in *TDAG51*$^{-/-}$ mice may affect vascular homeostasis.

Despite the fact that *Chapter 3* of this thesis highlights GDF10 as a novel inhibitor of VC, additional animal studies are necessary to confirm these findings. Future experiments should investigate whether exogenous GDF10 treatment can inhibit VC in wild-type mice using either a CKD-associated or proof-of-principle vitamin D3 overload model of VC. Because there exists a compensatory increase in BMP3 in *GDF10*$^{-/-}$ mice, experiments utilizing *GDF10-BMP3* double knockout mice are also necessary to unequivocally validate GDF10 as an important regulator of mineralization. Given that similar to Bmp3, GDF10 is a negative regulator of osteoblast differentiation and mineralization future experiments examining skeletal health status in *GDF10*$^{-/-}$ and *GDF10-BMP3* double knockout mice are also of interest[172,173].

Identification of GDF10 as a novel systemic modulator of VC and hepatic lipid accumulation are particularly exciting. Previous findings demonstrate the vital role of circulating proteins in the regulation of conditions associated with MS. In clinical studies expression of another divergent member of the TGF-β superfamily, GDF15, has been correlated with obesity, insulin resistance, and risk of CVD[284]. Studies have also reported that plasma levels of KL, OPN, and fetuin-A are associated with CAC[68]. Similarly, systemic levels of proprotein convertase subtilisin/kexin type 9 (PCSK9) correlate with presence of calcific aortic valve stenosis, while patients treated with anti-PCSK9 antibodies

exhibit an attenuation of aortic stenosis progression[285,286]. Hence, identification of molecules that can effectively regulate GDF10 activity and expression are of great interest.

CHAPTER 6: REFERENCES

1 Wolinsky, H. & Glagov, S. Structural Basis for the Static Mechanical Properties of the Aortic Media. *Circulation research* **14**, 400-413, doi:10.1161/01.res.14.5.400 (1964).

2 Lacolley, P., Regnault, V., Segers, P. & Laurent, S. Vascular Smooth Muscle Cells and Arterial Stiffening: Relevance in Development, Aging, and Disease. *Physiol Rev* **97**, 1555-1617, doi:10.1152/physrev.00003.2017 (2017).

3 Chirinos, J. A., Segers, P., Hughes, T. & Townsend, R. Large-Artery Stiffness in Health and Disease: JACC State-of-the-Art Review. *J Am Coll Cardiol* **74**, 1237-1263, doi:10.1016/j.jacc.2019.07.012 (2019).

4 van Popele, N. M. *et al.* Association between arterial stiffness and atherosclerosis: the Rotterdam Study. *Stroke* **32**, 454-460, doi:10.1161/01.str.32.2.454 (2001).

5 Benetos, A. *et al.* Influence of age, risk factors, and cardiovascular and renal disease on arterial stiffness: clinical applications. *Am J Hypertens* **15**, 1101-1108, doi:10.1016/s0895-7061(02)03029-7 (2002).

6 Stehouwer, C. D., Henry, R. M. & Ferreira, I. Arterial stiffness in diabetes and the metabolic syndrome: a pathway to cardiovascular disease. *Diabetologia* **51**, 527-539, doi:10.1007/s00125-007-0918-3 (2008).

7 Willum-Hansen, T. *et al.* Prognostic value of aortic pulse wave velocity as index of arterial stiffness in the general population. *Circulation* **113**, 664-670, doi:10.1161/CIRCULATIONAHA.105.579342 (2006).

8 Laurent, S. & Boutouyrie, P. The structural factor of hypertension: large and small artery alterations. *Circulation research* **116**, 1007-1021, doi:10.1161/CIRCRESAHA.116.303596 (2015).

9 Chou, Y. H., Chu, T. S. & Lin, S. L. Role of renin-angiotensin system in acute kidney injury-chronic kidney disease transition. *Nephrology (Carlton)* **23 Suppl 4**, 121-125, doi:10.1111/nep.13467 (2018).

10 Lanzer, P. *et al.* Medial vascular calcification revisited: review and perspectives. *Eur Heart J* **35**, 1515-1525, doi:10.1093/eurheartj/ehu163 (2014).

11 Subbiah, A. K., Chhabra, Y. K. & Mahajan, S. Cardiovascular disease in patients with chronic kidney disease: a neglected subgroup. *Heart Asia* **8**, 56-61, doi:10.1136/heartasia-2016-010809 (2016).

12 Leopold, J. A. Vascular calcification: Mechanisms of vascular smooth muscle cell calcification. *Trends Cardiovasc Med* **25**, 267-274, doi:10.1016/j.tcm.2014.10.021 (2015).

13 Allam, A. H. *et al.* Atherosclerosis in ancient Egyptian mummies: the Horus study. *JACC Cardiovasc Imaging* **4**, 315-327, doi:10.1016/j.jcmg.2011.02.002 (2011).

14 Lacolley, P., Regnault, V. & Laurent, S. Mechanisms of Arterial Stiffening: From Mechanotransduction to Epigenetics. *Arteriosclerosis, thrombosis, and vascular biology* **40**, 1055-1062, doi:10.1161/ATVBAHA.119.313129 (2020).

15 Wang, X. R., Zhang, J. J., Xu, X. X. & Wu, Y. G. Prevalence of coronary artery calcification and its association with mortality, cardiovascular events in patients with chronic kidney disease: a systematic review and meta-analysis. *Ren Fail* **41**, 244-256, doi:10.1080/0886022X.2019.1595646 (2019).

16 Demer, L. L. & Tintut, Y. Vascular calcification: pathobiology of a multifaceted disease. *Circulation* **117**, 2938-2948, doi:10.1161/CIRCULATIONAHA.107.743161 (2008).

17 London, G. M. *et al.* Arterial media calcification in end-stage renal disease: impact on all-cause and cardiovascular mortality. *Nephrol Dial Transplant* **18**, 1731-1740, doi:10.1093/ndt/gfg414 (2003).

18 Okuno, S. *et al.* Presence of abdominal aortic calcification is significantly associated with all-cause and cardiovascular mortality in maintenance hemodialysis patients. *American journal of kidney diseases : the official journal of the National Kidney Foundation* **49**, 417-425, doi:10.1053/j.ajkd.2006.12.017 (2007).

19 Chiu, Y. W. *et al.* Coronary artery calcification and mortality in diabetic patients with proteinuria. *Kidney international* **77**, 1107-1114, doi:10.1038/ki.2010.70 (2010).

20 Chen, Y., Zhao, X. & Wu, H. Arterial Stiffness: A Focus on Vascular Calcification and Its Link to Bone Mineralization. *Arteriosclerosis, thrombosis, and vascular biology* **40**, 1078-1093, doi:10.1161/ATVBAHA.120.313131 (2020).

21 Kakani, E., Elyamny, M., Ayach, T. & El-Husseini, A. Pathogenesis and management of vascular calcification in CKD and dialysis patients. *Semin Dial* **32**, 553-561, doi:10.1111/sdi.12840 (2019).

22 Benz, K. *et al.* Vascular inflammation and media calcification are already present in early stages of chronic kidney disease. *Cardiovasc Pathol* **27**, 57-67, doi:10.1016/j.carpath.2017.01.004 (2017).

23 Moe, S. M. *et al.* Medial artery calcification in ESRD patients is associated with deposition of bone matrix proteins. *Kidney international* **61**, 638-647, doi:10.1046/j.1523-1755.2002.00170.x (2002).

24 Wang, N. *et al.* Radial artery calcification in end-stage renal disease patients is associated with deposition of osteopontin and diminished expression of alpha-smooth muscle actin. *Nephrology (Carlton)* **13**, 367-375, doi:10.1111/j.1440-1797.2008.00941.x (2008).

25 McCullough, P. A., Agrawal, V., Danielewicz, E. & Abela, G. S. Accelerated atherosclerotic calcification and Monckeberg's sclerosis: a continuum of advanced vascular pathology in chronic kidney disease. *Clin J Am Soc Nephrol* **3**, 1585-1598, doi:10.2215/CJN.01930408 (2008).

26 Schwarz, U. *et al.* Morphology of coronary atherosclerotic lesions in patients with end-stage renal failure. *Nephrol Dial Transplant* **15**, 218-223, doi:10.1093/ndt/15.2.218 (2000).

27 Russo, D., Palmiero, G., De Blasio, A. P., Balletta, M. M. & Andreucci, V. E. Coronary artery calcification in patients with CRF not undergoing dialysis.

American journal of kidney diseases : the official journal of the National Kidney Foundation **44**, 1024-1030, doi:10.1053/j.ajkd.2004.07.022 (2004).

28 Mihai, S. *et al.* Inflammation-Related Mechanisms in Chronic Kidney Disease Prediction, Progression, and Outcome. *J Immunol Res* **2018**, 2180373, doi:10.1155/2018/2180373 (2018).

29 Dai, L., Golembiewska, E., Lindholm, B. & Stenvinkel, P. End-Stage Renal Disease, Inflammation and Cardiovascular Outcomes. *Contrib Nephrol* **191**, 32-43, doi:10.1159/000479254 (2017).

30 Cottone, S. *et al.* Oxidative stress, inflammation and cardiovascular disease in chronic renal failure. *J Nephrol* **21**, 175-179 (2008).

31 Campean, V. *et al.* CD40-CD154 expression in calcified and non-calcified coronary lesions of patients with chronic renal failure. *Atherosclerosis* **190**, 156-166, doi:10.1016/j.atherosclerosis.2006.01.014 (2007).

32 Hill, N. R. *et al.* Global Prevalence of Chronic Kidney Disease - A Systematic Review and Meta-Analysis. *PLoS One* **11**, e0158765, doi:10.1371/journal.pone.0158765 (2016).

33 Stevens, P. E., Levin, A. & Kidney Disease: Improving Global Outcomes Chronic Kidney Disease Guideline Development Work Group, M. Evaluation and management of chronic kidney disease: synopsis of the kidney disease: improving global outcomes 2012 clinical practice guideline. *Ann Intern Med* **158**, 825-830, doi:10.7326/0003-4819-158-11-201306040-00007 (2013).

34 Metcalfe, W. How does early chronic kidney disease progress? A background paper prepared for the UK Consensus Conference on early chronic kidney disease. *Nephrol Dial Transplant* **22 Suppl 9**, ix26-30, doi:10.1093/ndt/gfm446 (2007).

35 Go, A. S., Chertow, G. M., Fan, D., McCulloch, C. E. & Hsu, C. Y. Chronic kidney disease and the risks of death, cardiovascular events, and hospitalization. *N Engl J Med* **351**, 1296-1305, doi:10.1056/NEJMoa041031 (2004).

36 van der Velde, M. *et al.* Lower estimated glomerular filtration rate and higher albuminuria are associated with all-cause and cardiovascular mortality. A collaborative meta-analysis of high-risk population cohorts. *Kidney international* **79**, 1341-1352, doi:10.1038/ki.2010.536 (2011).

37 Manjunath, G. *et al.* Level of kidney function as a risk factor for cardiovascular outcomes in the elderly. *Kidney international* **63**, 1121-1129, doi:10.1046/j.1523-1755.2003.00838.x (2003).

38 Mann, J. F., Gerstein, H. C., Pogue, J., Bosch, J. & Yusuf, S. Renal insufficiency as a predictor of cardiovascular outcomes and the impact of ramipril: the HOPE randomized trial. *Ann Intern Med* **134**, 629-636, doi:10.7326/0003-4819-134-8-200104170-00007 (2001).

39 Culleton, B. F. *et al.* Cardiovascular disease and mortality in a community-based cohort with mild renal insufficiency. *Kidney international* **56**, 2214-2219, doi:10.1046/j.1523-1755.1999.00773.x (1999).

40 Smith, G. L. *et al.* Renal impairment and outcomes in heart failure: systematic review and meta-analysis. *J Am Coll Cardiol* **47**, 1987-1996, doi:10.1016/j.jacc.2005.11.084 (2006).

41 Schiffrin, E. L., Lipman, M. L. & Mann, J. F. Chronic kidney disease: effects on the cardiovascular system. *Circulation* **116**, 85-97, doi:10.1161/CIRCULATIONAHA.106.678342 (2007).

42 Hillege, H. L. *et al.* Urinary albumin excretion predicts cardiovascular and noncardiovascular mortality in general population. *Circulation* **106**, 1777-1782, doi:10.1161/01.cir.0000031732.78052.81 (2002).

43 Brantsma, A. H. *et al.* Urinary albumin excretion and its relation with C-reactive protein and the metabolic syndrome in the prediction of type 2 diabetes. *Diabetes Care* **28**, 2525-2530, doi:10.2337/diacare.28.10.2525 (2005).

44 de Zeeuw, D. *et al.* Albuminuria, a therapeutic target for cardiovascular protection in type 2 diabetic patients with nephropathy. *Circulation* **110**, 921-927, doi:10.1161/01.CIR.0000139860.33974.28 (2004).

45 Goodman, W. G. & Quarles, L. D. Development and progression of secondary hyperparathyroidism in chronic kidney disease: lessons from molecular genetics. *Kidney international* **74**, 276-288, doi:10.1038/sj.ki.5002287 (2008).

46 Lindberg, J. S. *et al.* The calcimimetic AMG 073 reduces parathyroid hormone and calcium x phosphorus in secondary hyperparathyroidism. *Kidney international* **63**, 248-254, doi:10.1046/j.1523-1755.2003.00720.x (2003).

47 Brown, S. J., Ruppe, M. D. & Tabatabai, L. S. The Parathyroid Gland and Heart Disease. *Methodist Debakey Cardiovasc J* **13**, 49-54, doi:10.14797/mdcj-13-2-49 (2017).

48 Covic, A. *et al.* Bone and mineral disorders in chronic kidney disease: implications for cardiovascular health and ageing in the general population. *Lancet Diabetes Endocrinol* **6**, 319-331, doi:10.1016/S2213-8587(17)30310-8 (2018).

49 Ball, A. M. *et al.* Risk of hip fracture among dialysis and renal transplant recipients. *JAMA* **288**, 3014-3018, doi:10.1001/jama.288.23.3014 (2002).

50 Farhat, G. N. *et al.* Volumetric BMD and vascular calcification in middle-aged women: the Study of Women's Health Across the Nation. *Journal of bone and mineral research : the official journal of the American Society for Bone and Mineral Research* **21**, 1839-1846, doi:10.1359/jbmr.060903 (2006).

51 London, G. M. *et al.* Association of bone activity, calcium load, aortic stiffness, and calcifications in ESRD. *J Am Soc Nephrol* **19**, 1827-1835, doi:10.1681/ASN.2007050622 (2008).

52 Shanahan, C. M. *et al.* Medial localization of mineralization-regulating proteins in association with Monckeberg's sclerosis: evidence for smooth muscle cell-mediated vascular calcification. *Circulation* **100**, 2168-2176 (1999).

53 Ritter, C. S. & Slatopolsky, E. Phosphate Toxicity in CKD: The Killer among Us. *Clin J Am Soc Nephrol* **11**, 1088-1100, doi:10.2215/CJN.11901115 (2016).

54 Mar Papa Daouda, E. K. B., Perez-Castiñeira Jose Roman, Serrano Delgado Aurelio, Soukri Abdelaziz. Inorganic Pyrophosphatases: Study of Interest. *Advances in Bioscience and Biotechnology* **08**, 388-397, doi:10.4236/abb.2017.810028 (2017).

55 Kellum, J. A. Determinants of blood pH in health and disease. *Crit Care* **4**, 6-14, doi:10.1186/cc644 (2000).
56 Block, G. A., Hulbert-Shearon, T. E., Levin, N. W. & Port, F. K. Association of serum phosphorus and calcium x phosphate product with mortality risk in chronic hemodialysis patients: a national study. *American journal of kidney diseases : the official journal of the National Kidney Foundation* **31**, 607-617 (1998).
57 McGovern, A. P. *et al.* Serum phosphate as a risk factor for cardiovascular events in people with and without chronic kidney disease: a large community based cohort study. *PLoS One* **8**, e74996, doi:10.1371/journal.pone.0074996 (2013).
58 Adeney, K. L. *et al.* Association of serum phosphate with vascular and valvular calcification in moderate CKD. *J Am Soc Nephrol* **20**, 381-387, doi:10.1681/ASN.2008040349 (2009).
59 Razzaque, M. S. Phosphate toxicity and vascular mineralization. *Contrib Nephrol* **180**, 74-85, doi:10.1159/000346784 (2013).
60 Shroff, R. C. *et al.* Chronic mineral dysregulation promotes vascular smooth muscle cell adaptation and extracellular matrix calcification. *J Am Soc Nephrol* **21**, 103-112, doi:10.1681/ASN.2009060640 (2010).
61 El-Abbadi, M. M. *et al.* Phosphate feeding induces arterial medial calcification in uremic mice: role of serum phosphorus, fibroblast growth factor-23, and osteopontin. *Kidney international* **75**, 1297-1307, doi:10.1038/ki.2009.83 (2009).
62 Lau, W. L., Festing, M. H. & Giachelli, C. M. Phosphate and vascular calcification: Emerging role of the sodium-dependent phosphate co-transporter PiT-1. *Thromb Haemost* **104**, 464-470, doi:10.1160/TH09-12-0814 (2010).
63 Chertow, G. M., Burke, S. K., Raggi, P. & Treat to Goal Working, G. Sevelamer attenuates the progression of coronary and aortic calcification in hemodialysis patients. *Kidney international* **62**, 245-252, doi:10.1046/j.1523-1755.2002.00434.x (2002).
64 Russo, D. *et al.* The progression of coronary artery calcification in predialysis patients on calcium carbonate or sevelamer. *Kidney international* **72**, 1255-1261, doi:10.1038/sj.ki.5002518 (2007).
65 Steitz, S. A. *et al.* Smooth muscle cell phenotypic transition associated with calcification: upregulation of Cbfa1 and downregulation of smooth muscle lineage markers. *Circulation research* **89**, 1147-1154 (2001).
66 Long, J. Z. *et al.* A smooth muscle-like origin for beige adipocytes. *Cell Metab* **19**, 810-820, doi:10.1016/j.cmet.2014.03.025 (2014).
67 Nguyen, A. T. *et al.* Smooth muscle cell plasticity: fact or fiction? *Circulation research* **112**, 17-22, doi:10.1161/CIRCRESAHA.112.281048 (2013).
68 Rutsch, F., Nitschke, Y. & Terkeltaub, R. Genetics in arterial calcification: pieces of a puzzle and cogs in a wheel. *Circulation research* **109**, 578-592, doi:10.1161/CIRCRESAHA.111.247965 (2011).
69 Li, X., Yang, H. Y. & Giachelli, C. M. Role of the sodium-dependent phosphate cotransporter, Pit-1, in vascular smooth muscle cell calcification. *Circulation research* **98**, 905-912, doi:10.1161/01.RES.0000216409.20863.e7 (2006).

70 O'Donnell, C. J. *et al.* Evidence for heritability of abdominal aortic calcific deposits in the Framingham Heart Study. *Circulation* **106**, 337-341, doi:10.1161/01.cir.0000022663.26468.5b (2002).
71 Peyser, P. A. *et al.* Heritability of coronary artery calcium quantity measured by electron beam computed tomography in asymptomatic adults. *Circulation* **106**, 304-308, doi:10.1161/01.cir.0000022664.21832.5d (2002).
72 Herrmann, S. M. *et al.* Polymorphisms of the human matrix gla protein (MGP) gene, vascular calcification, and myocardial infarction. *Arteriosclerosis, thrombosis, and vascular biology* **20**, 2386-2393, doi:10.1161/01.atv.20.11.2386 (2000).
73 Munroe, P. B. *et al.* Mutations in the gene encoding the human matrix Gla protein cause Keutel syndrome. *Nat Genet* **21**, 142-144, doi:10.1038/5102 (1999).
74 Luo, G. *et al.* Spontaneous calcification of arteries and cartilage in mice lacking matrix GLA protein. *Nature* **386**, 78-81, doi:10.1038/386078a0 (1997).
75 Yao, Y. *et al.* Inhibition of bone morphogenetic proteins protects against atherosclerosis and vascular calcification. *Circulation research* **107**, 485-494, doi:10.1161/CIRCRESAHA.110.219071 (2010).
76 Price, P. A., Faus, S. A. & Williamson, M. K. Warfarin causes rapid calcification of the elastic lamellae in rat arteries and heart valves. *Arteriosclerosis, thrombosis, and vascular biology* **18**, 1400-1407, doi:10.1161/01.atv.18.9.1400 (1998).
77 Teichert, M. *et al.* Vitamin K epoxide reductase complex subunit 1 (VKORC1) polymorphism and aortic calcification: the Rotterdam Study. *Arteriosclerosis, thrombosis, and vascular biology* **28**, 771-776, doi:10.1161/ATVBAHA.107.159913 (2008).
78 Ohmori, R. *et al.* Plasma osteopontin levels are associated with the presence and extent of coronary artery disease. *Atherosclerosis* **170**, 333-337, doi:10.1016/s0021-9150(03)00298-3 (2003).
79 Steitz, S. A. *et al.* Osteopontin inhibits mineral deposition and promotes regression of ectopic calcification. *The American journal of pathology* **161**, 2035-2046, doi:10.1016/S0002-9440(10)64482-3 (2002).
80 Heiss, A. *et al.* Structural basis of calcification inhibition by alpha 2-HS glycoprotein/fetuin-A. Formation of colloidal calciprotein particles. *J Biol Chem* **278**, 13333-13341, doi:10.1074/jbc.M210868200 (2003).
81 Osawa, M., Tian, W., Horiuchi, H., Kaneko, M. & Umetsu, K. Association of alpha2-HS glycoprotein (AHSG, fetuin-A) polymorphism with AHSG and phosphate serum levels. *Hum Genet* **116**, 146-151, doi:10.1007/s00439-004-1222-7 (2005).
82 Jung, J. Y. *et al.* Association of AHSG gene polymorphisms and aortic stiffness in peritoneal dialysis patients. *Am J Nephrol* **31**, 510-517, doi:10.1159/000309789 (2010).
83 Andersen, G. *et al.* AHSG tag single nucleotide polymorphisms associate with type 2 diabetes and dyslipidemia: studies of metabolic traits in 7,683 white Danish subjects. *Diabetes* **57**, 1427-1432, doi:10.2337/db07-0558 (2008).

84 Stenvinkel, P. *et al.* Low fetuin-A levels are associated with cardiovascular death: Impact of variations in the gene encoding fetuin. *Kidney international* **67**, 2383-2392, doi:10.1111/j.1523-1755.2005.00345.x (2005).
85 Lehtinen, A. B. *et al.* Association of alpha2-Heremans-Schmid glycoprotein polymorphisms with subclinical atherosclerosis. *J Clin Endocrinol Metab* **92**, 345-352, doi:10.1210/jc.2006-0429 (2007).
86 Schafer, C. *et al.* The serum protein alpha 2-Heremans-Schmid glycoprotein/fetuin-A is a systemically acting inhibitor of ectopic calcification. *J Clin Invest* **112**, 357-366, doi:10.1172/JCI17202 (2003).
87 Roberts, F., Zhu, D., Farquharson, C. & Macrae, V. E. ENPP1 in the Regulation of Mineralization and Beyond. *Trends Biochem Sci* **44**, 616-628, doi:10.1016/j.tibs.2019.01.010 (2019).
88 Eller, P. *et al.* Impact of ENPP1 genotype on arterial calcification in patients with end-stage renal failure. *Nephrol Dial Transplant* **23**, 321-327, doi:10.1093/ndt/gfm566 (2008).
89 Johnson, K., Polewski, M., van Etten, D. & Terkeltaub, R. Chondrogenesis mediated by PPi depletion promotes spontaneous aortic calcification in NPP1-/- mice. *Arteriosclerosis, thrombosis, and vascular biology* **25**, 686-691, doi:10.1161/01.ATV.0000154774.71187.f0 (2005).
90 Ho, A. M., Johnson, M. D. & Kingsley, D. M. Role of the mouse ank gene in control of tissue calcification and arthritis. *Science* **289**, 265-270, doi:10.1126/science.289.5477.265 (2000).
91 St Hilaire, C. *et al.* NT5E mutations and arterial calcifications. *N Engl J Med* **364**, 432-442, doi:10.1056/NEJMoa0912923 (2011).
92 Favre, G. *et al.* The ABCC6 Transporter: A New Player in Biomineralization. *Int J Mol Sci* **18**, doi:10.3390/ijms18091941 (2017).
93 Wassel, C. L. *et al.* Associations of SNPs in ADIPOQ and subclinical cardiovascular disease in the multi-ethnic study of atherosclerosis (MESA). *Obesity (Silver Spring)* **19**, 840-847, doi:10.1038/oby.2010.229 (2011).
94 Xu, Y. & Sun, Z. Molecular basis of Klotho: from gene to function in aging. *Endocr Rev* **36**, 174-193, doi:10.1210/er.2013-1079 (2015).
95 Roth, D. E., Venta, P. J., Tashian, R. E. & Sly, W. S. Molecular basis of human carbonic anhydrase II deficiency. *Proc Natl Acad Sci U S A* **89**, 1804-1808, doi:10.1073/pnas.89.5.1804 (1992).
96 Luo, X. H. *et al.* Development of arterial calcification in adiponectin-deficient mice: adiponectin regulates arterial calcification. *Journal of bone and mineral research : the official journal of the American Society for Bone and Mineral Research* **24**, 1461-1468, doi:10.1359/jbmr.090227 (2009).
97 Sly, W. S. *et al.* Carbonic anhydrase II deficiency in 12 families with the autosomal recessive syndrome of osteopetrosis with renal tubular acidosis and cerebral calcification. *N Engl J Med* **313**, 139-145, doi:10.1056/NEJM198507183130302 (1985).

98 Spicer, S. S., Lewis, S. E., Tashian, R. E. & Schulte, B. A. Mice carrying a CAR-2 null allele lack carbonic anhydrase II immunohistochemically and show vascular calcification. *The American journal of pathology* **134**, 947-954 (1989).

99 Wu, M., Chen, G. & Li, Y. P. TGF-beta and BMP signaling in osteoblast, skeletal development, and bone formation, homeostasis and disease. *Bone Res* **4**, 16009, doi:10.1038/boneres.2016.9 (2016).

100 Galvin, K. M. *et al.* A role for smad6 in development and homeostasis of the cardiovascular system. *Nat Genet* **24**, 171-174, doi:10.1038/72835 (2000).

101 Dorai, H., Vukicevic, S. & Sampath, T. K. Bone morphogenetic protein-7 (osteogenic protein-1) inhibits smooth muscle cell proliferation and stimulates the expression of markers that are characteristic of SMC phenotype in vitro. *J Cell Physiol* **184**, 37-45, doi:10.1002/(SICI)1097-4652(200007)184:1<37::AID-JCP4>3.0.CO;2-M (2000).

102 Freedman, B. I. *et al.* Bone morphogenetic protein 7 (BMP7) gene polymorphisms are associated with inverse relationships between vascular calcification and BMD: the Diabetes Heart Study. *Journal of bone and mineral research : the official journal of the American Society for Bone and Mineral Research* **24**, 1719-1727, doi:10.1359/jbmr.090501 (2009).

103 Speer, M. Y. *et al.* Smooth muscle cells give rise to osteochondrogenic precursors and chondrocytes in calcifying arteries. *Circulation research* **104**, 733-741, doi:10.1161/CIRCRESAHA.108.183053 (2009).

104 Tyson, K. L. *et al.* Osteo/chondrocytic transcription factors and their target genes exhibit distinct patterns of expression in human arterial calcification. *Arteriosclerosis, thrombosis, and vascular biology* **23**, 489-494, doi:10.1161/01.ATV.0000059406.92165.31 (2003).

105 Graciolli, F. G. *et al.* Phosphorus overload and PTH induce aortic expression of Runx2 in experimental uraemia. *Nephrol Dial Transplant* **24**, 1416-1421, doi:10.1093/ndt/gfn686 (2009).

106 Byon, C. H. *et al.* Oxidative stress induces vascular calcification through modulation of the osteogenic transcription factor Runx2 by AKT signaling. *J Biol Chem* **283**, 15319-15327, doi:10.1074/jbc.M800021200 (2008).

107 Zhang, X. *et al.* Runx2 overexpression enhances osteoblastic differentiation and mineralization in adipose--derived stem cells in vitro and in vivo. *Calcified tissue international* **79**, 169-178, doi:10.1007/s00223-006-0083-6 (2006).

108 Lin, M. E., Chen, T., Leaf, E. M., Speer, M. Y. & Giachelli, C. M. Runx2 Expression in Smooth Muscle Cells Is Required for Arterial Medial Calcification in Mice. *The American journal of pathology* **185**, 1958-1969, doi:10.1016/j.ajpath.2015.03.020 (2015).

109 Lin, M. E. *et al.* Runx2 deletion in smooth muscle cells inhibits vascular osteochondrogenesis and calcification but not atherosclerotic lesion formation. *Cardiovasc Res* **112**, 606-616, doi:10.1093/cvr/cvw205 (2016).

110 Sun, Y. *et al.* Smooth muscle cell-specific runx2 deficiency inhibits vascular calcification. *Circulation research* **111**, 543-552, doi:10.1161/CIRCRESAHA.112.267237 (2012).

111 D'Souza, D. R. *et al.* Hyperglycemia regulates RUNX2 activation and cellular wound healing through the aldose reductase polyol pathway. *J Biol Chem* **284**, 17947-17955, doi:10.1074/jbc.M109.002378 (2009).

112 Patidar, A., Singh, D. K., Thakur, S., Farrington, K. & Baydoun, A. R. Uremic serum-induced calcification of human aortic smooth muscle cells is a regulated process involving Klotho and RUNX2. *Biosci Rep* **39**, doi:10.1042/BSR20190599 (2019).

113 Giachelli, C. M. The emerging role of phosphate in vascular calcification. *Kidney international* **75**, 890-897, doi:10.1038/ki.2008.644 (2009).

114 Platko, K. *et al.* TDAG51 (T-Cell Death-Associated Gene 51) Is a Key Modulator of Vascular Calcification and Osteogenic Transdifferentiation of Arterial Smooth Muscle Cells. *Arteriosclerosis, thrombosis, and vascular biology* **40**, 1664-1679, doi:10.1161/ATVBAHA.119.313779 (2020).

115 Koleganova, N. *et al.* Arterial calcification in patients with chronic kidney disease. *Nephrol Dial Transplant* **24**, 2488-2496, doi:10.1093/ndt/gfp137 (2009).

116 Yang, H., Curinga, G. & Giachelli, C. M. Elevated extracellular calcium levels induce smooth muscle cell matrix mineralization in vitro. *Kidney international* **66**, 2293-2299, doi:10.1111/j.1523-1755.2004.66015.x (2004).

117 Li, X., Yang, H. Y. & Giachelli, C. M. BMP-2 promotes phosphate uptake, phenotypic modulation, and calcification of human vascular smooth muscle cells. *Atherosclerosis* **199**, 271-277, doi:10.1016/j.atherosclerosis.2007.11.031 (2008).

118 Yang, Y. *et al.* AKT-independent activation of p38 MAP kinase promotes vascular calcification. *Redox Biol* **16**, 97-103, doi:10.1016/j.redox.2018.02.009 (2018).

119 Fujita, T. *et al.* Phosphate provides an extracellular signal that drives nuclear export of Runx2/Cbfa1 in bone cells. *Biochem Biophys Res Commun* **280**, 348-352, doi:10.1006/bbrc.2000.4108 (2001).

120 Ge, C. *et al.* Reciprocal Control of Osteogenic and Adipogenic Differentiation by ERK/MAP Kinase Phosphorylation of Runx2 and PPARgamma Transcription Factors. *J Cell Physiol* **231**, 587-596, doi:10.1002/jcp.25102 (2016).

121 Moerman, E. J., Teng, K., Lipschitz, D. A. & Lecka-Czernik, B. Aging activates adipogenic and suppresses osteogenic programs in mesenchymal marrow stroma/stem cells: the role of PPAR-gamma2 transcription factor and TGF-beta/BMP signaling pathways. *Aging Cell* **3**, 379-389, doi:10.1111/j.1474-9728.2004.00127.x (2004).

122 Jaiswal, R. K. *et al.* Adult human mesenchymal stem cell differentiation to the osteogenic or adipogenic lineage is regulated by mitogen-activated protein kinase. *J Biol Chem* **275**, 9645-9652, doi:10.1074/jbc.275.13.9645 (2000).

123 Sun, H. *et al.* Osteoblast-targeted suppression of PPARgamma increases osteogenesis through activation of mTOR signaling. *Stem Cells* **31**, 2183-2192, doi:10.1002/stem.1455 (2013).

124 Cao, J. *et al.* Impact of targeted PPARgamma disruption on bone remodeling. *Mol Cell Endocrinol* **410**, 27-34, doi:10.1016/j.mce.2015.01.045 (2015).

125 Nuttall, M. E. *et al.* Adipocytes and the regulation of bone remodeling: a balancing act. *Calcified tissue international* **94**, 78-87, doi:10.1007/s00223-013-9807-6 (2014).
126 Woldt, E. *et al.* The nuclear hormone receptor PPARgamma counteracts vascular calcification by inhibiting Wnt5a signalling in vascular smooth muscle cells. *Nature communications* **3**, 1077, doi:10.1038/ncomms2087 (2012).
127 Liu, L. *et al.* High phosphate-induced downregulation of PPARgamma contributes to CKD-associated vascular calcification. *J Mol Cell Cardiol* **114**, 264-275, doi:10.1016/j.yjmcc.2017.11.021 (2018).
128 Proudfoot, D. *et al.* Apoptosis regulates human vascular calcification in vitro: evidence for initiation of vascular calcification by apoptotic bodies. *Circulation research* **87**, 1055-1062, doi:10.1161/01.res.87.11.1055 (2000).
129 Reynolds, J. L. *et al.* Human vascular smooth muscle cells undergo vesicle-mediated calcification in response to changes in extracellular calcium and phosphate concentrations: a potential mechanism for accelerated vascular calcification in ESRD. *J Am Soc Nephrol* **15**, 2857-2867, doi:10.1097/01.ASN.0000141960.01035.28 (2004).
130 Shroff, R. C. *et al.* Dialysis accelerates medial vascular calcification in part by triggering smooth muscle cell apoptosis. *Circulation* **118**, 1748-1757, doi:10.1161/CIRCULATIONAHA.108.783738 (2008).
131 Dong, Y. *et al.* Role of endoplasmic reticulum stress signalling in diabetic endothelial dysfunction and atherosclerosis. *Diab Vasc Dis Res* **14**, 14-23, doi:10.1177/1479164116666762 (2017).
132 Shanahan, C. M. & Furmanik, M. Endoplasmic Reticulum Stress in Arterial Smooth Muscle Cells: A Novel Regulator of Vascular Disease. *Curr Cardiol Rev* **13**, 94-105, doi:10.2174/1573403X12666161014094738 (2017).
133 Masuda, M., Miyazaki-Anzai, S., Levi, M., Ting, T. C. & Miyazaki, M. PERK-eIF2alpha-ATF4-CHOP signaling contributes to TNFalpha-induced vascular calcification. *J Am Heart Assoc* **2**, e000238, doi:10.1161/JAHA.113.000238 (2013).
134 Miyazaki-Anzai, S. *et al.* Endoplasmic reticulum stress effector CCAAT/enhancer-binding protein homologous protein (CHOP) regulates chronic kidney disease-induced vascular calcification. *J Am Heart Assoc* **3**, e000949, doi:10.1161/JAHA.114.000949 (2014).
135 Muller, K. H. *et al.* Poly(ADP-Ribose) Links the DNA Damage Response and Biomineralization. *Cell Rep* **27**, 3124-3138 e3113, doi:10.1016/j.celrep.2019.05.038 (2019).
136 Chow, W. Y. *et al.* NMR spectroscopy of native and in vitro tissues implicates polyADP ribose in biomineralization. *Science* **344**, 742-746, doi:10.1126/science.1248167 (2014).
137 Wang, C. *et al.* Poly(ADP-ribose) polymerase 1 accelerates vascular calcification by upregulating Runx2. *Nature communications* **10**, 1203, doi:10.1038/s41467-019-09174-1 (2019).

138 Fuselier, T. T. & Lu, H. PHLD Class Proteins: A Family of New Players in the p53 Network. *Int J Mol Sci* **21**, doi:10.3390/ijms21103543 (2020).
139 Lemmon, M. A., Ferguson, K. M. & Abrams, C. S. Pleckstrin homology domains and the cytoskeleton. *FEBS Lett* **513**, 71-76, doi:10.1016/s0014-5793(01)03243-4 (2002).
140 Lemmon, M. A. & Ferguson, K. M. Signal-dependent membrane targeting by pleckstrin homology (PH) domains. *Biochem J* **350 Pt 1**, 1-18 (2000).
141 Chae Gyu Park, S. Y. L., Gokul Kandala, Sang Yull Lee, Yongwon Choi. A novel gene product that couples TCR Signaling to Fas(CD95) expression in activation-induced cell death. *Immunity* **4**, 583-591 (1996).
142 Neef, R., Kuske, M. A., Prols, E. & Johnson, J. P. Identification of the human PHLDA1/TDAG51 gene: down-regulation in metastatic melanoma contributes to apoptosis resistance and growth deregulation. *Cancer Res* **62**, 5920-5929 (2002).
143 Nagai, M. A. Pleckstrin homology-like domain, family A, member 1 (PHLDA1) and cancer. *Biomed Rep* **4**, 275-281, doi:10.3892/br.2016.580 (2016).
144 Hayashida, N. *et al.* A novel HSF1-mediated death pathway that is suppressed by heat shock proteins. *EMBO J* **25**, 4773-4783, doi:10.1038/sj.emboj.7601370 (2006).
145 Basseri, S. *et al.* Loss of TDAG51 results in mature-onset obesity, hepatic steatosis, and insulin resistance by regulating lipogenesis. *Diabetes* **62**, 158-169, doi:10.2337/db12-0256 (2013).
146 Kastrati, I., Canestrari, E. & Frasor, J. PHLDA1 expression is controlled by an estrogen receptor-NFkappaB-miR-181 regulatory loop and is essential for formation of ER+ mammospheres. *Oncogene* **34**, 2309-2316, doi:10.1038/onc.2014.180 (2015).
147 Toyoshima, Y. *et al.* TDAG51 mediates the effects of insulin-like growth factor I (IGF-I) on cell survival. *J Biol Chem* **279**, 25898-25904, doi:10.1074/jbc.M400661200 (2004).
148 Coutinho-Camillo, C. M. *et al.* Expression of PAR-4 and PHLDA1 is prognostic for overall and disease-free survival in oral squamous cell carcinomas. *Virchows Arch* **463**, 31-39, doi:10.1007/s00428-013-1438-9 (2013).
149 Li, G., Wang, X., Hibshoosh, H., Jin, C. & Halmos, B. Modulation of ErbB2 blockade in ErbB2-positive cancers: the role of ErbB2 Mutations and PHLDA1. *PLoS One* **9**, e106349, doi:10.1371/journal.pone.0106349 (2014).
150 Nagai, M. A., Fregnani, J. H., Netto, M. M., Brentani, M. M. & Soares, F. A. Down-regulation of PHLDA1 gene expression is associated with breast cancer progression. *Breast Cancer Res Treat* **106**, 49-56, doi:10.1007/s10549-006-9475-6 (2007).
151 Gomes, I., Xiong, W., Miki, T. & Rosner, M. R. A proline- and glutamine-rich protein promotes apoptosis in neuronal cells. *J Neurochem* **73**, 612-622 (1999).
152 Hossain, G. S. *et al.* Deficiency of TDAG51 protects against atherosclerosis by modulating apoptosis, cholesterol efflux, and peroxiredoxin-1 expression. *J Am Heart Assoc* **2**, e000134, doi:10.1161/JAHA.113.000134 (2013).

153 Carlisle, R. E. *et al.* TDAG51 mediates epithelial-to-mesenchymal transition in human proximal tubular epithelium. *Am J Physiol Renal Physiol* **303**, F467-481, doi:10.1152/ajprenal.00481.2011 (2012).
154 Morikawa, M., Derynck, R. & Miyazono, K. TGF-beta and the TGF-beta Family: Context-Dependent Roles in Cell and Tissue Physiology. *Cold Spring Harb Perspect Biol* **8**, doi:10.1101/cshperspect.a021873 (2016).
155 Massague, J. TGFbeta signalling in context. *Nat Rev Mol Cell Biol* **13**, 616-630, doi:10.1038/nrm3434 (2012).
156 Heldin, C. H., Miyazono, K. & ten Dijke, P. TGF-beta signalling from cell membrane to nucleus through SMAD proteins. *Nature* **390**, 465-471, doi:10.1038/37284 (1997).
157 Constam, D. B. Regulation of TGFbeta and related signals by precursor processing. *Semin Cell Dev Biol* **32**, 85-97, doi:10.1016/j.semcdb.2014.01.008 (2014).
158 Heldin, C. H. & Moustakas, A. Role of Smads in TGFbeta signaling. *Cell Tissue Res* **347**, 21-36, doi:10.1007/s00441-011-1190-x (2012).
159 Pardali, E. & Ten Dijke, P. TGFbeta signaling and cardiovascular diseases. *Int J Biol Sci* **8**, 195-213, doi:10.7150/ijbs.3805 (2012).
160 Oshima, M., Oshima, H. & Taketo, M. M. TGF-beta receptor type II deficiency results in defects of yolk sac hematopoiesis and vasculogenesis. *Dev Biol* **179**, 297-302, doi:10.1006/dbio.1996.0259 (1996).
161 West, J. *et al.* Pulmonary hypertension in transgenic mice expressing a dominant-negative BMPRII gene in smooth muscle. *Circulation research* **94**, 1109-1114, doi:10.1161/01.RES.0000126047.82846.20 (2004).
162 Lijnen, P. J., Petrov, V. V. & Fagard, R. H. Association between transforming growth factor-beta and hypertension. *Am J Hypertens* **16**, 604-611, doi:10.1016/s0895-7061(03)00847-1 (2003).
163 Cogan, J. D. *et al.* Gross BMPR2 gene rearrangements constitute a new cause for primary pulmonary hypertension. *Genet Med* **7**, 169-174, doi:10.1097/01.gim.0000156525.09595.e9 (2005).
164 Bobik, A. *et al.* Distinct patterns of transforming growth factor-beta isoform and receptor expression in human atherosclerotic lesions. Colocalization implicates TGF-beta in fibrofatty lesion development. *Circulation* **99**, 2883-2891, doi:10.1161/01.cir.99.22.2883 (1999).
165 Kalinina, N. *et al.* Smad expression in human atherosclerotic lesions: evidence for impaired TGF-beta/Smad signaling in smooth muscle cells of fibrofatty lesions. *Arteriosclerosis, thrombosis, and vascular biology* **24**, 1391-1396, doi:10.1161/01.ATV.0000133605.89421.79 (2004).
166 Stary, H. C. *et al.* A definition of advanced types of atherosclerotic lesions and a histological classification of atherosclerosis. A report from the Committee on Vascular Lesions of the Council on Arteriosclerosis, American Heart Association. *Circulation* **92**, 1355-1374, doi:10.1161/01.cir.92.5.1355 (1995).
167 Shao, J. S., Cai, J. & Towler, D. A. Molecular mechanisms of vascular calcification: lessons learned from the aorta. *Arteriosclerosis, thrombosis, and*

vascular biology **26**, 1423-1430, doi:10.1161/01.ATV.0000220441.42041.20 (2006).

168 Balderman, J. A. *et al.* Bone morphogenetic protein-2 decreases microRNA-30b and microRNA-30c to promote vascular smooth muscle cell calcification. *J Am Heart Assoc* **1**, e003905, doi:10.1161/JAHA.112.003905 (2012).

169 Liberman, M., Johnson, R. C., Handy, D. E., Loscalzo, J. & Leopold, J. A. Bone morphogenetic protein-2 activates NADPH oxidase to increase endoplasmic reticulum stress and human coronary artery smooth muscle cell calcification. *Biochem Biophys Res Commun* **413**, 436-441, doi:10.1016/j.bbrc.2011.08.114 (2011).

170 Liu, T. *et al.* BMP-2 promotes differentiation of osteoblasts and chondroblasts in Runx2-deficient cell lines. *J Cell Physiol* **211**, 728-735, doi:10.1002/jcp.20988 (2007).

171 Wei, X. *et al.* Bone Morphogenetic Proteins 2/4 Are Upregulated during the Early Development of Vascular Calcification in Chronic Kidney Disease. *Biomed Res Int* **2018**, 8371604, doi:10.1155/2018/8371604 (2018).

172 Daluiski, A. *et al.* Bone morphogenetic protein-3 is a negative regulator of bone density. *Nat Genet* **27**, 84-88, doi:10.1038/83810 (2001).

173 Gamer, L. W., Cox, K., Carlo, J. M. & Rosen, V. Overexpression of BMP3 in the developing skeleton alters endochondral bone formation resulting in spontaneous rib fractures. *Dev Dyn* **238**, 2374-2381, doi:10.1002/dvdy.22048 (2009).

174 Takao, M. *et al.* Identification of rat bone morphogenetic protein-3b (BMP-3b), a new member of BMP-3. *Biochem Biophys Res Commun* **219**, 656-662, doi:10.1006/bbrc.1996.0289 (1996).

175 Upadhyay, G. *et al.* Stem cell antigen-1 enhances tumorigenicity by disruption of growth differentiation factor-10 (GDF10)-dependent TGF-beta signaling. *Proc Natl Acad Sci U S A* **108**, 7820-7825, doi:10.1073/pnas.1103441108 (2011).

176 Hino, J., Matsuo, H. & Kangawa, K. Bone morphogenetic protein-3b (BMP-3b) gene expression is correlated with differentiation in rat calvarial osteoblasts. *Biochem Biophys Res Commun* **256**, 419-424, doi:10.1006/bbrc.1999.0341 (1999).

177 Matsumoto, Y. *et al.* Bone morphogenetic protein-3b (BMP-3b) inhibits osteoblast differentiation via Smad2/3 pathway by counteracting Smad1/5/8 signaling. *Mol Cell Endocrinol* **350**, 78-86, doi:10.1016/j.mce.2011.11.023 (2012).

178 Hino, J., Kangawa, K., Matsuo, H., Nohno, T. & Nishimatsu, S. Bone morphogenetic protein-3 family members and their biological functions. *Front Biosci* **9**, 1520-1529, doi:10.2741/1355 (2004).

179 Lichtman, M. K., Otero-Vinas, M. & Falanga, V. Transforming growth factor beta (TGF-beta) isoforms in wound healing and fibrosis. *Wound Repair Regen* **24**, 215-222, doi:10.1111/wrr.12398 (2016).

180 Dituri, F., Cossu, C., Mancarella, S. & Giannelli, G. The Interactivity between TGFbeta and BMP Signaling in Organogenesis, Fibrosis, and Cancer. *Cells* **8**, doi:10.3390/cells8101130 (2019).

181 Roberts, A. B. *et al.* Transforming growth factor type beta: rapid induction of fibrosis and angiogenesis in vivo and stimulation of collagen formation in vitro. *Proc Natl Acad Sci U S A* **83**, 4167-4171, doi:10.1073/pnas.83.12.4167 (1986).

182 Sime, P. J., Xing, Z., Graham, F. L., Csaky, K. G. & Gauldie, J. Adenovector-mediated gene transfer of active transforming growth factor-beta1 induces prolonged severe fibrosis in rat lung. *J Clin Invest* **100**, 768-776, doi:10.1172/JCI119590 (1997).

183 Yang, L. *et al.* Transforming growth factor beta signaling in hepatocytes participates in steatohepatitis through regulation of cell death and lipid metabolism in mice. *Hepatology* **59**, 483-495, doi:10.1002/hep.26698 (2014).

184 George, J., Roulot, D., Koteliansky, V. E. & Bissell, D. M. In vivo inhibition of rat stellate cell activation by soluble transforming growth factor beta type II receptor: a potential new therapy for hepatic fibrosis. *Proc Natl Acad Sci U S A* **96**, 12719-12724, doi:10.1073/pnas.96.22.12719 (1999).

185 Zhao, J. *et al.* Smad3 deficiency attenuates bleomycin-induced pulmonary fibrosis in mice. *Am J Physiol Lung Cell Mol Physiol* **282**, L585-593, doi:10.1152/ajplung.00151.2001 (2002).

186 Sato, M., Muragaki, Y., Saika, S., Roberts, A. B. & Ooshima, A. Targeted disruption of TGF-beta1/Smad3 signaling protects against renal tubulointerstitial fibrosis induced by unilateral ureteral obstruction. *J Clin Invest* **112**, 1486-1494, doi:10.1172/JCI19270 (2003).

187 Li, P. *et al.* Targeting secreted cytokine BMP9 gates the attenuation of hepatic fibrosis. *Biochim Biophys Acta Mol Basis Dis* **1864**, 709-720, doi:10.1016/j.bbadis.2017.12.008 (2018).

188 Desroches-Castan, A. *et al.* Bone Morphogenetic Protein 9 Is a Paracrine Factor Controlling Liver Sinusoidal Endothelial Cell Fenestration and Protecting Against Hepatic Fibrosis. *Hepatology* **70**, 1392-1408, doi:10.1002/hep.30655 (2019).

189 Vukicevic, S. *et al.* Osteogenic protein-1 (bone morphogenetic protein-7) reduces severity of injury after ischemic acute renal failure in rat. *J Clin Invest* **102**, 202-214, doi:10.1172/JCI2237 (1998).

190 Gravesen, E. *et al.* Exogenous BMP7 in aortae of rats with chronic uremia ameliorates expression of profibrotic genes, but does not reverse established vascular calcification. *PLoS One* **13**, e0190820, doi:10.1371/journal.pone.0190820 (2018).

191 Hsiao, E. C. *et al.* Characterization of growth-differentiation factor 15, a transforming growth factor beta superfamily member induced following liver injury. *Mol Cell Biol* **20**, 3742-3751, doi:10.1128/mcb.20.10.3742-3751.2000 (2000).

192 Zhang, Y. *et al.* Over-expression of growth differentiation factor 15 (GDF15) preventing cold ischemia reperfusion (I/R) injury in heart transplantation through Foxo3a signaling. *Oncotarget* **8**, 36531-36544, doi:10.18632/oncotarget.16607 (2017).

193 Hassanpour Golakani, M. *et al.* MIC-1/GDF15 Overexpression Is Associated with Increased Functional Recovery in Traumatic Spinal Cord Injury. *J Neurotrauma* **36**, 3410-3421, doi:10.1089/neu.2019.6421 (2019).
194 Li, S. *et al.* GDF10 is a signal for axonal sprouting and functional recovery after stroke. *Nat Neurosci* **18**, 1737-1745, doi:10.1038/nn.4146 (2015).
195 Platko, K. *et al.* GDF10 blocks hepatic PPARgamma activation to protect against diet-induced liver injury. *Mol Metab* **27**, 62-74, doi:10.1016/j.molmet.2019.06.021 (2019).
196 Hino, J. *et al.* Overexpression of bone morphogenetic protein-3b (BMP-3b) in adipose tissues protects against high-fat diet-induced obesity. *Int J Obes (Lond)* **41**, 483-488, doi:10.1038/ijo.2017.15 (2017).
197 Hirt-Burri, N., Scaletta, C., Gerber, S., Pioletti, D. P. & Applegate, L. A. Wound-healing gene family expression differences between fetal and foreskin cells used for bioengineered skin substitutes. *Artif Organs* **32**, 509-518, doi:10.1111/j.1525-1594.2008.00578.x (2008).
198 Fischer, K. D. & Agrawal, D. K. Vitamin D regulating TGF-beta induced epithelial-mesenchymal transition. *Respir Res* **15**, 146, doi:10.1186/s12931-014-0146-6 (2014).
199 Ding, N. *et al.* A vitamin D receptor/SMAD genomic circuit gates hepatic fibrotic response. *Cell* **153**, 601-613, doi:10.1016/j.cell.2013.03.028 (2013).
200 Sun, K., Wang, Q. & Huang, X. H. PPAR gamma inhibits growth of rat hepatic stellate cells and TGF beta-induced connective tissue growth factor expression. *Acta Pharmacol Sin* **27**, 715-723, doi:10.1111/j.1745-7254.2006.00299.x (2006).
201 Burgess, H. A. *et al.* PPARgamma agonists inhibit TGF-beta induced pulmonary myofibroblast differentiation and collagen production: implications for therapy of lung fibrosis. *Am J Physiol Lung Cell Mol Physiol* **288**, L1146-1153, doi:10.1152/ajplung.00383.2004 (2005).
202 Zou, R. *et al.* PPARgamma agonists inhibit TGF-beta-PKA signaling in glomerulosclerosis. *Acta Pharmacol Sin* **31**, 43-50, doi:10.1038/aps.2009.174 (2010).
203 Hao, G. H., Niu, X. L., Gao, D. F., Wei, J. & Wang, N. P. Agonists at PPAR-gamma suppress angiotensin II-induced production of plasminogen activator inhibitor-1 and extracellular matrix in rat cardiac fibroblasts. *Br J Pharmacol* **153**, 1409-1419, doi:10.1038/bjp.2008.21 (2008).
204 Cunningham, N. S. *et al.* Growth/differentiation factor-10: a new member of the transforming growth factor-beta superfamily related to bone morphogenetic protein-3. *Growth Factors* **12**, 99-109, doi:10.3109/08977199509028956 (1995).
205 Hino, J. *et al.* Coordination of BMP-3b and cerberus is required for head formation of Xenopus embryos. *Dev Biol* **260**, 138-157, doi:10.1016/s0012-1606(03)00223-9 (2003).
206 Ripamonti, U., Crooks, J., Matsaba, T. & Tasker, J. Induction of endochondral bone formation by recombinant human transforming growth factor-beta2 in the baboon (Papio ursinus). *Growth Factors* **17**, 269-285, doi:10.3109/08977190009028971 (2000).

207 Hino, J., Miyazawa, T., Miyazato, M. & Kangawa, K. Bone morphogenetic protein-3b (BMP-3b) is expressed in adipocytes and inhibits adipogenesis as a unique complex. *Int J Obes (Lond)* **36**, 725-734, doi:10.1038/ijo.2011.124 (2012).
208 Berger, J. & Moller, D. E. The mechanisms of action of PPARs. *Annu Rev Med* **53**, 409-435, doi:10.1146/annurev.med.53.082901.104018 (2002).
209 Nolte, R. T. *et al.* Ligand binding and co-activator assembly of the peroxisome proliferator-activated receptor-gamma. *Nature* **395**, 137-143, doi:10.1038/25931 (1998).
210 Werman, A. *et al.* Ligand-independent activation domain in the N terminus of peroxisome proliferator-activated receptor gamma (PPARgamma). Differential activity of PPARgamma1 and -2 isoforms and influence of insulin. *J Biol Chem* **272**, 20230-20235, doi:10.1074/jbc.272.32.20230 (1997).
211 Gearing, K. L., Gottlicher, M., Teboul, M., Widmark, E. & Gustafsson, J. A. Interaction of the peroxisome-proliferator-activated receptor and retinoid X receptor. *Proc Natl Acad Sci U S A* **90**, 1440-1444, doi:10.1073/pnas.90.4.1440 (1993).
212 Burns, K. A. & Vanden Heuvel, J. P. Modulation of PPAR activity via phosphorylation. *Biochim Biophys Acta* **1771**, 952-960, doi:10.1016/j.bbalip.2007.04.018 (2007).
213 Grygiel-Gorniak, B. Peroxisome proliferator-activated receptors and their ligands: nutritional and clinical implications--a review. *Nutr J* **13**, 17, doi:10.1186/1475-2891-13-17 (2014).
214 Hamblin, M., Chang, L., Fan, Y., Zhang, J. & Chen, Y. E. PPARs and the cardiovascular system. *Antioxid Redox Signal* **11**, 1415-1452, doi:10.1089/ARS.2008.2280 (2009).
215 Farmer, S. R. Regulation of PPARgamma activity during adipogenesis. *Int J Obes (Lond)* **29 Suppl 1**, S13-16, doi:10.1038/sj.ijo.0802907 (2005).
216 Ahmadian, M. *et al.* PPARgamma signaling and metabolism: the good, the bad and the future. *Nat Med* **19**, 557-566, doi:10.1038/nm.3159 (2013).
217 Wang, F., Mullican, S. E., DiSpirito, J. R., Peed, L. C. & Lazar, M. A. Lipoatrophy and severe metabolic disturbance in mice with fat-specific deletion of PPARgamma. *Proc Natl Acad Sci U S A* **110**, 18656-18661, doi:10.1073/pnas.1314863110 (2013).
218 Gross, B., Pawlak, M., Lefebvre, P. & Staels, B. PPARs in obesity-induced T2DM, dyslipidaemia and NAFLD. *Nat Rev Endocrinol* **13**, 36-49, doi:10.1038/nrendo.2016.135 (2017).
219 Pettinelli, P. & Videla, L. A. Up-regulation of PPAR-gamma mRNA expression in the liver of obese patients: an additional reinforcing lipogenic mechanism to SREBP-1c induction. *J Clin Endocrinol Metab* **96**, 1424-1430, doi:10.1210/jc.2010-2129 (2011).
220 Matsusue, K. *et al.* Liver-specific disruption of PPARgamma in leptin-deficient mice improves fatty liver but aggravates diabetic phenotypes. *J Clin Invest* **111**, 737-747, doi:10.1172/JCI17223 (2003).

221 Yamauchi, T. *et al.* Inhibition of RXR and PPARgamma ameliorates diet-induced obesity and type 2 diabetes. *J Clin Invest* **108**, 1001-1013, doi:10.1172/JCI12864 (2001).
222 Cheng, L., Zhang, L., Yang, J. & Hao, L. Activation of peroxisome proliferator-activated receptor gamma inhibits vascular calcification by upregulating Klotho. *Exp Ther Med* **13**, 467-474, doi:10.3892/etm.2016.3996 (2017).
223 Jeon, M. J. *et al.* Activation of peroxisome proliferator-activated receptor-gamma inhibits the Runx2-mediated transcription of osteocalcin in osteoblasts. *J Biol Chem* **278**, 23270-23277, doi:10.1074/jbc.M211610200 (2003).
224 Feng, H. *et al.* Peroxisome Proliferator-Activated Receptor-gamma Coactivator-1alpha Inhibits Vascular Calcification Through Sirtuin 3-Mediated Reduction of Mitochondrial Oxidative Stress. *Antioxid Redox Signal* **31**, 75-91, doi:10.1089/ars.2018.7620 (2019).
225 Metz, R. P., Patterson, J. L. & Wilson, E. Vascular smooth muscle cells: isolation, culture, and characterization. *Methods Mol Biol* **843**, 169-176, doi:10.1007/978-1-61779-523-7_16 (2012).
226 Hossain, G. S. *et al.* TDAG51 is induced by homocysteine, promotes detachment-mediated programmed cell death, and contributes to the cevelopment of atherosclerosis in hyperhomocysteinemia. *J Biol Chem* **278**, 30317-30327, doi:10.1074/jbc.M212897200 (2003).
227 Nelson, A. J. *et al.* Targeting Vascular Calcification in Chronic Kidney Disease. *JACC Basic Transl Sci* **5**, 398-412, doi:10.1016/j.jacbts.2020.02.002 (2020).
228 Agatston, A. S. *et al.* Quantification of coronary artery calcium using ultrafast computed tomography. *J Am Coll Cardiol* **15**, 827-832, doi:10.1016/0735-1097(90)90282-t (1990).
229 Pasch, A. *et al.* Nanoparticle-based test measures overall propensity for calcification in serum. *J Am Soc Nephrol* **23**, 1744-1752, doi:10.1681/ASN.2012030240 (2012).
230 Chiva-Blanch, G. *et al.* Liquid Biopsy of Extracellular Microvesicles Maps Coronary Calcification and Atherosclerotic Plaque in Asymptomatic Patients With Familial Hypercholesterolemia. *Arteriosclerosis, thrombosis, and vascular biology* **39**, 945-955, doi:10.1161/ATVBAHA.118.312414 (2019).
231 Leopold, J. A. MicroRNAs Regulate Vascular Medial Calcification. *Cells* **3**, 963-980, doi:10.3390/cells3040963 (2014).
232 Berezin, A. E. & Kremzer, A. A. Circulating osteopontin as a marker of early coronary vascular calcification in type two diabetes mellitus patients with known asymptomatic coronary artery disease. *Atherosclerosis* **229**, 475-481, doi:10.1016/j.atherosclerosis.2013.06.003 (2013).
233 Krzanowski, M. *et al.* Elevated Circulating Osteoprotegerin Levels in the Plasma of Hemodialyzed Patients With Severe Artery Calcification. *Ther Apher Dial* **22**, 519-529, doi:10.1111/1744-9987.12681 (2018).
234 Westenfeld, R. *et al.* Effect of vitamin K2 supplementation on functional vitamin K deficiency in hemodialysis patients: a randomized trial. *American journal of*

kidney diseases : the official journal of the National Kidney Foundation **59**, 186-195, doi:10.1053/j.ajkd.2011.10.041 (2012).

235 Diaz-Tocados, J. M. *et al.* Dietary magnesium supplementation prevents and reverses vascular and soft tissue calcifications in uremic rats. *Kidney international* **92**, 1084-1099, doi:10.1016/j.kint.2017.04.011 (2017).

236 Geurtzen, K. *et al.* Mature osteoblasts dedifferentiate in response to traumatic bone injury in the zebrafish fin and skull. *Development* **141**, 2225-2234, doi:10.1242/dev.105817 (2014).

237 Furmanik, M. & Shanahan, C. M. ER stress regulates alkaline phosphatase gene expression in vascular smooth muscle cells via an ATF4-dependent mechanism. *BMC Res Notes* **11**, 483, doi:10.1186/s13104-018-3582-4 (2018).

238 Liu, F. *et al.* Tauroursodeoxycholic acid attenuates inorganic phosphate-induced osteoblastic differentiation and mineralization in NIH3T3 fibroblasts by inhibiting the ER stress response PERK-eIF2alpha-ATF4 pathway. *Drug Discov Ther* **9**, 38-44, doi:10.5582/ddt.2015.01008 (2015).

239 Tani, T., Orimo, H., Shimizu, A. & Tsuruoka, S. Development of a novel chronic kidney disease mouse model to evaluate the progression of hyperphosphatemia and associated mineral bone disease. *Sci Rep* **7**, 2233, doi:10.1038/s41598-017-02351-6 (2017).

240 Jia, T. *et al.* A novel model of adenine-induced tubulointerstitial nephropathy in mice. *BMC Nephrol* **14**, 116, doi:10.1186/1471-2369-14-116 (2013).

241 Lee, D. H. *et al.* Gender difference in bone loss and vascular calcification associated with age. *Korean Circ J* **43**, 453-461, doi:10.4070/kcj.2013.43.7.453 (2013).

242 Lessmann, N. *et al.* Sex Differences in Coronary Artery and Thoracic Aorta Calcification and Their Association With Cardiovascular Mortality in Heavy Smokers. *JACC Cardiovasc Imaging* **12**, 1808-1817, doi:10.1016/j.jcmg.2018.10.026 (2019).

243 Tou, L., Quibria, N. & Alexander, J. M. Transcriptional regulation of the human Runx2/Cbfa1 gene promoter by bone morphogenetic protein-7. *Mol Cell Endocrinol* **205**, 121-129, doi:10.1016/s0303-7207(03)00151-5 (2003).

244 Javed, A. *et al.* Specific residues of RUNX2 are obligatory for formation of BMP2-induced RUNX2-SMAD complex to promote osteoblast differentiation. *Cells Tissues Organs* **189**, 133-137, doi:10.1159/000151719 (2009).

245 Matsubara, T. *et al.* BMP2 regulates Osterix through Msx2 and Runx2 during osteoblast differentiation. *J Biol Chem* **283**, 29119-29125, doi:10.1074/jbc.M801774200 (2008).

246 Kim, H. N. *et al.* Combination of Runx2 and BMP2 increases conversion of human ligamentum flavum cells into osteoblastic cells. *BMB Rep* **44**, 446-451, doi:10.5483/BMBRep.2011.44.7.446 (2011).

247 Watson, K. E. *et al.* TGF-beta 1 and 25-hydroxycholesterol stimulate osteoblast-like vascular cells to calcify. *J Clin Invest* **93**, 2106-2113, doi:10.1172/JCI117205 (1994).

248 Lin, S., Svoboda, K. K., Feng, J. Q. & Jiang, X. The biological function of type I receptors of bone morphogenetic protein in bone. *Bone Res* **4**, 16005, doi:10.1038/boneres.2016.5 (2016).
249 ten Dijke, P. *et al.* Identification of type I receptors for osteogenic protein-1 and bone morphogenetic protein-4. *J Biol Chem* **269**, 16985-16988 (1994).
250 Ebisawa, T. *et al.* Characterization of bone morphogenetic protein-6 signaling pathways in osteoblast differentiation. *J Cell Sci* **112 (Pt 20)**, 3519-3527 (1999).
251 Aoki, H. *et al.* Synergistic effects of different bone morphogenetic protein type I receptors on alkaline phosphatase induction. *J Cell Sci* **114**, 1483-1489 (2001).
252 Gamer, L. W., Nove, J., Levin, M. & Rosen, V. BMP-3 is a novel inhibitor of both activin and BMP-4 signaling in Xenopus embryos. *Dev Biol* **285**, 156-168, doi:10.1016/j.ydbio.2005.06.012 (2005).
253 Allendorph, G. P., Isaacs, M. J., Kawakami, Y., Izpisua Belmonte, J. C. & Choe, S. BMP-3 and BMP-6 structures illuminate the nature of binding specificity with receptors. *Biochemistry* **46**, 12238-12247, doi:10.1021/bi700907k (2007).
254 Sinha, A. & Vyavahare, N. R. High-glucose levels and elastin degradation products accelerate osteogenesis in vascular smooth muscle cells. *Diab Vasc Dis Res* **10**, 410-419, doi:10.1177/1479164113485101 (2013).
255 Chen, D. *et al.* Differential roles for bone morphogenetic protein (BMP) receptor type IB and IA in differentiation and specification of mesenchymal precursor cells to osteoblast and adipocyte lineages. *J Cell Biol* **142**, 295-305, doi:10.1083/jcb.142.1.295 (1998).
256 Zhang, J. *et al.* Identification of the haematopoietic stem cell niche and control of the niche size. *Nature* **425**, 836-841, doi:10.1038/nature02041 (2003).
257 Schroeder, T. M., Jensen, E. D. & Westendorf, J. J. Runx2: a master organizer of gene transcription in developing and maturing osteoblasts. *Birth Defects Res C Embryo Today* **75**, 213-225, doi:10.1002/bdrc.20043 (2005).
258 Hassan, M. Q. *et al.* Dlx3 transcriptional regulation of osteoblast differentiation: temporal recruitment of Msx2, Dlx3, and Dlx5 homeodomain proteins to chromatin of the osteocalcin gene. *Mol Cell Biol* **24**, 9248-9261, doi:10.1128/MCB.24.20.9248-9261.2004 (2004).
259 Franceschi, R. T. & Xiao, G. Regulation of the osteoblast-specific transcription factor, Runx2: responsiveness to multiple signal transduction pathways. *J Cell Biochem* **88**, 446-454, doi:10.1002/jcb.10369 (2003).
260 Lian, J. B. *et al.* Regulatory controls for osteoblast growth and differentiation: role of Runx/Cbfa/AML factors. *Crit Rev Eukaryot Gene Expr* **14**, 1-41 (2004).
261 Vimalraj, S., Arumugam, B., Miranda, P. J. & Selvamurugan, N. Runx2: Structure, function, and phosphorylation in osteoblast differentiation. *Int J Biol Macromol* **78**, 202-208, doi:10.1016/j.ijbiomac.2015.04.008 (2015).
262 Liu, T. M. & Lee, E. H. Transcriptional regulatory cascades in Runx2-dependent bone development. *Tissue Eng Part B Rev* **19**, 254-263, doi:10.1089/ten.TEB.2012.0527 (2013).

263 Zhang, Y. W. *et al.* A RUNX2/PEBP2alpha A/CBFA1 mutation displaying impaired transactivation and Smad interaction in cleidocranial dysplasia. *Proc Natl Acad Sci U S A* **97**, 10549-10554, doi:10.1073/pnas.180309597 (2000).
264 Sarafidis, P. A., Whaley-Connell, A., Sowers, J. R. & Bakris, G. L. Cardiometabolic syndrome and chronic kidney disease: what is the link? *J Cardiometab Syndr* **1**, 58-65, doi:10.1111/j.0197-3118.2006.05470.x (2006).
265 Yun, H. R. *et al.* Obesity, Metabolic Abnormality, and Progression of CKD. *American journal of kidney diseases : the official journal of the National Kidney Foundation* **72**, 400-410, doi:10.1053/j.ajkd.2018.02.362 (2018).
266 DeBoer, M. D. *et al.* Metabolic Syndrome Severity and Risk of CKD and Worsened GFR: The Jackson Heart Study. *Kidney Blood Press Res* **43**, 555-567, doi:10.1159/000488829 (2018).
267 Targher, G., Byrne, C. D., Lonardo, A., Zoppini, G. & Barbui, C. Non-alcoholic fatty liver disease and risk of incident cardiovascular disease: A meta-analysis. *J Hepatol* **65**, 589-600, doi:10.1016/j.jhep.2016.05.013 (2016).
268 Mantovani, A. *et al.* Nonalcoholic fatty liver disease increases risk of incident chronic kidney disease: A systematic review and meta-analysis. *Metabolism* **79**, 64-76, doi:10.1016/j.metabol.2017.11.003 (2018).
269 Byrne, C. D. & Targher, G. NAFLD as a driver of chronic kidney disease. *J Hepatol* **72**, 785-801, doi:10.1016/j.jhep.2020.01.013 (2020).
270 Musso, G. *et al.* Association of non-alcoholic fatty liver disease with chronic kidney disease: a systematic review and meta-analysis. *PLoS Med* **11**, e1001680, doi:10.1371/journal.pmed.1001680 (2014).
271 Jaruvongvanich, V., Wirunsawanya, K., Sanguankeo, A. & Upala, S. Nonalcoholic fatty liver disease is associated with coronary artery calcification: A systematic review and meta-analysis. *Dig Liver Dis* **48**, 1410-1417, doi:10.1016/j.dld.2016.09.002 (2016).
272 Cho, Y. K. *et al.* The impact of non-alcoholic fatty liver disease and metabolic syndrome on the progression of coronary artery calcification. *Sci Rep* **8**, 12004, doi:10.1038/s41598-018-30465-y (2018).
273 Oni, E. *et al.* Nonalcoholic Fatty Liver Disease Is Associated With Arterial Distensibility and Carotid Intima-Media Thickness: (from the Multi-Ethnic Study of Atherosclerosis). *Am J Cardiol* **124**, 534-538, doi:10.1016/j.amjcard.2019.05.028 (2019).
274 Kim, D. *et al.* Nonalcoholic fatty liver disease is associated with coronary artery calcification. *Hepatology* **56**, 605-613, doi:10.1002/hep.25593 (2012).
275 Mellinger, J. L. *et al.* Hepatic steatosis and cardiovascular disease outcomes: An analysis of the Framingham Heart Study. *J Hepatol* **63**, 470-476, doi:10.1016/j.jhep.2015.02.045 (2015).
276 Eshraghian, A. Bone metabolism in non-alcoholic fatty liver disease: vitamin D status and bone mineral density. *Minerva Endocrinol* **42**, 164-172, doi:10.23736/S0391-1977.16.02587-6 (2017).
277 Alhasson, F. *et al.* NKT cell modulates NAFLD potentiation of metabolic oxidative stress-induced mesangial cell activation and proximal tubular toxicity.

Am J Physiol Renal Physiol **310**, F85-F101, doi:10.1152/ajprenal.00243.2015 (2016).

278 Alhasson, F. *et al.* High circulatory leptin mediated NOX-2-peroxynitrite-miR21 axis activate mesangial cells and promotes renal inflammatory pathology in nonalcoholic fatty liver disease. *Redox Biol* **17**, 1-15, doi:10.1016/j.redox.2018.04.002 (2018).

279 Saklayen, M. G. The Global Epidemic of the Metabolic Syndrome. *Curr Hypertens Rep* **20**, 12, doi:10.1007/s11906-018-0812-z (2018).

280 Araujo, A. R., Rosso, N., Bedogni, G., Tiribelli, C. & Bellentani, S. Global epidemiology of non-alcoholic fatty liver disease/non-alcoholic steatohepatitis: What we need in the future. *Liver Int* **38 Suppl 1**, 47-51, doi:10.1111/liv.13643 (2018).

281 Starkel, P. & Leclercq, I. A. Animal models for the study of hepatic fibrosis. *Best Pract Res Clin Gastroenterol* **25**, 319-333, doi:10.1016/j.bpg.2011.02.004 (2011).

282 Kristiansen, M. N. *et al.* Obese diet-induced mouse models of nonalcoholic steatohepatitis-tracking disease by liver biopsy. *World J Hepatol* **8**, 673-684, doi:10.4254/wjh.v8.i16.673 (2016).

283 Ailhaud, G. Adipose tissue as a secretory organ: from adipogenesis to the metabolic syndrome. *C R Biol* **329**, 570-577; discussion 653-575, doi:10.1016/j.crvi.2005.12.012 (2006).

284 Mullican, S. E. & Rangwala, S. M. Uniting GDF15 and GFRAL: Therapeutic Opportunities in Obesity and Beyond. *Trends Endocrinol Metab* **29**, 560-570, doi:10.1016/j.tem.2018.05.002 (2018).

285 Poggio, P. *et al.* PCSK9 Involvement in Aortic Valve Calcification. *J Am Coll Cardiol* **72**, 3225-3227, doi:10.1016/j.jacc.2018.09.063 (2018).

286 Bergmark, B. A. *et al.* An Exploratory Analysis of Proprotein Convertase Subtilisin/Kexin Type 9 Inhibition and Aortic Stenosis in the FOURIER Trial. *JAMA Cardiol* **5**, 709-713, doi:10.1001/jamacardio.2020.0728 (2020).

APPENDICES

APPENDIX 1-ER stress in response to vitamin D3

Supplemental Figure 1

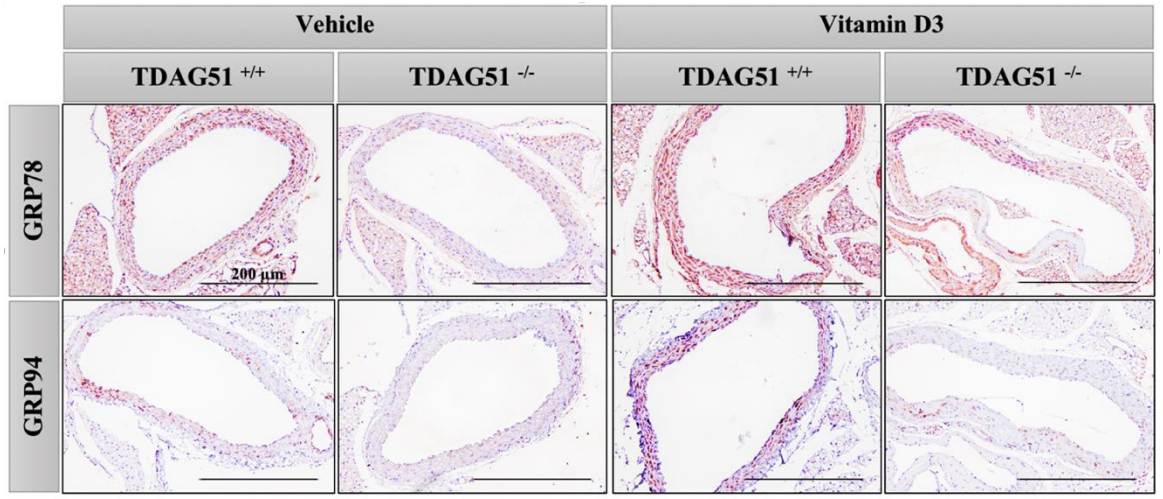

Supplemental Figure S1: Aortas from *TDAG51*$^{-/-}$ mice exhibit an attenuation of ER stress in response to vitamin D3 treatment. Eight week old *TDAG51*$^{+/+}$ and *TDAG51*$^{-/-}$ male mice were randomly selected to either treatment or vehicle control groups. The treatment group was injected with 555000 IU/kg/day of active vitamin D3 for 3 consecutive days[1]. Mice were sacrificed on day 7 of the study. Abdominal aortas were harvested, fixed in formalin, embedded in paraffin and sectioned at a thickness of 4 µm. Sections were deparaffinized in three changes of xylene and dehydrated in 3 changes of ethanol. Sections were then blocked for 30 minutes and incubated with primary antibody overnight. Following the incubation with primary antibody, sections were washed and subsequently incubated with secondary antibody. Nuclei were counterstained using Gill's Hematoxylin**.** Staining was detected using Nova Red Solution.

APPENDIX 2-Adenine model of VC pilot

Various animal models have been developed to examine CKD-associated VC. The large majority of available models are dependent on surgical or genetic manipulation. The most commonly used method to induce renal dysfunction is surgical reduction of kidney mass by 2/3, 3/4 or 5/6, which eventually leads to uremia and other CKD-related complication[2]. However, surgical models pose a substantial risk of mortality. Induction of CKD using dietary administration of adenine is an alternative model in which renal impairment occurs as a result of nephrotoxicity due to an accumulation of precipitated adenine crystals in the renal tubules and urinary track[2]. Adenine-based models of VC are predominantly used in rat studies and have been demonstrated to produce somewhat inconsistent results in mice on a C57BL/6J genetic background due to resistance to ectopic mineral accumulation[2].

In recent years, two separate groups have successfully demonstrated an induction adenine-mediated kidney injury in mice[3,4]. In their study, Jia *et al.*[3] carried out an 8-week experiment in which mice were fed either a casein-based control diet or casein-based diet supplemented with varying concentrations of adenine. Schematic view of study design adapted from the original manuscript is shown in *Supplemental Figure S2A* below. This study demonstrated a reliable non-surgical method of inducing CKD-like renal damage in mice, however VC was not examined. Even though a substantial increase in circulating serum P_i was observed in the adenine group, it is unclear whether VC would be present in these animals given that no additional P_i supplementation was provided. In a separate study, Tani *et al.*[4] demonstrated that although adenine feeding leads to renal impairment similar to that observed previously, adenine alone is not sufficient to lead to VC in the absence of

additional P_i supplementation. Based on these observations, we adopted the protocol for CKD induction and P_i loading developed by Tani and colleagues[4]. Schematic view of our study design is shown in *Supplemental Figure S2B* below. Other components of the diet, such as calcium, magnesium, and vitamin D3 were comparable to Jia *et al.*[3] because the experimental procedure in the study described by Tani *et al.*[4] did not disclose the exact proportions. The exact proportions of micro and macro nutrients are outlined in *Supplemental Table 1*.

The designed study was not carried out to completion because of substantial weight loss, which occurred as a result of reduced food consumption, and increased mortality rates in the adenine and adenine+P_i groups (*Figure S3A*). Weight loss further increased when a combination of high P_i and adenine was introduced, leading to termination of the experiment (*Figure S3A*). The limited data from this study demonstrate that in line with previous observations adenine feeding results in renal tubular inflammation and increased adipocyte content in the femurs of mice fed diet containing 0.2% adenine (*Figure S3B and C*)[3,4]. Additionally, an increase in serum phosphate and creatinine was also observed in adenine fed mice (*Figure S3D*). No significant increase in aortic mineral content was observed in the adenine+Pi or adenine alone groups (*Figure S3E*). Given that mice were only fed high P_i containing diet for approximately one week, and that Tani *et al.*[4] demonstrated that adenine alone does not induce VC, it is not surprising that no increase in mineral content in the aortas was observed.

To overcome the limitations of the study described above, experimental approach was modified to incrementally increase P_i content in the diet util it reached 1.8%. Schematic

view of modified study design is shown in *Supplemental Figure S4A*. Additionally, to help maintain body weight, diet was supplemented with a high calorie dietary supplement recommended by the animal facility staff. Given that vehicle control samples were available from previous experiment, this pilot study only included the adenine and adenine+ P_i groups. Although, the study was carried out to completion with minimal weight loss, no difference in aortic mineral content between adenine+P_i group and previously tested vehicle control group was observed (*Figure S4B and C*). Lack of expected phenotype was attributed to high concentration of vitamin K in the dietary supplement (Ensure).

Supplemental Figure S2 (1/1)

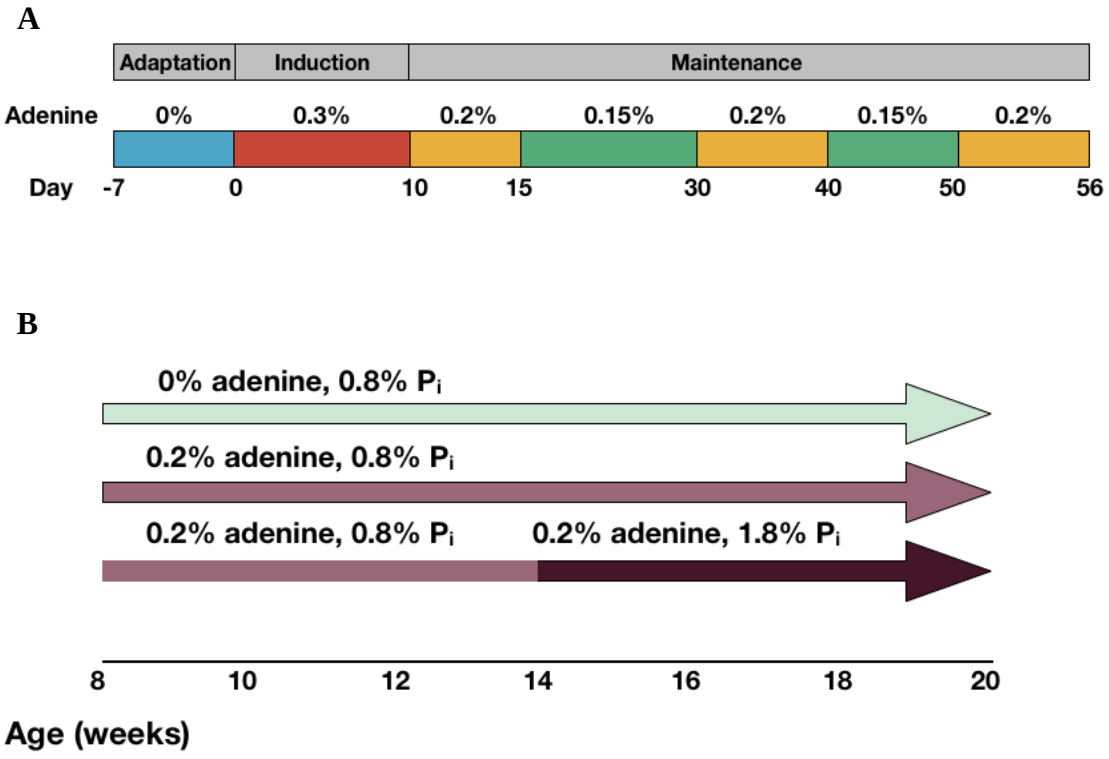

Supplemental Figure S2: A schematic representation of adenine-mediated CKD models. (A) Adenine model of renal damage employed by Jia *et al*[3]. (B) Study design for induction of CKD-associated VC based on Tani *et al*[4].

Supplemental Figure S3 (1/2)

A

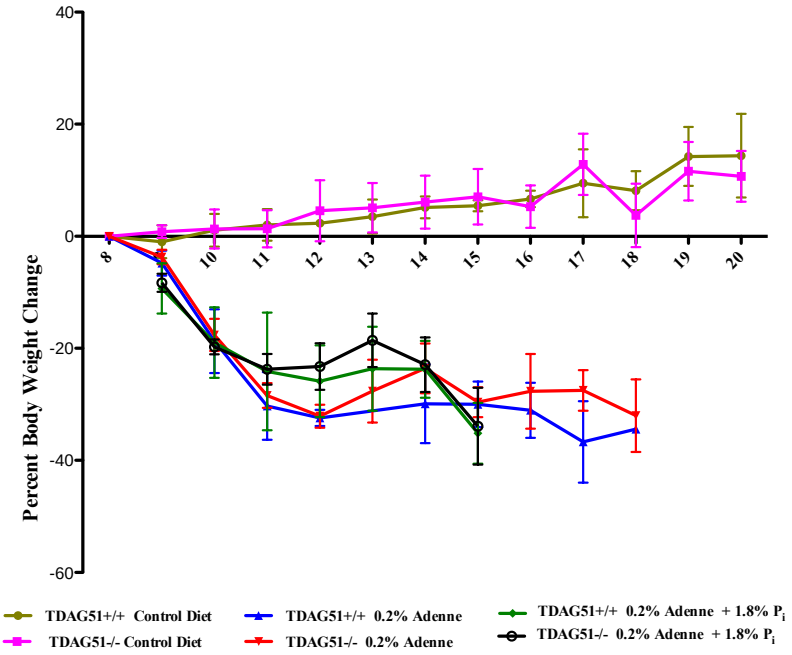

B

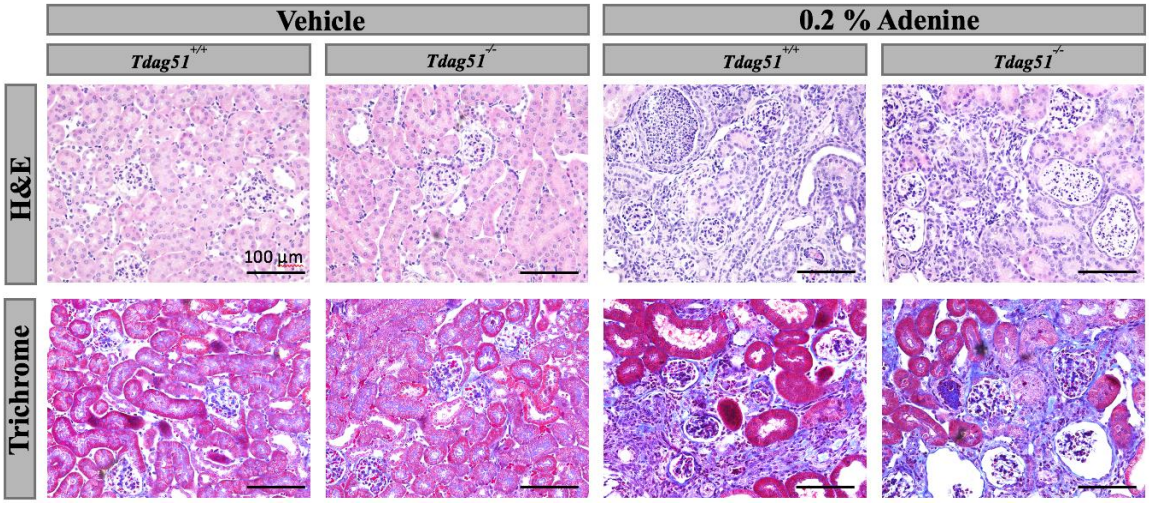

Supplemental Figure S3 (2/2)

C

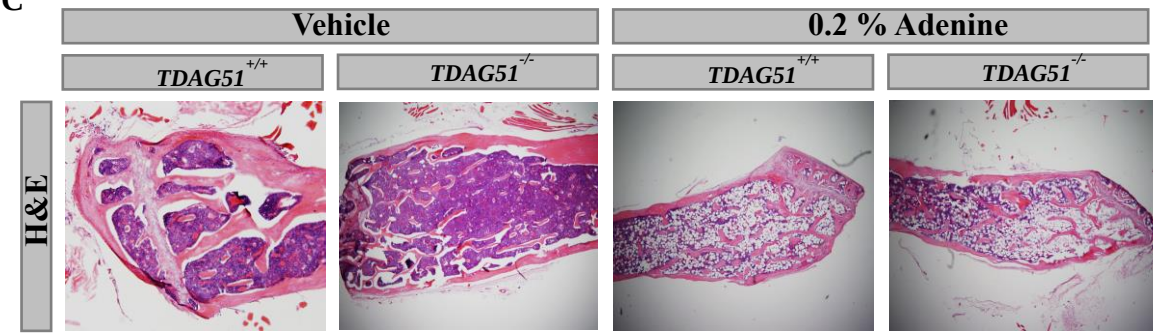

D

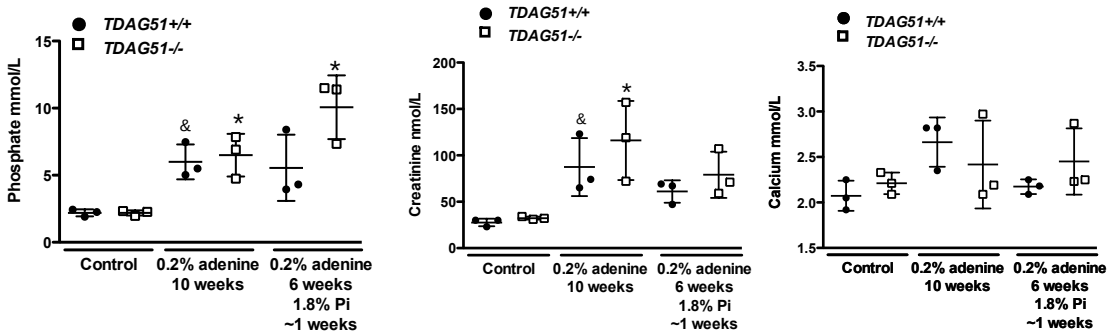

*, $p<0.05$, vs. *TDAG51*$^{+/+}$ Vehicle ; &, $p<0.05$, vs. *TDAG51*$^{-/-}$ 0.2% Adenine

E

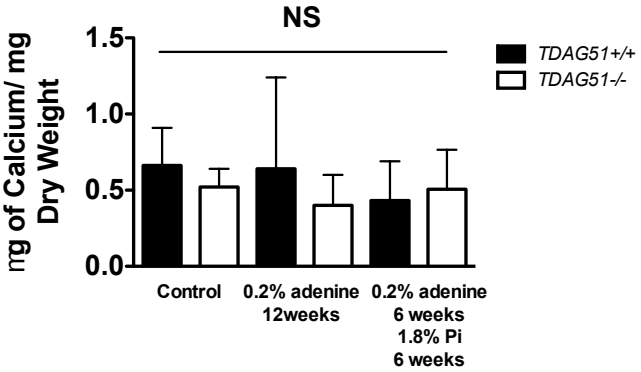

Supplemental Figure S3: Assessment of adenine-mediated model of renal damage and VC . (A) Percent body weight change (n=3-5 per group). (B) Representative H&E and Trichrome staining in the kidney tissue. (C) Representative H&E staining in the femur tissue. (D) Quantification of serum phosphate, creatinine, and calcium (n=3 per group). (E) Quantification of calcium deposition in the aortas (n=3-5 per group). All data represented as mean and error bars as standard deviation.

Supplemental Figure S4

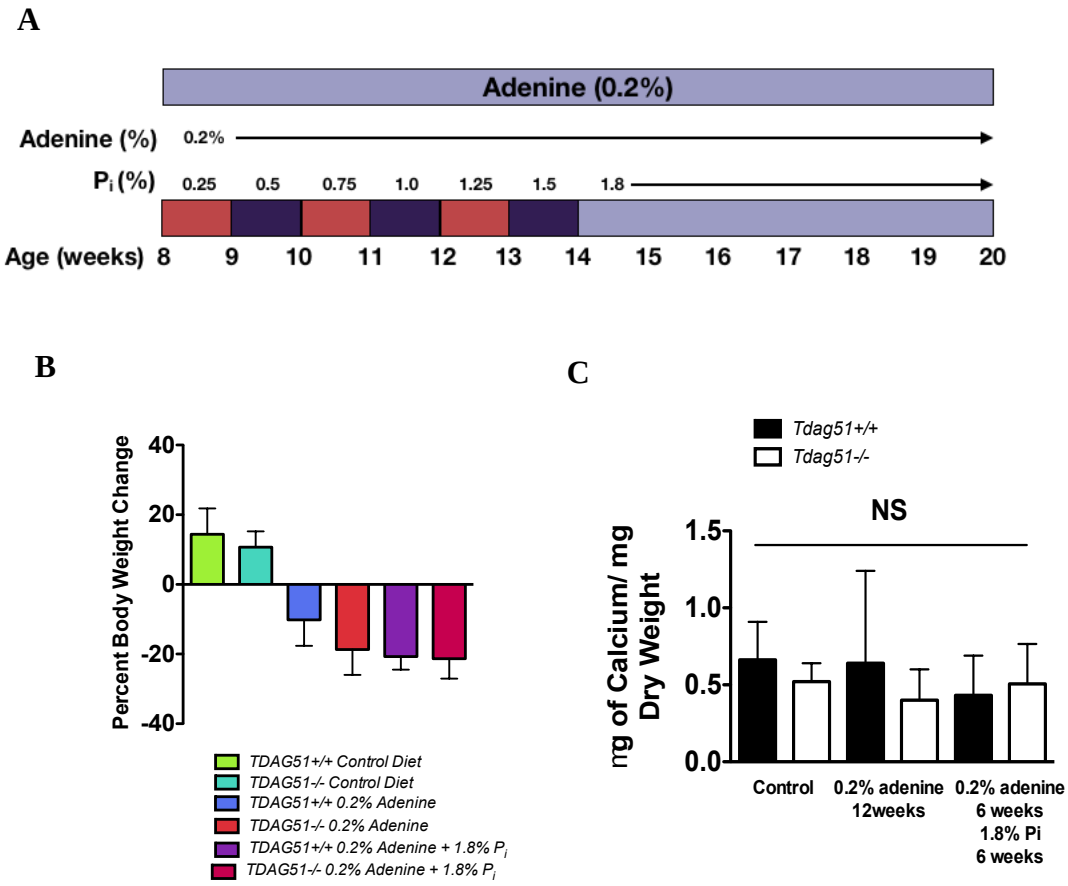

Supplemental Figure S4: Assessment of adapted adenine model of renal damage and VC . (A) A schematic representation of adapted experimental design. (B) Percent body weight change (n=5-7 per group; control groups from previous experiment). (C) Quantification of calcium deposition in the aortas (n=5-7 per group; control groups from previous experiment). All data represented as mean and error bars as standard deviation.

Supplemental Table 1: Diet compositions

	Diets		
Diet Formula	**Control**	**0.2% Adenine**	**0.2% Adenine + 1.8% P_i**
Adenine (%)	0	0.2	0
Phosphate (%)	0.8	0.8	0.8
Calcium (%)	1.07	1.07	1.07
Magnesium (%)	0.24	0.24	0.24
Vitamin D3 (IU)	1.37	1.37	1.37
Casein (g/kg)	200.0	200.0	200.0
L-Cystine (g/kg)	3.0	3.0	3.0
Corn Starch (g/kg)	367.4366	365.4366	340.9368
Maltodextrin (g/kg)	132.0	132.0	132.0
Sucrose (g/kg)	100.0	100.0	100.0
Soybean Oil (g/kg)	70.0	70.0	70.0
Cellulose (g/kg)	50.0	50.0	50.0
Mineral Mix (g/kg)	13.39	13.39	13.39
Calcium Phosphate, monobasic, monohydrate (g/kg)	26.42	26.42	67.07
Calcium Carbonate (g/kg)	16.15	16.15	
Potassium Phosphate, monobasic (g/kg)	0.44	0.44	0.44
Magnesium Oxide (g/kg)	3.123	3.123	3.123
Vitamin Mix (g/kg)	15.0	15.0	15.0
Vitamin A Palmitate (500, 000 IU/g) (g/kg)	0.012	0.012	0.012
Vitamin D3 in (50, 000 IU/g in sucrose) (g/kg)	0.0274	0.0274	0.0274
Vitamin E, DL-alpha tocopheryl acetate (500 IU/g) (g/kg)	0.225	0.225	0.225
Choline Bitartrate (g/kg)	2.75	2.75	2.75
Thiamine (81%) (g/kg)	0.01	0.01	0.01
Vitamin K, phylloquinone (g/kg)	0.002	0.002	0.002
TBHQ antioxidant (g/kg)	0.014	0.014	0.014

Nutrient information

	% kcal from		
Protein	19.5	19.5	20
Carbohydrate	62.7	62.7	61.7
Fat	17.8	17.8	18.3
Kcal/g	3.6	3.6	3.5

APPENDIX 3-Structural similarity between mouse TGF-β and GDF10 active ligands

Protein sequence of mouse TGF-β1 and GDF10 were compared using the NCBI Protein Blast online tool. Query input is summarized in *Supplemental Table 2*. Graphical summary of comparison of protein sequences demonstrates only 40-50% similarity in the carboxy terminal domain between TGF-β1 and GDF10 (*Figure S5*).

Supplemental Table 2: NCBI protein blast input summary

	TGF-β	GDF10
Species	Mouse	Mouse
Peptide length (amino acids)	390	476
Predicted Molecular Mass (Da)	44,310	52,575
UniProt Sequence Identifier	Q3UNK5	P97797

Supplemental Figure S5

A

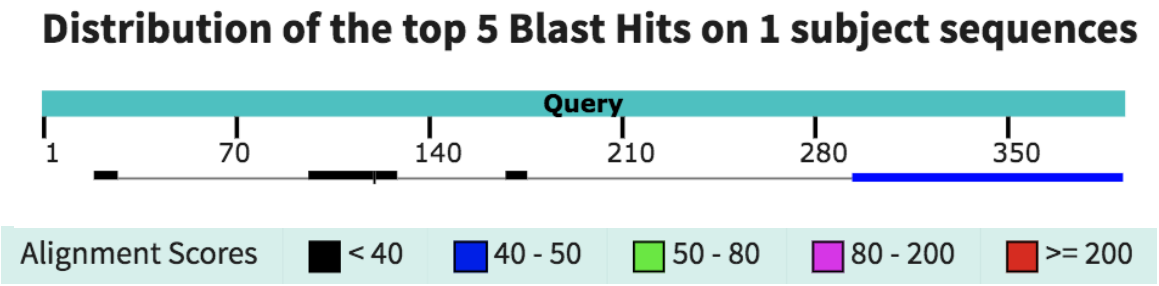

B

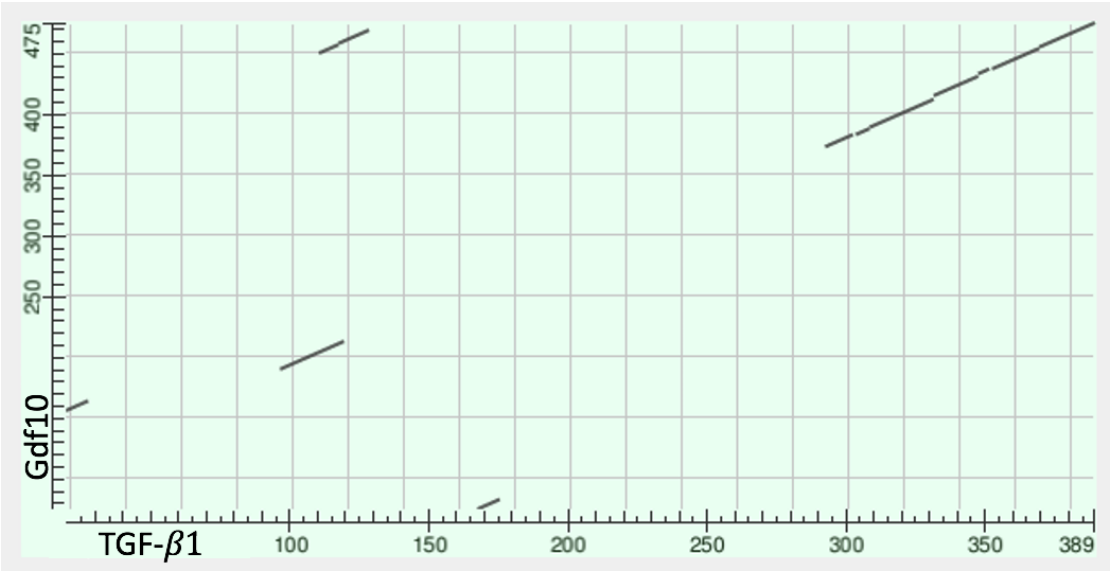

Supplemental Figure S5: Comparison of Gdf10 and TGF-β protein sequences. (A) Graphical summary. (B) Dot plot summary.

APPENDIX 4-HDAC3 expression in VSMCs from *TDAG51*$^{+/+}$ and *TDAG51*$^{-/-}$ mice

Supplemental Figure 6

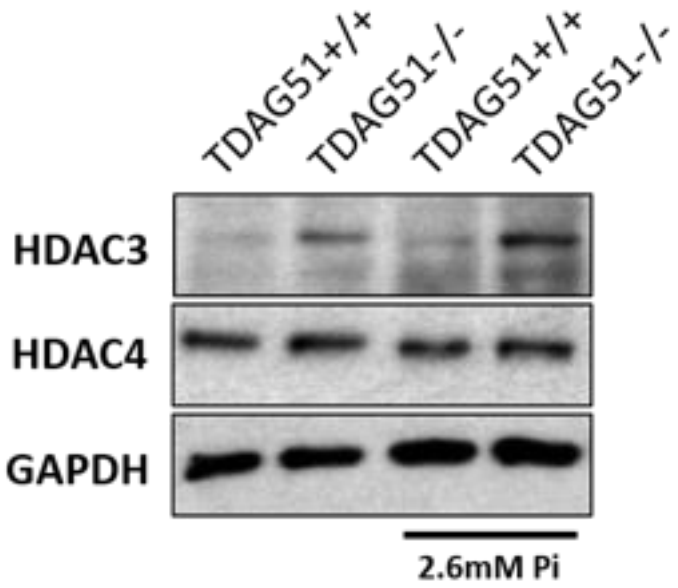

Supplemental Figure 6: *TDAG51*$^{-/-}$ VSMCs exhibit increase expression of HDAC3. *TDAG51*$^{+/+}$ and *TDAG51*$^{-/-}$ VSMCs were either untreated or treated with 2.6 mM Pi for 3 days. Protein concentrations of whole cell lysates were measured using a modified Lowry assay. The samples were resolved by SDS-PAGE and subsequently transferred to nitrocellulose membranes. The membranes were then blocked using 5% w/v skimmed milk and subsequently incubated with respective primary antibodies overnight. Following the incubation with primary antibody, membranes were incubated with respective secondary antibodies and the signal was detected using a Konica Minolta X-ray film processor or ChemiDoc XRS+.

APPENDIX REFERENCES

1. Kang, Y. H., Jin, J. S., Yi, D. W. & Son, S. M. Bone morphogenetic protein-7 inhibits vascular calcification induced by high vitamin D in mice. *Tohoku J Exp Medicine* **221**, 299–307 (2010).

2. Shobeiri, N., Adams, M. A. & Holden, R. M. Vascular calcification in animal models of CKD: A review. *Am J Nephrol* **31**, 471–481 (2010).

3. Jia, T. *et al.* A novel model of adenine-induced tubulointerstitial nephropathy in mice. *Bmc Nephrol* **14**, 116 (2013).

4. Tani, T., Orimo, H., Shimizu, A. & Tsuruoka, S. Development of a novel chronic kidney disease mouse model to evaluate the progression of hyperphosphatemia and associated mineral bone disease. *Sci Rep-uk* **7**, 2233 (2017).